Copyright Warning & Restrictions

The copyright law of the United States (Title 17, United States Code) governs the making of photocopies or other reproductions of copyrighted material.

Under certain conditions specified in the law, libraries and archives are authorized to furnish a photocopy or other reproduction. One of these specified conditions is that the photocopy or reproduction is not to be "used for any purpose other than private study, scholarship, or research." If a, user makes a request for, or later uses, a photocopy or reproduction for purposes in excess of "fair use" that user may be liable for copyright infringement,

This institution reserves the right to refuse to accept a copying order if, in its judgment, fulfillment of the order would involve violation of copyright law.

Please Note: The author retains the copyright while the New Jersey Institute of Technology reserves the right to distribute this thesis or dissertation

Printing note: If you do not wish to print this page, then select "Pages from: first page # to: last page #" on the print dialog screen

ABSTRACT

Behavior of High Strength Concrete and Slender Reinforced Concrete Columns With and Without Steel Fibers

by
Lin Showmay Hsu

A series of compression tests are conducted on 3 in. by 6 in. cylindrical specimens using a modified testing method that give the complete stress-strain behavior for both plain and fibrous high strength concretes with or without tie confinements. The volume fractions of fiber in the concrete are 0%, 0.5%, 0.75%, and 1.0%, respectively. Empirical equations are proposed herein to represent the complete stress-strain relationships of high strength and high strength fibrous concretes with compressive strength exceeding 10,000 psi. Various parameters are studied and their relationships are experimentally determined. The comparison between the experimental and analytical results shows to have good agreement.

The proposed empirical stress-strain equations for high strength and high strength steel fiber concretes are used as material properties to modify the existing computer program of biaxially loaded slender reinforced concrete columns. This computer program evaluates the complete biaxial load-deflection and moment-curvature relationships of slender columns from zero load until failure. A total of nine high strength and five high strength steel fiber slender reinforced concrete columns are tested to compare their experimental load-deformation results with the analytical values derived from the present theoretical studies. A satisfactory agreement is attained for both ascending and descending branches of the load-deformation curves.

Behavior of High Strength Concrete and Slender Reinforced Concrete Columns With and Without Steel Fibers

by
Lin Showmay Hsu

A Dissertation
Submitted to the Faculty of
New Jersey Institute of Technology
in Partial Fulfillment of the Requirements for the
Degree of Doctor of Philosophy Department of
Civil and Environmental Engineering
October, 1992

APPROVAL PAGE

Behavior of High Strength Concrete and Slender Reinforced Concrete Columns With and Without Steel Fibers

by
Lin Showmav Hsu

Dr. Cheng-Tzu Thomas Hsu, Dissertation Adviser
Associate Chairperson and Professor of Civil and Environmental Engineering, NJIT

Dr. Dorairaja Raghu, Committee Member
Professor of Civil and Environmental Engineering, NJIT

Dr. Farhad Ansari, Committee Member
Professor of Civil and Environmental Engineering, NJIT

Dr. Methi Wecharatana, Committee Member
Professor of Civil and Environmental Engineering, NJIT

Dr. Rong-Yaw Chen, Committee Member
Professor of Mechanical and Industrial Engineering, NJIT

BIOGRAPHICAL SKETCH

Author: Lin Showmay Hsu.

Degree: Doctor of Philosophy.

Date: October, 1992.

Undergraduate and Graduate Education:

- Doctor of Philosophy in Civil and Environmental Engineering,
  New Jersey Institute of Technology, Newark, NJ, 1992.
- Master of Science in Civil Engineering,
  New Jersey Institute of Technology, Newark, NJ, 1988.
- Bachelor of Science in Civil Engineering,
  Chung Yuan University, Chungli, Taiwan, Republic of China, 1985.

Major: Civil Engineering

Position Held:

9/91-9/92	Graduate Assistant, Structure and Concrete Laboratory, Department of Civil and Environmental Engineering, New Jersey Institute of Technology, Newark, NJ.
12/88-9/92	Teaching Assistant, Engineering Mechanics, Department of Civil and Environmental Engineering, New Jersey Institute of Technology, Newark, NJ.
5/88-12/88	Graduate assistant, Computer Laboratory, Department of Civil and Environmental Engineering, New Jersey Institute of Technology, Newark, NJ.

This dissertation is dedicated to
my beloved mother
A-Jaw Lee
and
my husband
Dr. Peming Hsu

ACKNOWLEDGMENTS

I would like to express my sincere thanks and gratitude to Dr. C. T. Thomas Hsu whose guidance and advice has been instrumental to the successful completion of this research work. His constructive criticism and his help with proper organization of the contents of this dissertation have been a valuable experience.

I would also like to thank my Dissertation Committee Members: Drs. Dorairaja Raghu, Farhad Ansari, Methi Wecharatana, and Rong-Yaw Chen for their invaluable suggestions.

Special thanks to Mr. Suk-Ki Kim, Mr. Chai Jaturapitakkul, Dr. Wen-Hu Tsao, and Mr. Allen Luke who shared their experiences with me and helped me carry out the experimental tests, and to Mr. John Eimess who helped to fabricate the circular-hoop. In addition, I would like to acknowledge the following colleagues who assisted me with the experimental preparations: Mr. P. S. Wu, Mr. T. Z. Wu, Mr. H. P. Savalia, Mr. M. S. Parikh, Mr. Chun-Tse Hsu, and Mr. Sang K. Shin.

Special thanks should also go to Dr. Methi Wecharatana for having donated many experimental materials.

The experiments were performed using the MTS testing system which was purchased under the NSF grant, No. CEE 8308339. Financial support to purchase the research materials from several New Jersey corporations and companies, graduate assistantship from NJIT which enabled the author to complete this study, are also greatly acknowledged.

TABLE OF CONTENTS

LIST OF TABLES

LIST OF FIGURES

LIST OF SYMBOLS

Chapter 2

A_S Area of Steel Wire

E_c Secant Modulus of Elasticity

E_{it} Initial Tangential Modulus

R.I. Reinforcing Index ($V_f * \ell / d$)

S Spacing of Hoops

T Toughness (the Area Under the Stress-Strain Curve)

T.I. Toughness Index which is Defined as Ratio of Toughness of Fibrous Concrete to that of Plain Concrete

V_f Fiber Volume Fraction

a Constant

f_c the Stress in General

f_c' Maximum Compressive Strength (Peak Stress) of Unconfined Concrete

f_{cc}' Maximum Compressive Strength (Peak Stress) of Confined Concrete

f_y Yield Strength of Transverse Steel

k_d Constant

ℓ / d Aspect Ratio of Steel Fiber (Length/Diameter)

n Coefficient in the Proposed Stress-Strain Equation

x Normalized Strain

x_d Strain at $0.3f_c'$ and $0.6f_c'$ in the Descending Portion of the Stress-Strain Curve of Plain and Fibrous Concrete, respectively

β Material Parameter for Unconfined Concrete

β_c Material Parameter for Confined Concrete

ε Strain in General

ε_o Strain Corresponding to Peak Stress

ε_{oc} Strain Corresponding to Peak Stress of Confined Concrete

η Normalized Stress

ρ Volumetric Ratio i.e. Ratio of Volume of Binder to Volume of Confined Concrete

Chapter 3

$(E_s)_k$ Secant Modulus of Elasticity for Element k

$M_{x(1)}, M_{y(1)}$ Maximum Moment Capacity from the Experimental Result

$M_{x(2)}, M_{y(2)}$ Maximum Moment Capacity from the Analytical Result

$M_{x(c)}, M_{y(c)}$ Calculated Value for the Bending Moment Components in X,Y Axis under Biaxial Bending and Axial Compression

$M_{x(lc)}, M_{y(lc)}$ Biaxial Bending Moment at the Middle Segment

$P_{(c)}$ Calculated Value for the Axial Load P under Biaxial Bending and Axial Compression

S the Lateral Tie Spacing

a_k Area of Element

d_i Represents the Reading from the Dial gage for each Increment of Loading

d_o Represents the Initial Reading from the Dial Gage

d_x, d_y Deflection in X,Y Axis

e_x, e_y Eccentricity in X,Y Axis

x,y Centroidal Coordinates for any Element in Cross Section

x_k, y_k Centroidal Coordinates for Element k in the Cross Section

ℓ_i Represents the Length of Mechanical Strain Gage at each Loading

ℓ_o Represents the Initial Length of Mechanical Strain Gage at Zero Loading

ε_o Strain at Coordinate Origin in the Principal Axes

ε_k Strain at Element k which is Subjected to Biaxial Bending and Axial Compression

ϕ_x, ϕ_y Curvature with Respect to M_X,M_y

CHAPTER ONE

INTRODUCTION

1.1 Statement of Originality

Recently, the increasing use of high strength cement-based composite in engineering construction has made it more important to understand the behavior of these structural materials.

The behavior of structure members can be rationally predicted by the given material properties, cross-sectional properties, and loading conditions, when the computerized nonlinear structural analysis techniques are employed. For this purpose, materials properties can be best described by their stress-strain relationship. However, in the existing literature, there is no published equation to predict the complete stress-strain curve of high strength cement based composite, particular for concrete cylinder with (and without) steel fibers and ties. In this study, attempts are made to experimentally obtain the complete stress-strain curve in compression and to develop empirical equations in terms of this measured curve for high strength cement-based composite.

In practice some columns are subjected to bending about principal axes simultaneously, especially the corner columns of buildings or columns in bridges. There is no published data to date, which discuss the behavior of high-strength slender columns with (and without) steel fibers under combined biaxial bending and axial compression. Thus, fourteen slender columns, with and without steel fibers, were tested to study the complete experimental load-deformation behavior including ascending and descending branches of the curves. The above proposed equations of stress-strain curve will be incorporated into the existing computer program to study the complete theoretical load-deformation behavior of biaxially loaded slender columns. This slender column computer program was recently developed at NJIT.

1.2 Literature Review

1.2.1 General

In recent years, applications of high strength concrete in the construction of tall buildings have increased in many countries. The main advantages of using high strength concrete are the economic benefits due to the reduced size of structural members and a reduction in the amount of reinforcement (Smith 1989). Furthermore, the high strength concrete is more durable and more resistant to corrosion and abrasion than that of the conventional concrete (Gregerson 1991).

As development of high strength concrete continues, the definition of high strength concrete varies in time and on a geographical basis due to lack of a standard criterion for the strength that is required to qualify as a high strength concrete. Several definitions of a high strength concrete have been made by various investigators. Freedman (Freedman 1970) defined the high strength concrete as a concrete which possessed compressive strength of at least 6,000 psi at 28 days. Bertero (Bertero 1979) defined it as a concrete with compressive strengths higher than 6,000 psi for normal weight concrete, and higher than 4,000 psi for light weight concrete. Albinger and co-workers (Albinger et al. 1981) defined the high strength concrete as a concrete with compressive strength between 6,000-11,000 psi for normal weight concrete and from 5,000-8,000 psi for light weight concrete at 56 days. Saucier (Saucier 1979) divided high strength concrete into three stages, (i) the present range of 5,000-10,000 psi (ii) the available range of 10,000-15,000 psi and (iii) the exotic area of 15,000 psi. In general, the definition of high strength concrete has been defined by ACI committee 363-High Strength Concrete (ACI 1984) as a concrete with specified compressive strength for design of 6,000 psi (41 MPa) or greater.

The material selection and mix proportioning of high strength concrete are more critical than those for a normal strength concrete. Each constituent such as cement, sand, coarse aggregate, concrete mixture, and pozzolans must be evaluated as to the type, strength characteristics, gradation, fineness, and interaction in combination with other ingredients. Many trial mix proportions are required to generate the data that allow the choice of optimum material and proportions. In particular, a high strength concrete generally has a lower water-cement ratio.

However, there are several ways to produce a high strength concrete. Many researchers have successfully made high strength concrete by using special techniques and changing the mix proportions between matrix compositions and admixtures. Peterman and co-workers (Peterman et al. 1986) made a high strength concrete by the adjustments to mix proportions such as water-cement and cement-sand ratios. Mather (Mather 1965) made a high strength concrete by using the high density materials. Mather used magnetite or limonite aggregates, which have unit weights of about 230 lb/ft^3, instead of normal coarse aggregates. Compressive strength of 9,000 psi at 7 days and 11,000 psi at 28 days were achieved. Macinnis and co-workers (Macinnis 1970) proposed three special techniques (high speed slurry mixing, seeding, and revibration) and two admixtures (fly ash and lignosulfonic acid water-reducing agent) to produce a high compressive strength concrete in the range of 6,000-11,000 psi. Another method to produce a high strength concrete is the use of mineral admixtures, such as silica fume (SF) and fly ash. They are kinds of pozzolanic mineral admixtures which are added as filler (extra fine aggregate) to improve the strength of cement composites using the so called "packing effect" to produce denser concrete. In addition, chemical admixtures, such as superplasticizers and water reducing agents , have been widely used in producing a higher strength concrete and even an ultra high strength concrete with compressive strength over 20,000 psi (Jahren, 1985 Sellevold 1983, and Sandvik 1986). During the past decade, Jahren (Jahren 1983) and ACI Committee 226 (ACI 1984) have used silica

fume (SF) to improve the strength of high strength concrete. Swamy (Swamy 1986) also made a high strength concrete with one-day strengths of 8,700 to 11,600 psi (60 to 80 N/mm^2), by using the granite aggregates and the ultrafine portland cement with a specific surface of about 750 m^2/kg. In summary, the strength and quality of high strength concrete are continually being improved and produced everyday. This continuing progress has resulted in a need to better understand the behavior of HSC.

1.2.2 Behavior of High Strength Concrete

1.2.2.1 High Strength Concrete Without Fiber. High strength concrete, generally, is brittle and lacks toughness, As a building material understanding its mechanical properties and failure characteristics becomes urgently necessary. One of the most important indications of mechanical behavior of any structural material is its stress-strain curve. For a rational design of concrete structure, both the ascending and descending parts of stress-strain curve are significant. The need to know the complete stress-strain curve of a material was clearly discussed by Bertero (Betero 1979). However, in the existing literature, only a few authors have discussed the complete stress-strain curves for a high strength concrete (Shah 1981). One of the reasons why there are insufficient experimental results on the complete stress-strain curve is that it is very difficult to measure the descending portion of the curve.

The shape of the ascending part of the stress-strain curve is more linear and steeper for a high strength concrete than for a normal concrete. Also, the slope of the descending branch of the curve is steeper for a high strength concrete (ACI-363 1984). It is difficult to obtain the descending part of the stress-strain curve experimentally because the interaction between the testing system and the specimen is critical (Shah 1981). If the stiffness of the machine is greater than the absolute value of the stiffness of the specimen in the descending part, then a stable descending part can be experimentally obtained (Hundson 1972). Some investigators have developed techniques to increase the stiffness

of the testing machine which is costly, and may not be available in a normal quality control laboratory (Ahmad 1979). However, Wang and co-workers (Wang et al. 1978) introduced a simple method to eliminate the strain energy release of the testing machine. In their testing, concrete cylinders were loaded in parallel with a hardened steel tubes. This design ensures that the sum of the load carried by the steel tubes and the concrete cylinder is always increasing up to a strain of 0.006. Thus, no release of energy comes from the testing machine. During loading, the strains in the steel tube were measured. Thus, knowing the total load and the corresponding steel strain, the stress-strain relationship for a concrete could be obtained. Although the method is relatively simple and gives reproducible descending portion of the stress-strain curve, it has certain limitations. The maximum strain that can be obtained is limited to the elastic range of the tubing material. Also, the size of the concrete cylinder that can be tested by the reduced capacity of the testing machine.

So far, two reports have discussed the complete stress-strain curve of a high strength concrete (from 10,000 psi to 13,000 psi) by using a circumferential control method. Shah and co-workers (Shah et al. 1981) developed a special measuring device. The specimens were loaded in two different control modes: a constant rate of axial strain and the controlled rate of circumferential strain. They used the circumferential strain control to obtain the complete stress-strain curve of a high strength concrete for larger sizes of specimens (4x8 and 3x9 in.). During their experiments, the axial strain rate was varied while the circumferential strain rate was held constant. Recently Taerwe (Taerwe 1992) modified the Shah's circumferential device to obtain the complete stress-strain curve.

1.2.2.2 High Strength Concrete With Fiber. The application of a high strength concrete in practice is somehow limited because it is more brittle than normal concrete. However, this brittle property of the material can be overcome by adding fibers. Fibers

have been used to reinforce the brittle materials since ancient times, such as straw in sunbaked bricks and horsehair in reinforced plaster. Recently, fibers have been produced from steel, plastic, glass, and natural materials in various shapes and sizes (ACI 544 1985).

Steel fiber reinforced concrete (SFRC) is concrete made of hydraulic cements containing fine and coarse aggregates and discontinuous discrete steel fibers. During past twenty years, SFRC has been increasingly used in a variety of structural applications. Currently, most of the applications for SFRC are in the areas of highway, airport pavement, tunnel linings, refractories, hydraulic structures, beam and beam-column junctions (Shah 1987).

To design or analyze the structures using SFRC, a complete stress-strain curve of SFRC in compression is needed. Many researchers have studied the mechanical properties of SFRC (ACI 1978, ACI 1982 Glavind 1991, Chen 1971, and Shah 1976). The results show that the addition of steel fibers leads to a greater improvement in ductility and toughness, (Glavind 1991, Fanella 1985, and Hughes 1977). Craig and co-workers (Craig et al. 1984) have also reported that adding fibers to a reinforced concrete column improved its compressive strength, shear strength, and ductility.

1.2.3 Empirical Equations of Complete Stress-Strain Curve for High Strength Concrete

1.2.3.1 Stress-Strain Curve without Fiber

1.2.3.1.1 Without Confinement. Although a number of empirical equations of complete stress-strain curve for a normal concrete have been proposed (Popovics 1970, Hsu 1974), only one published paper has ever discussed an empirical formula of complete stress-strain curve for the normal weight concretes with strengths up to 11,000 psi (Wang 1978). Wang and co-workers proposed an analytic expression with four constant

parameters. The parameters depend on the properties of both the ascending and the descending portions of the stress-strain curve and can be evaluated from the knowledge of four key points of the curve. The coordinates of the four key points are expressed in function of the compressive strength of concrete so as to allow prediction of the entire curve solely from the knowledge of the compressive strength. Thus, this section only discusses the recent development of stress-strain law for a normal concrete. In 1985, Carreira and co-worker (Carreira et al. 1985) proposed an equation to represent the complete stress-strain relationship of a plain normal concrete. They concluded that the shape of the stress-strain curve was strongly affected by some factors, such as strain rate, stiffness of the testing machine, the quality of the cement matrix, and the aggregate characteristics and their content. The parameters in the empirical equation are physically significant and can be estimated from the experiments. Other complete stress-strain equations for normal concrete were summarized by Hsu (Hsu 1974). Appendix A lists various empirical stress-strain relationships of concrete.

1.2.3.1.2 With Confinement. Several researchers have developed empirical equations to represent the complete stress-strain curve of normal strength concrete with different kinds of tie confinements. Appendix A lists the published empirical equations for confined concrete.

For high strength confined concrete, Ahamd and co-worker (Ahmad et al. 1982) proposed a model to predict the stress-strain curves of confined concrete based on properties of the hoop reinforcement and the stress-strain relationship of plain high strength concrete.

1.2.3.2 Stress-Strain Curve of High Strength Concrete with Fiber

1.2.3.2.1 Without Confinement. Very few empirical expressions of complete stress-strain curve for a normal concrete with fibers have been proposed, none of them

discusses an empirical formula for a high strength concrete with fibers (Ezeldin 1989). Therefore, this section only discusses the stress-strain law for a normal concrete with fibers. Ezeldin (Ezeldin 1989) proposed an empirical equation to express the stress-strain relationship for a normal concrete reinforced with steel fiber by extending the Carreira's equation (Carreira 1985).

Fanella and co-worker (Fanella et al. 1985) proposed an analytical model to predict the complete stress-strain curve of fiber reinforced mortar or concrete using the modified form of Wang's equation. Four parameters in Fanell's equation were derived from the fiber shape, volume fraction, and fiber geometry.

1.2.3.2.2 With Confinement. In existing literature, there are no published data and equations which discuss the stress-strain law or curve for a high strength concrete with fibers and confinement.

CHAPTER TWO

BEHAVIOR OF PLAIN AND FIBROUS HIGH STRENGTH CONCRETE UNDER COMPRESSION

2.1 Introduction

High strength concrete (HSC) in recent years has gained acceptance from engineers and contractors. Many new high-rise reinforced concrete buildings have been using concrete with compressive strength as high as 12,000 psi (Gregerson 1991). With the increasing use of high strength concrete as a structural material, more information on its mechanical properties is needed.

It is well-known that the high strength concrete is more brittle than the normal strength concrete. The application of high strength concrete in practice is severely limited by its more brittle behavior. However, this brittle property can be overcome by adding fibers and/or tie confinements. It has been shown that addition of fibers to concrete increased the ductility of the concrete (Craig 1984) and fatigue strength (Kwak 1991). During the last twenty years, steel fiber concrete has been increasingly used in structural application. Research has been made on the subject of using steel fibers for reinforcing structural members in combination with conventional reinforcing. .

For a rational design of concrete structure, the complete stress-strain curve of its material becomes a necessity. A number of empirical expressions for the stress-strain relationship of concrete have been proposed from the literature (see Appendix A). However, no one has ever discussed the expression for stress-strain behavior of plain high strength and high strength steel fiber reinforced concrete with or without tie confinement.

In this investigation, high strength concrete is defined as concrete with a compressive strength exceeding 10,000 psi. High strength steel fiber reinforced concrete

is made by adding steel fiber at different volume fraction to a concrete matrix. Attempts are made to use a relatively simple experimental technique to obtain a complete stress-strain curve of high strength cement-based composite concrete with compressive strength over 10,000 psi. The analytic expressions for the stress-strain relation of high strength cement-based composite concrete are thus proposed to predict their physical and mechanical behavior.

2.2 Objectives

(1) To investigate a suitable strain rate for a complete stress-strain curve of high strength concrete under uniaxial compression. The stress-strain curve of a high strength concrete hardly shows any strain softening behavior at an unsuitable strain rate. In other words, after the peak stress, the descending branch of the curve is almost vertical and the specimen shows an explosive failure. Thus, it is necessary to find a suitable strain rate in order to attain a complete stress-strain curve.

(2) To experimentally obtain the complete stress-strain curves of unconfined and confined (by circular-hoop-reinforcement without longitudinal reinforcement) concrete, in uniaxial compression for high strength cement-based composite concrete. The influence of parameters (spacing, fiber volume fraction) on the peak stress and its corresponding strain, the shape of the stress-strain curve (particularly its descending branch), and the toughness of the composite concrete are analyzed.

(3) To develop empirical equations for the complete stress-strain curve of high strength concrete with (and without) fibers and with (and without) tie confinements, under compression test.

(4) To compare the proposed analytic stress-strain equations with the experimental data based on present research and others.

2.3 Experimental Scheme

2.3.1 Material and Mixing Proportion

2.3.1.1 Material. The materials consisted of Type I cement satisfying with ASTM 150, sand from local source, crushed stone and basalt with maximum aggregate size of 3/8 in., tap water, silica fume (SF) in a powder form to achieve a higher strength, and the superplasticizers (SP) to maintain good workability.

The steel fibers at different volume fractions of 0.5%, 0.75%, and 1% in high strength concrete, were mixed homogeneously . These steel fibers are made from low carbon, cold draw, and steel wire, hooked at both ends, and glued together on sides with water soluble glue to form bundles(collated). The aspect ratio (ℓ / d) of steel fiber is 60 and its specific gravity is 490 lb/ft^3.

The tie confinement with circular hoops was constructed by steel wire (12-gage, f_y= 66.1 ksi). The circular hoops at different pitches of 1, 2, and 3 in, were put into cardboard-mold (3 in. by 6 in. cylinder) as shown in Fig. 2.1. In order to fix the tie confinements in the position, the circular ties were connected with one another by 22-gage soft wire. Fig. 2.2 shows the details of the fabricated structure. Table 2.1 shows the conversion values from the tie spacing to the volumetric ratio which is defined as the ratio of volume of the binder to the volume of the confined concrete.

2.3.1.2 Mixing Proportion. Table 2.2 lists the mixing proportions of a high strength concrete for this research. With this mixing proportion, the compressive strength of concrete is approximately 10,000 psi at 14 days after casting with curing.

2.3.2 Mixing, Casting, and Curing

To minimize scattering, all specimens followed the same procedures for material mixing, casting, and curing.

All materials as described in previous Sec. 2.3.1 in Table 2.2, were mixed by a rotary mixer. The 3 in. by 6 in. cylinder mold were prepared and lubricated with oil before the concrete was poured. When mixing with fibers, it is difficult to disperse uniformly throughout the mixture. Therefore, this mixing step shall be inspected experimentally. The mixing sequence used was as follows: Firstly, the coarse and fine aggregates were loaded into the mixer and dry mixed for 2 to 3 minutes. Next, the cement and silica fume were added and mixed for another 1 to 2 minutes. Then, 80% of the water was added to cementitious material. The remainder of 20% of the water were first mixed with the superplasticizers and later were added to the cementitious material over 2 minutes to form a uniform mixture. The steel fibers were later added to this uniform mixture in a gradual manner to prevent segregation or balling and to insure random distribution of the fibers. Finally, all fibers were spread to the matrix, the small rotary mixer had to continue mixing for few minutes, until a homogeneous mixture was achieved. The resulting mixture was then molded into 3 in. by 6 in. cylindrical specimens.

During casting, both table vibrator and steel bar were used to compact the specimens. All specimens were covered by plastic sheets right after casting and were left at the room for 24 hours to get hardened. These specimens were then demolded and cured in a lime saturated water until the day before testing. The age of the specimens at the time of testing varied from 2 to 56 days, the majority of the tests have been carried out 28 days after casting.

2.3.3 Experimental Setup

The stress-strain curve of concrete is measured in the NJIT structural laboratory by an uniaxial compression test.

Prior to testing, each cylinder was capped with sulfur compound at both ends to ensure parallel and smooth surfaces of the test specimens and to maintain a constant

length for all cylinders. The 3 in. by 6 in. cylinder specimens were tested in an uniaxial compression under the Material Testing System (MTS) servo-controlled, close-loop machine. The maximum load capacity of the MTS is 100 kips. To obtain a complete stress-strain curve, a slow strain rate of 1.67×10^{-5} strain/sec, was employed. The axial deformations were measured by two clip-on gages which were mounted to the specimen as shown in Fig. 2.3. In order to record the average axial displacements, the signals from the two strain gages were averaged and fed back to the controller to constantly adjust the applied load. An IBM electronic data acquisition system running the Unkelscope program was used to record the strain values and corresponding loads.

2.4 Results and Discussion

The behavior of high strength cement-based concrete was investigated in this study. The high strength concrete without fiber is called herein as a plain high strength concrete, and the high strength concrete with fiber termed as a high strength fiber-reinforced concrete or fibrous high strength concrete in this study. Both types of the concrete were also studied the effect of tie confinement on their stress-strain behavior. The main objective of this study was to obtain the complete stress-strain curves for these concretes. Empirical equations were then proposed to get the best curve fitting on these complete stress-strain curves. The parameters of the proposed equations for unconfined and confined concretes, were analyzed to relate to the compressive strength, f_c', or volumetric ratio, ρ, respectively. Furthermore, other experimental data were compared with the present proposed equations with a given single value of compressive strength, f_c'. This compressive strength was used to derive the parameters of the proposed equations.

2.4.1 Uniaxial Compression Test

Plain and fibrous high strength concrete (with and without tie confinement), were tested to study their stress-strain behavior subjected to an uniaxial compression. The failure

surface of concrete was recorded and reported after testing. The aging effect on the strength of concrete and the fiber effect on the toughness of concrete were also investigated.

2.4.1.1 Plain High Strength Concrete

2.4.1.1.1 Compressive Strength. Uniaxial compressive strength over 10,000 psi for a normal weight concrete can be obtained by using the available component materials without the use of exotic techniques in mixing, placing, or curing. In this research, A-H superplasticizers were used to attain the necessary workability for the low water-cement ratio of concrete.

The compressive strength of cement-based composites changes with materials, mix proportions, and conditions, such as aging, curing. Table 2.3 shows some values for the compressive strength (also called peak stress) with its corresponding strain (also called peak strain) from the literature (Carreira 1985) and from the present mixing proportions (as shown in Table 2.2) at different aging. On the average, the peak strain for the high strength concrete is greater than that for the normal strength concrete as seen in Table 2.3. Other investigators (Carrasquillo 1981) also reported similar results that the peak strain for the high strength concrete is slightly greater than that for the normal strength concrete. Therefore, the constant value for the ultimate strain of 0.003, as specified by the ACI Committee 318 (ACI 318 1989), could be conservative.

2.4.1.1.2 Strength Gain with Age. In this study, the compressive strength of 10,000 psi for concrete can be achieved at 14-16 days.

Fig. 2.4 shows the typical complete stress-strain curves of high strength concrete at different ages. The compressive strength increases with increasing age. The compressive strengths were measured at 9, 16, 23, 31, 44, and 56-day after casting. At

each age, at least two cylinders were tested and the average of the test values was taken as the compressive strength.

Fig. 2.5 shows a typical normalized ratio strength of high strength concrete as function of age. The normalized ratio strength is the ratio of compression strength to compressive strength at 56 days. By observing this curve, a higher rate of strength gains for a high strength concrete occurred at early ages. At later ages, however the difference is not significant. Typical ratio of 9-day to 56-day strength is 72% for a high strength concrete at present study. Other researches (Carrasquillo 1981, and Parrott 1969) also obtained similar results for the rate of development of strength for a high strength concrete. It is believed that the higher rate of strength development of a high strength concrete at early age is caused by an increase in the internal curing temperature in the concrete cylinders due to a higher heat of hydration, because of the low water-cement ratio in the high strength concrete (Carrasquillo 1981).

2.4.1.1.3 Stress-Strain Behavior. Fig. 2.4 shows the typical stress-strain curves of concrete for a compressive strength up to 13,000 psi at different ages in an uniaxial compression. It shows that the compressive strength increases with the increasing ages as indicated previously. The higher strength concrete exists less internal microcracking than the lower strength concrete for a given imposed axial strain (Carrasquillo 1981). The shape of the ascending branch of the stress-strain curve is more linear and steeper as the compressive strength increases, which is due to less bond cracking and higher stress-strength ratio to form the continuous crack patterns (Carrasquillo 1981). After reaching the maximum strength, the higher the compressive strength is, the larger the decrease of the descending rate is. In other words, the descending part of the stress-strain curve exhibits a more brittle characteristic as the compressive strength increases. For a heterogeneous material like concrete, cracking is a dominant factor for its brittle behavior as described in Sec. 2.4.1.1.5.

Fig. 2.4 also shows that the peak strain slightly increases with the increasing compressive strength. Carrasquillo and co-workers (Carrasquillo et al. 1981) also concluded a similar result on both normal and high strength concretes.

2.4.1.1.4 Modulus of Elasticity. The secant modulus of elasticity is defined as the secant slope of the uniaxial stress-strain curve at a stress level of 45 percent of the compressive strength. Fig. 2.6 shows the relationship of modulus of elasticity and its corresponding strength as summarized by ACI committee 363 (ACI-363 1987) and the present study. Based on the results of Fig. 2.6, it may be concluded that present ACI recommendation for the modulus of elasticity is only applicable to the concrete with the compressive strength up to 6,000 psi.

Table 2.4 summaries the compressive strength ($f_c^{'}$), strain (ε_o) at peak stress, and modulus of elasticity (E_c) from both this study and Carrasquillo's report (Carrasquillo 1981). A comparison of experimentally determined values for the modulus of elasticity with those predicted by the expression given in ACI 318-77, is given in Table 2.4. under columns 5 and 6, respectively. They indicate that ACI equation overestimates the modulus of elasticity for a high strength concrete. Table 2.4 also indicates some minor difference in modulus of elasticity. This slight discrepancy is mainly due to the different coarse aggregates used in the concrete mix. The elastic modulus of the high strength concrete is strongly influenced by the elastic properties of coarse aggregates (Baalbaki 1991). Aitcin and co-worker (Aitcin et al. 1990) also reported that both compressive strength and elastic modulus of concrete were shown to be significantly influenced by the mineralogical characteristics of aggregates used in the concrete mix.

2.4.1.1.5 Failure Mode. The mode of failure of high strength concrete observed during testing was clearly different from that of normal concrete. In general, the normal concrete gradually fails after reaching its peak load; whereas, the high strength concrete suddenly explodes at the peak load. Therefore, it is difficulty to obtain a complete stress-

strain curve for a high strength concrete. With the technique developed in this study, it is possible to obtain a gradually failure of the high strength concrete and an external crack pattern at the lower strain rates.

Fig. 2.7 (a) and 2.7 (b) show two typical failure modes for the high strength concrete at different strain rates, 1.67×10^{-5} and 13.89×10^{-5} strain/sec, respectively. Fig. 2.7 (a) shows that the cracks progressively propagate in the loading direction. And the complete stress-strain curve can be obtained under this gradually failing at this strain rate, 1.67×10^{-5} strain/sec. Fig. 2.7 (b) shows a suddenly explosion at the peak load. Thus, the descending part of stress-strain curve is dropped suddenly.

Both crack patterns in the Fig. 2.7 clearly show that the broken surfaces pass through the aggregate and mortar. Therefore, the broken surface exhibits a more smooth surface. This indicates that the strength of the mortar is at least higher than that of the aggregate. Since the strength of the mortar-matrix is higher than that of the aggregate, the crack initiates through the aggregate by forming a much smoother cracked surface. This phenomenon is different from the behavior in the normal strength concrete (Carrasquillo 1981). The normal strength concrete develops a highly irregular failure surfaces including a large amount of bond failure. Taerwe (Taerwe 1992) also showed the similar results. Kurt (Kurt 1979) reported that failure surfaces of the high strength concrete are more likely to pass through the aggregate particles because of the proportionately greater matrix strength. For this reason, the aggregate strength and stiffness should be a more important parameter in a high strength concrete than in a normal concrete.

2.4.1.2 High Strength Fiber-Reinforced Concrete

2.4.1.2.1 Stress-Strain behavior. Figs. 2.8 and 2.9 show the typical complete stress-strain curves of high strength fiber-reinforced concrete at different ages for fiber contents of 0.5% and 1.0%, respectively. It shows that the compressive strength increases with the increasing ages.

Fig. 2.10 and 2.11 show the ratio of compressive strength to compressive strength at 56-day, as function of ages for fiber contents of 0.5%, and 1.0%, respectively. For both fiber contents at early ages, a higher rate of strength is developed, and, at later ages, the difference is not significant. Typical ratios of 9-day to 56-day strength are 70% for fiber volume fraction at 0.5% and 71% for fiber volume fraction at 1.0%, respectively. The rate of development of strength for fibrous high strength concrete is similar to that of the high strength concrete without fiber.

Fig. 2.12 shows the stress-strain curves for a high strength fiber-reinforced concrete at different fiber contents. It clearly shows that the post-peak segment of stress-strain curve is affected by the addition of fibers. An increase in the slope of the descending part of the stress-strain curve is also observed by increasing the fiber volume fraction.

Fig. 2.13 shows two curves for the peak stress and the strain corresponding to the peak stress, as a function of fiber volume fraction. It clearly shows that the addition of steel fibers is found to increase the strain corresponding to the peak stress, but does not produce any significant changes in the compressive strength (peak stress). This may be attributed to the reduced workability by adding fibers to a lower water-cement ratio matrix. This reduced workability causes more amount of air being entrapped after compacting. The other possible reason may be caused by the aggregate. In the concrete matrix, the aggregate may affect fiber orientation, the fibers parallel to the loading direction may even produce lower strength due to buckling of the fibers (Hughes 1977). The fibers perpendicular to the loading direction, however, can increase the compressive strength, which is because the fibers tend to confine the lateral expansion of the specimen thereby reducing the propagation of cracking. Several investigators have reported test results for the compressive strength ranging from a loss to as much as a 40% increase for using the conventional steel fiber-reinforced concrete (ACI 544 1987).

Generally speaking, one of the main advantage to add the fiber to the concrete mix is to make the material to become more ductile.

2.4.1.2.2 Toughness Index. The toughness of a concrete is related to its ability to absorb energy. It can be estimated by using the area under a stress-strain curve. A convenient way to quantify the increase in toughness is using the toughness index which is defined as the ratio of the toughness of the fibrous concrete to that of the plain concrete (Fanella 1985). In this study the toughness index is defined as the area under a stress-strain curve of fibrous concrete up to a strain of 0.012, which is divided by the area under a stress-strain curve of plain concrete up to a strain of 0.012.

Table 2.5 lists the toughness index (T.I.) at different fiber contents. To quantitatively assess the influence of reinforcing index (R.I.) versus toughness due to the steel fibers, the average value of the toughness index versus the reinforcing index for each test series is plotted in Fig. 2.14. A square-fitting line is also derived and given by, $T.I. = 1.421(R.I.) + 1.035$.

2.4.1.2.3 Failure Mode. Fig. 2.15 shows the inside view of failure surface of the specimen for fibrous high strength concrete after testing. Several randomly fibers are pull out from the surface of failed concrete. The irregular failure surface can be seen in this failed concrete, which is in contrast to that of the plain high strength concrete. During the compression test, the popping sound of the fiber failed in being pull out is one of its special phenomena for fibrous high strength concrete tests. It seems that the hooded ends of the fibers have contributed to the increase in bonding between the steel fibers and the concrete matrix.

Two distinct types of failure modes were observed during the tests. Fig. 2.16 shows these two types of failure modes. The first type of failure specimen, shown in Fig. 16 (a), is a high strength concrete without fibers. The crack propagates parallel to the loading direction. The second type of failure specimen, shown in Fig. 2.16 (b), is a high

strength concrete with fibers. This type of failure is marked by bulging of specimen in the lateral direction with the specimen cracking up along the outer surface near the middle zone. This type of failure demonstrates that the addition of fiber can improve the ductility in a high strength concrete. In other words, the hooded-end fiber provides its capacity as a crack arrestor. Therefore, the presence of fiber in the concrete alters the mode of failure and also makes the concrete less brittle.

Fig. 2.17 shows the failure pattern of specimens after testing for plain and fibrous high strength concrete with (and without) tie confinement. The numbers indicate the fiber volume fraction, V_f, and the spacing of the circular hoops, in percentage and in inches, respectively.

2.4.1.3 Effect of Tie Confinement on Plain and Fibrous High Strength Concrete. Figs. 2.18 and 2.19 show the typical stress-strain curves at different tie spacing for plain and fibrous high strength concrete, respectively. Observing the curves from the figures, compressive strength and its corresponding strain increase with increasing tie confinements. There is not much difference in the initial portion of the stress-strain curves for confined and unconfined concrete. Since the confinement, provided by lateral circular-hoop-reinforcement, is a reaction to the lateral expansion of concrete, lateral reinforcement becomes effective only after considerable deformations have taken place in the axial direction (Sargin 1971, and Desayi 1978).

2.4.2 Analytic Expressions for High Strength Concrete

The following conditions must be considered, when the equations are being proposed to represent the stress-strain relationship of high strength cement based composite.

1. The equation or equations should compare favorably with all experimental data.

2. Ascending and descending branches of the stress-strain curve should be implied, and the equation or equations should represent both ascending and descending branches of the curve.
3. The mathematical form should be as simple as possible and can be easily used in any analysis.
4. The equation should be based on physically significant parameters that can be experimentally determined. At point of origin, $f_c = 0$ and $d(f_c)/d\varepsilon = E_{it}$, where f_c is the concrete stress, ε is the concrete strain, and E_{it} is the initial tangential modulus. At point of maximum stress, $d(f_c)/d\varepsilon = 0$.

The most common parameters with physical significance used to define the stress-strain relationship include following:

1. $f_c^{'}$ is the maximum compressive stress, usually considered as the concrete strength.
2. ε_o is the strain corresponding with the maximum compressive stress $f_c^{'}$.
3. E_c is the modulus of elasticity.
4. E_{it} is the slope at the origin or initial tangent modulus.

Various empirical stress-strain relationships for concrete have been studied and reported in Appendix A. One of the empirical equations in the appendix A, proposed by Carreira and Chu (Carreira and Chu 1985) for an uniaxial compression of plain concrete, is modified herein to investigate into the stress-strain characteristics for both plain and fibrous high strength concrete.

2.4.2.1 Plain High Strength Concrete. The following section discusses the complete stress-strain curves of unconfined and confined concretes for this study. The expression for complete stress-strain relationship under uniaxial compression can be represented by the following equations.

$$\eta = \frac{n\beta x}{n\beta - 1 + x^{n\beta}} \qquad \text{for } 0 \le x < x_d \qquad (2.1)$$

where

$$\eta = \frac{f_c}{f_c'} \qquad (2.2)$$

$$x = \frac{\varepsilon}{\varepsilon_o} \qquad (2.3)$$

$$\beta = \frac{1}{1 - \frac{f_c'}{\varepsilon_o E_{it}}} \qquad \text{for } \beta \ge 1.0 \qquad (2.4)$$

where β and n are the material parameters. β depends on the shape of the stress-strain diagram, and n depends on the strength of material. η is the normalized stress, x is the normalized strain, f_C is the stress in general, ε is the strain in general, f_c' the peak stress of concrete, ε_o is strain corresponding to the peak stress, x_d is the strain at $0.3f_c'$ in the descending portion of the stress-strain curve.

Eq. (2.1) is a modified form of stress-strain equation proposed by Carreira (Carreira, 1985). n is added to the original equation proposed by Carreira (Carreira, 1985). Also the parameters are modified and corrected for the present unconfined high strength concrete.

$$\eta = \eta_d \exp\left[-k_d (x - x_d)^a\right] \quad \text{for } x_d \le x \qquad (2.5)$$

where η_d is equal to 0.3 which correspond to 0.3 $f_c^{'}$ in the descending portion of the stress-strain curve, k_d = 0.8, and a=0.5.

Eqs. (2.1) through (2.5) are defined in terms of $f_c^{'}$, ε_o, n, and β or E_{it}. These parameters can be obtained from the uniaxial compression tests under a constant strain rate.

The relationships of parameters n, β, ε_o, and E_{it} with $f_c^{'}$ will be discussed in section 2.4.4.1 Thus, the stress strain relationship can be generated by knowing a single value, $f_c^{'}$, the maximum compressive strength of the concrete.

It should be noted that Eqs. (2.1) through (2.4) are employed for a confined concrete and Eqs. (2.1) through (2.5) are employed for an unconfined concrete, respectively.

2.4.2.2 High strength Fiber-Reinforced Concrete. The expressions of complete stress-strain relationships for unconfined high strength fiber-reinforced concrete are similar to that for the plain high strength concrete. Therefore, Eqs. (2.1) through (2.5) are used again to describe the stress-strain behavior for fiber-reinforced concrete. Here, η_d for high strength fiber-reinforced concrete is equal to 0.6, which corresponds to $0.6f_c^{'}$ in the descending portion of the stress strain curve, k_d=0.7, and a=0.8. x_d for high strength fiber reinforced concrete is the strain corresponding at $0.6f_c^{'}$ in the descending portion of the stress-strain curve. The rest of the parameters are the same as the ones in the previous section. These parameters can be obtained from compression tests under the constant strain rate. Section 2.4.4.2 will discuss the relationships between the parameters, n, β, ε_o, and E_{it}, and $f_c^{'}$. Therefore, the complete stress- strain curve can be generated by knowing a single value, $f_c^{'}$, the maximum compressive strength of the fibrous concrete.

Eqs. (2.1) through (2.4) are again employed for a confined high strength fiber-reinforced concrete with the different values of parameters.

2.4.3 Fitting Proposed Equations to Experimental Data

This section discusses the parameters in the proposed equations to fit both the ascending and descending parts of the stress-strain curve from the experimental data.

2.4.3.1 Plain High Strength Concrete. To fit the proposed Eqs. (2.1) to (2.5) of stress-strain curve to the experimental data, the parameters of proposed equations must be firstly determined. The parameters $f_c^{'}$, ε_o, and E_{it} can be obtained experimentally. Eq. (2.4) was used to obtain β's value. Then n's value was determined by the best fitting curve in the descending part. Therefore, x_d can be set with corresponding to 0.3 $f_c^{'}$ for the plain high strength concrete. The parameters k_d and a in Eq. (2.5) can be obtained by using a minimization of square of error technique.

There are two conditions for the plain high strength concrete due to confinement of the tie reinforcement as follows:

2.4.3.1.1 Without Confinement. Figs. 2.20 through 2.23 show the stress-strain curves of different compressive strength at different n parameter values. The descending part of the stress-strain curve obviously changes with different n's values. Furthermore, for the best curve fitting, n's value increases with increasing compressive strength, $f_c^{'}$. The relationship of n parameter and $f_c^{'}$ will be discussed in Sec. 2.4.4.1.1. Appendix B shows the results of best curve fitting for the stress-strain curve of plain high strength concrete without confinement.

2.4.3.1.2 With Confinement. Figs. 2.24 through 2.26 show the stress-strain curves at different volumetric ratio, ρ. The best curve fitting for confined concrete is to set n=1. Appendix C also shows the results of best curve fitting for the stress-strain curve of plain high strength concrete with confinements.

2.4.3.2 High Strength Fiber-Reinforced Concrete. All the fitting procedures for high strength fiber-reinforced concrete are the same as for the plain high strength concrete in Sec. 2.4.3.1. The only exception is to set x_d which corresponds to 0.6 $f_c^{'}$ for a high strength fiber-reinforced concrete.

There are also two conditions for the following high strength fiber-reinforced concrete: namely, without confinement and with confinement.

2.4.3.2.1 Without Confinement. Figs. 2.27 through 2.29 show the stress-strain curves of different fiber volume fractions at different n parameter values. The descending part of the stress-strain curve obviously changes with different n's values. Furthermore, for the best curve fitting, n's value increases with increasing compressive strength, $f_c^{'}$. The relationship of n parameter and $f_c^{'}$ will be discussed in Sec. 2.4.4.1.2. Appendix D shows the best curve fitting for the stress-strain curve of high strength fiber-reinforced concrete without confinement at different fiber volume fraction.

2.4.3.2.2 With Confinement. Figs. 2.30 through 2.32 show the stress-strain curves of different volumetric ratio, ρ, at 0.5% fiber volume fraction. The best fitting curve for a confined concrete is to set that n equal to 1. Appendix E shows the best curve fitting for the stress-strain curve of high strength fiber-reinforced concrete with confinement at different fiber volume fraction.

2.4.4 Analytical Expressions to Estimate Parameters of Proposed Equations

The main objective of this analysis is to develop the useful relationships of the parameters used in the complete stress-strain curve for a high strength concrete. For examples, the parameters n, β, and ε_o, can be related to the compressive strength, $f_c^{'}$. The reason that $f_c^{'}$ is used to estimate the other parameters is that only the specified compressive strength is known during the design stages of most structures. There are two types of high strength concrete in this study: Plain high strength concrete and high

strength fiber-reinforced concrete. The following two cases will be studied: without tie-confinement and with tie-confinement, respectively.

2.4.4.1 Parameters for Plain High Strength Concrete

2.4.4.1.1 Unconfined Concrete.

(1) β parameter:

Eq. (2.1) is used to generate a set of compressive stress-strain curves at different β's values while other parameters are kept constant. As seen in Fig. 2.33 the slope of the descending branch is affected by the β's value; for an example a flatter curve is obtained with the reduction of β's. The shape of the stress-strain curve is strongly dependent upon the parameter β. As it is known, the shape of the ascending branch of stress-strain is more linear and steeper and the slope of the descending branch becomes more steeper for high strength concrete than those for normal concrete. Specially, the higher the strength in the concrete is, the more steeper slope in the descending part of stress-strain curve it becomes. Table 2.6 summarizes the values of β and $f_c^{'}$. Hence, using the present experimental results, a best fitting statistical analysis was performed to obtain a relationship between the parameter, β, and the compressive strength, $f_c^{'}$. Fig. 2.34 shows the curve of β as a function of $f_c^{'}$ for cylindrical specimen test. β's value can be predicted by the following equation.

$$\beta = \left(\frac{f_c^{'}}{9.46}\right)^3 + 2.59 \tag{2.6}$$

where $f_c^{'}$ is the compressive strength of concrete in [ksi].

(2) n parameter:

In order to develop a better curve to fit the descending portion of the stress-strain curve, n's values are proposed herein as a function of the compressive strength, $f_c^{'}$.

The values of n are obtained by the following conditions:

For $0 \leq x \leq 1$, then

$$n=1 \tag{2.7}$$

For $1 < x \leq x_d$, then n=1, if,

$$0 \text{ (ksi)} < f_c^{'} < 9 \text{ (ksi)} \tag{2.8}$$

then n=2, if,

$$9 \text{ (ksi)} \leq f_c^{'} < 11 \text{ (ksi)} \tag{2.9}$$

then n=3, if,

$$11 \text{ (ksi)} \leq f_c^{'} < 13 \text{ (ksi)} \tag{2.10}$$

then n=5, if,

$$13 \text{ (ksi)} \leq f_c^{'} \text{ (ksi)} \tag{2.11}$$

(3) ε_o and E_{it} parameters:

Table 2.6 also lists the values of ε_o, E_{it}, and $f_c^{'}$. To quantify the effect of the compressive strength on the peak strain and initial tangential modulus, a regression analysis was performed to establish a relationship between the compressive strength, $f_c^{'}$, and the peak strain, ε_o, or the initial modulus ,E_{it}. Figs 2.29 and 2.30 show the curves of ε_o, E_{it} as a function of $f_c^{'}$, respectively.

Therefore, the curves of ε_o and E_{it} can be represented by the following equations.

$$\varepsilon_o = 8.9\times10^{-5} f_c' + 2.114\times10^{-3} \quad (2.12)$$

$$E_{it} = 1.2431\times10^{2} f_c' + 3.28312\times10^{3} \quad (2.13)$$

where ε_o is [in/in], E_{it} [ksi], and f_c' [ksi].

(4) x_d

After obtaining the curve of Eq. (2.1) by substituting the parameters, such as β, n, f'_C, and ε_O, then, the strain (x_d) can be determined, The strain x_d is a strain which corresponds to the stress value of $0.3f'_C$ (ksi) in the descending branch of stress-strain curve..

2.4.4.1.2 Confined Concrete

The expressions of stress-strain curve for a confined concrete are the same as the ones for an unconfined concrete, excepting n=1 and β_c a material parameter that depends on the confinement of volumetric ratio, ρ. It is noted that Eqs.(2.1) through (2.4) can represent the stress-strain behavior in both ascending and descending branches of stress-strain curve. Eq. (2.5) is not needed for a confined concrete.

Table 2.7 lists the compressive strength, the peak strain, β_c, and the volumetric ratio (ρ,) i.e. the ratio of the volume of binder to the volume of confined concrete. As a result, both compressive strength and peak strain, increase with increasing volumetric ratio, ρ. And β_c is decreasing with increasing volumetric ratio, ρ. This is due to the fact that tie confinements in concrete support its ductile behavior.

To find out the effect of confinements on compressive behavior of the high strength concrete, a regression analysis was performed to establish a relationship between the volumetric ratio, ρ, and the compressive strength or the peak strain or β_c. The

following equations are obtained by using the regression analysis, the data are derived from Table 2.8. The results are shown in Figs. 2.37 through 2.39.

$$f_{cc}^{'} = 214.73\rho + f_{c}^{'} \tag{2.14}$$

$$\varepsilon_{oc} = 0.18134\rho + \varepsilon_{o} \tag{2.15}$$

$$\beta_{c} = \beta \exp\left[-1.6\rho^{0.2}\right] \tag{2.16}$$

$$\rho = \frac{4A_{s}}{DS} \tag{2.17}$$

where S [in], D [in], and A_S [in^2] are shown in Fig. 2.40. $f_{cc}^{'}$ [ksi] is the peak stress of confined concrete, ε_{oc} [in/in] is the strain corresponding to the peak stress of confined concrete, β_c is a material parameter for confined concrete, ρ is a volumetric ratio, and $f_{c}^{'}$, ε_o, and β are the parameters for unconfined concrete.

Fig. 2.41 shows the typical complete stress-strain curves for a high strength concrete with compressive strength of 11.80 ksi at different volumetric ratio (ρ), which are generated by the present analytical equations discussed in this section.

2.4.4.2 Parameters for High Strength Fiber-Reinforced Concrete. Fig. 2.12 shows the typical curves for high strength fiber-reinforced concrete at different fiber volume fraction as seen in the figure, the increase of fiber volume fraction develops a more ductile behavior in the descending branch of the stress-strain curve.

2.4.4.2.1 Unconfined Concrete

(1) β Parameter:

Table 2.9 summarizes the test results of β and $f_{c}^{'}$ at different fiber volume fraction for cylindrical specimens of high strength fiber-reinforced concrete;

Fig. 2.42 shows that β is a function of $f_c^{'}$ at different fiber volume fraction, V_f. By using the experimental results, a best curve fitting by statistical analysis was performed to obtain a relationship between the parameters β and $f_c^{'}$ in the following:

$$\beta = \left[\frac{f_c^{'}}{A}\right]^3 + C \tag{2.18}$$

Where A [ksi] and C [dimensionless] are summarized in Table 2.10

The relationships of parameters, A or C, with fiber volume fraction, V_f, are shown in the following equations:

$$A = 1.717(V_f)^3 + 8.501 \tag{2.19}$$

$$C = -0.26V_f + 2.742 \tag{2.20}$$

Where V_f is the fiber volume fraction in percentage (%).

(2) n Parameter:

To develop a better curve to fit the descending portion of the stress-strain curve for a high strength fiber-reinforced concrete, n parameter is proposed in the analytical model and n's value is dependent on the compressive strength, $f_c^{'}$. For a high strength fiber-reinforced concrete, the slope of descending branch as shown in Fig. 2.12 increases with increasing fiber volume fraction, V_f. Table 2.11 summarizes the relationship between n and $f_c^{'}$ at different fiber volume fraction, V_f.

(3) ε_o and E_{it} Parameters:

For the high strength fiber-reinforced concrete at different fiber volume fraction, Table 2.9 lists the parameters ε_o, initial tangential modulus, E_{it} , and

$f_c^{'}$. Figs. 2.43 through 2.45 and 2.46 through 2.48 show the curves of ε_o and E_{it} as the function of $f_c^{'}$, respectively. A regression analysis was performed to establish a relationship between ε_o or E_{it} , and $f_c^{'}$ at different fiber volume fraction. The following expressions show their relationships:

$$\varepsilon_o = a_1 f_c^{'} + C_1 \tag{2.21}$$

$$E_{it} = a_2 f_c^{'} + C_2 \tag{2.22}$$

Where the parameters a_1 [1/ksi], a_2, C_1, and C_2 [ksi] are listed in Table 2.12.

(4) x_d parameter:

Once the parameters n, β, and ε_o are obtained by a given value of $f_c^{'}$ according to the above formulas, a complete stress-strain curve can therefore be constructed. It should be noted that the strain x_d is appointed to correspond to $0.6f_c^{'}$ (ksi) in the descending branch of stress-strain curve.

2.4.4.2.2 Confined Concrete. The complete stress-strain curve for confined high strength fiber-reinforced concrete can be expressed by Eqs. (2.1) through (2.4), where n=1, and β is a material parameter that depends on the confinement of volumetric ratio, ρ , and the shape of the stress-strain curve. Table 2.13 through 2.15 list the compressive strength, $f_{cc}^{'}$, peak strain, ε_{oc}, initial tangential modulus, E_{it}, and β_c, at different fiber volume fraction, V_f, and volumetric ratio, ρ. Table 2.16 also lists the average parameters of compressive strength, strain at peak stress, β_c, for different volumetric ratio (ρ) at different fiber volume fraction (V_f).

Fig. 2.49 presents the values of compressive stress as a function of fiber volume fraction at different volumetric ratio. Fig. 2.50 shows the values of compressive stress as a function of volumetric ratio at different fiber volume fraction . These figures show the results that the compressive strength does not significantly increase with increasing fiber

volume fraction at a constant volumetric ratio, however the compressive strength increases with noticeably increasing volumetric ratio at a constant fiber volume fraction.

Fig 2.51 shows the values of strain at peak stress as a function of fiber volume fraction at different volumetric ratio; Fig. 2.52 also presents the values of strain at peak stress as a function of volumetric ratio at different fiber volume fraction. Both figures show that the strain at peak stress increases with increasing fiber volume fraction or volumetric ratio. By comparing the strain values in Fig. 2.51 with the values in Fig. 2.52, it seems that the values of strain at peak stress increase significantly by the tie confinements than that by the steel fibers. As a result, the increase in strain (ε_o) at peak stress by the confinements is more effective than by the steel fibers. This is due to the fact that the tie confinement is a continuous circular-hoop, and the steel fiber is only randomly discontinuous phase in the concrete (Shah 1970).

Table 2.16 and Fig. 2.53 show that both β and β_c decrease with increasing both the fiber volume fraction and volumetric ratio. The combined effects of the steel fiber and tie confinement in the concrete make it more ductile.

In order to find out the effect of tie confinements on the compressive behavior of high strength steel fiber reinforced concrete, a regression analysis was performed to establish a relationship between compressive strength (f'_{cc}), the strain at peak stress (ε_{oc}), and β_c with different volumetric ratio (ρ) at different fiber contents. Tables 2.17 and 2.18 list these related equations, which are obtained by using a regression analysis with the data from Table 2.16, and are shown in Figs. 2.53 through 2.59.

Fig. 2.60 shows the complete stress-strain curves for fibrous high strength concrete with the compressive strength of 11.98 ksi and fiber volume fraction of 1.0% at different volumetric ratio, which are generated by the present analytical equations for fibrous high strength concrete.

2.4.5 Comparison Between Experimental Results and Analytical Equations

2.4.5.1 Plain High Strength Concrete. The parameters of complete stress-strain curve in Eqs. (2.1) through (2.5) can be obtained by a given single value of compressive strength, $f_c^{'}$. Sec. 2.4.4 lists the proposed analytical equations to relate these parameters with a given single value of $f_c^{'}$ [ksi]. This section shows some results of comparison between the complete stress-strain curves from the present experimental results with the analytical curves obtained by a single value of $f_c^{'}$ [ksi].

2.4.5.1.1 Unconfined Concrete. The complete stress-strain curve under axial compression for an unconfined high strength concrete can be described by Eqs (2.1) through (2.5). Parameters for stress-strain curve are the Maximum compressive strength ($f_c^{'}$), the strain (ε_o) at the maximum compressive strength, β, n, and x_d. These parameters have been found to be a function of the compressive strength, $f_c^{'}$, as described in Sec. 2.4.4. For a given compressive strength, Eq. (2.6) can be used to compute β, Eqs. (2.8) through (2.11) are used to determine n parameter for the descending portion of stress-strain curve, and Eq. (2.12) is used to calculate the strain (ε_o) corresponding to the peak stress.

Appendix F illustrates the comparative results of complete normalized stress-strain curves between the experimental results and the analytical equations based on a given compressive strength ($f_c^{'}$). A good agreement is achieved between these comparisons.

2.4.5.1.2 Confined Concrete. The complete stress-strain equations of high strength concrete under axial compression with confinement was discussed in Sec. 2.4.4.1.2. The volumetric ratio (ρ) is defined in Eq. (2.17). Maximum compressive strength ($f_{cc}^{'}$), its corresponding strain (ε_{oc}) and β_c's value can be obtained by a given volumetric ratio (ρ) in Eqs. (2.14), (2.15), and (2.16), respectively. The value of n is equal to an unit.

Appendix G includes the figures for comparative studies of high strength concrete with confinement. They show two complete normalized stress-strain curves for high strength concrete with confinement; one from experimental data, the other one from the analytical equations of a given maximum compressive strength ($f_c^{'}$) and volumetric ratio (ρ). As the results, the figures show a good agreement between these two curves.

2.4.5.2 Fibrous High Strength Concrete. By the given values of maximum compressive strength ($f_c^{'}$) and volumetric ratio (ρ) at different fiber volume fraction, the parameters of complete stress-strain curve in , Eqs. (2.1) through (2.5) can be obtained. Sec. 2.4.4 lists the proposed analytical equations to attain these parameters. This section compares the complete stress-strain curves from the present experimental results with the curves obtained by the proposed analytical equations.

2.4.5.2.1 Unconfined Concrete. The complete stress-strain equations for fibrous high strength concrete are shown in Eqs (2.1) through (2.5). The parameters for the stress-strain curve are the maximum compressive strength ($f_c^{'}$), the strain (ε_o) at the maximum compressive strength, β, n, and x_d. These parameters can be attained by a given compressive strength ($f_c^{'}$) at certain fiber volume fraction, which are described in Sec. 2.4.4. For a given maximum compressive strength at constant fiber volume fraction, Eqs. (2.18) through (2.20) are used to calculate β, Table 2.11 is used to compute n parameter for the descending portion of stress-strain curve, and Eq. (2.21) is used to obtain the strain (ε_o) corresponding to the peak stress.

Appendix H shows the comparative studies of fibrous high strength concrete without confinement at different fiber volume fraction. They show two complete normalized stress-strain curves for fibrous high strength concrete; one from the experimental data, the other one from the analytical equations based on a given maximum compressive strength ($f_c^{'}$) at certain fiber content. The comparative studies show a good agreement between them.

2.4.5.2.2 Confined Concrete. The stress-strain curve of fibrous high strength concrete with confinement was discussed in Sec. 2.4.4.2.2. Maximum compressive strength (f'_{cc}) and its corresponding strain (ε_{oc}) can be obtained from Table 2.17. β_c's value is given in Table 2.18. The value of n is equal to an unit.

Appendix I includes the figures of comparison on fibrous high strength concrete with confinement at different fiber volume fraction. Two complete normalized stress-strain curves are compared for fibrous high strength concrete with confinement; one from the experimental data, and the other one from the analytical equations based on a given maximum compressive strength (f'_c) and volumetric ratio (ρ) at certain fiber content. As a result of this comparison, it shows that a good agreement is achieved between these two curves.

2.4.6 Comparison Between Proposed Analytical Equations and Experimental Data by Others.

Two experiment data from the literature, Wang and co-workers (Wang et al. 1978) and Shah and co-workers (Shah et al. 1981), are used to compare with the proposed stress-strain equations. They tested several 3-in by 6-in cylinders of plain high strength concrete without tie confinement. The proposed equations are listed in Eqs. (2.1) through (2.5). As mentioned previously, the parameters of proposed equations can be predicted by a given single value of maximum compressive strength, f'_c. Therefore, the only value is needed from any experimental data is the maximum compressive strength, f'_c.

Figs. 2.61 through 2.63 show a good agreement for the complete stress-strain curves between the proposed equations and the experimental data by Wang and co-workers (Wang et al. 1971) and Shah and co-workers (Shah et al. 1981). It must be emphasized that the maximum compressive strength, f'_c, is the only value needed in the proposed formulas. Those figures also show n parameter is not equal to an unit for the high strength concrete as seen in Figs. 2.61 through 2.63.

Table 2.1 Conversion of Volumetric Ratio from Tie Spacing.

Tie Spacing (in.)	Volumetric Ratio (ρ)
1	0.01155
2	0.0057732
3	0.0038488

Table 2.2 Mixing Proportions for High Strength Concrete.

Mixing Proportions		
Materials	Weight Ratio	Weight (lb/yd^3)
Water	0.28	244
Cement	1.00	870
Sand	1.40	1218
Aggregate	2.20	1914
Silica Fume	0.05	44
SP (fl.oz)	40 fl.oz/100 lb of cement	348

Table 2.3 Parameters of Compressive Strength, its Corresponding Strain, and β for Normal and High Strength Concrete.

Investigator	Age (days)	f_c' (ksi)	ε_o (in./in.)	β
Carreirra (1985)	3	1.11*	0.0015	1.9
	15	2.20*	0.0022	2.85
	22	2.60*	0.00195	2.5
	42	3.56*	0.00195	2.2
	84	3.95*	0.0020	2.1
	2	3.00*	0.0029	2.8
	To	5.82*	0.0029	5.3
		7.30*	0.00295	5.2
	125	10.75*	0.00345	6.9
	56	10.20*	0.0032	8.5
	-	10.60*	0.00295	7.0
Present study		9.55	0.003083	3.5
	9	11.32	0.003183	4.33
		11.37	0.003085	4.42
	To	11.66	0.003144	4.25
		11.88	0.003121	4.93
	44	12.15	0.00331	4.49
		13.25	0.003326	5.4

f_c' : Maximum Compressive Strength

ε_o : Strain at Peak Stress

β : Material Parameter

Table 2.4 Modulus of Elasticity for High Strength Concrete

Investigator	Coarse Aggregate	f_c' (psi)	ε_o (in./in.)	E_c (10^6 psi)	E_c* (10^6 psi)
Carrasquillo (1981)	Crushed Limestone	10,670	0.0029	5.01	5.89
		11,050	0.0030	5.30	5.99
		11,100	0.0029	5.33	6.00
	Gravel	9,290	0.0028	4.05	5.49
		9,520	0.0031	3.66	5.56
		9,500	0.0030	3.70	5.55
		10,570	0 0036	3.72	5.86
Present Study	Basalt	9,549	0.003038	4.497	5.57
		10,945	0.003023	4.770	5.96
		11,660	0.003144	4.840	6.15
		12,154	0.003310	4.735	6.28
		13,258	0.003326	4.781	6.56
	Crushed Stone	11,493	0.003250	3.876	6.11
		11,673	0.003417	3.759	6.16
		12,060	0.003583	3.667	6.26

* ACI 318-77

$$E_c = 57000\sqrt{f_c'}\,\text{psi}$$

f_c' : Maximum Compressive Strength

ε_o : Strain at Peak Stress

E_c : Modulus of Elasticity

Table 2.5 Toughness Index for High Strength Fiber-Reinforced Concrete.

Specimen No.	R.I.	f_c' (ksi)	ε_o (in./in.)	T (ksi)	T.I.
HS1	0	11.293	0.002979	1.64	
HS2		11.556	0.003009	1.79	
Avg.				1.71	1
HF1	0.30	11.843	0.00358	2.32	
HF2		12.072	0.00377	2.72	
HF3		12.264	0.00371	2.79	
HF4		13.044	0.00387	2.60	
HF5		12.359	0.00361	2.76	
Avg.				2.64	1.54
HF6	0.45	13.097	0.00351	3.06	
HF7		11.867	0.00420	2.84	
HF8		11.714	0.00331	2.82	
HF9		13.000	0.00353	2.84	
HF10		12.868	0.00355	2.63	
Avg.				2.84	1.66
HF11	0.60	12.498	0.00366	3.21	
HF12		12.571	0.00356	3.15	
HF13		12.405	0.00410	3.19	
HF14		12.603	0.00362	3.16	
Avg.				3.18	1.86

R.I. : Reinforcing Index (R.I.= V_f x ℓ / d)

f_c' : Maximum Compressive Strength

ε_o : Strain at Peak Stress

T : Toughness (Area Limited to ε_o= 0.012)

T.I. : Toughness Index

Table 2.6 Fitting Parameters for High Strength Concrete Without Confinement.

Specimen No.	f_c' (ksi)	ε_o (in./in.)	E_{it} (ksi)	β
S01	9.54886	0.003038	4400.72	3.50
S02	10.94499	0.003023	4683.65	4.40
S03	11.37145	0.003085	4762.64	4.42
S04	11.6596	0.003144	4808.25	4.37
S05	12.15421	0.00331	4721.55	4.50
S06	13.25814	0.00326	4891.76	5.40

f_c' : Maximum Compressive Strength

ε_o : Strain at Peak Stress

E_{it} : Initial Tangential Modulus

β : Material parameter

Table 2.7 Fitting Parameters for High Strength Concrete With Confinement.

ρ	Specimen No.	f'_{cc} (ksi)	ε_{oc} (in./in.)	E_{it} (ksi)	β_c
0.0038488	S31	12.05873	0.003760	4647.79	3.23
	S32	12.46497	0.003849	4748.01	3.15
	S33	12.04352	0.003833	4650.84	3.08
Avg.		12.18907	0.003814		3.15
0.0057732	S21	12.99607	0.004556	4743.74	2.51
	S22	12.80013	0.004589	4649.39	2.5
	S23	12.93295	0.004570	4695.99	2.52
	S24	13.32193	0.004507	4697.75	2.7
Avg.		13.01264	0.004556		2.56
0.01155	S11	14.00280	0.005222	4697.83	2.33
	S12	13.99718	0.005154	4660.60	2.4
	S13	14.29558	0.005294	4741.67	2.32
	S14	14.12480	0.005186	4759.31	2.34
	S15	14.15614	0.005217	4850.56	2.27
Avg.		14.1153	0.005215		2.33

f'_{cc} : Maximum Compressive Strength of Confined Concrete

ε_{oc} : Strain at Peak Stress of Confined Concrete

E_{it} : Initial Tangential Modulus

β_C : Material parameter of Confined Concrete

ρ : Volumetric Ratio

Table 2.8 Average of Fitting Parameters for High Strength Concrete.

ρ	f'c (f'cc) (ksi)	εo (εoc) (in./in.)	Eit (ksi)	β(β_c)
0	11.722	0.003157	4740.28	4.50
0.0038488	12.18907	0.003814	4682.21	3.15
0.0057732	13.01264	0.004556	4692.72	2.56
0.01155	14.1153	0.005215	4741.99	2.33

$f_c^{'}, f_{cc}^{'}$: Maximum Compressive Strength of Unconfined and Confined Concrete

$\varepsilon_o, \varepsilon_{oc}$: Strain at Peak Stress of Unconfined and Confined Concrete

β, β_c: Material Parameter of Unconfined and Confined Concrete

E_{it} : Initial Tangential Modulus

ρ : Volumetric Ratio

Table 2.9 Fitting Parameters for High Strength Fiber-Reinforced Concrete Without Confinement.

V_f (%)	Specimen No.	f'_c (ksi)	ε_o (in./in.)	E_{it} (ksi)	β
0.5	M01	9.11793	0.003180	4003.47	3.52
	M02	9.12190	0.003198	4013.93	3.46
	M03	10.67766	0.003222	4116.39	5.13
	M04	11.78803	0.003464	4172.62	5.42
	M05	11.79983	0.003478	4212.04	5.14
	M06	12.75779	0.003784	4106.40	5.30
0.75	D01	11.71385	0.003499	4253.63	4.7
	D02	11.80029	0.003549	4195.64	4.82
	D03	11.86748	0.003571	4203.79	4.77
	D04	12.00021	0.003680	4244.78	4.31
	D05	12.04887	0.003655	4152.97	4.85
	D06	12.34969	0.003604	4239.84	5.21
	D07	12.55436	0.003633	4254.07	5.32
1.0	F01	9.62024	0.003383	4101.83	3.26
	F02	11.40159	0.003591	4253.77	3.94
	F03	11.72992	0.003772	4136.73	4.07
	F04	11.84591	0.003750	4195.38	4.05
	F05	12.02028	0.003777	4201.38	4.12
	F06	12.32278	0.003883	4193.61	4.11

f'_c : Maximum Compressive Strength

ε_o : Strain at Peak Stress

E_{it} : Initial Tangential Modulus

β : Material parameter

V_f : Fiber Volume Fraction

Table 2.10 Parameters in Eq. (2.18) for High Strength Fiber-Reinforced Concrete Without Confinement.

V_f (%)	A	C
0.5	8.70	2.61
0.75	9.25	2.55
1.0	10.21	2.48

* $\beta = (\frac{f_c'}{A})^3 + C$

f_c' is a Maximum Compressive Strength in ksi.

where $A = 1.717(V_f)^3 + 8.501$

$C = -0.26V_f + 2.742$

Table 2.11 n Parameter for High Strength Fiber-Reinforced Concrete Without Confinement.

V_f (%)	$0 \le X \le 1$	$1 < X \le X_d$
0.5	n=1	n=1.0, if $f_c' < 11.5$ n=1.5, if $11.5 \le f_c' < 12$ n=2.0, if $12 \le f_c'$
0.75	n=1	n=1.0, if $f_c' < 11.5$ n=1.5, if $11.5 \le f_c' < 12.5$ n=2.0, if $12.5 \le f_c'$
1.0	n=1	n=1.0, if $f_c' < 12$ n=1.5, if $12 \le f_c'$

X_d : Strain Corresponding to 0.6 f_c'
f_c' in ksi

Table 2.12 Parameters in Eqs. 2.21 and 2.22 for High Strength Fiber-Reinforced Concrete Without Confinement.

V_f (%)	a_1	C_1	a_2	C_2
0.5	0.000142	0.001837	43.66	3629.24
0.75	0.000118	0.002172	35.51	3792.86
1.0	0.000178	0.001645	33.77	3792.59

* $\varepsilon_o = a_1 f_c' + C_1$ (2.21)

* $E_{it} = a_2 f_c' + C_2$ (2.22)

Table 2.13 Fitting Parameters at V_f of 0.5% with Confinement.

ρ	Specimen No.	f'_{cc} (ksi)	ε_{oc} (in./in.)	E_{it} (ksi)	β_c
0.0038488	M31	13.10663	0.004644	4125.21	3.17
	M32	12.79955	0.004595	4076.07	3.16
	M33	12.29565	0.004575	4203.64	2.94
	M34	12.68036	0.004462	3901.10	3.4
	M35	12.86164	0.004523	4102.11	3.26
Avg.		**12.74877**	**0.0045598**		**3.19**
0.0057732	M21	13.39995	0.005397	4001.27	2.64
	M22	13.19913	0.005366	3996.36	2.60
	M23	13.39063	0.005233	4047.33	2.72
	M24	13.18322	0.005341	4005.02	2.61
	M25	13.03674	0.005174	3845.96	2.90
Avg.		**13.24193**	**0.005302**		**2.69**
0.01155	M11	14.00259	0.006041	4103.09	2.30
	M12	13.77063	0.006020	3994.63	2.34
	M13	14.36273	0.006219	4099.80	2.29
	M14	14.04175	0.006109	3988.09	2.36
	M15	14.38778	0.006200	3992.61	2.39
Avg.		**14.11310**	**0.0061180**		**2.34**

f'_{cc}: Compressive Strength of Confined Concrete

ε_{oc}: Strain at Peak Stress of Confined Concrete

β_c: Material Parameter of Confined Concrete

Table 2.14 Fitting Parameters at V_f of 0.75% with Confinement.

ρ	Specimen No.	f'_{cc} (ksi)	ε_{oc} (in./in.)	E_{it} (ksi)	β_c
0.0038488	D31	12.79264	0.004803	4097.85	2.86
	D32	12.71972	0.004759	4102.79	2.87
	D33	12.94367	0.004901	4193.36	2.70
Avg.		**12.81867**	**0.004821**		**2.81**
0.0057732	D21	13.29856	0.005450	4136.88	2.44
	D22	12.93684	0.005401	4041.77	2.45
Avg.		**13.11770**	**0.005426**		**2.44**
0.01155	D11	14.09897	0.006302	4088.52	2.21
	D12	14.18085	0.006308	4088.17	2.22
Avg.		**14.13991**	**0.006305**		**2.22**

f'_{cc}: Compressive Strength of Confined Concrete

ε_{oc}: Strain at Peak Stress of Confined Concrete

β_c: Material Parameter of Confined Concrete

Table 2.15 Fitting Parameters at V_f of 1.0 % with Confinement.

ρ	Specimen No.	f'_{cc} (ksi)	ε_{oc} (in./in.)	E_{it} (ksi)	β_c
0.0038488	F31	12.84848	0.005161	4144.77	2.50
	F32	12.71670	0.005555	4209.58	2.19
	F33	12.73166	0.005115	4197.86	2.46
Avg.		**12.76561**	**0.005277**		**2.38**
0.0057732	F21	13.10025	0.005728	4194.78	2.20
	F22	13.42345	0.005800	4293.71	2.17
	F23	13.31097	0.005730	4435.16	2.10
	F24	13.17758	0.005675	4196.14	2.24
Avg.		**13.25306**	**0.005733**		**2.18**
0.01155	F11	14.11252	0.006550	4186.50	2.06
	F12	14.11069	0.006599	4192.88	2.07
	F13	14.32465	0.006637	4088.02	2.08
Avg.		**14.18262**	**0.006595**		**2.07**

f'_{cc}: Compressive Strength of Confined Concrete

ε_{oc}: Strain at Peak Stress of Confined Concrete

β_c: Material Parameter of Confined Concrete

Table 2.16 Average of Fitting Parameters at Different Fiber Content and Tie Confinement.

ρ	V_f (%)	f'_c (f'_{cc}) (ksi)	ε_o (ε_{oc}) (in./in)	β (β_c)
0	0.5	11.804	0.003513	5.11
	0.75	11.96	0.003583	4.71
	1.0	11.98	0.003776	4.10
0.0038488	0.5	12.75	0.004560	3.19
	0.75	12.82	0.004821	2.81
	1.0	12.77	0.005277	2.38
0.0057732	0.5	13.24	0.005302	2.69
	0.75	13.12	0.005426	2.44
	1.0	13.25	0.005733	2.18
0.01155	0.5	14.11	0.006118	2.34
	0.75	14.14	0.006305	2.22
	1.0	14.18	0.006595	2.07

f'_c, f'_{cc}: Compressive Strength of Unconfined and Confined Concrete

$\varepsilon_o, \varepsilon_{oc}$: Strain at Peak Stress of Unconfined and Confined Concrete

β, β_c: Material Parameter of Unconfined and Confined Concrete

V_f : Fiber Volume Fraction

Table 2.17 Parameters of f'_{cc} and ε_{oc} for High Strength Fiber-Reinforced Concrete.

Vf (%)	f'_{cc} (ksi)	ε_{oc} (in./in)
0.5	$197.95\rho + f'_c$	$0.2252\rho + \varepsilon_o$
0.75	$186.76\rho + f'_c$	$0.2322\rho + \varepsilon_o$
1.0	$190.47\rho + f'_c$	$0.2360\rho + \varepsilon_o$

Table 2.18 Constant Parameters of β_c for High Strength Fiber-Reinforced Concrete.

V_f (%)	β	K	a
0.5	5.11	5.7	0.44
0.75	4.71	3.3	0.33
1.0	4.10	1.7	0.2

$*\beta_c = \beta \mathrm{EXP}(-K\rho^a)$

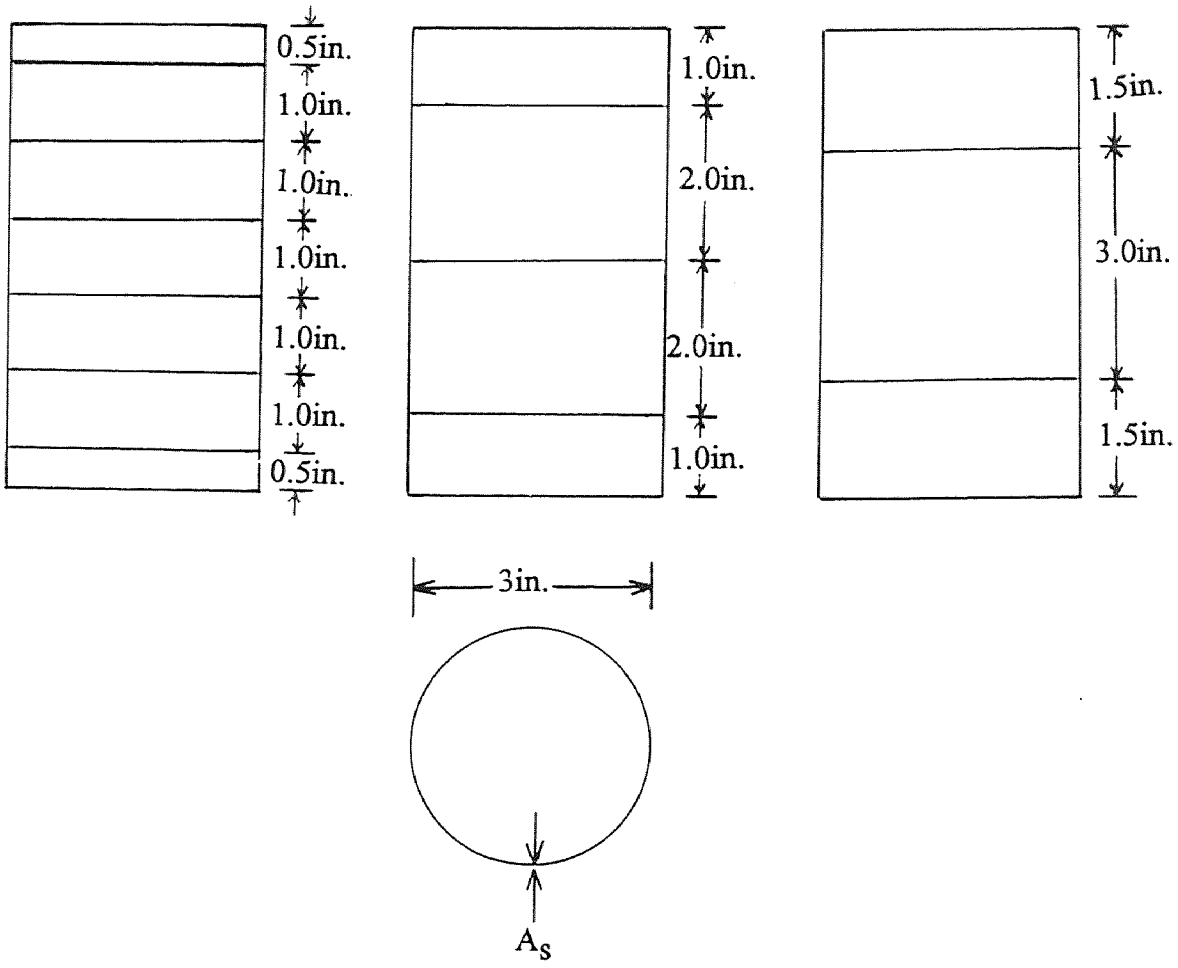

Figure 2.1 Position of Circular-Hoop Inside Specimens.

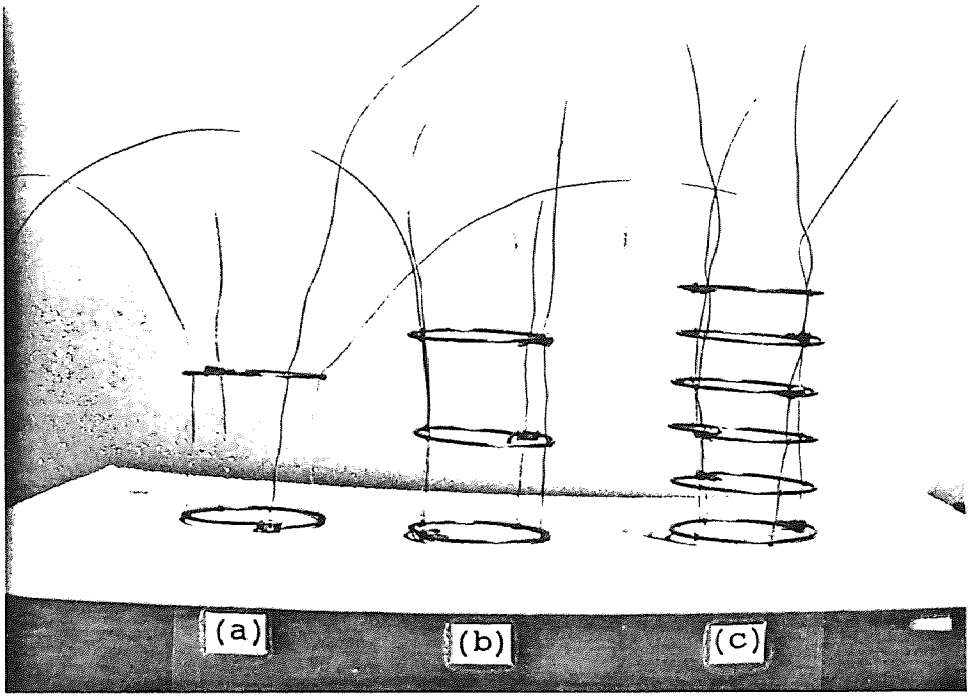

Figure 2.2 Tie Confinement with Circular-Hoop in Detains:
(a) S=3", (b) S=2", and (c) S=1".

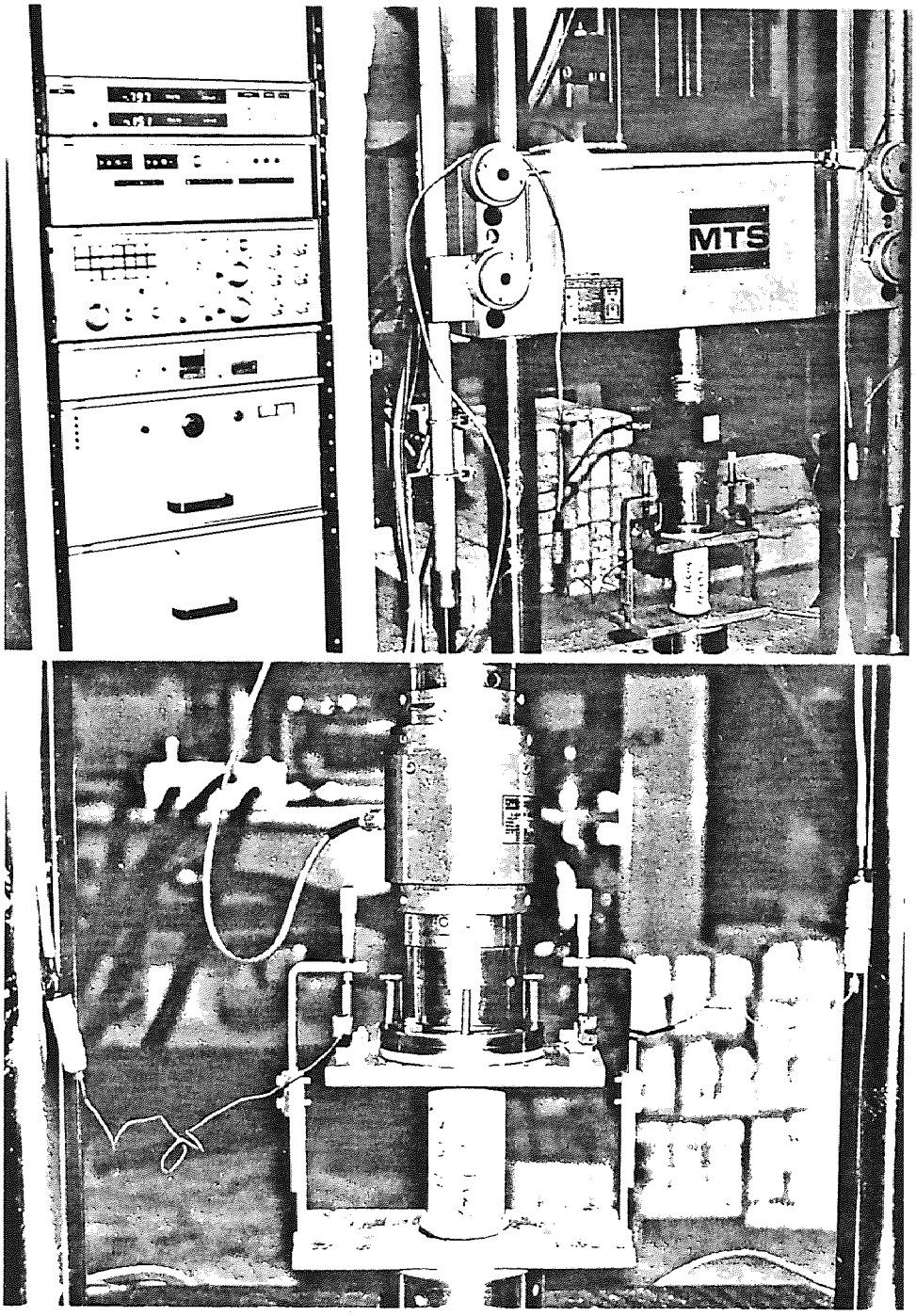

Figure 2.3 Experimental Setup for Cylinder in Compressive Test.

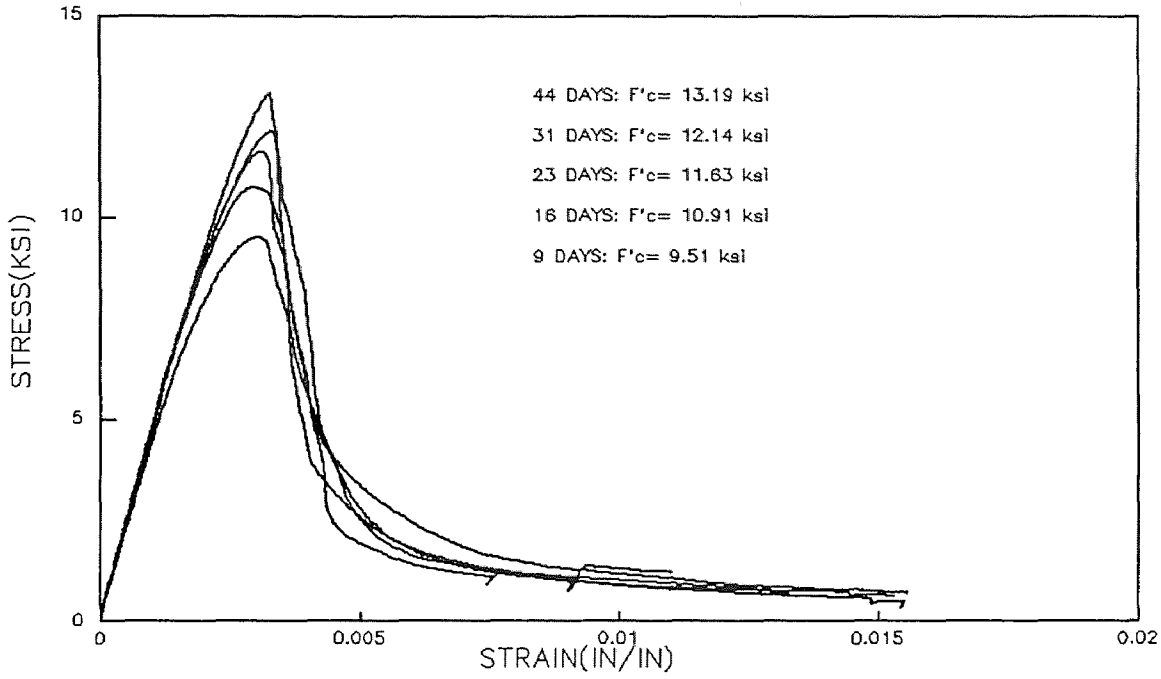

Figure 2.4 Stress-Strain Curves for HSC at Different Ages.

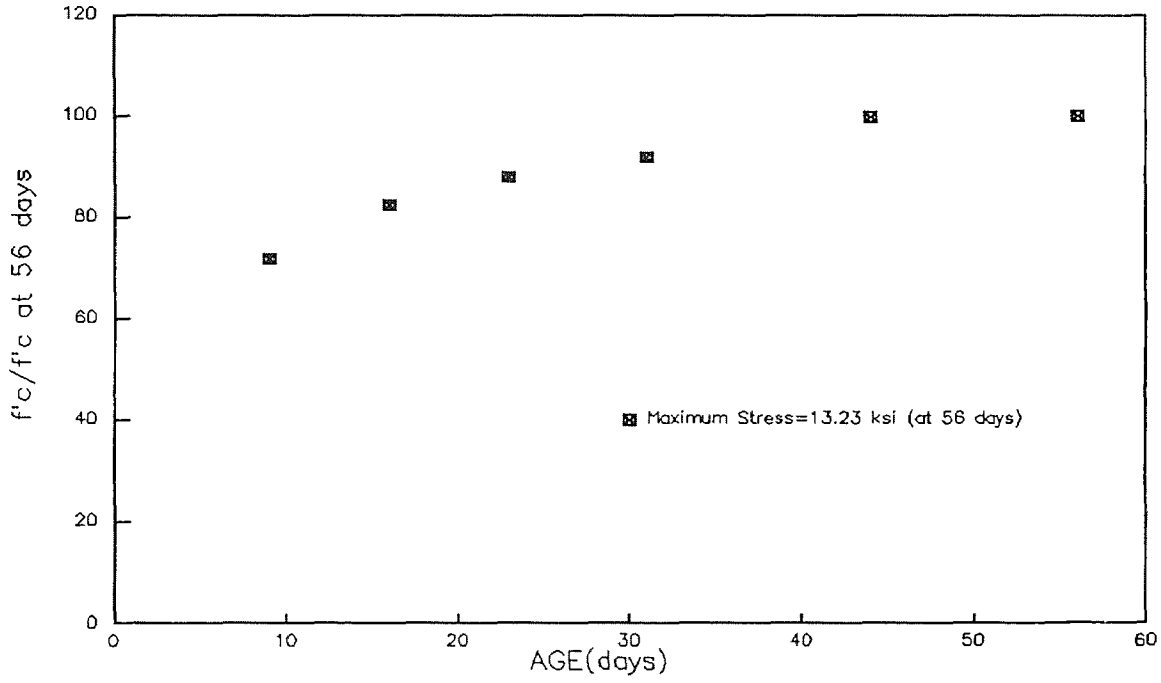

Figure 2.5 Normalized Strength Gain with Age for HSC.

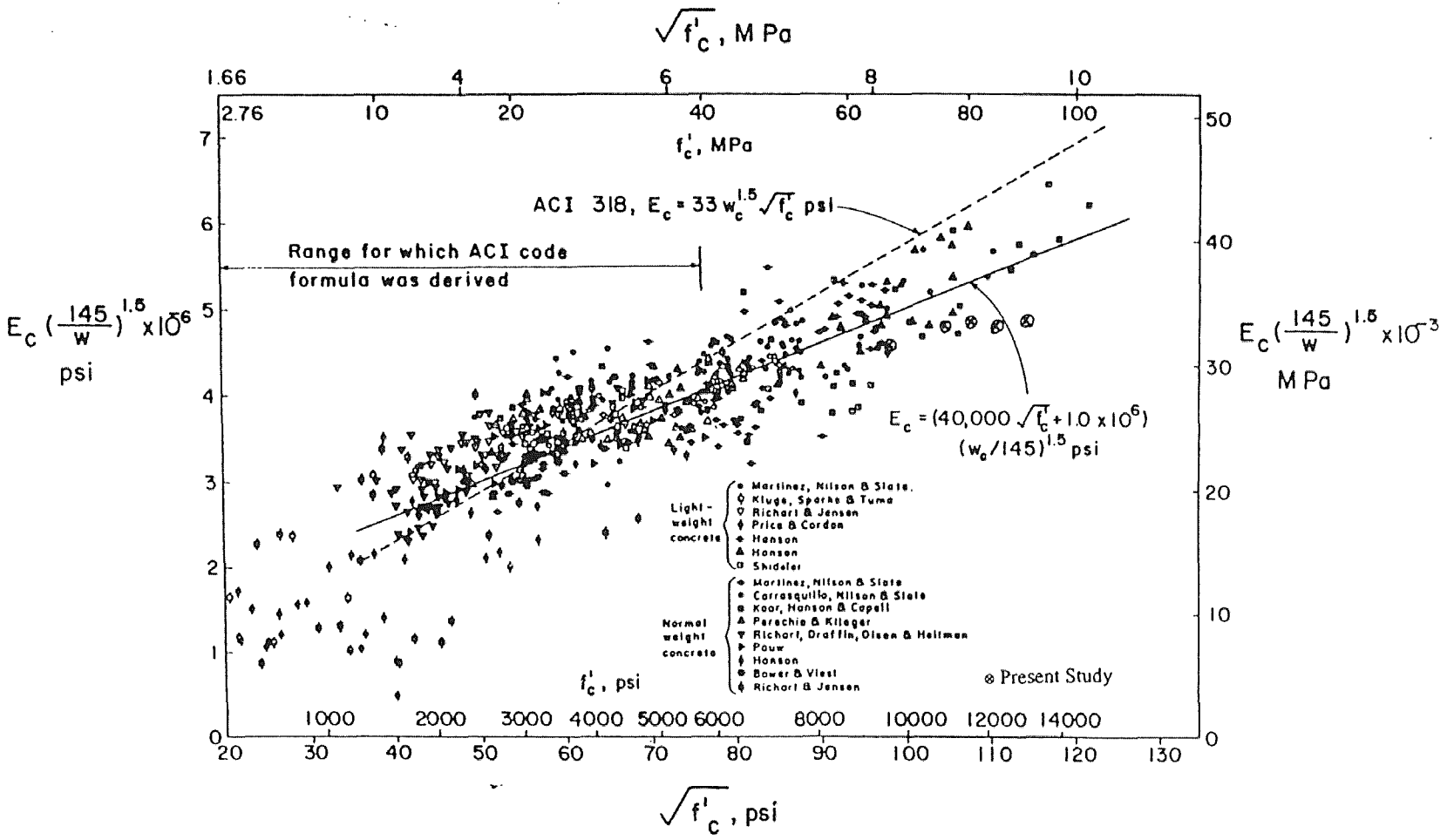

Figure 2.6 Modulus of Elasticity Versus Concrete Strength (ACI-363).

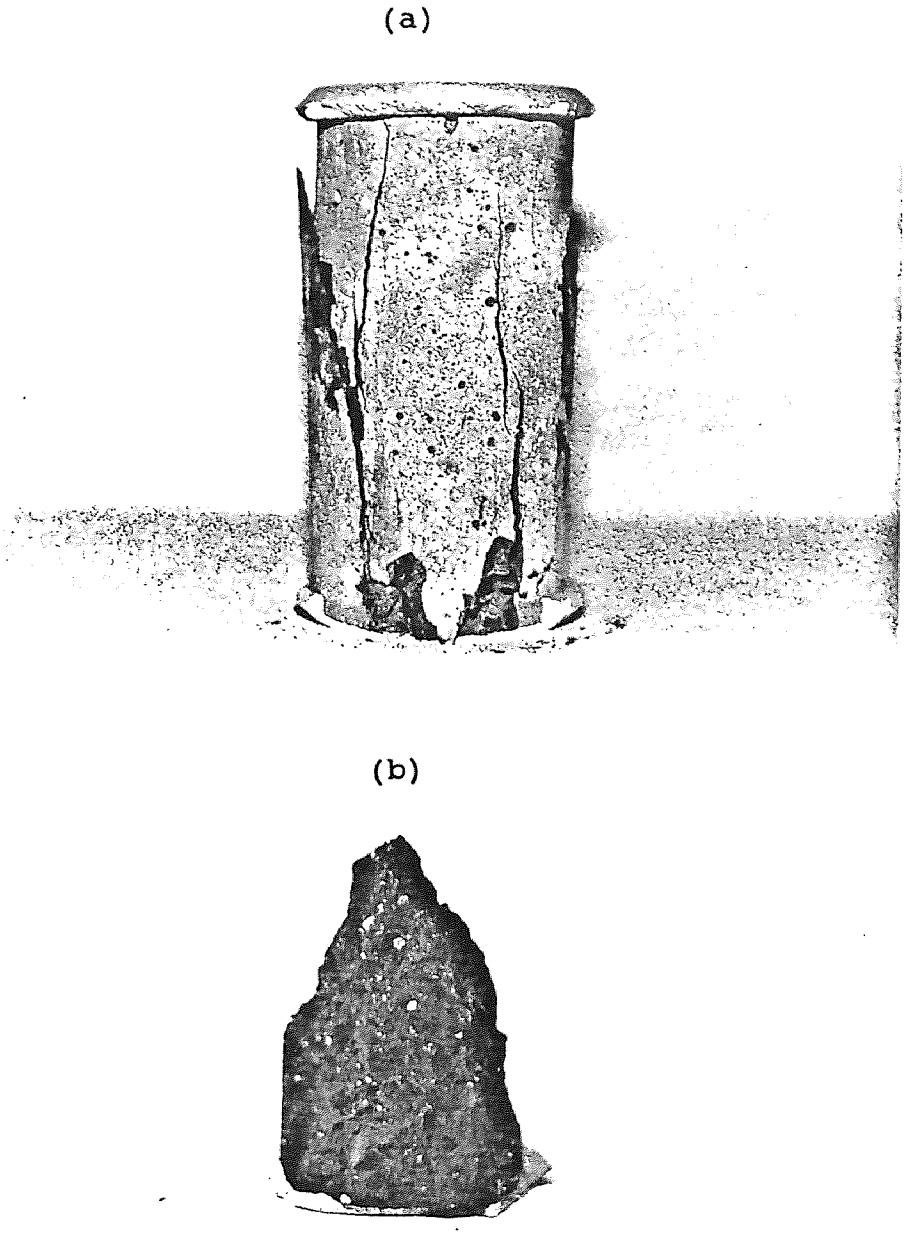

Figure 2.7 Typical Failure mode for HSC in Compression Test at Different Strain Rate: (a) Slow Strain Rate, and (b) Regular Strain Rate.

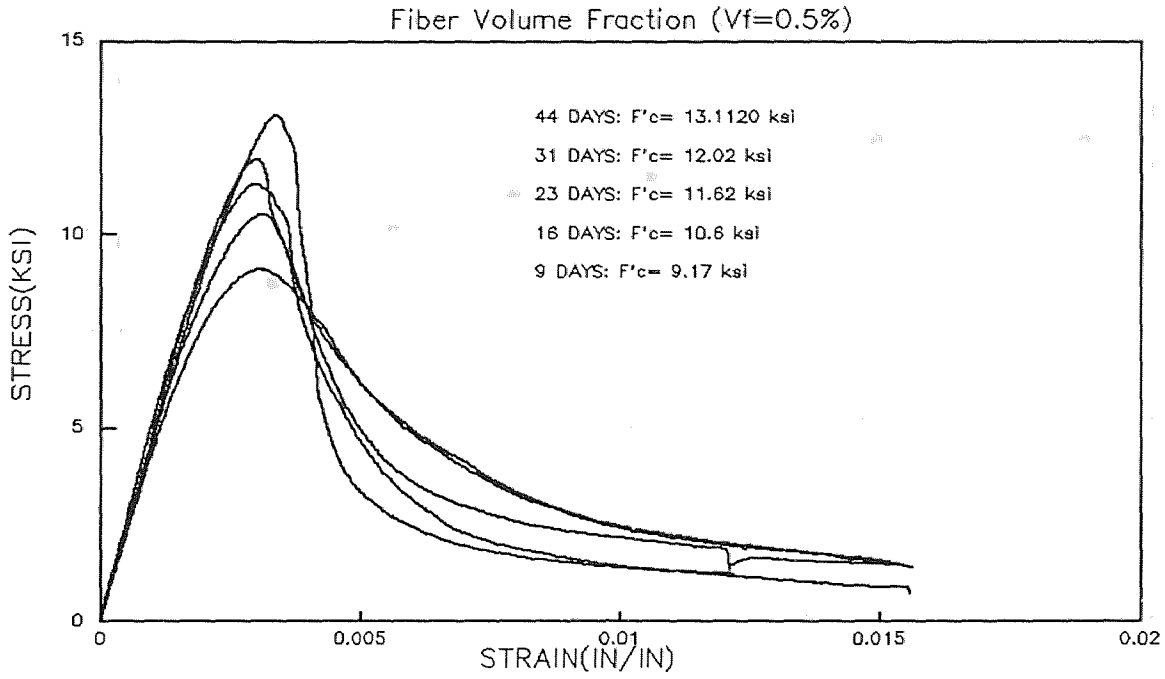

Figure 2.8 Stress-Strain Curves for High Strength Fiber-Reinforced Concrete at Different Ages, V_f=0.5%.

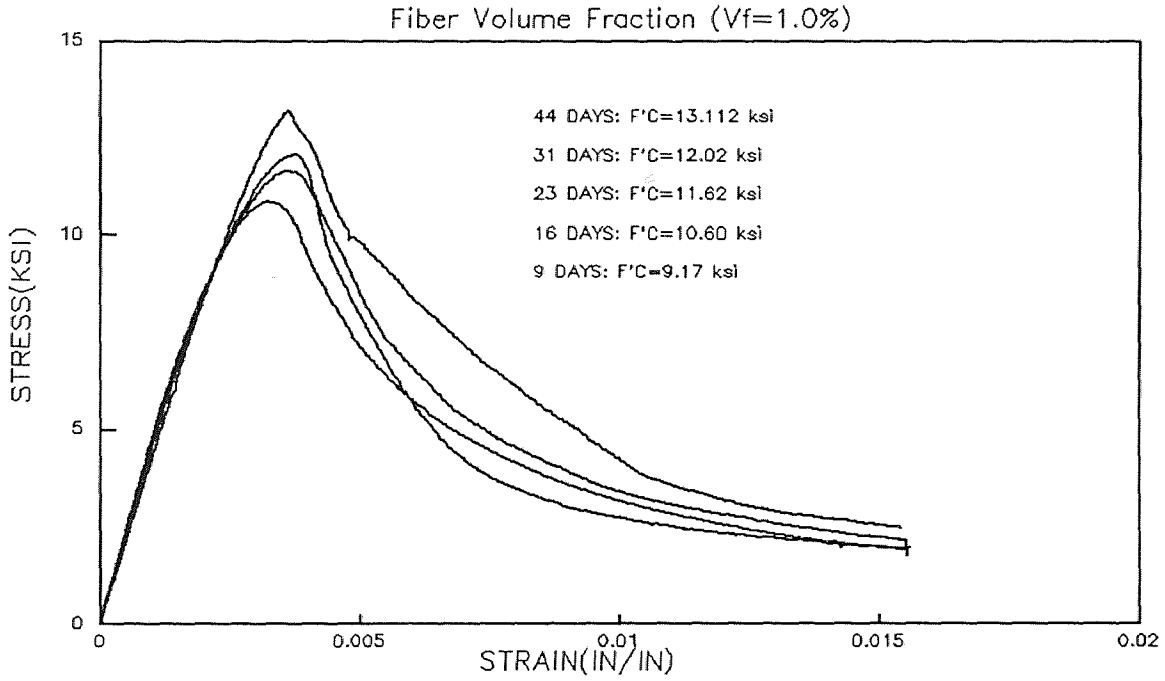

Figure 2.9 Stress-Strain Curves for High Strength Fiber-Concrete at Different Ages, V_f=1.0%.

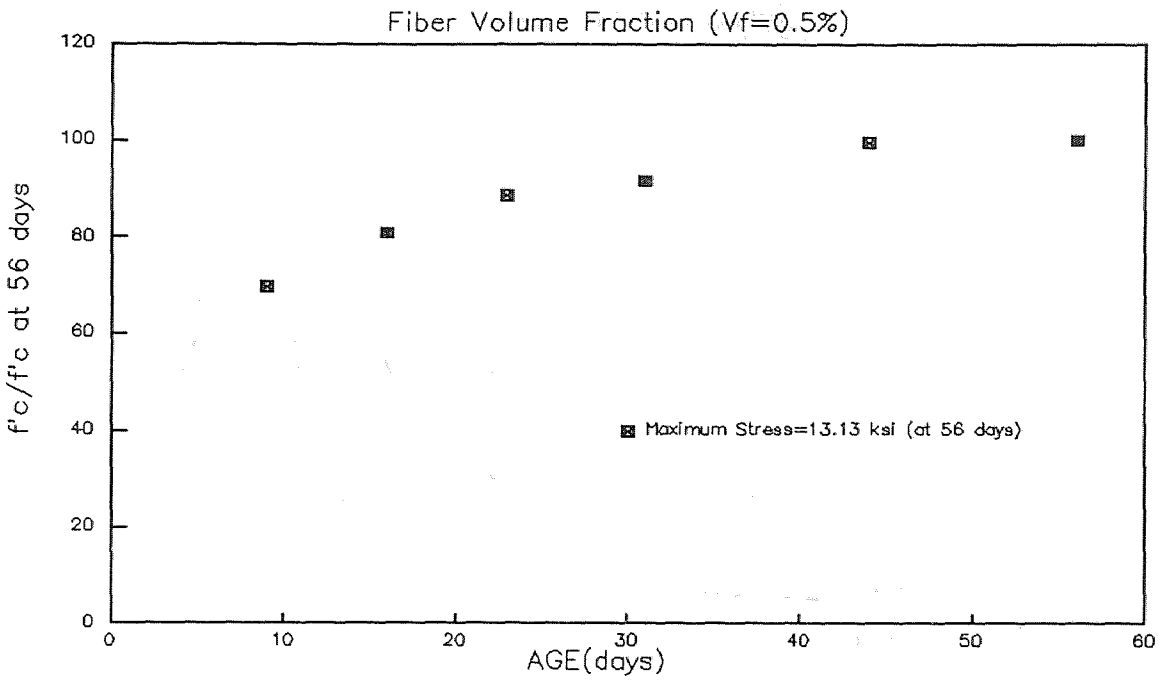

Figure 2.10 Nomalized Strength Gain with Ages for High Strength Fiber-Reinforced Concrete, V_f=0.5%.

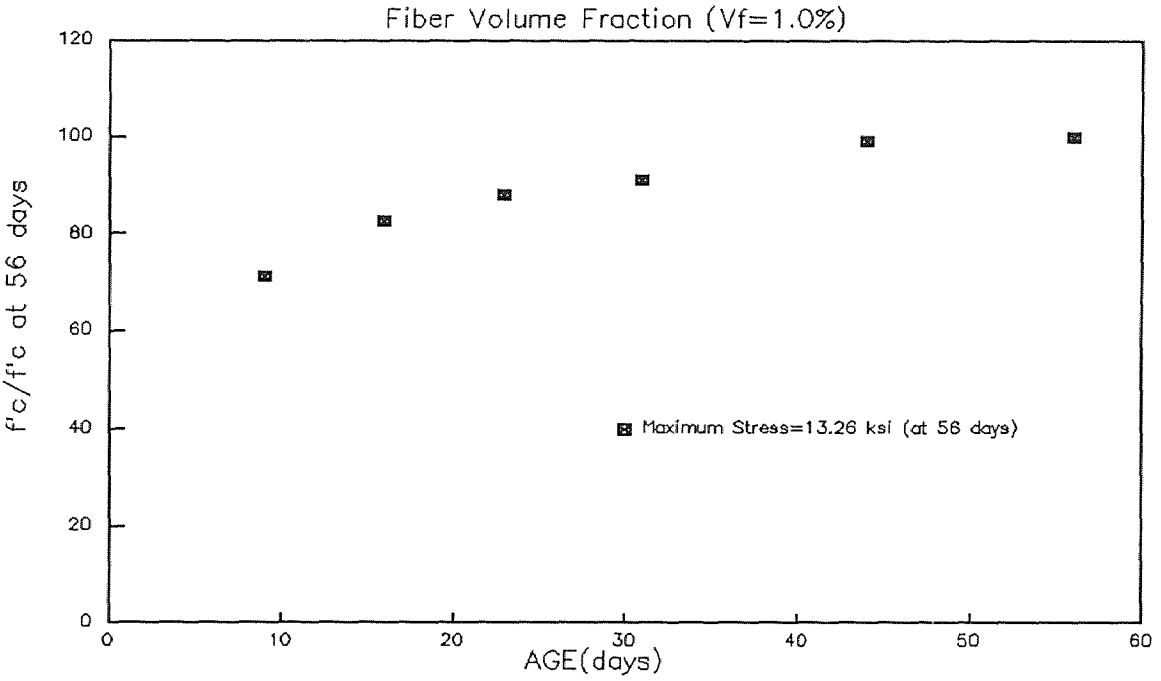

Figure 2.11 Normalized Strength Gain with Age for High Strength Fiber-Reinforced Concrete, V_f=1.0%.

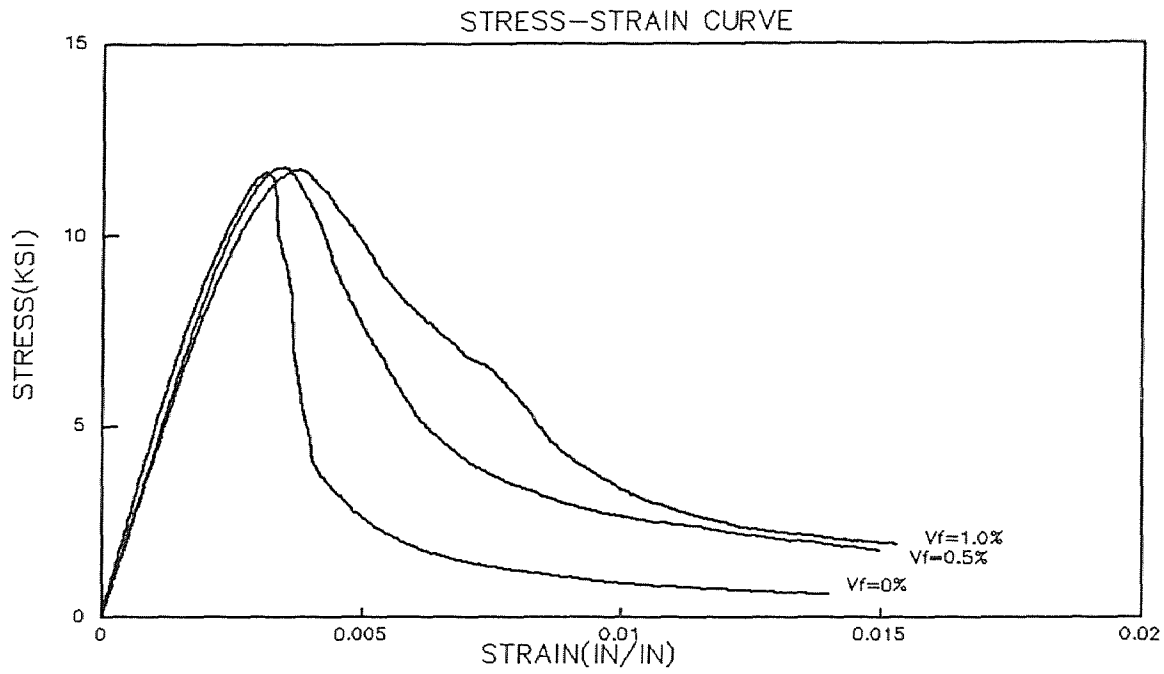

Figure 2.12 Influence of Volume Fraction of Fiber on Compressive Stress-Strain Curves.

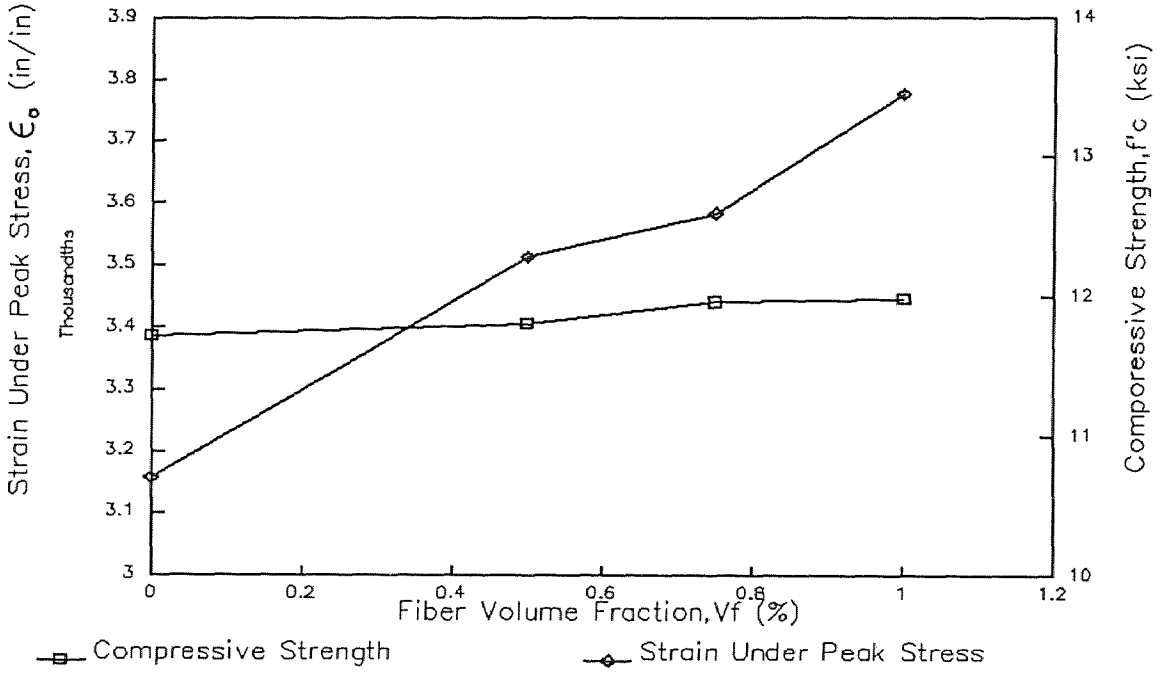

Figure 2.13 Comparison of Strength and Its Strain at Different Fiber Content.

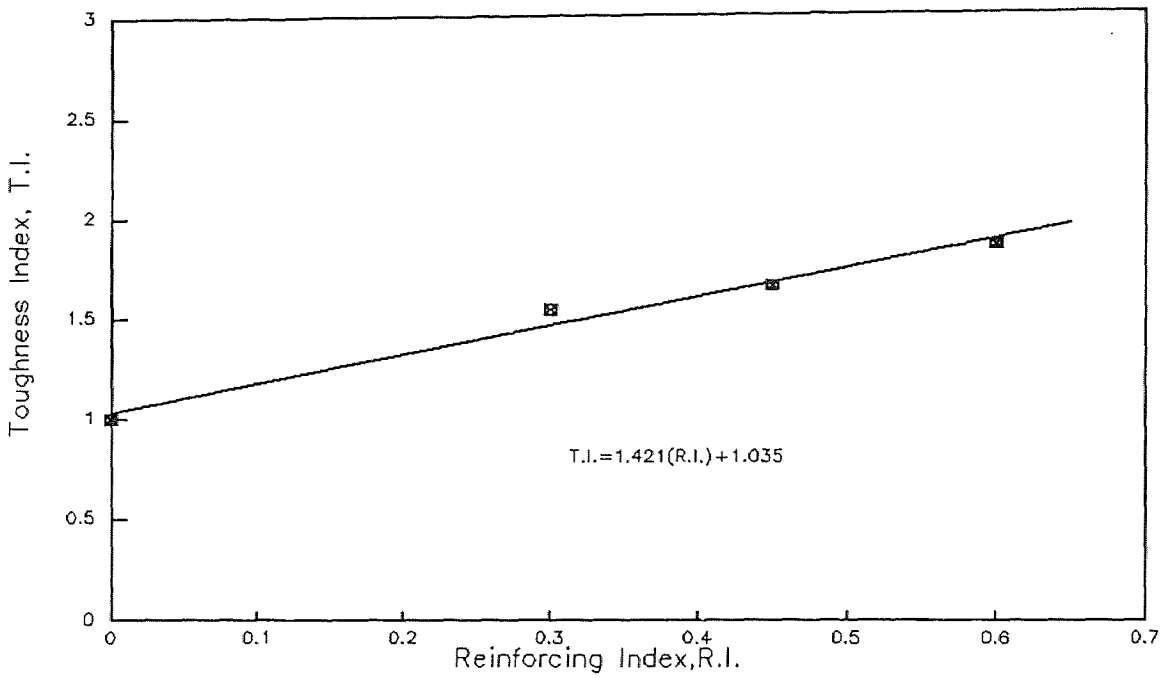

Figure 2.14 Variation of Toughness Index with the Reinforcing Index.

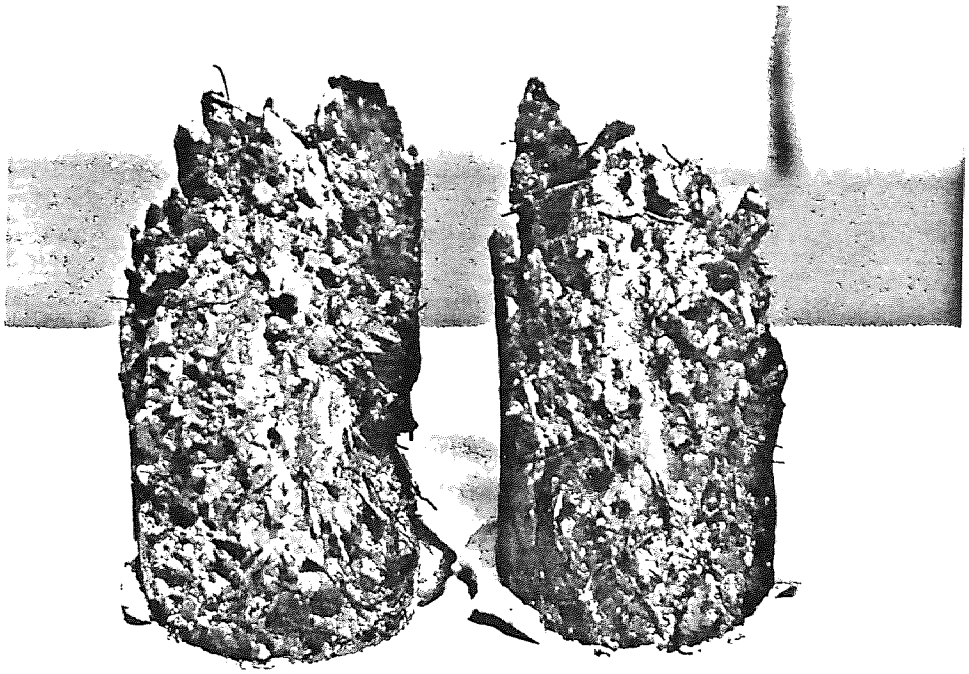

Figure 2.15 Typical Failure Mode for High Strength Fiber-Reinforced Concrete in Compressing Test, After Taking Broken Surface out of Cylinder.

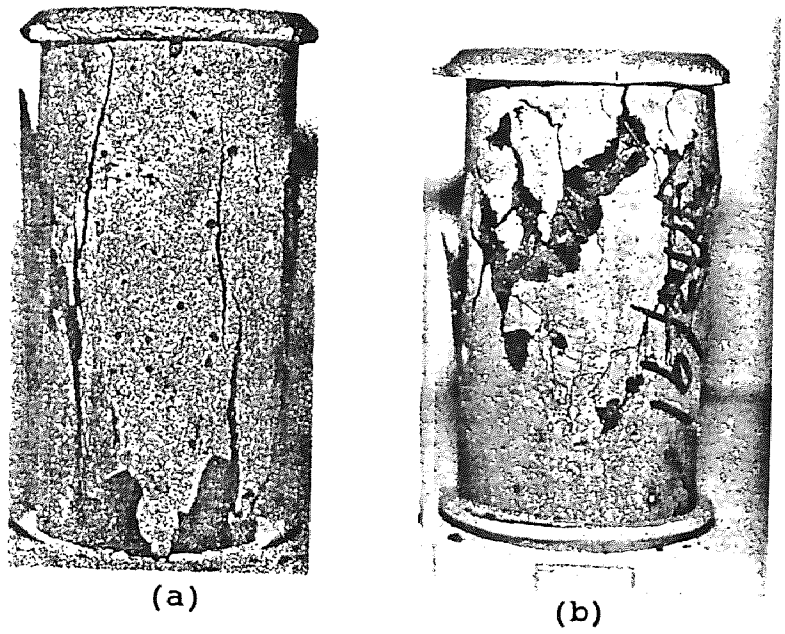

Figure 2.16 Typical Failure Mode of High Strength Concrete in Compression Test: (a) Without fiber, (b) With Fiber.

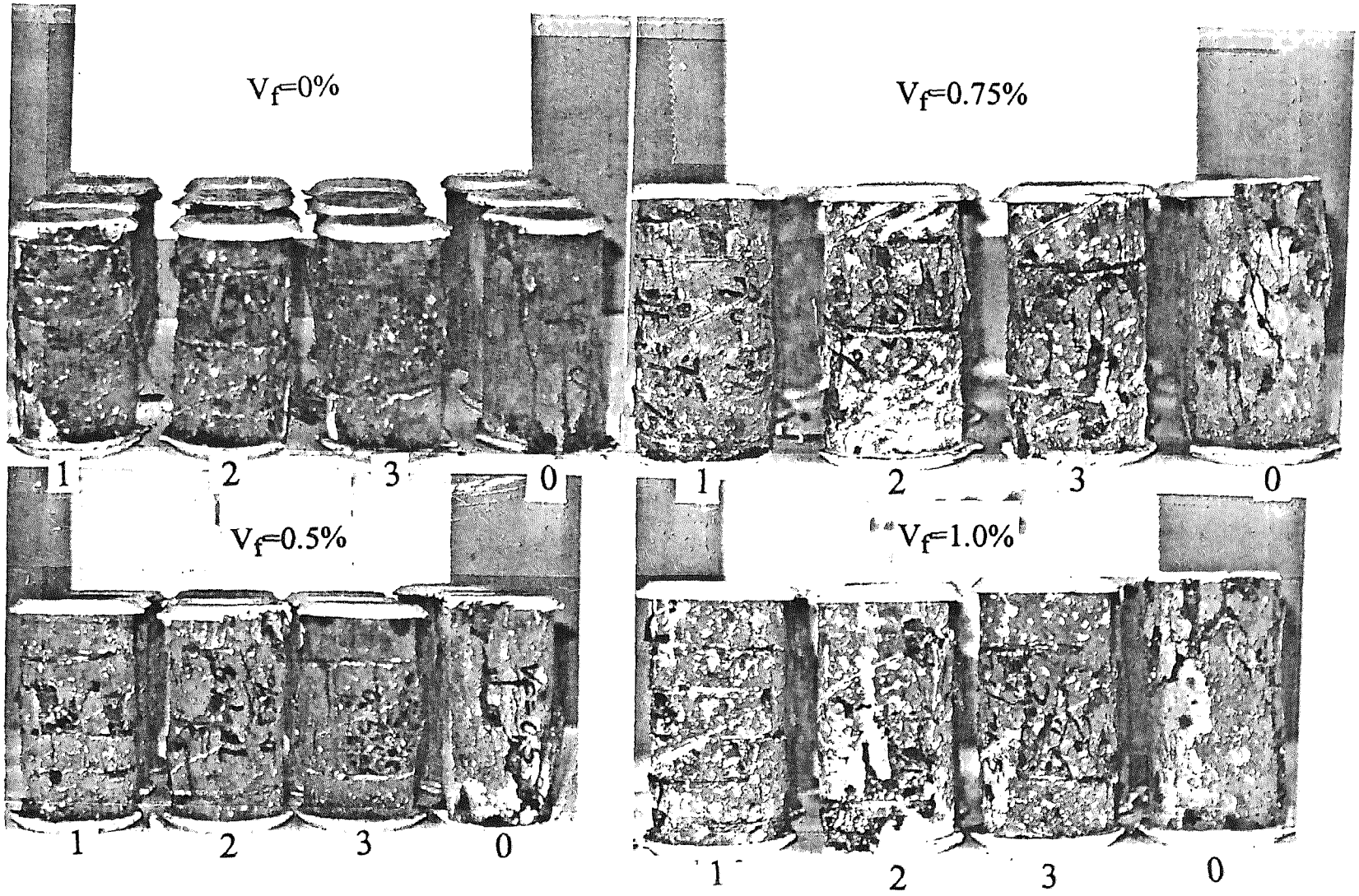

Figure 2.17 Some of the Cylindrical Specimens after Testing.

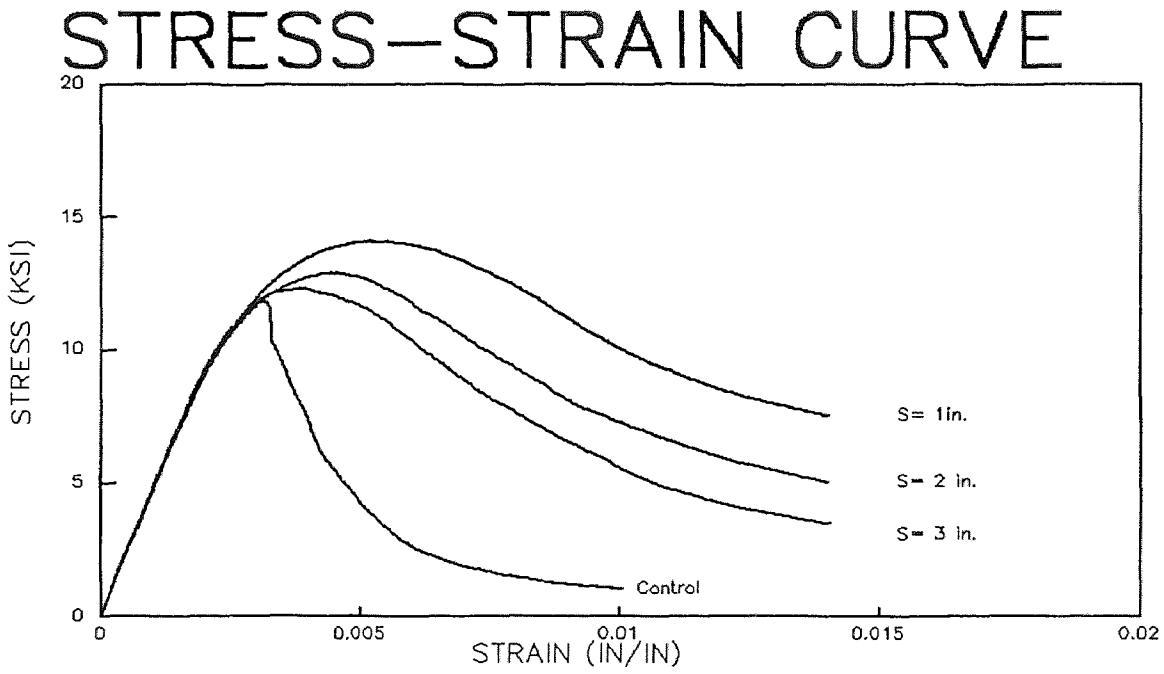

Figure 2.18 Stress-Strain Curve for HSC at Different Tie Spacing.

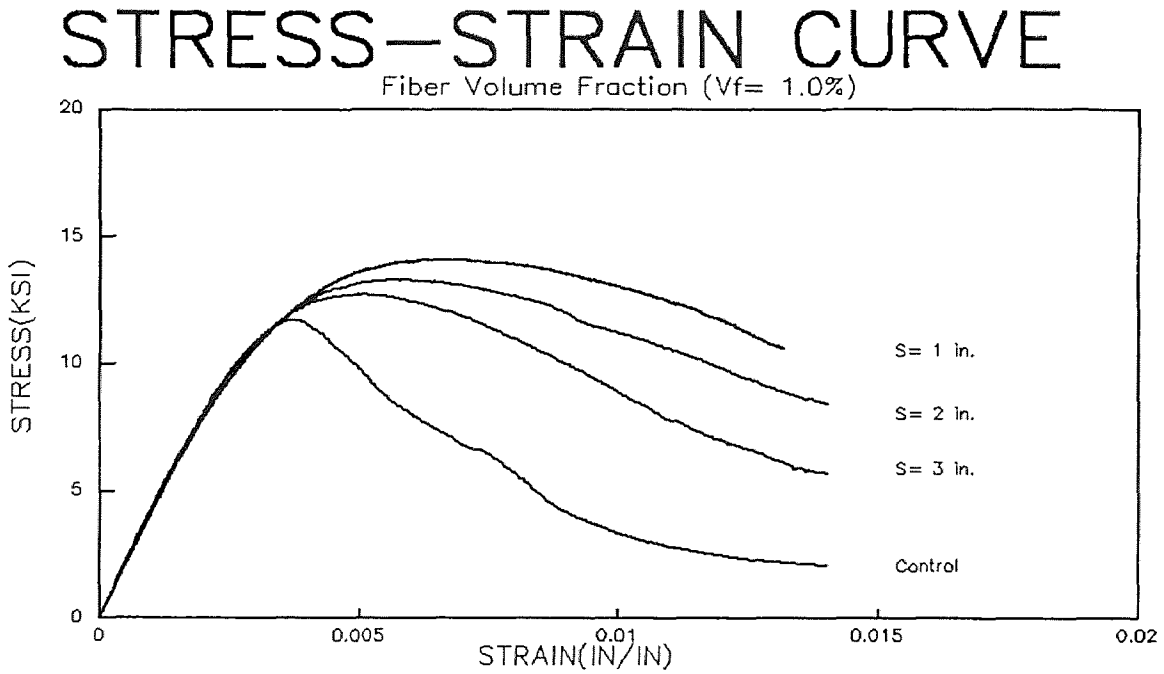

Figure 2.19 Stress-Strain Curves for Fibrous High Strength Concrete at Different Tie Spacing.

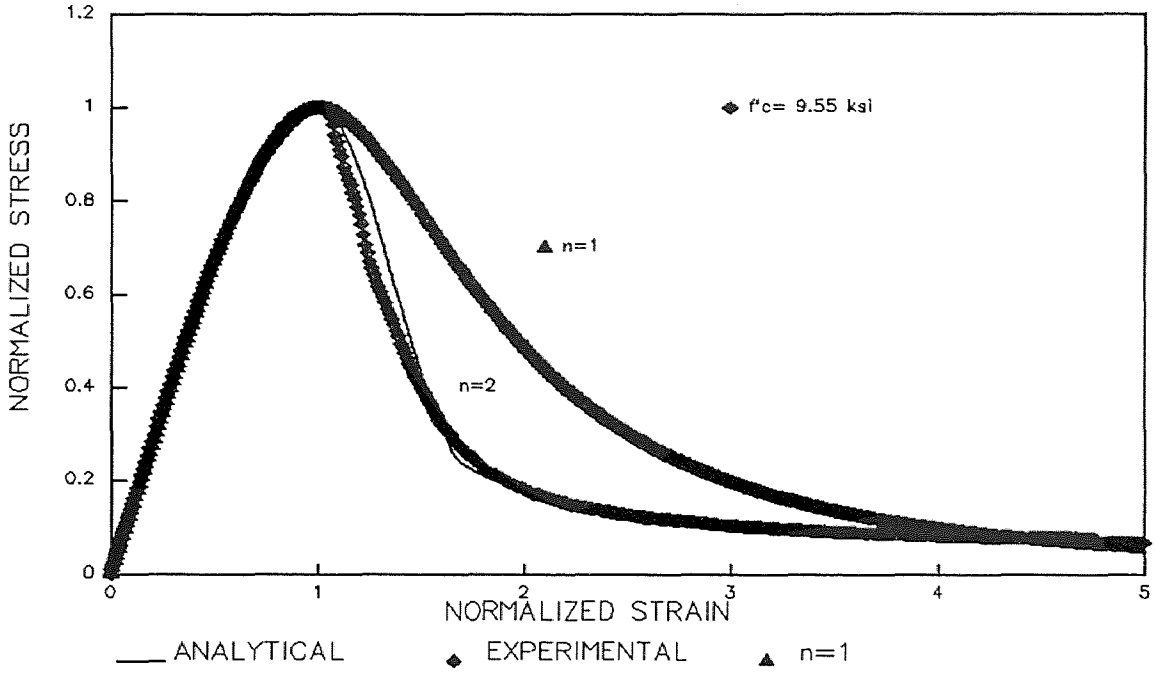

Figure 2.20 Influence of n Parameter on Descending Part of Compressive Stress-Strain Curve for HSC.

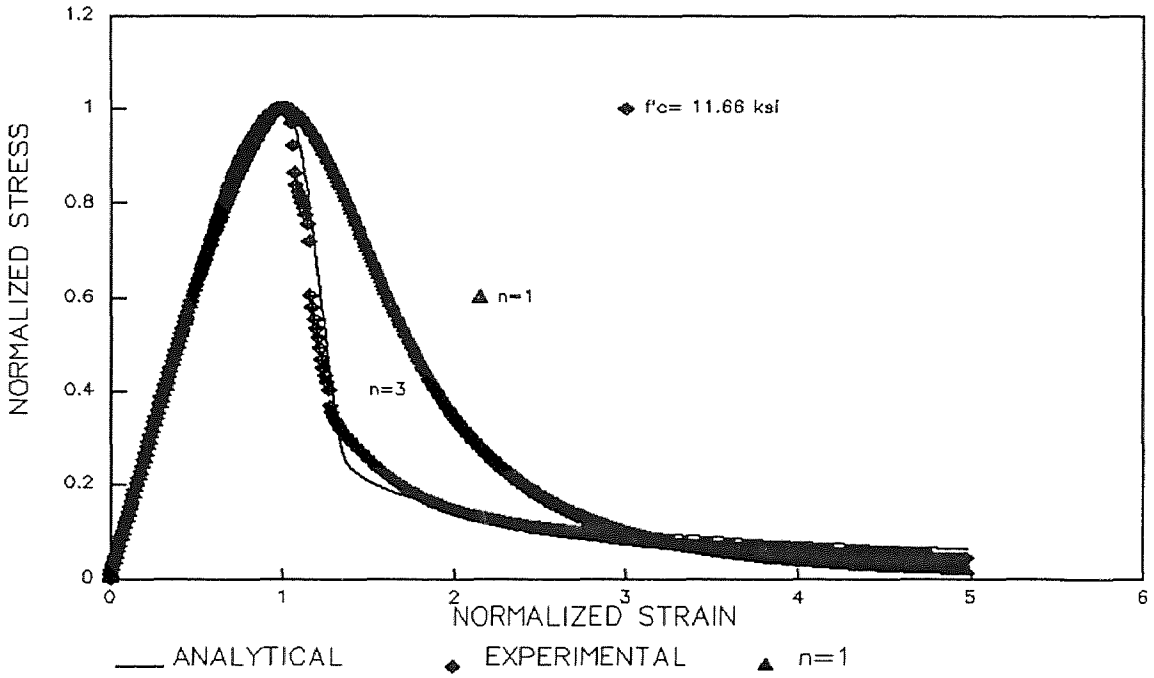

Figure 2.21 Influence of n Parameter on Descending Part of Compressive Stress-Strain Curve for HSC.

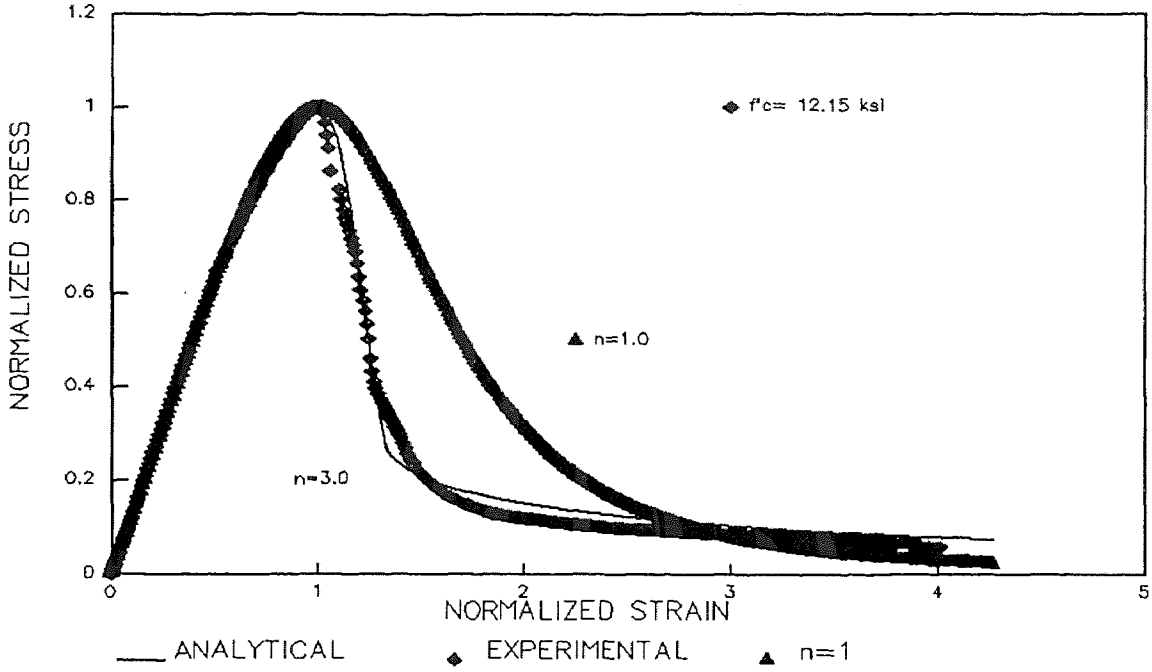

Figure 2.22 Influence of n Parameter on Descending Part of Compressive Stress-Strain Curve for HSC.

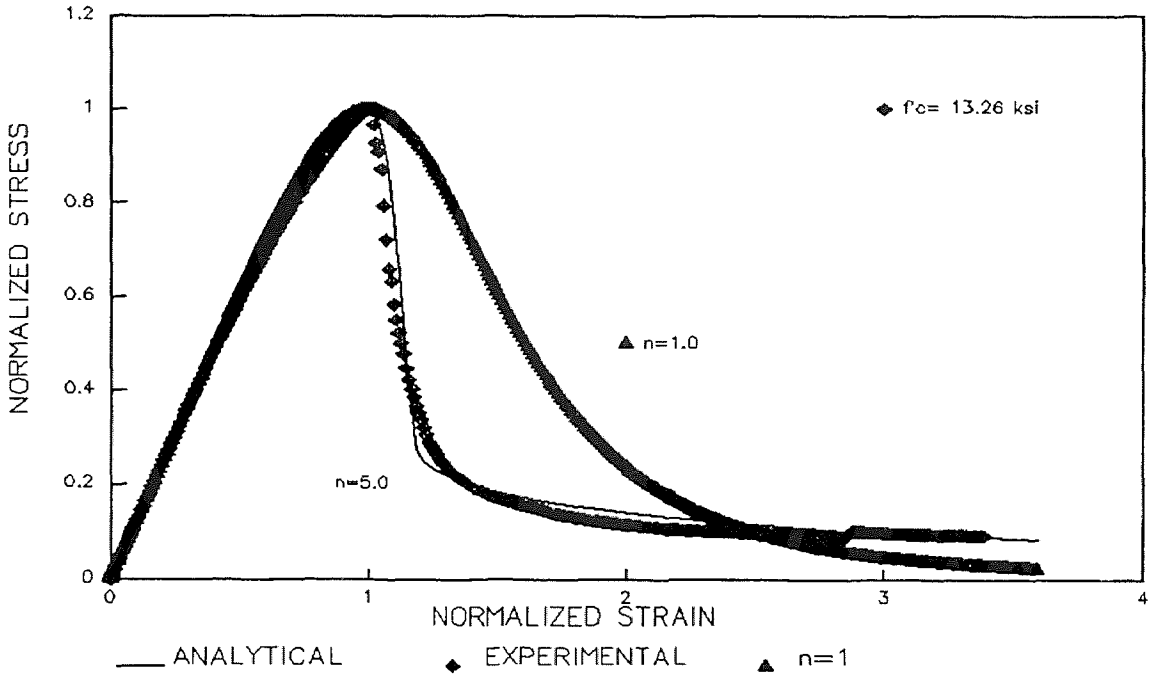

Figure 2.23 Influence of n Parameter on Descending Part of Compressive Stress-Strain Curve for HSC.

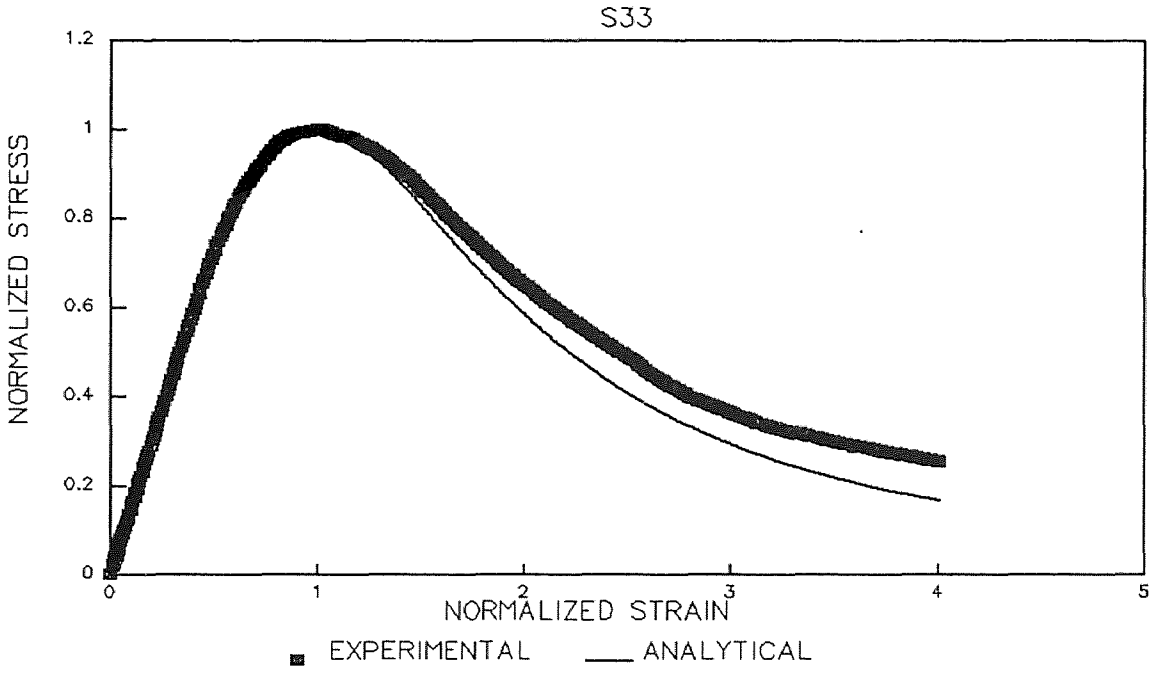

Figure 2.24 Fitting Proposed Equations to Experimental Data at Tie Spacing of 3 in.

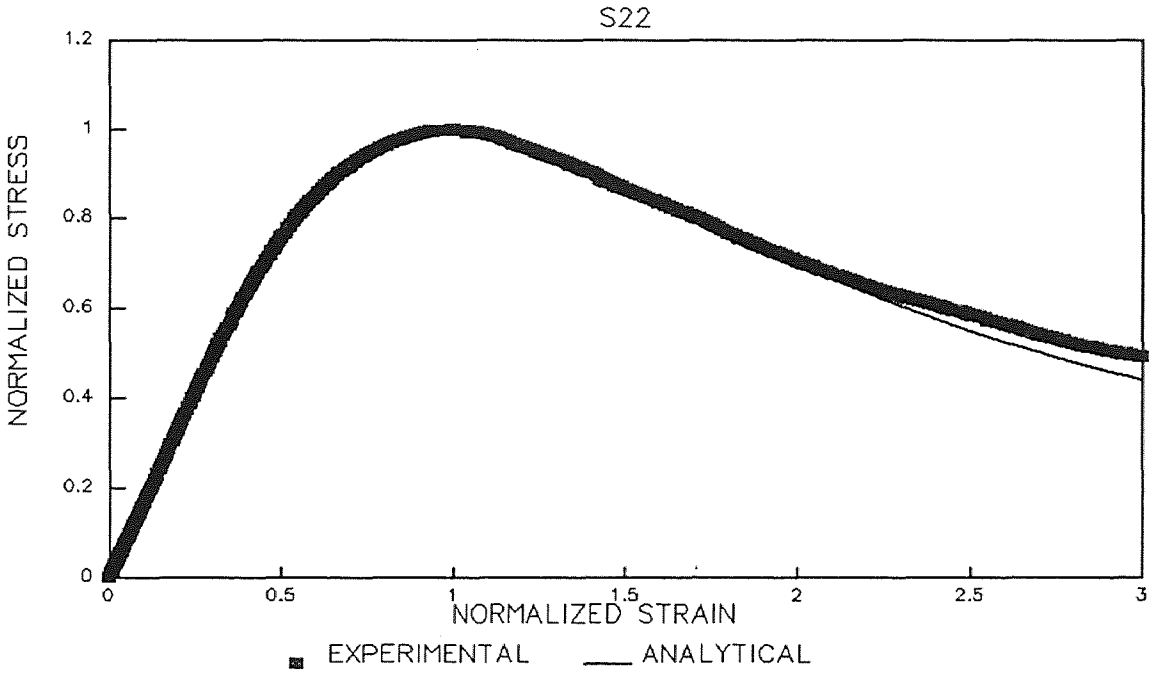

Figure 2.25 Fitting Proposed Equations to Experimental Data at Tie Spacing of 2 in.

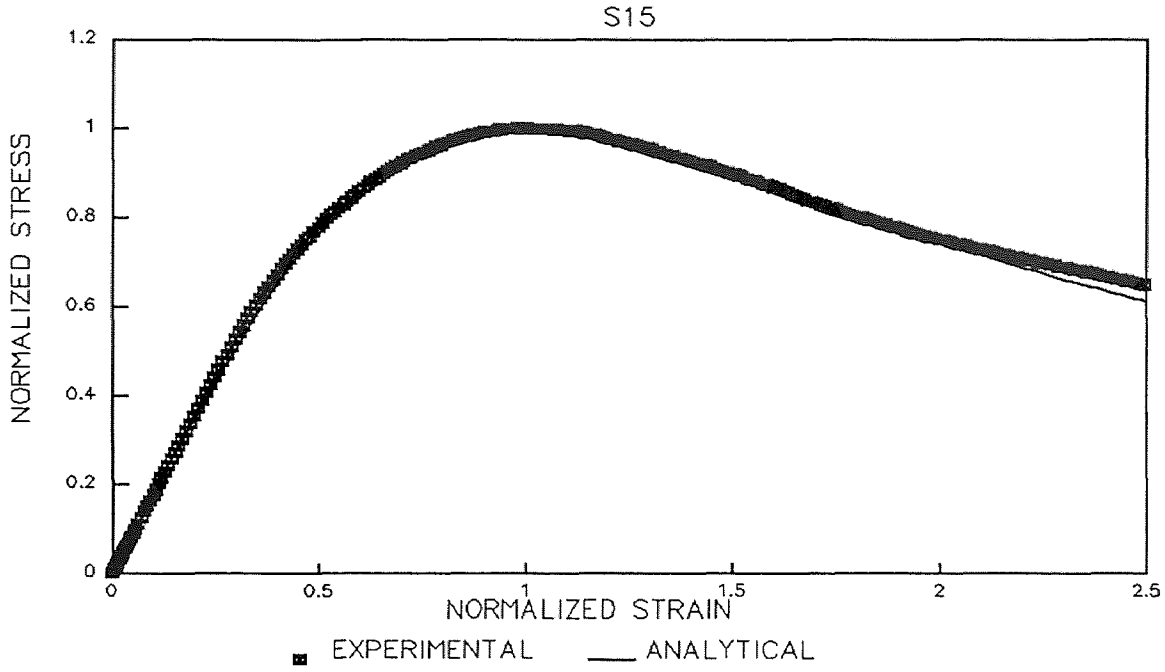

Figure 2.26 Fitting Proposed Equations to Experimental Data at Tie Spacing of 1 in.

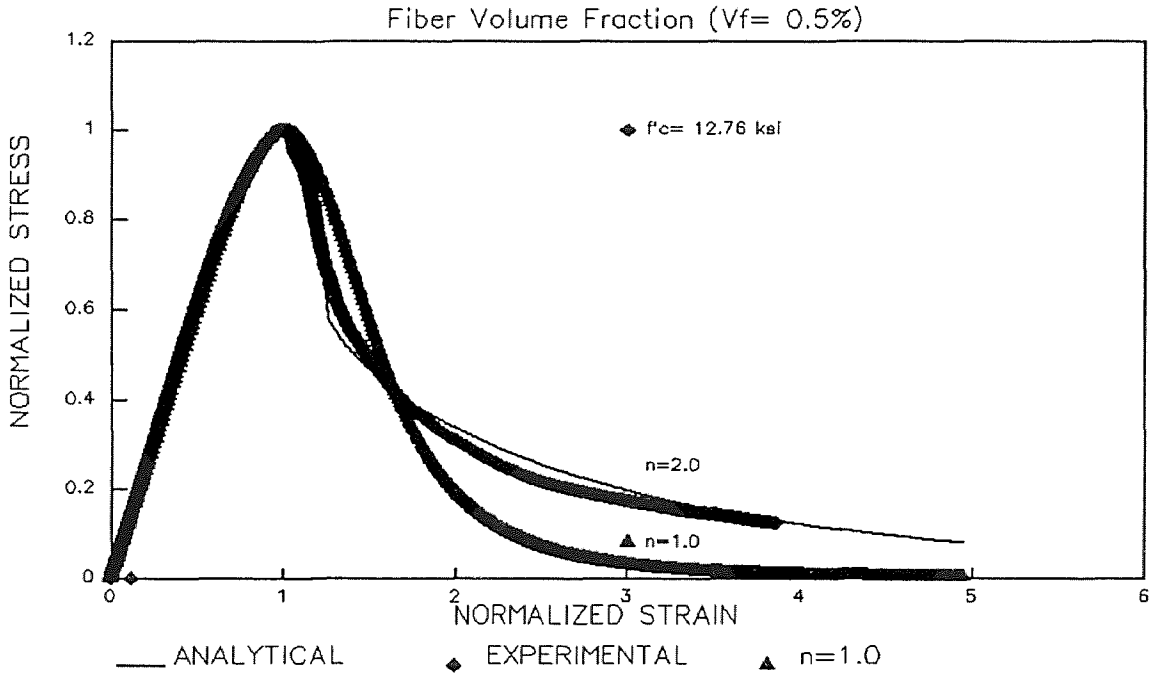

Figure 2.27 Influence of n Parameter on Descending Part of Compressive Stress-Strain Curve for HSC at 0.5% Fiber Volume Fraction.

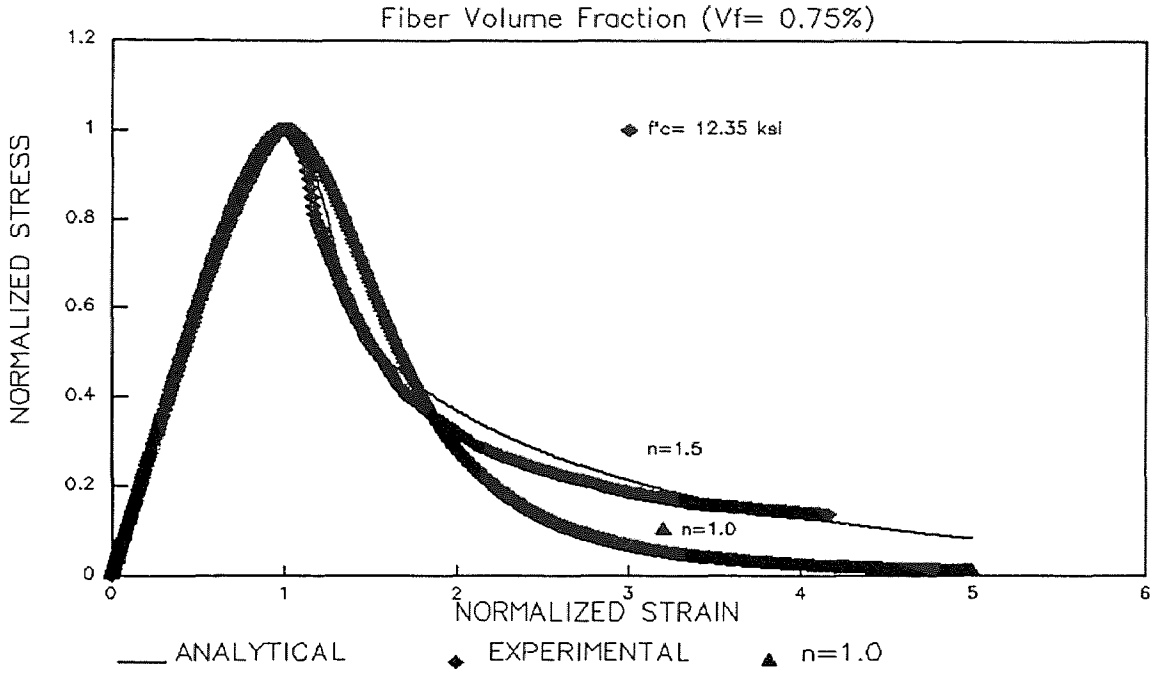

Figure 2.28 Influence of n Parameter on Descending Part of Compressive Stress-Strain Curve for HSC at 0.75% Fiber Volume Fraction.

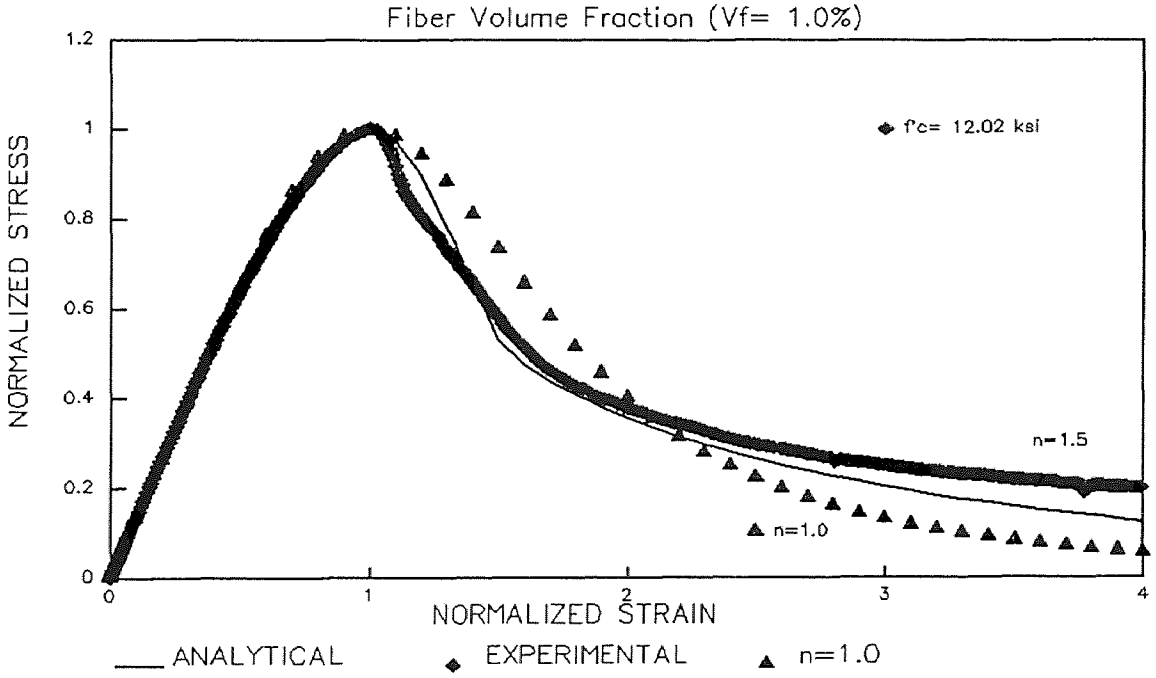

Figure 2.29 Influence of n Parameter on Descending Part of Compressive Stress-Strain Curve for HSC at 1.0% Fiber Volume Fraction.

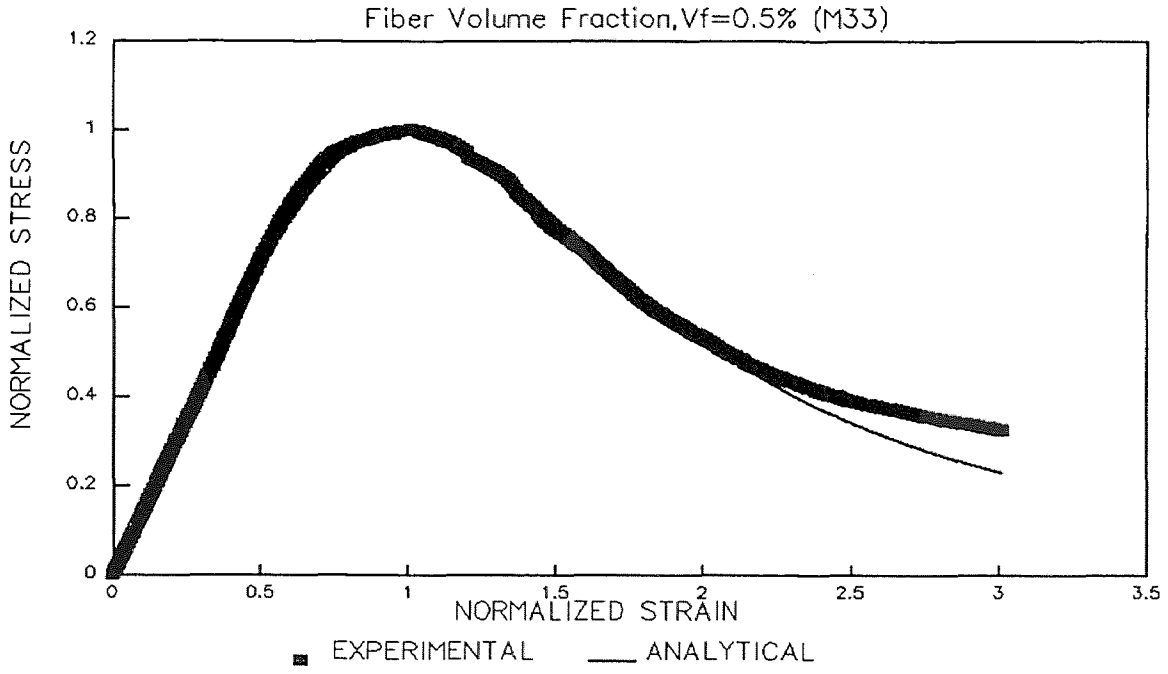

Figure 2.30 Fitting Proposed Equations to Experimental Data for HSC at Tie Spacing of 3 in. and 0.5% Fiber Volume Fraction.

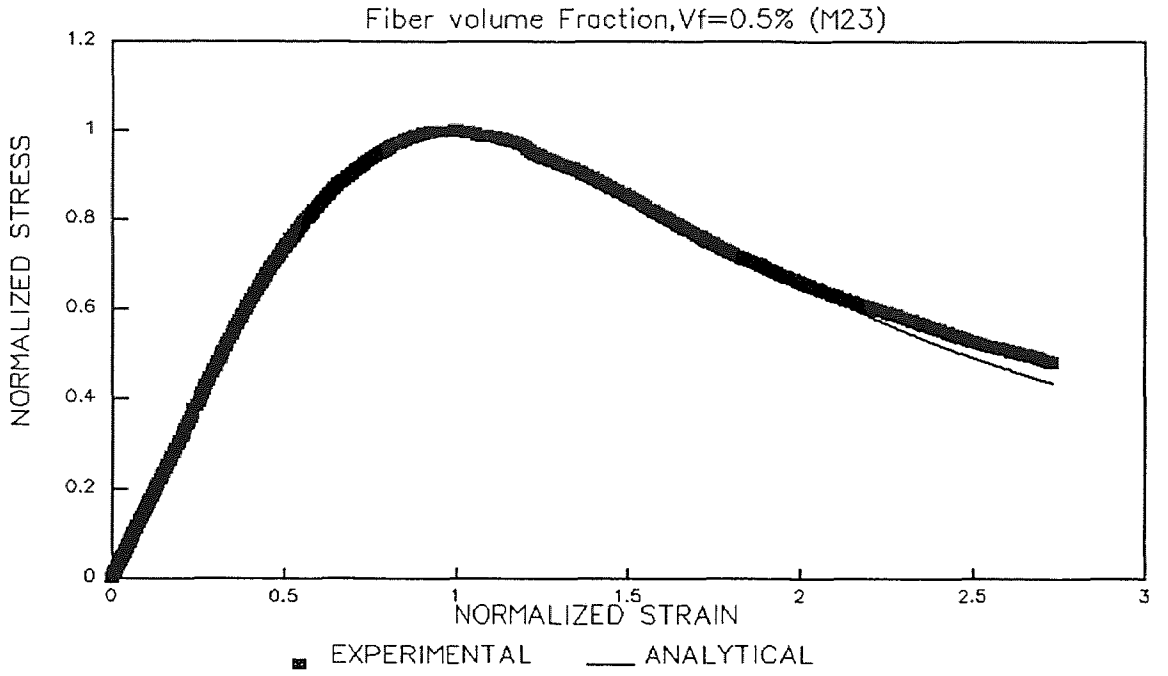

Figure 2.31 Fitting Proposed Equations to Experimental Data for HSC at Tie Spacing of 2 in. and 0.5% Fiber Volume Fraction.

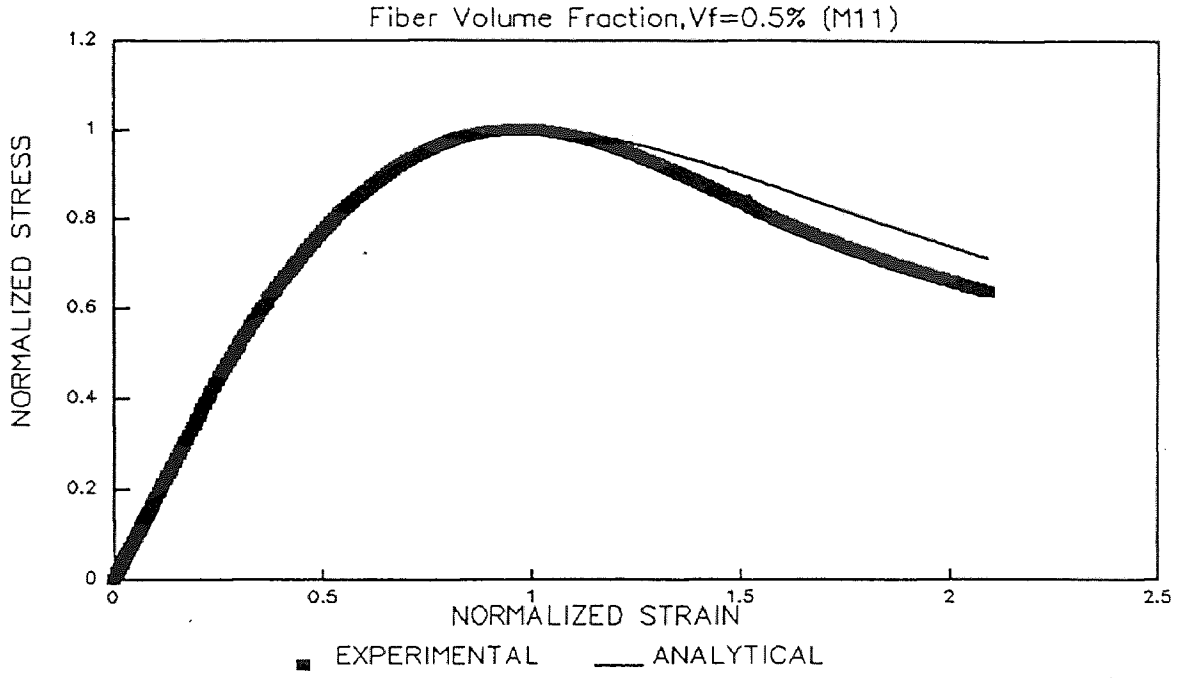

Figure 2.32 Fitting Proposed Equations to Experimental Data for HSC at Tie Spacing of 1 in. and 0.5% Fiber Volume Fraction.

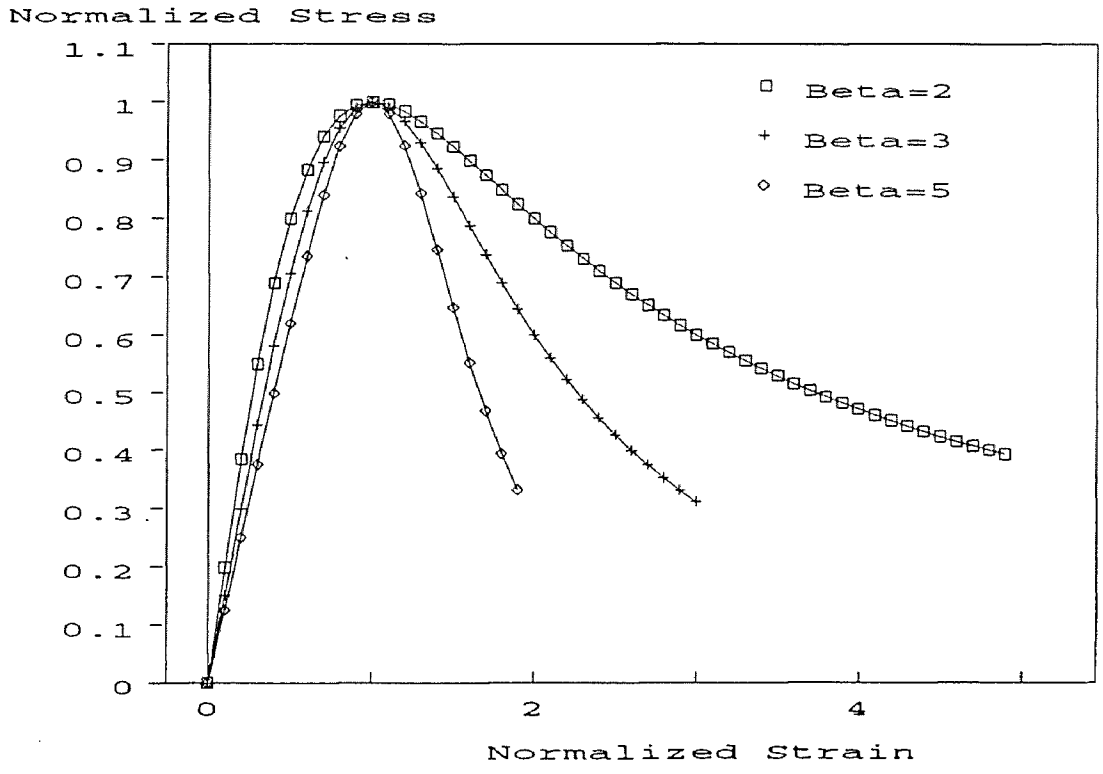

Figure 2.33 Effect of Beta on Generated Compressive Stress-Strain Curves.

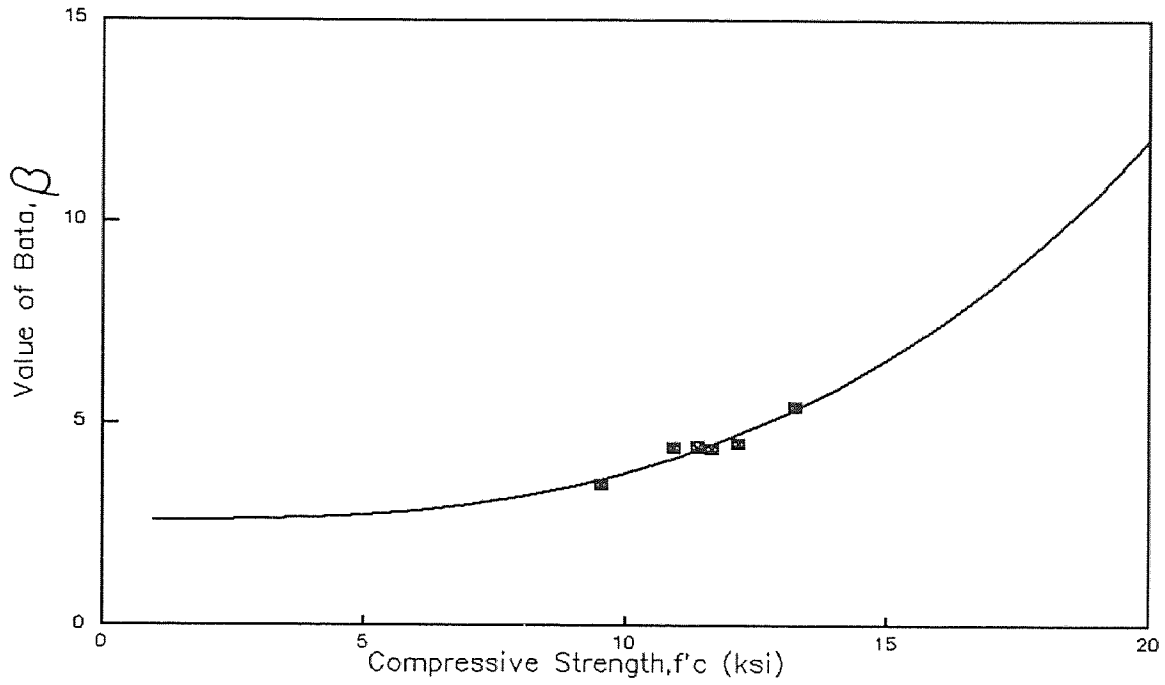

Figure 2.34 Relationship Between f'_c and ß for HSC.

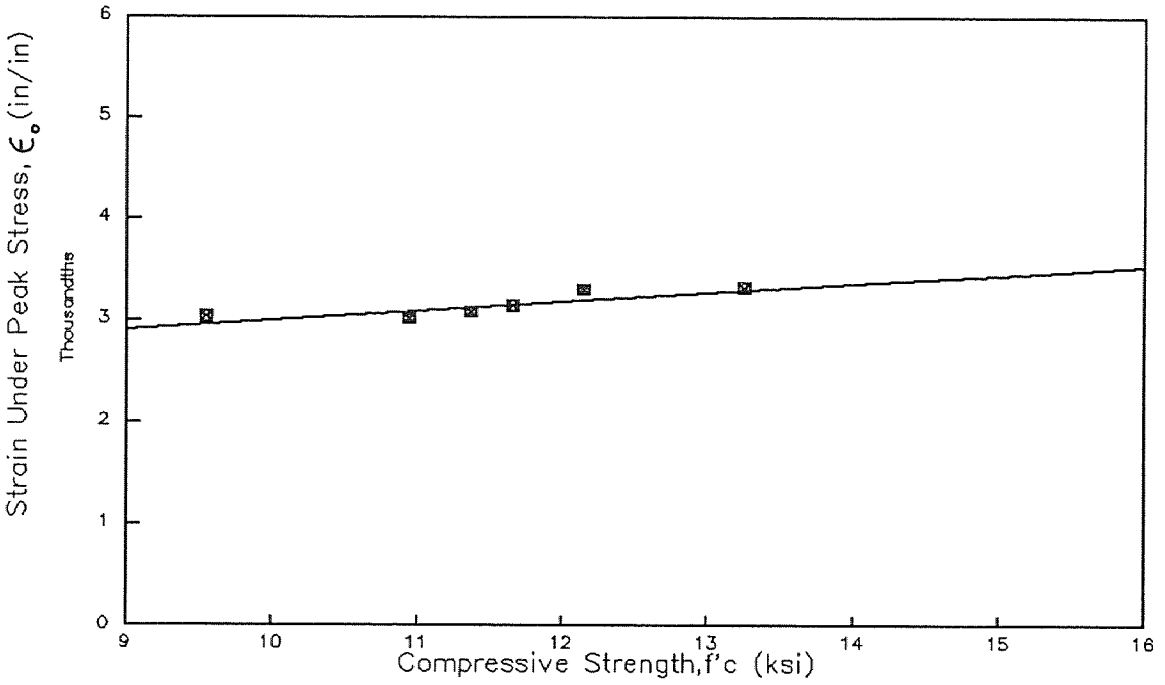

Figure 2.35 Relationship Between f'_c and ϵ_o for HSC.

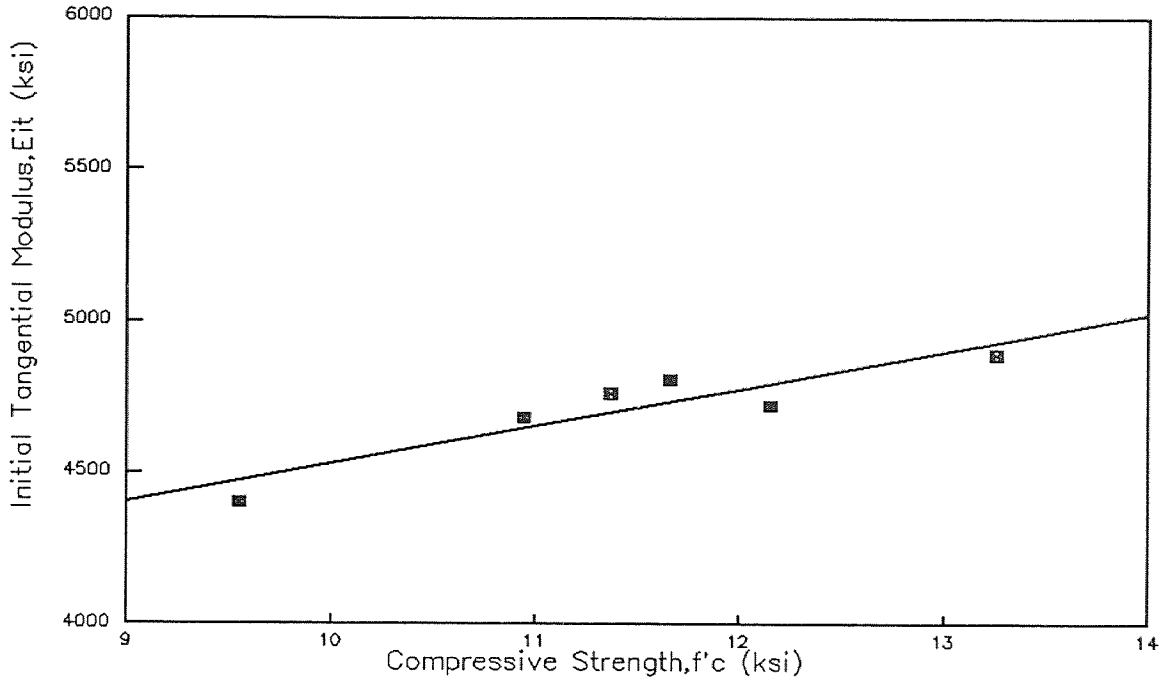

Figure 2.36 Relationship Between f'_c and E_{it} for HSC.

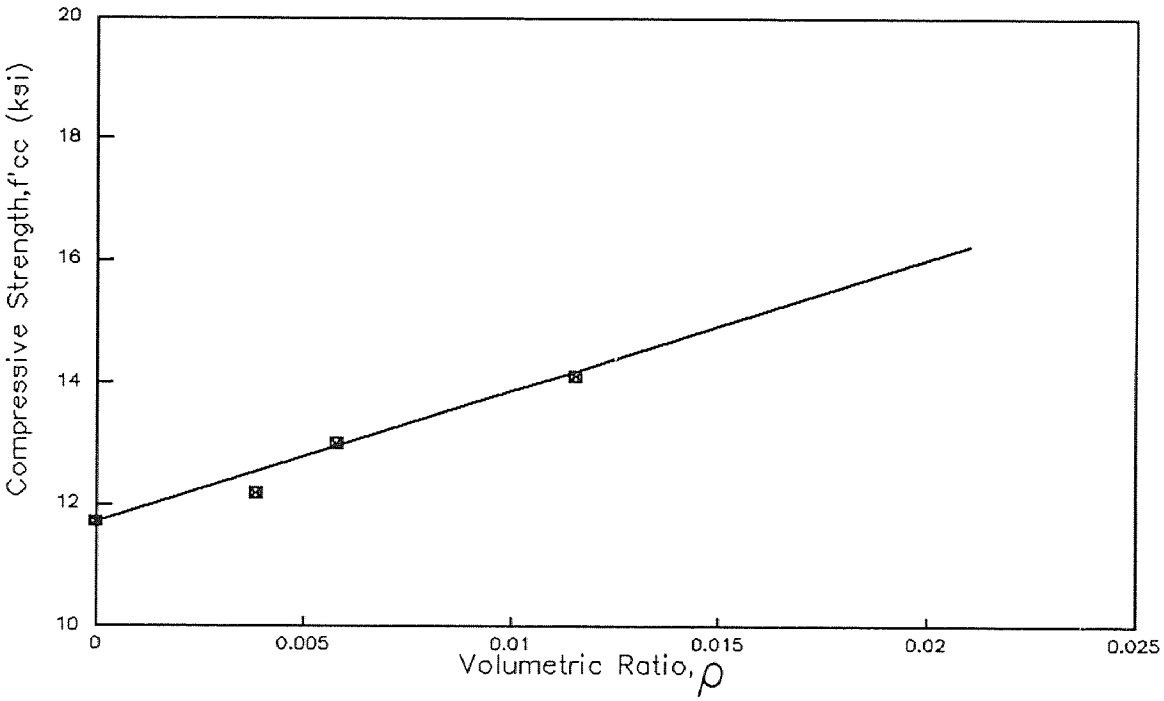

Figure 2.37 Relationship Between ρ and f'_{cc} for HSC.

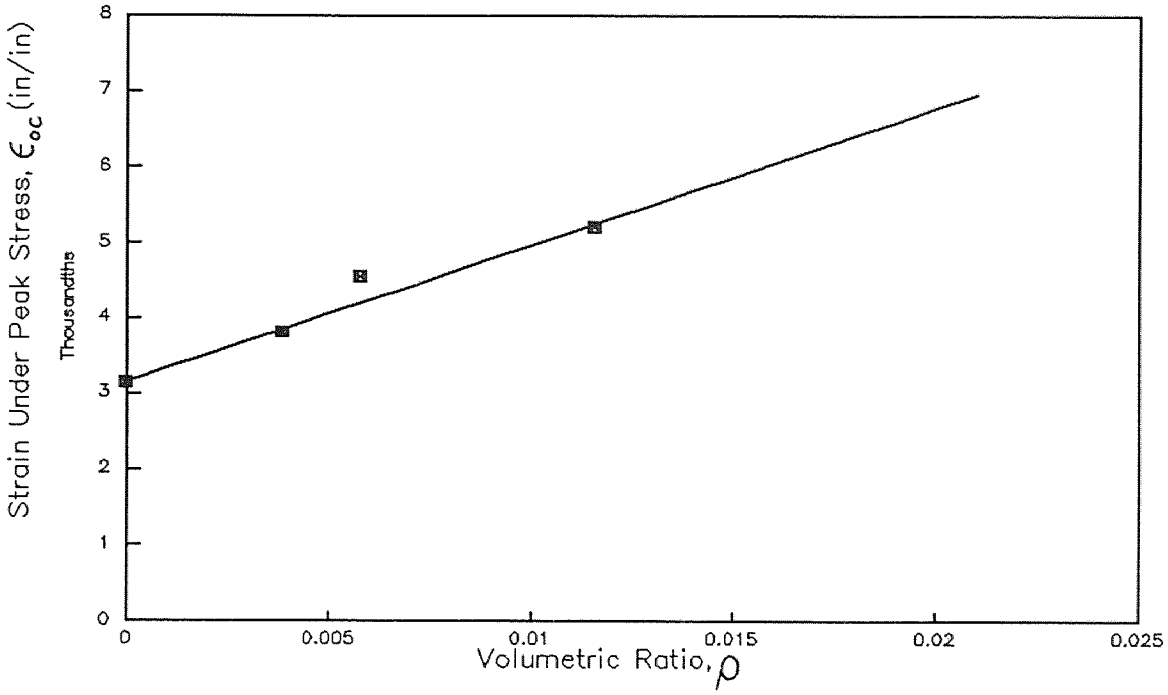

Figure 2.38 Relationship Between ρ and ϵ_{oc} for HSC.

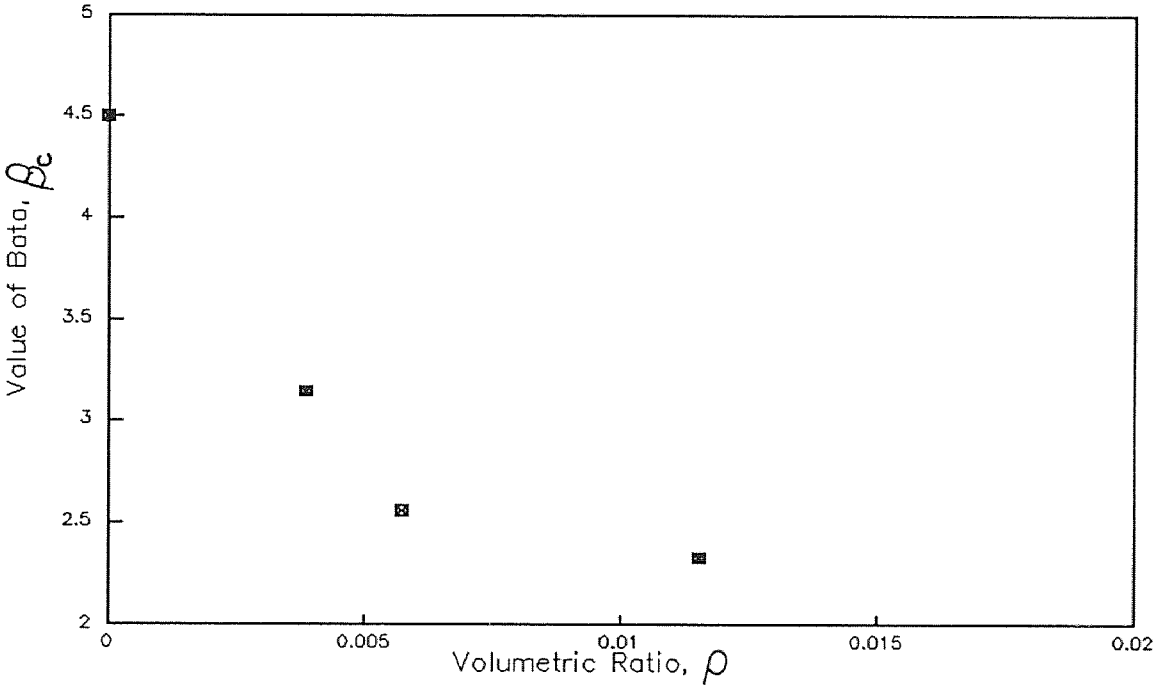

Figure 2.39 Relationship Between ρ and β_c for HSC.

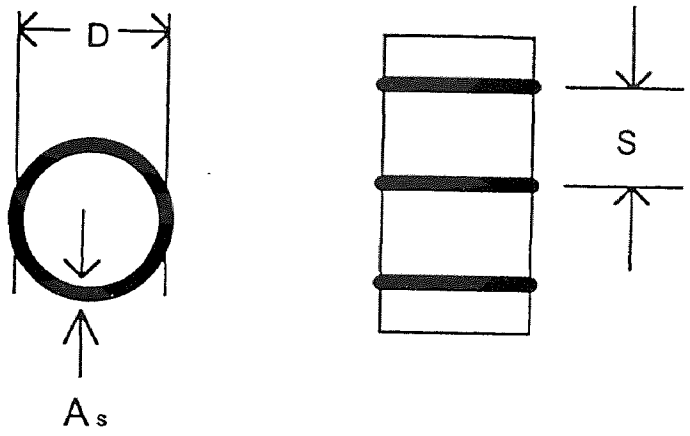

Figure 2.40 Scheme for Circular Hoop of Cylinder Concrete.

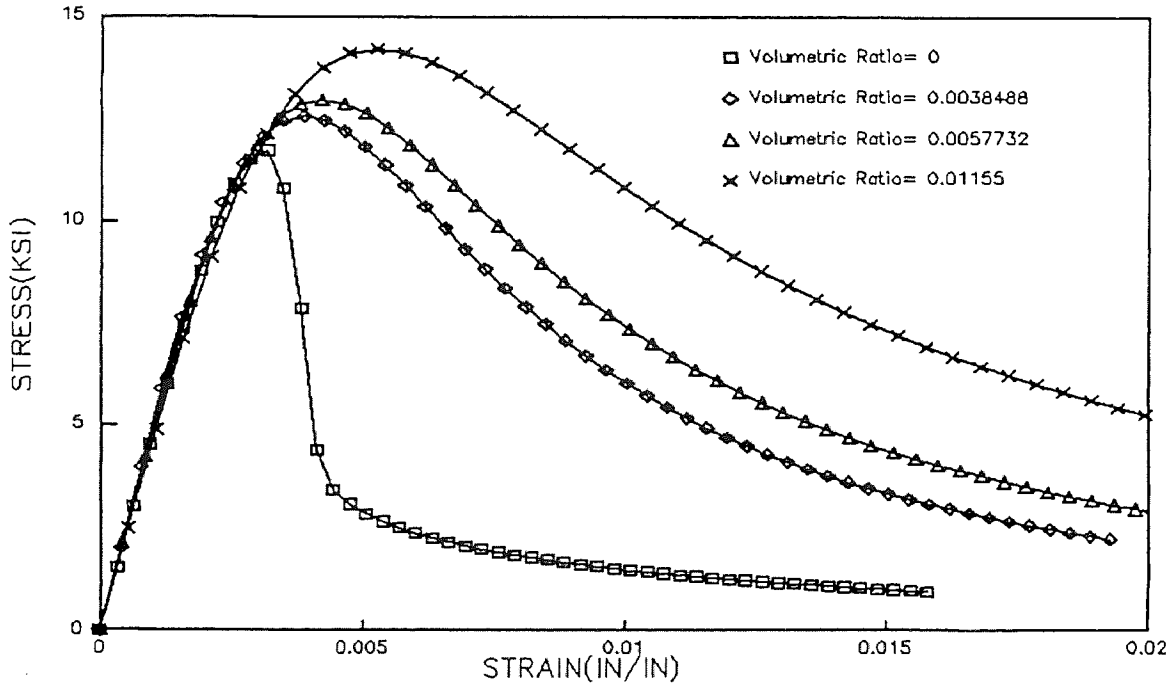

Figure 2.41 Generated Analytical Stress-Strain Curves at Different Tie Spacing

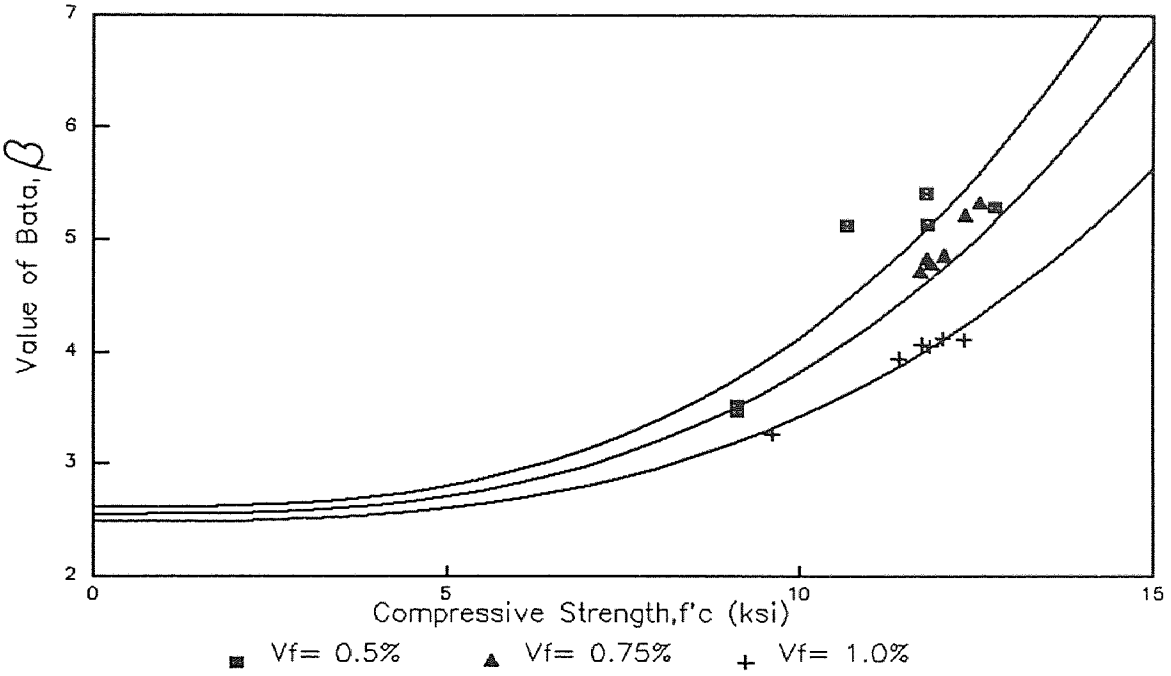

Figures 2.42 Relationship Between f' $_c$ and ß for HSC at Different Fiber Content (V_f=0.5%, 0.75%, 1.0%).

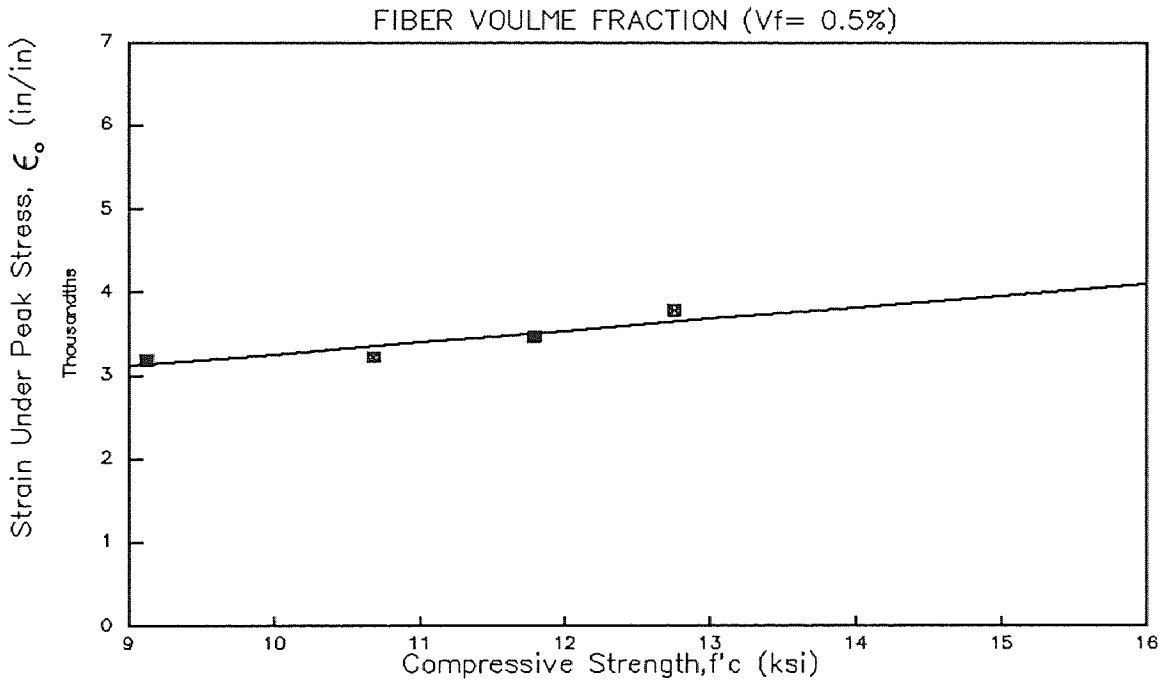

Figure 2.43 Relationship Between f' $_c$ and ϵ_o for HSC at 0.5% Fiber Volume Fraction.

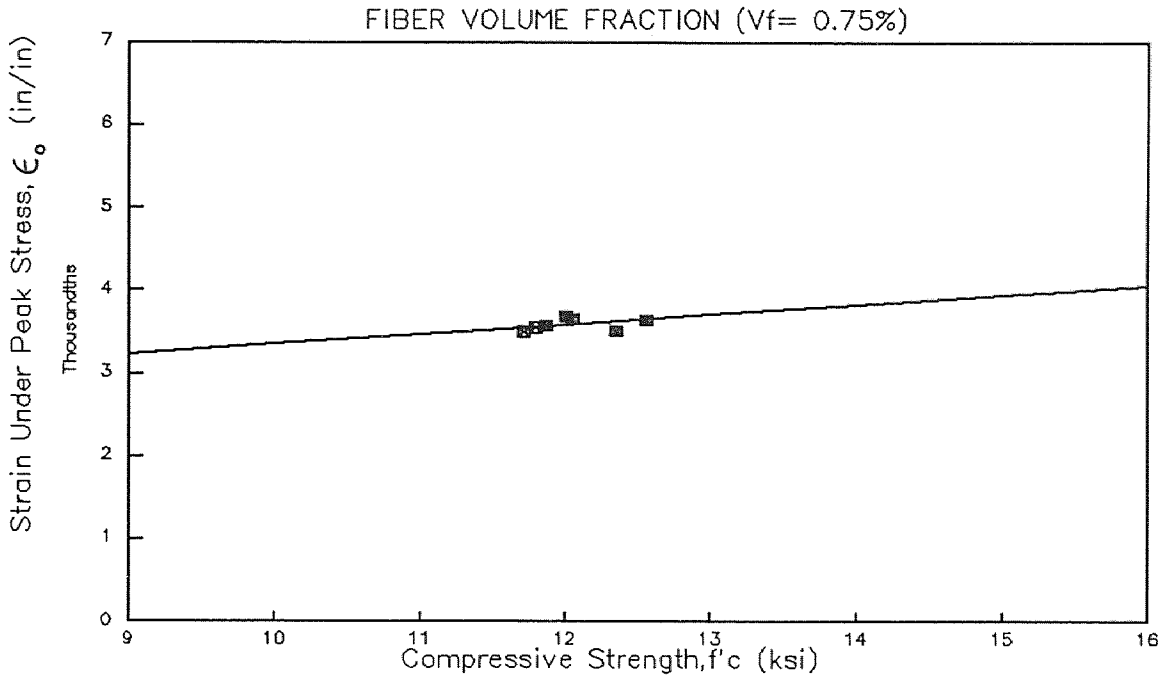

Figure 2.44 Relationship Between f'$_c$ and ϵ_o for HSC at 0.75% Fiber Volume Fraction.

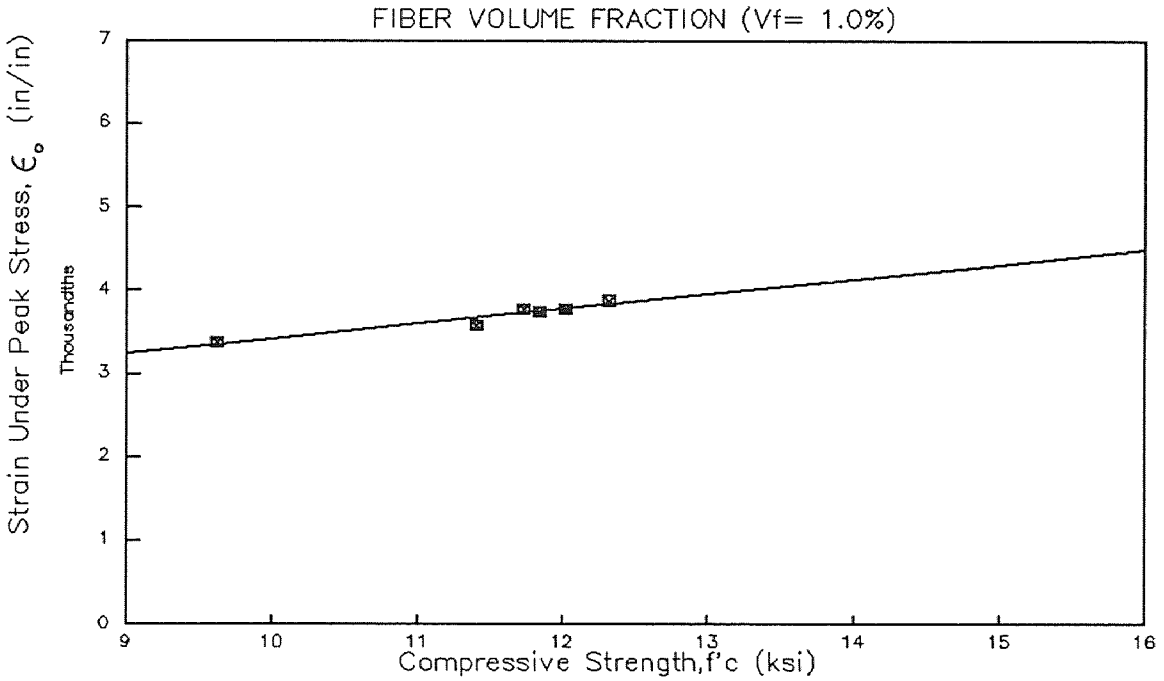

Figure 2.45 Relationship Between f'$_c$ and ϵ_o for HSC at 1.0% Fiber Volume Fraction.

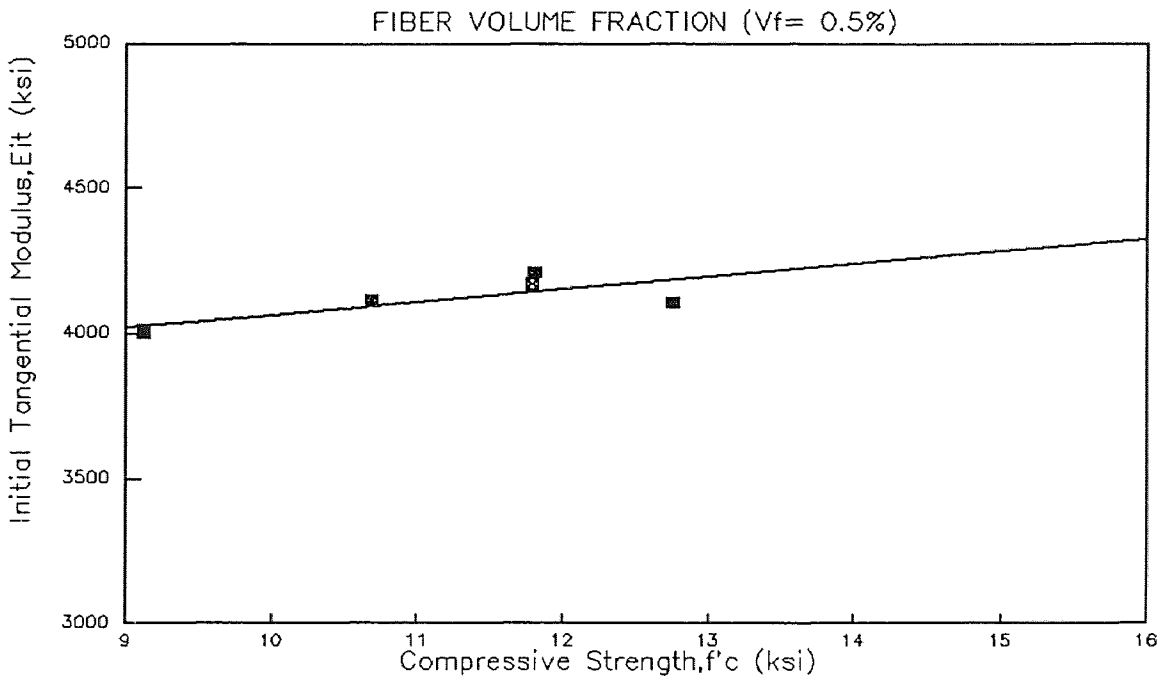

Figure 2.46 Relationship Between f'_c and E_{it} for HSC at 0.5% Fiber Volume Fraction.

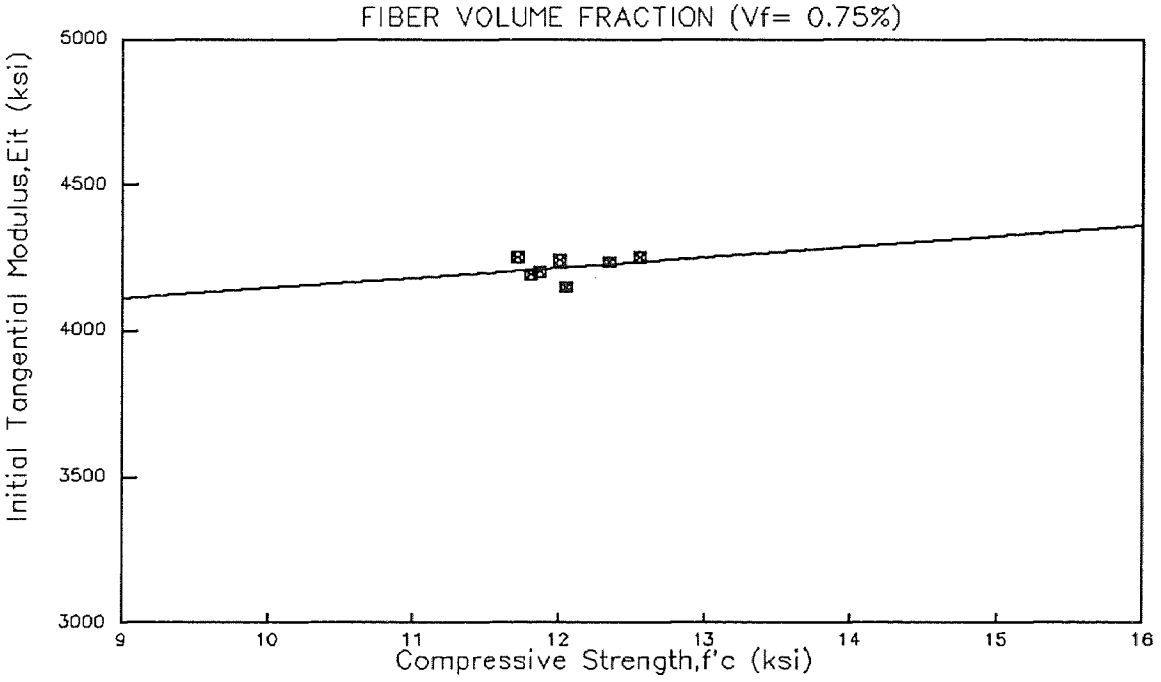

Figure 2.47 Relationship Between f'_c and E_{it} for HSC at 0.75% Fiber Volume Fraction.

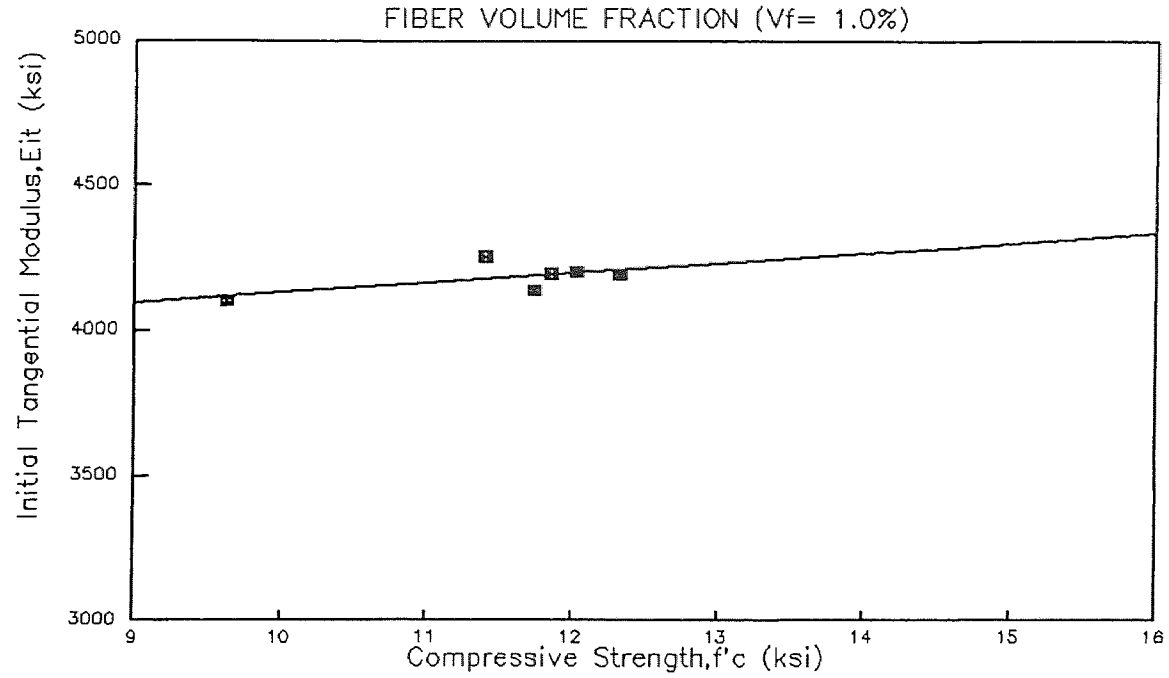

Figure 2.48 Relationship Between f'_c and E_{it} for HSC at 1.0% Fiber Volume Fraction.

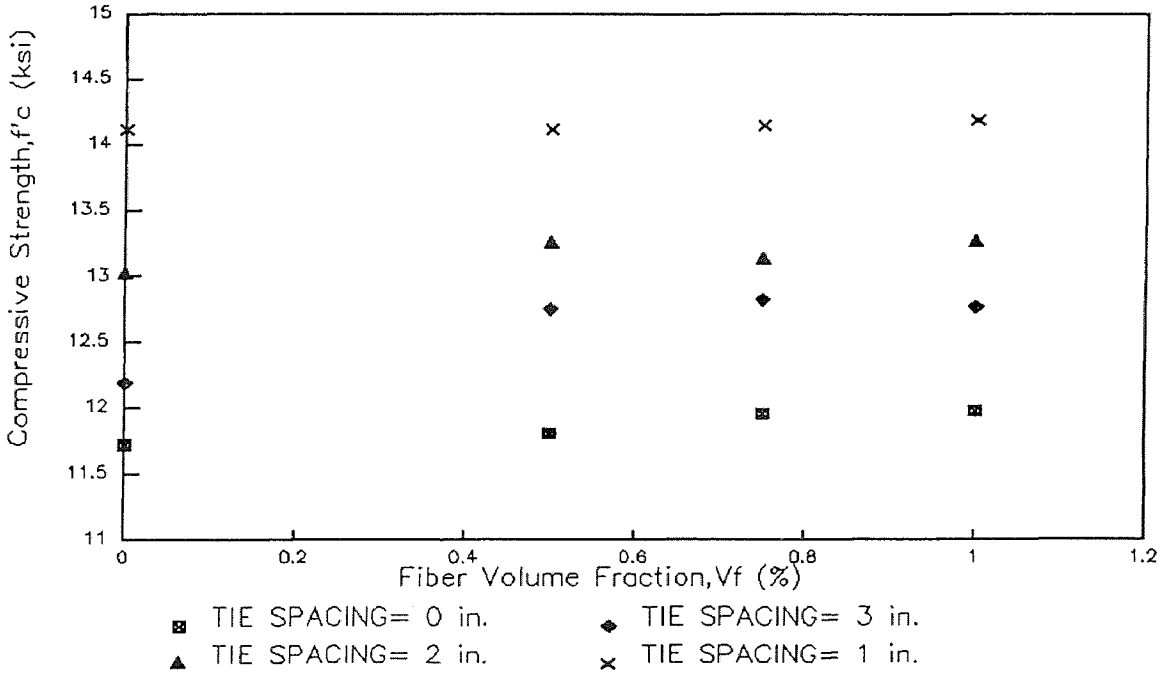

Figure 2.49 Relationship Between V_f and f'_c at Different Tie Spacing.

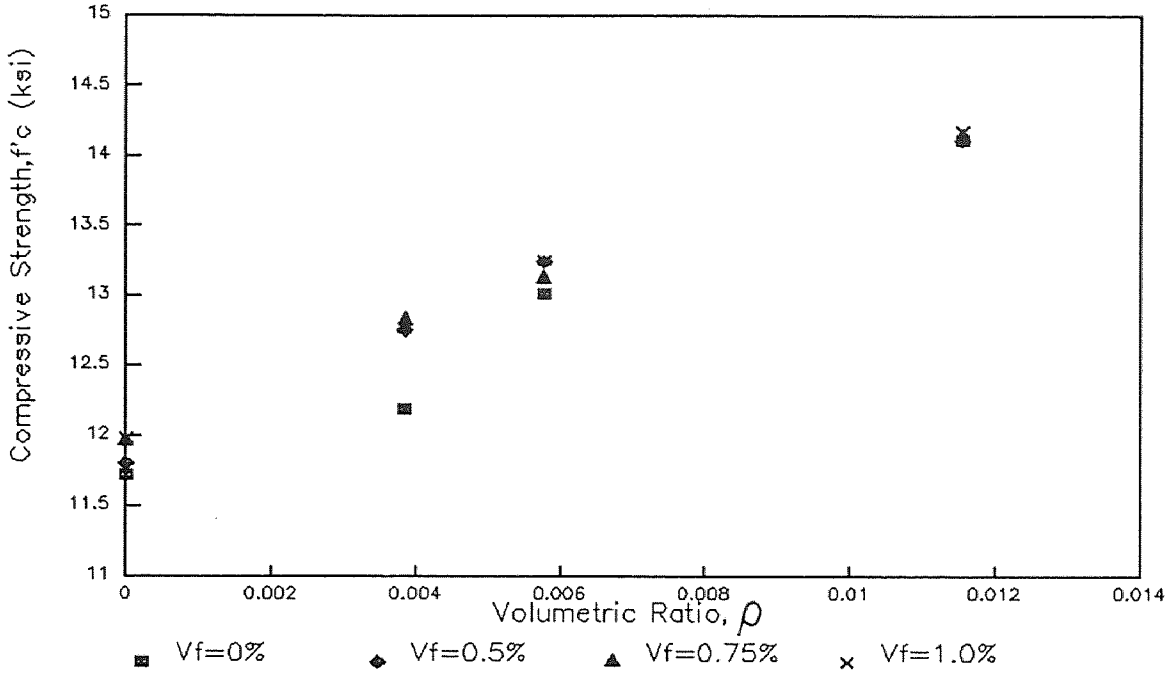

Figure 2.50 Relationship Between ρ and f' $_c$ at Different Fiber Content.

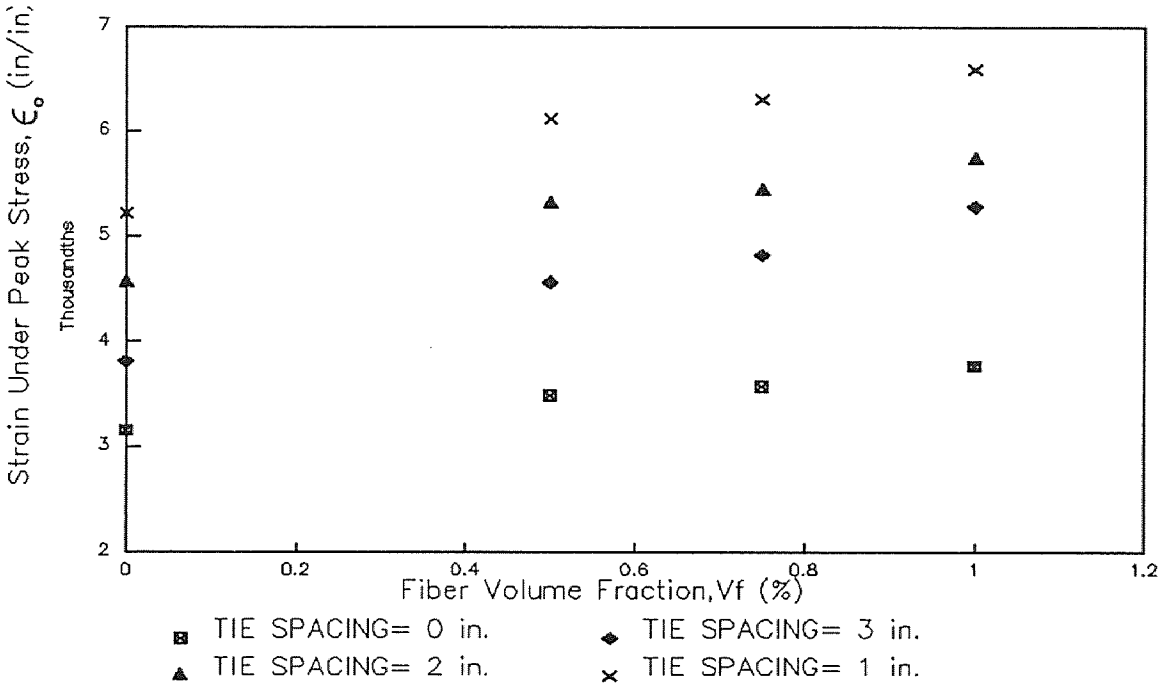

Figure 2.51 Relationship Between V $_f$ and ϵ $_o$ at Different Tie Spacing

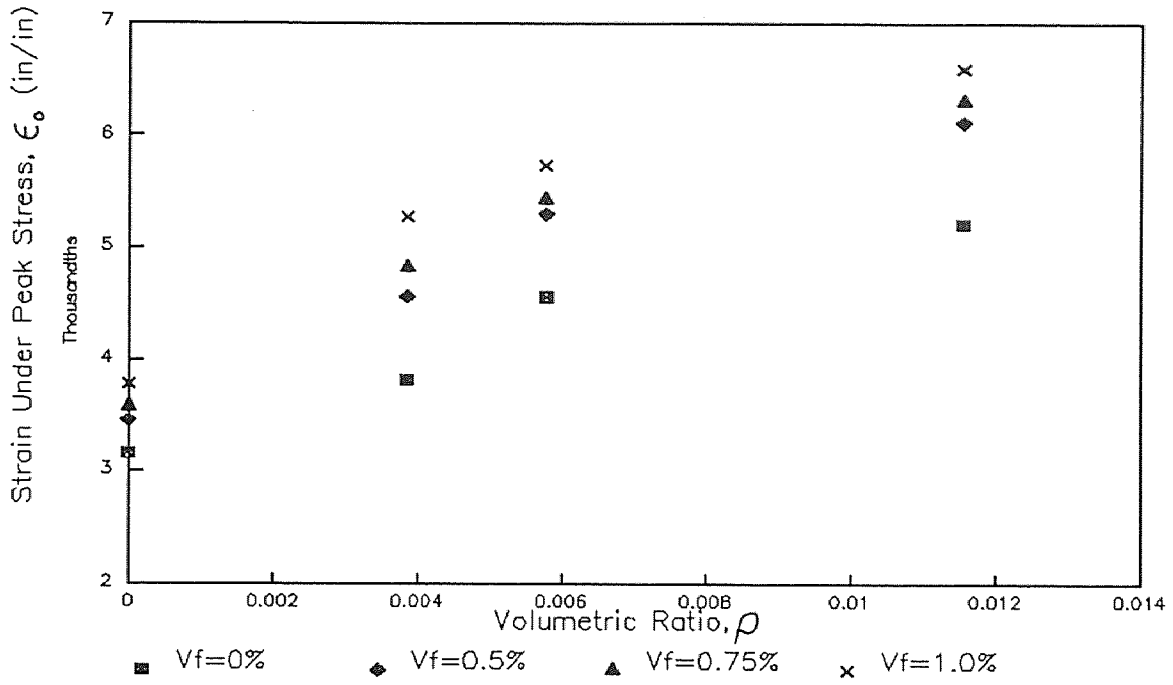

Figure 2.52 Relationship Between ρ and ϵ_o at Different Fiber Content.

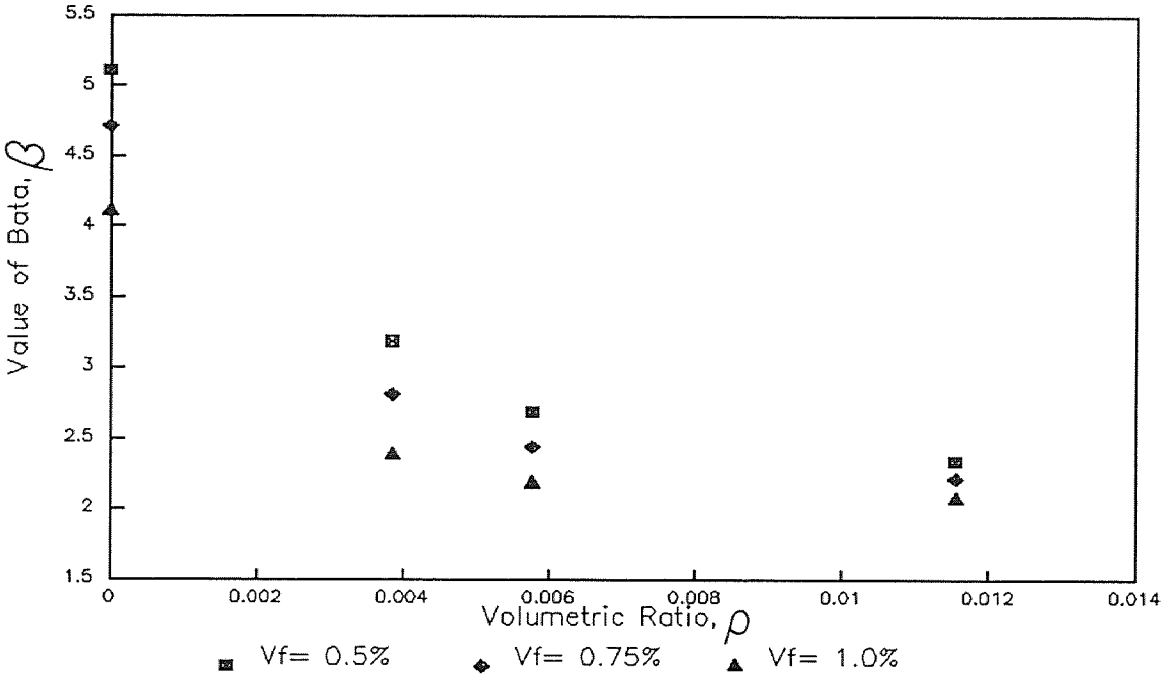

Figure 2.53 Relationship Between ρ and β_c at Different Fiber Content.

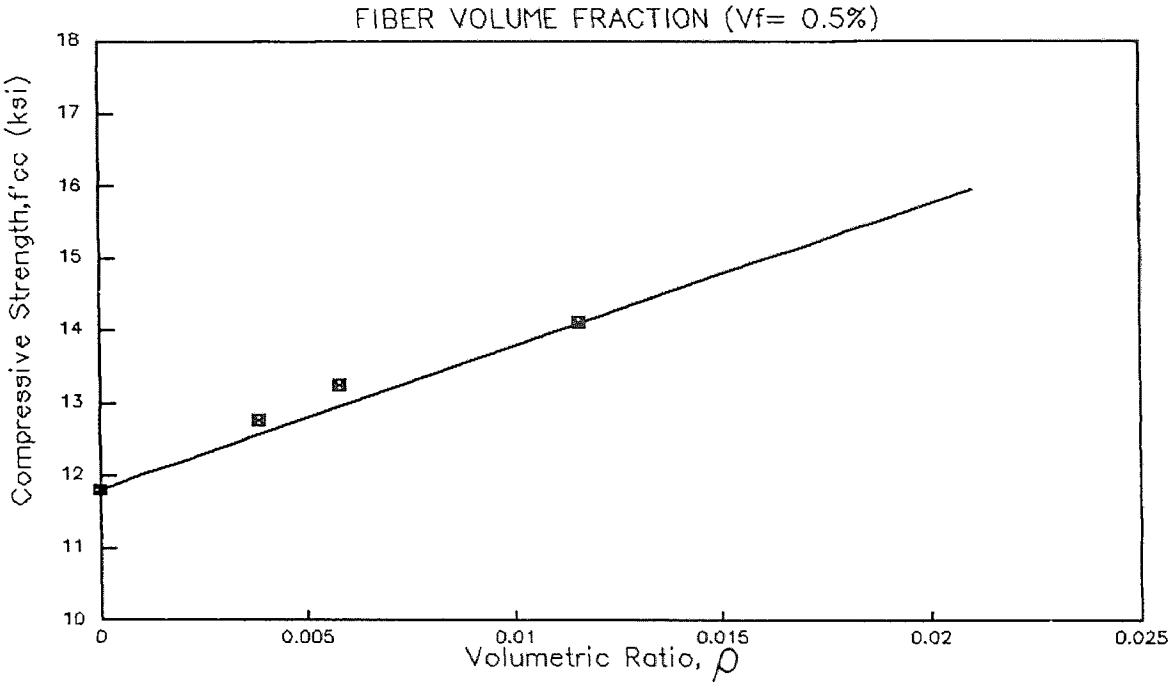

Figure 2.54 Relationship Between ρ and f'_{cc} for HSC at 0.5% Fiber Volume Fraction.

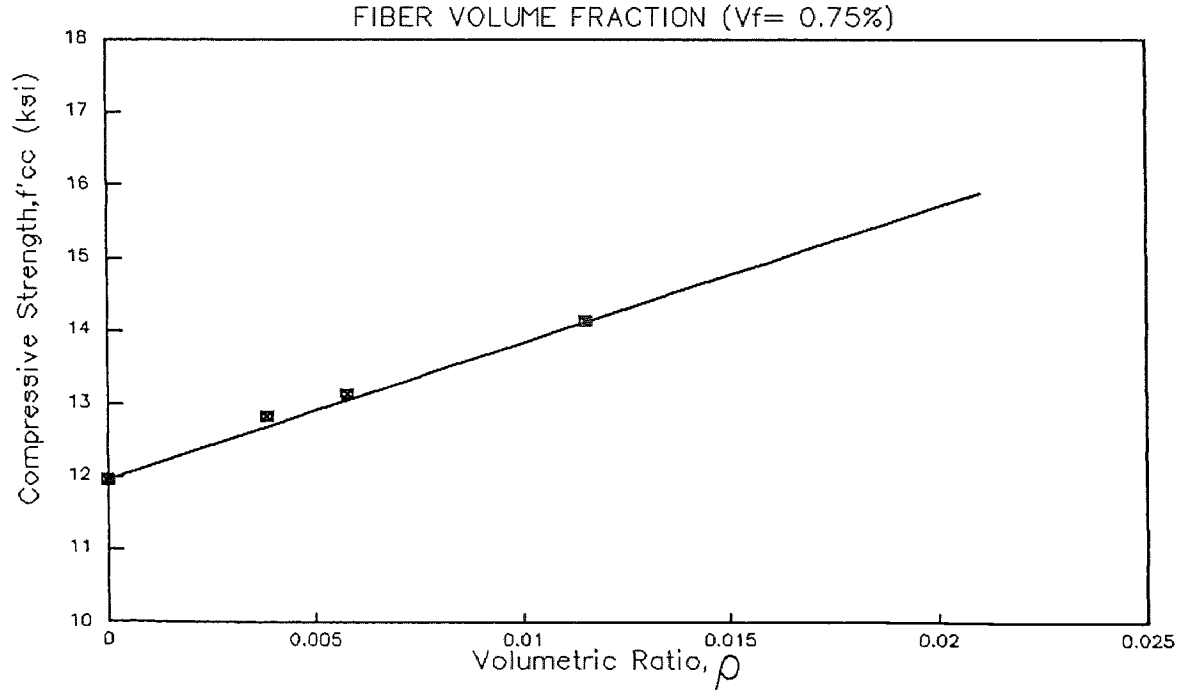

Figure 2.55 Relationship Between ρ and f'_{cc} for HSC at 0.75% Fiber Volume Fraction.

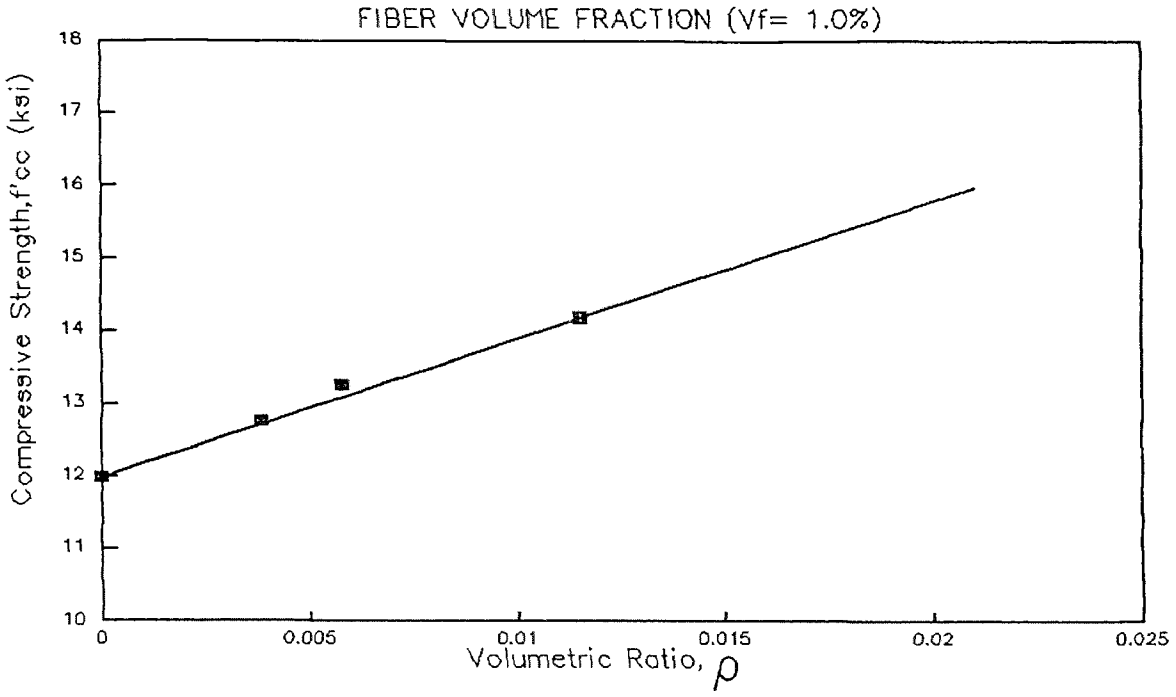

Figure 2.56 Relationship Between ρ and f'_{cc} for HSC at 1.0% Fiber Volume Fraction.

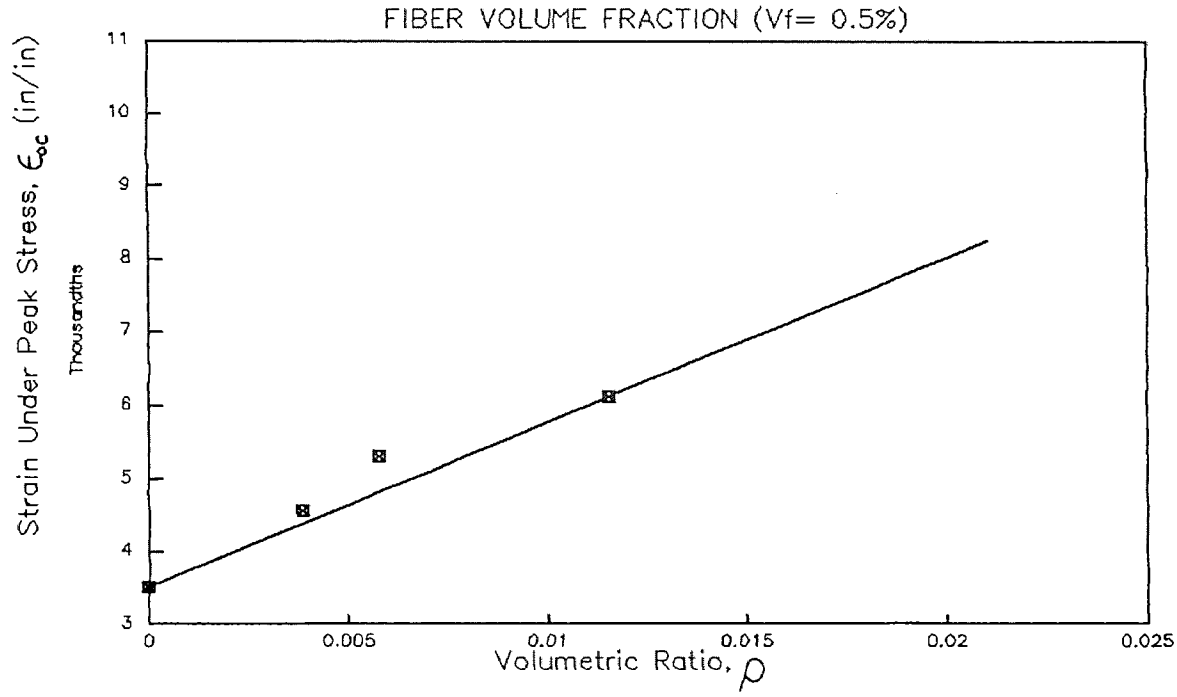

Figure 2.57 Relationship Between ρ and ϵ_{oc} for HSC at 0.5% Fiber Volume Fraction.

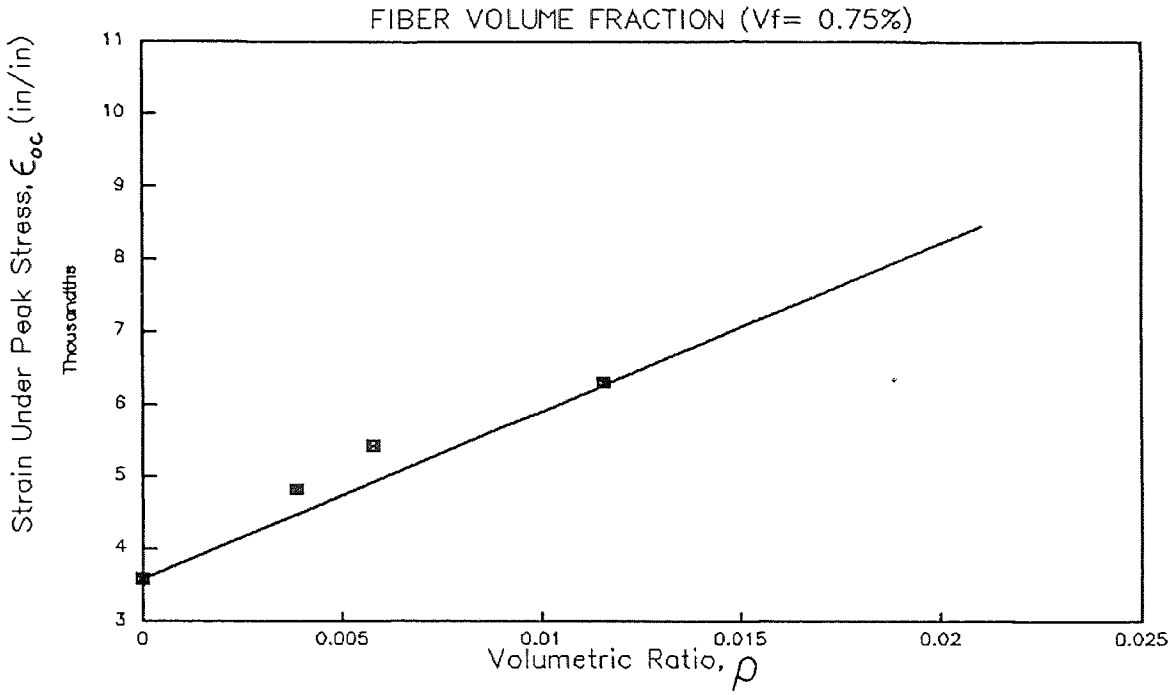

Figure 2.58 Relationship Between ρ and ϵ_{oc} for HSC at 0.75% Fiber Volume Fraction.

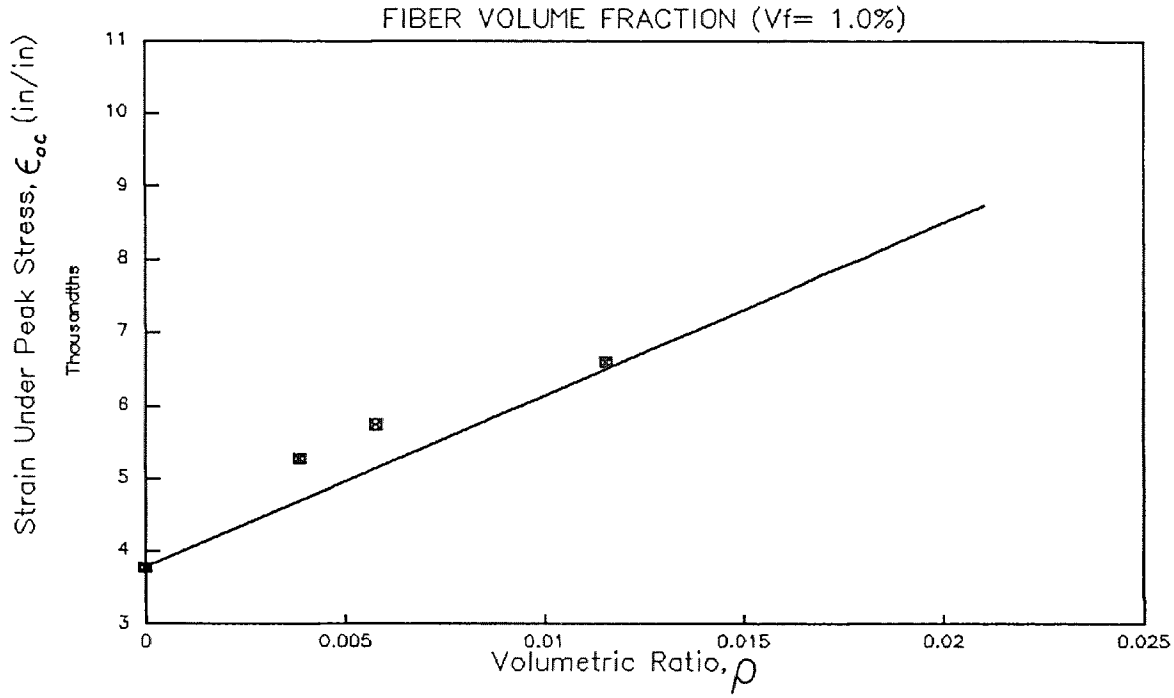

Figure 2.59 Relationship Between q and ϵ_{oc} for HSC at 1.0% Fiber Volume Fraction.

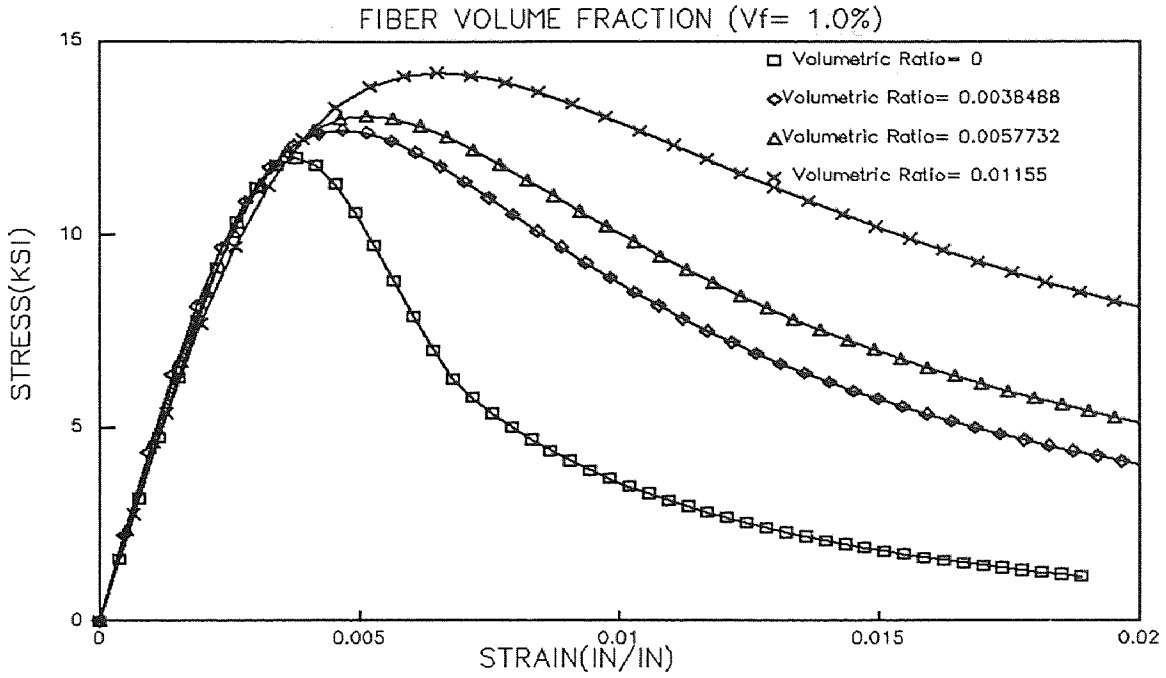

Figure 2.60 Generated Analytical Stress-Strain Curve for Fibrous High Strength Concrete (V_f=1.0%) at Different Tie Spacing.

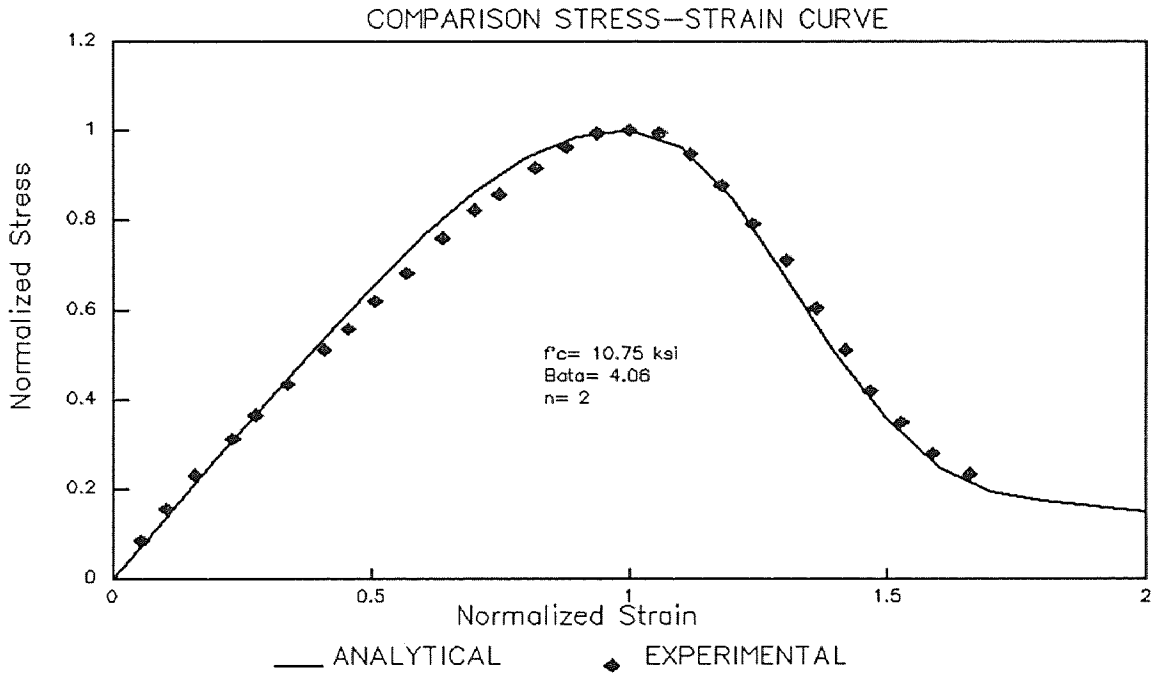

Figure 2.61 Proposed Model vs Wang's Experimental Data (Wang,1978).

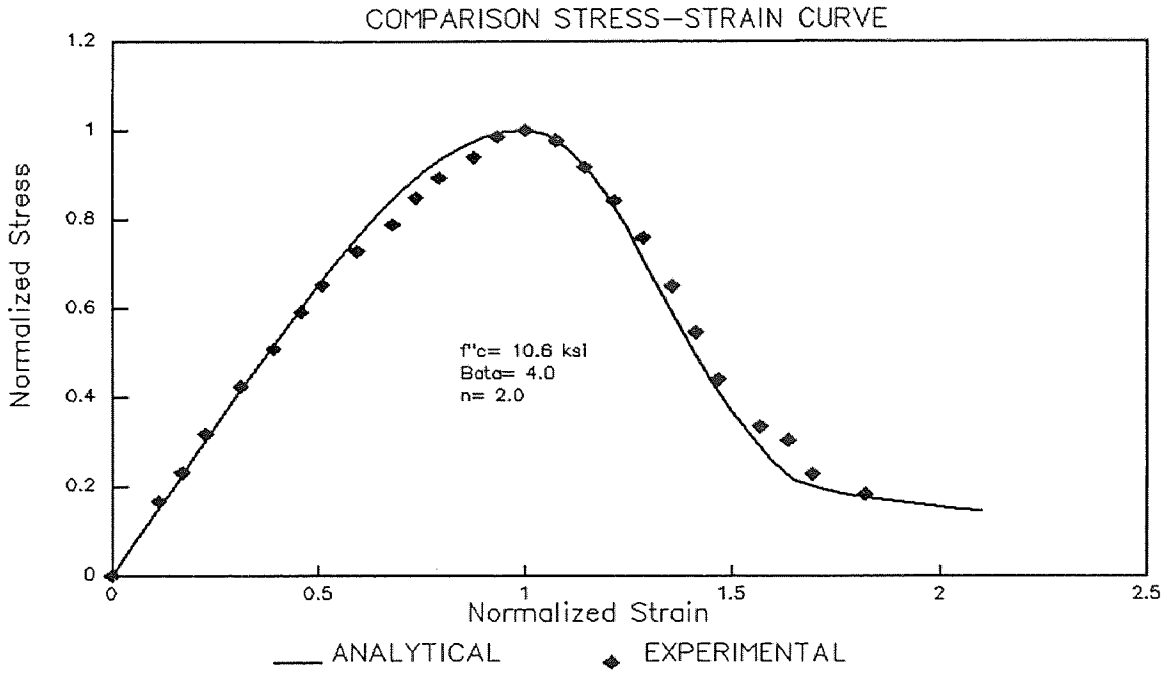

Figure 2.62 Proposed Model vs Wnag's Experimental Data (Wang,1978).

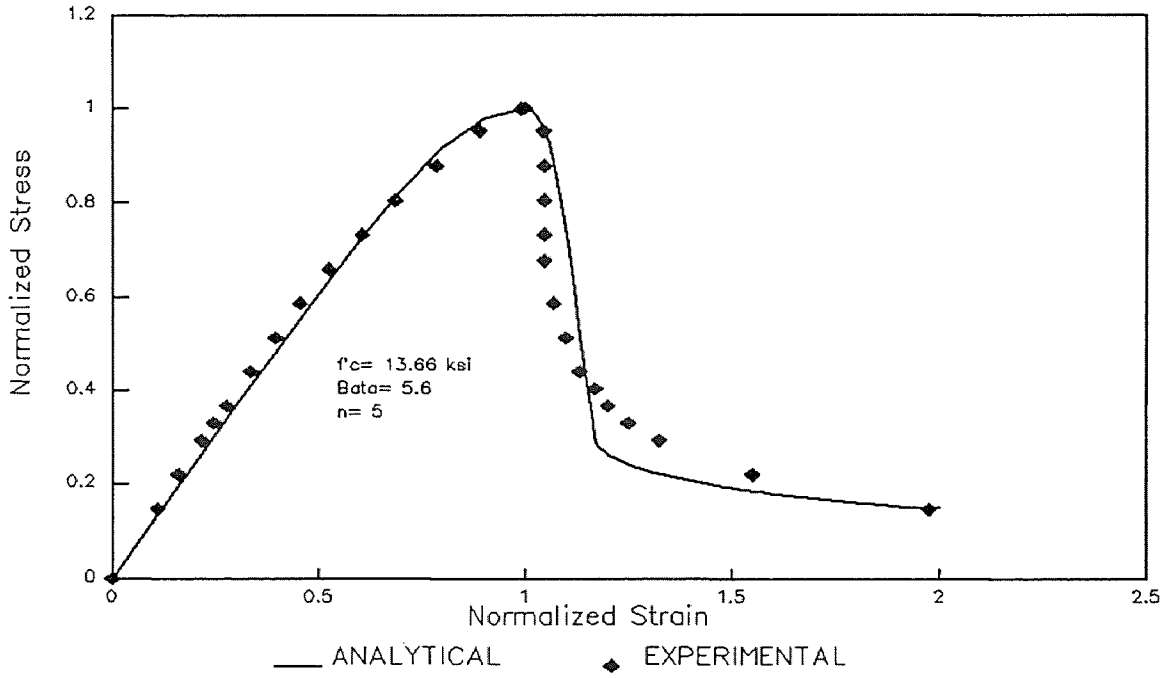

Figure 2.63 Proposed Model vs Shah's Experimental Data (Shah,1981).

CHAPTER THREE

BEHAVIOR OF BIAXIALLY LOADED PLAIN AND STEEL FIBER HIGH STRENGTH REINFORCED CONCRETE SLENDER COLUMNS

3.1 Introduction

The use of high strength concrete in the columns of high-rise buildings has a significant economic benefit. As far as the high strength concrete columns are concerned, most of the previous research work has concentrated on members subjected to axial compression only. In practice, some columns are subjected to bending about both principal axes simultaneously, especially the corner columns of the buildings or the columns in the bridges.

The use of high strength concrete column can reduce its column size, but, becomes more brittle due to its inherent behavior of high strength concrete. There are, in general, two ways to improve the ductility of the column. One is to increase the lateral ties of the column, and the other is to add the steel fibers to the high strength concrete column. In this study, primary objective for these column tests is to study the complete load-deformation behavior of biaxially loaded slender columns with (and without) steel fibers. To study the ductility of the columns, different spacing of lateral ties and fiber volume fraction are being examined. All columns were constructed using the concrete with compressive strength ranging from 10 ksi to 12 ksi.

Two types of columns were tested: plain high strength columns and high strength steel fiber columns. L-series was designated for high strength columns and FL-series was designated for the high strength steel fiber columns, respectively. These columns were tested under combined biaxial bending and axial compression. Different eccentricities, the amount of tie confinement, and the fiber content were used to characterize the behavior of the slender columns.

Tensile test for main reinforcing bars (steel), #2 and #3, were done by Tinus & Olsen tension & compression test machine. All concrete cylinders and columns were tested using the MTS servo-control close-loop system. The experimental results for the load-deformation behavior of biaxially loaded slender columns are compared with theoretical results developed in the following.

3.2 Objectives

The objectives for the study of this chapter are as follows:

i) To test and study the behavior of high strength slender columns with (and without) steel fibers under combined biaxial bending and axial compression. The proportional loading and pinned-ended condition are used for the present column tests.

ii) To compare the present experimental results with the theoretical analysis developed for the load-deformation behavior of high strength slender columns. The theoretical result is obtained by modifying an existing computer program of slender columns developed recently at NJIT (Wang and Hsu 1990, Tsao 1991). The empirical stress-strain equations developed in chapter 2 are used to characterize the stress-strain behavior of the concrete in the computer program.

3.3 Theoretical Analysis of Standard Shaped Slender Column Under Combined Biaxial Flexure and Axial Load

To study the complete load-deflection and moment-curvature curves of standard shaped slender columns subjected to biaxial bending and axial compression under monotonic loading, the strain compatibility and equilibrium of forces and moments which can account for any loading condition and material properties, must be utilized.

The present computer analysis is based on the following assumptions:

1. Plane section remains plane before and after bending.

2. Strains in the steel and concrete at their interfaces are assumed to be compatible.
3. Effect of creep and shrinkage are neglected.
4. No initial deflection in the undeformed columns exists.
5. Axial deformation, shear deformation and torsional effects are all neglected.
6. Monotonic loading is used.

The cross section of a standard shaped slender column can be divided into several small elements as shown in Fig. 3.1. Consider for each small element k, with its centroidal coordinates (x_k,y_k), the strain, ε_k, is assumed to be uniformly distributed across the element k. According to the assumptions that plane section remains plane, and for an element that is subjected to biaxial bending and axial compression, the strain, ε_k, can be expressed in the following form:

$$\varepsilon_k = \varepsilon_o + \phi_x y + \phi_y x \tag{3.1}$$

where

ε_o : strain at the coordinate origin of the principal axis.

ϕ_x : curvature with respect to M_x. ϕ_x is positive when it can produce compressive strains in the positive y direction.

ϕ_y : curvature with respect to M_y. ϕ_y is positive when it can produce compressive strains in the positive x direction.

An idealized piecewise linear stress-strain curve for steel (Fig. 3.2) and the empirical equations for the stress-strain curves of high strength concretes from the previous chapter have been used for the reinforcing steel and concrete elements, respectively. For a value of strain ε_k, a value of the secant modulus of elasticity $(E_s)_k$ for steel or concrete element can be obtained from the steel stress-strain curve and concrete stress-strain curve (unconfined and confined), respectively. The secant modulus of

elasticity can be assured to give the positive values of $(E_S)_k$ and to prevent the singularity problem in the matrix operation. The equilibrium equation in the cross section with n elements for the axial load P, bending moment components M_X, M_Y can be expressed in the following forms:

$$P_{(c)} = \sum_{k=1}^{n} (E_s)_k \varepsilon_k a_k \tag{3.2}$$

$$M_{x(c)} = \sum_{k=1}^{n} (E_s)_k \varepsilon_k a_k y_k \tag{3.3}$$

$$M_{y(c)} = \sum_{k=1}^{n} (E_s)_k \varepsilon_k a_k x_k \tag{3.4}$$

where

$(E_S)_k$: the secant modulus of elasticity in the element k

ε_k: strain of element k

a_k: area of element k

x_k, y_k: coordinates at the centroid of element k

The subscript (c) from $P_{(c)}$, $M_{X(c)}$, $My_{(c)}$ expresses the calculated values in an iteration cycle.

The finite difference method was introduced to calculate the deflections which satisfy the compatibility equations.

For slender column, the second order effect is important and for the case of proportional loading. Let d_X, d_Y be expressed the deflections of column in x and y axis, respectively. Therefor, the biaxial bending moment $M_{x(lc)}$, $M_{y(lc)}$ at the middle segment can be calculated as follows:

$$M_{x(lc)} = P_{(c)}(e_y + d_{y(lc)}) \tag{3.5}$$

$$M_{y(lc)} = P_{(c)}(e_x + d_{x(lc)}) \tag{3.6}$$

Other details of the theoretical analysis can be found in the reference by Wang and Hsu (1990), and Tsao (1991).

3.4 Experimental Scheme

3.4.1 Material and Mixing proportion

The materials consisted of Type I cement satisfying with ASTM 150, sand from the local source, basalt with maximum aggregate size of 3/8 in., tap water, silica fume (SF) in powder form with 96% of SiO_2, and the superplasticizers (SP) to maintain a good workability. The mix proportions are shown in Table 2.2.

Hooked ends steel fiber with aspect ratio (ℓ / d) of 60 were used. These steel fibers are made from low carbon, cold draw steel wire. They were glued together on sides with water soluble glue to form bundles (collated). The specific gravity of fiber is 490 lb/ft^3. The steel fibers at different volume fraction of 0.5%, and 1.0% were randomly mixed into the high strength concrete.

The reinforcement consisted of four No. 2 or No. 3 deformed bars which are tied by 12 gage steel wires (f_y=66.1 ksi) at spacing 2 in. or 3 in. intervals.

3.4.2 Mixing, Casting, and Curing

A rotating drum mixer was used to mix the components. The mixed material for each batch made enough one column and some control cylinders.

For steel fiber concrete, the same mixing procedure mentioned in chapter 2 was used. The high strength concrete column with fiber contents was at 0.5% and 1.0%, respectively.

To determine the compressive strength of concrete, five 3 in. by 6 in. control cylinders were cast and cured under conditions identical to the test column specimens.

For making a column, the reinforcements were assembled into a unit before it placing in the mold as shown in Fig. 3.3. Two forms were built by using 5/8 in. thick plywood as shown in Fig. 3.4. To prevent bulging of side walls, the plywood was braced horizontally. Before casting the column, the form was cleaned and oiled with a thin layer of motor oil to facilitate the easy removal of specimens. The columns were cast in the plywood forms in a horizontal position so that both the strength and fibers can assure better uniformity and randomly distributed. An electrically driven vibrator and steel rod were used to vibrate and compact the concrete. After 24 hours, the column and cylinders were removed from their forms and cured in water until one day before testing.

3.4.3 Test Specimens

Nine square high strength columns and five square high strength steel fiber columns were cast for this study. Table 3.1 and 3.2 list their specifications. The dimensions of column is 3-in. by 3-in. square and 48-in. long. The details of geometry of specimens are shown in Fig. 3.5. Two loading brackets were provided at each column end to assist with the application of biaxially eccentric loads. These brackets were heavily reinforced to prevent any premature failure. The variable parameters are main bars, the eccentricity of axial compression, steel fiber content and the spacing of tie confinement.

The columns were reinforced with four No. 2 or No. 3 steel bars as main bars. The typical stress-strain curve for No. 2 and No. 3 deformed bar are shown in Figs. 3.6 through 3.8.

The cover with 0.5-in-thickness to the longitudinal bars was to protect the steel bars. 12-gage plain steel wire was used for the lateral ties.

3.4.4 Experimental Setup

The main objective for the column tests was to study the complete load-deformation behavior of biaxially loaded slender columns with and without steel fibers.

The columns were loaded with different eccentricities by using a stroke control at a strain rate of 0.05 in./min. on MTS testing machine. Thus, the results caused a combined axial compression and biaxial bendings about x and y axis .

To avoid local failure at the column ends, steel plates were attached to each end of the specimens. The axial load was transmitted to column at each end by the steel plate. Hinged end conditions were provided at both ends for all test columns. The details of experimental setup are shown in Fig. 3.9 and Fig. 3.10.

To obtain a complete ascending and descending branches of biaxial load-deflection curve, stroke control was used during the test. Loads were applied in a small increments. After each increment, the cracks on the specimens were examined and the readings were recorded from the dial gages and demec gages (mechanical strain gage). All experiments were carried out beyond the peak load and were terminated when the pined-ends can not rotate any longer.

Eight Ames dial gages were used to measure the defections at the beginning of brackets and at the mid-height of the column in both x- and y- directions. These dial gages were located near the centroid of the compression side. If the dial gages moved away from the centroid of the compression side during the test (due to the column deflection), they were adjusted. If the concrete was crushed and spalled off exactly at the place where the dial gages located, further measurements were not recorded. The mechanical strain gages were provided to measure the strain at the central portion of the column so that the average curvatures in both x- and y- directions at mid-height can be

attained. Fig. 3.11 shows the arrangements of mechanical strain gages for the present slender column specimens. If the concrete spalled off outside the 6 in. measured range (3 in. each side from the mid-height of the columns), further measurements were not recorded. It is because at this time, the plastic hinge does not rotate at the mid-height as desired.

3.5 Method for Analysis of Test Results

The applied load, P, can be determined directly from the MTS system. The deflections (d_x and d_y) and deformations at mid-height of the column are visually recorded by the dial gages and mechanical strain gages, respectively.

The experimental values of bending moments in x- and y-direction, M_x and M_y, are computed using the experimental axial load values and the load eccentricities (e_x and e_y) which are corrected for the mid-height deflections of the column (i.e. $M_x = P(e_y+d_y)$ and $M_y = P(e_x+d_x)$). The experimental ultimate load and moment capacities (P_{max}, M_x, and M_y) of the plain high strength and fibrous high strength columns are summarized in Table 3.3 and 3.4, respectively.

The deflection, d, can be calculated by $d = d_i - d_o$, where d_i represents the readings from the dial gage for each increment of loading, and d_o represents the initial reading from the dial gage . There are two dial gages in both x- and y-direction at mid-height of the column. Thus, the average deflections in x- and y-direction can be computed for each increment of loading.

The strains, ε, can be calculated by $\varepsilon = (\ell_i - \ell_o)/\ell_o$, where ℓ_o represents the initial length of mechanical strain gages at zero loading and ℓ_i represents the length of the mechanical strain gages at each loading. After determining the strains from mechanical strain gage points which locate at 1, 2, 3 and 4 for x-direction and at 5, 6, 7, and 8 for y-direction, the strain-position curves are drawn as shown in Appendix J for

plain high strength column and in Appendix M for fibrous high strength column. The slope of the strain-position curve represents its corresponding curvature which is shown in Appendix J and K for plain high strength and fibrous high strength columns, respectively. Usually, a strain distribution curve is linear. If the strain distribution curve is not linear, a straight line by a linear regression method is used to compute its curvature value.

3.6 Results and Discussion

3.6.1 Plain High Strength Concrete Column

Table 3.1 lists the dimensions of the plain high strength concrete columns and their experimental conditions. Specimen L1 is a trial column specimen. Its test results are not reported. Table 3.3 lists the experimental values of the maximum axial load and moment capacity for plain high strength columns.

The effect of tie confinement on high strength column was investigated using different tie spacing. Two kinds of tie spacing, 2-in and 3-in, respectively, were used in this study.

Table 3.3, lists the maximum axial load and moment capacity for L3 and L8 columns with 3-in and 2-in tie spacing, respectively. The results seemingly indicate that the tie confinement does not affect the ultimate strength of the column,

When the biaxially load is applied to a high strength column, an unfavorable explosive type of failure occurs after reaching the peak load. This is due to brittle behavior of a high strength concrete. The use of tie confinements helps minimize the violence of this brittle failure. Table 3.5 lists the failure phenomena of different column specimens. In the Table, the length of spalled-off for column L8 is shorter than that for column L3. As a result, tie confinement affects the failure behavior. Sometimes, the

failure zone of the column does not locate at its critical section (center of column). This phenomenon indicates that the column does not bend in a symmetrical curvature.

The failure patterns of the high strength columns are shown in Appendix L. Cracking behavior was observed during testing. The columns showed some flexure cracks before reaching its peak load. Fig. 3.12. shows the high strength columns after testing to failure.

Fig. 3.13 shows typical normalized load-deflection curves for column L3 (tie spacing = 3 in) and L8 (tie spacing = 2 in) at different amount of confinement. The figure shows that the slope of descending curve of L8 is higher than that of L3, which indicates that the load-carrying capacity drops slowly with increasing confinement. Thus, the addition of confinements to column results in an improvement of its ductility.

3.6.2 High Strength Steel Fiber Reinforced Concrete Column

Table 3.2 lists the dimensions of five high strength fibrous columns and their experimental conditions. Table 3.4 lists their experimental values of the maximum axial load and moment capacity.

Both the column L3 and column FL1 (with fiber) were constructed and tested using the same conditions except that the specimen FL1 had fibers at volume fraction of 1.0%. By comparing their ultimate capacities as seen in Tables 3.3 and 3.4, it shows that the addition of fibers does not affect their ultimate load and moment capacity of the column. Fig. 3.14 shows the typical normalized load-deflection curves for column L3 and FL1 (with fiber) . This figure shows that the slope of descending curve of FL1 is higher than that of L3, which indicates that the load-carrying capacity drops slowly for the column with steel fibers. Thus, the addition of fibers to a column results in an improvement of its ductility, however only a slightly increase. Craig and co-workers (Craig 1984) also showed that the ductility for a normal strength fibrous column was only slightly increased with increasing steel fibers. To significantly improve the column

ductility, the fibers need to be placed in the outer cover of the column in order to help confine the concrete core.

The typical failure and crushed modes of high strength steel fiber columns are shown in the photographs of Appendix M. Fig. 3.15 shows the high strength fibrous columns after testing to failure. During the phases of each test, cracking behavior was observed and recorded (Table 3.6). On the average, the crack length for high strength fibrous column is shorter than that for plain high strength columns (see Table 3.5 and 3.6). The shorter crack length is due to the fact that the fibers help confine the concrete and delay the crack propagation. During the column test, the high strength column has an unfavorable explosive type of failure as indicated in the previous section. This explosive type of the failure has been reduced by adding the fibers to the column.

3.6.3 Comparison of Experimental Results and Theoretical Model

3.6.3.1 Plain High Strength Concrete Column

3.6.3.1.1 Ultimate Load and Load-Deflection Curves. Experimental values of the axial-load capacity shown in Table 3.7 are obtained directly from the tests and the theoretical values are calculated based on the computer analysis and program developed by Wang and Hsu (Wang and Hsu 1990) and Tsao (Tsao 1991), respectively. This computer analysis program has been modified for this study. $P_{test}/P_{analysis}$ represents the ratio of P_{max} obtained from the experimental result to P_{max} calculated from the theoretical analysis by a computer program. Table 3.5 also lists the values of $P_{test}/P_{analysis}$ and its average value of 1.04. Therefore, an examination of the results shows a good agreement between the experimental ultimate load and the computed values with various parameters, f'_c, f_y, e_x, e_y, and S.

The load-deflection curves of plain high strength columns from the theoretical analysis and from the experimental results are shown in Appendix N. Generally

speaking, the load-deflection curves between the theoretical analysis and the experimental results show a good agreement from zero load up to peak load, P_{max}; after the peak load, the present computer analysis slightly overestimates the descending branch of curve. The results indicate that the use of the proposed stress-strain model (see Chapter 2) in the theoretical analysis give a reasonable accuracy in predicating the behavior of the high strength reinforced concrete slender columns subjected to combined biaxial bending and axial load.

3.6.3.1.2 Ultimate Moment Capacity and Moment-Curvature Curves. Table 3.8 shows two maximum moment capacities, one by using the theoretical model, $M_{x(2)}$ and $M_{y(2)}$, another one from the experimental result, $M_{x(1)}$ and $M_{y(1)}$. As the results, both ratios of $(M_{x(1)}/M_{x(2)})$ and $(M_{y(1)}/M_{y(2)})$ are 1.066 and 1.085, respectively, which indicate a good agreement between the experimental and theoretical results.

For a slender column, the maximum moment is not always occurred at the maximum load of the column due to second order effect. In other words, the maximum moment is not necessary to correspond to its maximum load all the time. The comparison of the present theoretical and experimental moment-curvature curves are shown in Appendix L The comparisons between the experiment and the analysis show a satisfactory agreement. Some moment-curvature curves from the experimental data do not show a descending branch. This termination of the measurement was due to the disloading of mechanical strain gages or the crushing of concrete has occurred outside the critical section, i.e. the plastic hinge does not locate at mid-height of the column.

3.6.3.2 High Strength Steel Fiber Reinforced Concrete Column

3.6.3.2.1 Ultimate Load and Load-Deflection Curve. Experimental values of axial-load capacity for the high strength fibrous reinforced concrete columns shown in Table 3.9 are obtained directly from the tests and the theoretical values are calculated based on

the computer analysis that was developed by Wang and Hsu (Wang and Hsu 1990), Tsao (Tsao 1991), respectively. The present analysis is a modification of Tsao's computer program. Table 3.9 also lists the values of $P_{test}/P_{analysis}$ and its average value of 1.06. An examination of the results shows that a good agreement is achieved between the experimental ultimate load and the computed values with various parameters, f'_c, f_y, e_x, e_y, and V_f.

The load-deflection curves of high strength fibrous concrete columns from the present theoretical analysis and from the experimental results are shown in Appendix O. Generally speaking, the biaxial load-deflection curves between the theoretical analysis and experimental results show a good agreement.

In a high strength fibrous reinforced concrete column, the descending branch of the experimental load-deflection curve does not behave steeply as that in the plain high strength column. This behavior shows that the addition of the steel fibers definitely improves its ductility. Craig and co-workers (Craig, 1984) reported that the ductility of the column was improved by adding the steel fibers in the column.

3.6.3.2.2 Ultimate Moment Capacity and Moment-Curvature Curve. Table 3.10 shows the capacities of the maximum bending moments about x- and y-axis; In the Table, $M_{x(1)}$ and $M_{y(1)}$, $M_{x(2)}$ and $M_{y(2)}$ represent the maximum moments from the experimental result and the present theoretical analysis, respectively. As shown, the ratios of $(M_{x(1)}/M_{x(2)})$ and $(M_{y(1)}/M_{y(2)})$ are 1.00 and 0.99, respectively, which yield an excellent agreement between the experimental and theoretical results.

The comparisons of the theoretical and experimental moment-curvature curves for high strength steel fiber reinforced concrete columns are shown in Appendix O. These comparisons also show a good agreement. It is noted that the fibrous columns usually achieves a better comparison than that for the plain column of it load-deformation curves.

The above results indicate that the use of the proposed stress-strain relationship for a high strength fibrous concrete present in Chapter 2 gives a reasonable accuracy to predict the behavior of a high strength fibrous columns under combined biaxial bending and axial compression. The present analysis enables one to calculate the biaxial moment-curvature, load-deflection curves of the column from zero load up to failure, including the descending branch of the curves, Thus this study gives a complete information on the load-deformation behavior of the biaxially loaded fibrous reinforced concrete columns.

3.6.4 Comparison Between Normal and High Strength Concrete Columns

Fig. 3.16(a) shows two typical load-deflection curves for high strength (HSC) and normal strength (NSC) (Tsao 1991) columns with a compressive strength ($f_c^{'}$) of 10.715 ksi and 2.695 ksi, respectively. Their normalized load-deflection curves are shown in Fig. 3.16(b). Both specimens were constructed and tested using the same conditions except their compressive strength. As excepted, the deflection of HSC is lower than that of NSC. This beneficial effect is mainly due to a higher moldulus of elasticity for a high strength concrete. The experimental results show that the normal strength column undergoes a larger deflection than that for the high strength column under the same loading condition. Thus, the high strength column exhibits a steeper and more linear in the ascending branch of the curve than that for the normal strength column. The descending branch of HSC and NSC indicates that the load-carrying capacity drops faster for HSC than that for NSC. Therefore, one can conclude that the high strength column behaves more brittle than that for the normal strength column. To overcome this weakness for the high strength column tie confinements and/or addition of the fibers are found to be a necessity.

Fig. 3.17 shows the typical normalized load-deflection curves with different amount of confinements and steel fibers. The curves indicate that the load-carrying capacities drop slower with increasing tie confinement or steel fibers.

Table 3.1 High Strength Column Specimens

Specimen No.	Main Bars	f_v (ksi)	S (in)	e_x (in)	e_y (in)	L (ft)	ρ_g (%)	α (deg)	f'_c (ksi)
L1	4-#2	63.00	3	0.924	0.383	4	2.18	22.5	11.16
L2	4-#2	63.00	3	0.707	0.707	4	2.18	45	10.00
L3	4-#3	77.05	3	0.707	0.707	4	4.90	45	10.72
L4	4-#3	77.05	3	2.121	2.121	4	4.90	45	11.37
L5	4-#3	77.05	3	1.732	1.000	4	4.90	30	10.30
L6	4-#3	77.05	3	1.732	1.000	4	4.90	30	11.00
L7	4-#3	77.05	3	2.598	1.500	4	4.90	30	11.03
L8	4-#3	77.05	2	0.707	0.707	4	4.90	45	10.02
L9	4-#3	61.00	2	2.121	2.121	4	4.90	45	10.40

α: Arctan (e_y/e_x)

L: Total length of column

e_x: Eccentricity along x-axis

e_y: Eccentricity along y-axis

S: Spacing of lateral reinforcement

f_y: Steel yield stress

f'_c: Maximum Compressive strength of concrete

ρ_g: Steel percentage in gross cross-section area

Table 3.2 High Strength Steel Fiber Column Specimens

Specimen No.	Main Bars	f_y (ksi)	S (in)	e_x (in)	e_y (in)	L (ft)	ρ_g (%)	α (deg)	V_f (%)	f'_c (ksi)
FL1	4-#3	77.05	3	0.707	0.707	4	4.9	45	1.0	12.17
FL2	4-#3	77.05	3	1.848	0.765	4	4.9	22.5	1.0	11.48
FL3	4-#3	77.05	3	1.848	0.765	4	4.9	22.5	0.5	11.63
FL4	4-#2	63.00	3	0.924	0.383	4	2.18	22.5	1.0	10.58
FL5	4-#3	77.05	3	2.121	2.121	4	4.9	45	1.0	10.50

α: Arctan (e_y/e_x)

L: Total length of column

e_x: Eccentricity along x-axis

e_y: Eccentricity along y-axis

S: Spacing of lateral reinforcement

f_y: Steel yield stress

f'_c: Maximum Compressive strength of concrete

ρ_g: Steel percentage in gross cross-section area

V_f: Fiber volume fraction

Table 3.3 Ultimate Load and Moment from Experimental Results

Test Results of L-Series Columns			
Specimen Number	**P_{max} (kip)**	**M_x (kip-in)**	**M_y (kip-in)**
L1+	24.08	-	-
L2	22.51	25.18	24.87
L3	29.42	30.87	31.20
L4	9.43	25.4	24.89
L5	14.02	19.32	32.85
L6	15.44	19.71	35.30
L7	11.40	22.39	36.72
L8	28.30	28.64	31.64
L9	9.21	24.81	24.38

* P_{max}: Maximum load
* M_x: Maximum moment in x-direction
* M_y: Maximum moment in y-direction
* +: Trial specimen

Table 3.4 Ultimate Load and Moment from Experimental Results (with Fibers)

Test Results of FL-Series Columns			
Specimen Number	**P_{max} (kip)**	**M_x (kip-in)**	**M_y (kip-in)**
FL1	28.90	32.57	30.30
FL2	15.80	16.06	40.17
FL3	16.09	17.25	35.32
FL4	27.00	17.16	40.19
FL5	11.10	30.01	29.68

* P_{max}: Maximum load
* M_x: Maximum moment in x-direction
* M_y: Maximum moment in y-direction

Table 3.5 Failure Condition for High Strength Column Specimens

Test Results of L-Series Columns			
Specimen Number	**Location of Plastic Hinge**	**Length of Plastic Hinge**	**No. of buckled Bars**
L1+	At mid-height	2.36in.to 3in.	None
L2	At mid-height	3.54in. to 4in.	None
L3	At mid-height	5.12in. to 5.5in.	None
L4	At mid-height	7.48in. to 7.5 in.	None
L5	Between upper bracket and middle	2.56in. to 3in.	None
L6	Close to lower bracket	3.15in. to 3.5in.	None
L7	Close to lower bracket	9.45in. to 9.5in.	None
L8	At mid-height	3.54in. to 4in.	None
L9	Between lower bracket and middle	3.35in. to 4in.	None

* +: Trial specimen

Table 3.6 Failure Condition for High Strength Steel Fiber Column Specimens

Test Results of FL-Series Columns			
Specimen Number	**Location of Plastic Hinge**	**Length of Plastic Hinge**	**No. of buckled Bars**
FL1	At mid-height	3.15in. to 3.3in.	None
FL2	At mid-height	2.76in. to 3.0in.	None
FL3	Near mid-height	2.76in. to 3.0in.	None
FL4	Between lower bracket and middle	2.76in. to 3.0in.	None
FL5	Between lower bracket and middle	2.76in. to 3.0in.	None

Table 3.7 Ultimate Load Capacity for High Strength Column Specimens

Maximum Axial Load and Deflection Results							
Specimen Number	Test			Analysis			$\frac{P_{tset}}{P_{analysis}}$
	P_{max} (kip)	d_x (in)	d_y (in)	P_{max} (kip)	d_x (in)	d_y (in)	
L1+	24.08	-	-	26.66	-	-	0.90
L2	22.51	0.398	0.411	26.05	0.350	0.350	0.86
L3	29.42	0.353	0.342	24.85	0.350	0.350	1.18
L4	9.43	0.517	0.575	9.57	0.470	0.470	0.99
L5	14.02	0.611	0.378	13.88	0.579	0.350	1.01
L6	15.44	0.555	0.277	13.90	0.576	0.350	1.11
L7	11.40	0.623	0.464	9.69	0.604	0.350	1.18
L8	28.30	0.411	0.305	24.11	0.350	0.350	1.17
L9	9.21	0.526	0.579	9.57	0.590	0.590	0.96
Avg.							1.04

* P_{max}: Maximum load
* d_x: Deflection of the middle in the x-direction
* d_y: Deflection of the middle in the y-direction
* +: Trial specimen

Table 3.8 Ultimate Moment Capacity for High Strength Column Specimens

Maximum Moment Results						
Specimen Number	**Test**		**Analysis**		$\frac{M_{X(1)}}{M_{X(2)}}$	$\frac{M_{y(1)}}{M_{y(2)}}$
	$M_{X(1)}$ **(kip-in)**	$M_{y(1)}$ **(kip-in)**	$M_{X(2)}$ **(kip-in)**	$M_{y(2)}$ **(kip-in)**		
L1+	-	-	-	-	-	-
L2	25.18	24.87	27.54	27.54	0.91	0.90
L3	30.87	31.2	26.69	26.69	1.16	1.17
L4	25.42	24.89	25.31	25.31	1.00	0.98
L5	19.32	32.85	18.74	32.08	1.03	1.02
L6	19.71	35.30	18.79	32.08	1.05	1.10
L7	22.39	36.72	18.49	29.55	1.21	1.24
L8	28.64	31.64	24.15	24.15	1.19	1.31
L9	24.81	24.38	25.36	25.36	0.98	0.96
Avg.					**1.066**	**1.085**

* M_X: Maximum moment in x-direction
* M_Y: Maximum moment in y-direction
* +: Trial specimen

Table 3.9 Ultimate Load Capacity for High Strength Steel Fiber Column Specimens

Maximum Axial Load and Deflection Results							
Specimen Number	**Test**			**Analysis**			$\frac{P_{test}}{P_{analysis}}$
	P_{max} (kip)	**d_x (in.)**	**d_y (in.)**	**P_{max} (kip)**	**d_x (in.)**	**d_y (in.)**	
FL1	28.90	0.465	0.420	26.45	0.470	0.470	1.09
FL2	15.80	0.695	0.251	15.14	0.844	0.410	1.04
FL3	16.09	0.752	0.307	14.85	0.754	0.350	1.08
FL4	27.00	0.565	0.252	27.22	0.502	0.230	0.99
FL5	11.10	0.553	0.582	9.97	0.710	0.710	1.11
Avg.							**1.06**

* P_{max}: Maximum load
* d_x: Deflection of the middle in x-direction
* d_y: Deflection of the middle in y-direction

Table 3.10 Ultimate Moment Capacity for High Strength Steel Fiber Column Specimens

Maximum Moment Results						
Specimen Number	**Test**		**Analysis**		$\frac{M_{X(1)}}{M_{X(2)}}$	$\frac{M_{y(1)}}{M_{y(2)}}$
	$M_{X(1)}$ (kip-in)	**$M_{y(1)}$ (kip-in)**	**$M_{X(2)}$ (kip-in)**	**$M_{y(2)}$ (kip-ib)**		
FL1	32.57	30.30	31.13	31.13	1.05	0.97
FL2	16.06	40.17	17.79	40.76	0.90	0.99
FL3	17.25	35.32	17.18	38.65	1.00	0.91
FL4	17.16	40.19	17.75	39.44	0.97	1.02
FL5	30.01	29.68	28.22	28.36	1.06	1.05
Avg.					**1.00**	**0.99**

* M_X: Maximum moment in x-direction
* M_y: Maximum moment in y-direction

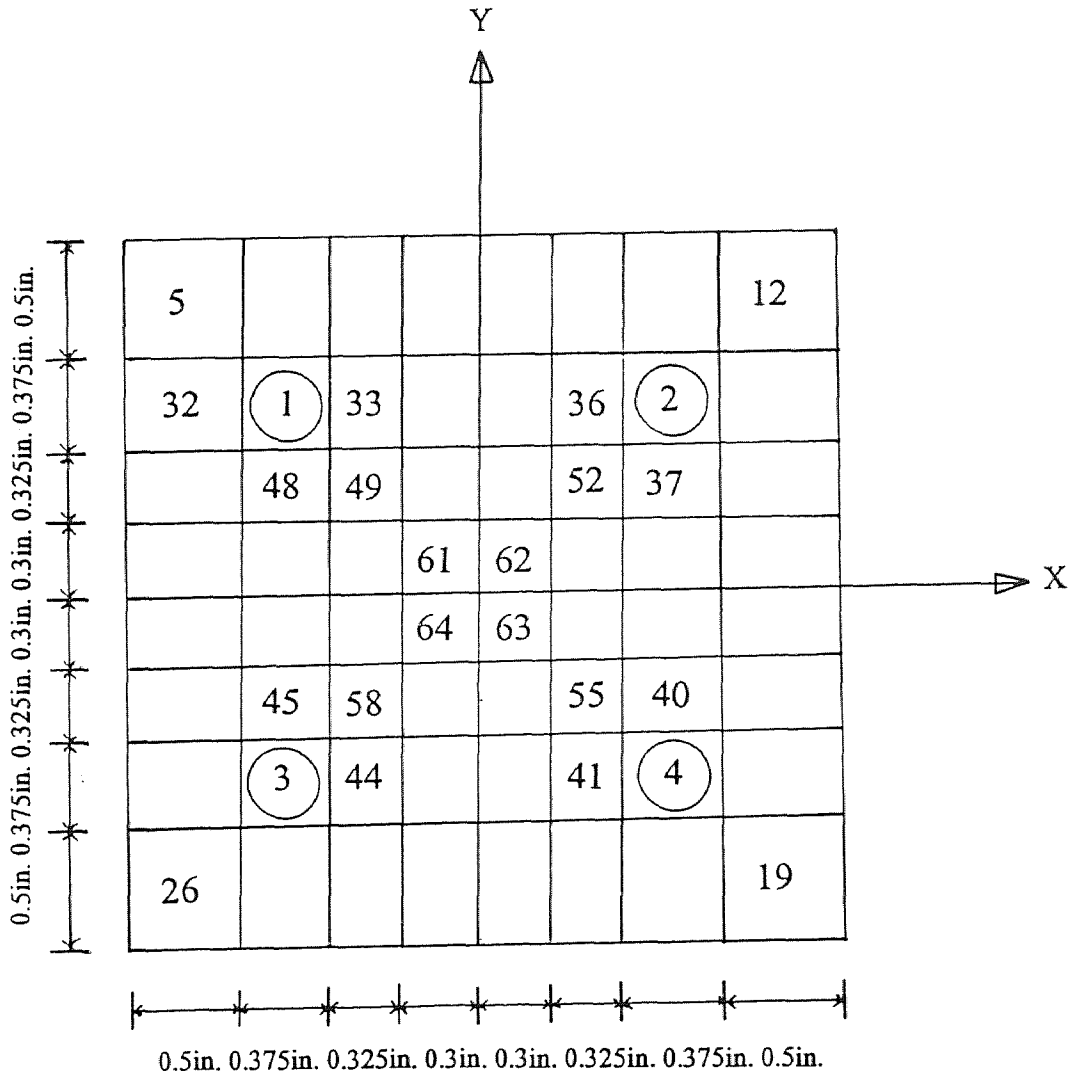

* Element 1 to 4 steel element
* Element 5 to 32 unconfined concrete element
* Element 33 to 64 confined concrete element

Figure 3.1 Cross Section of Square Slender Column for Computer Analysis.

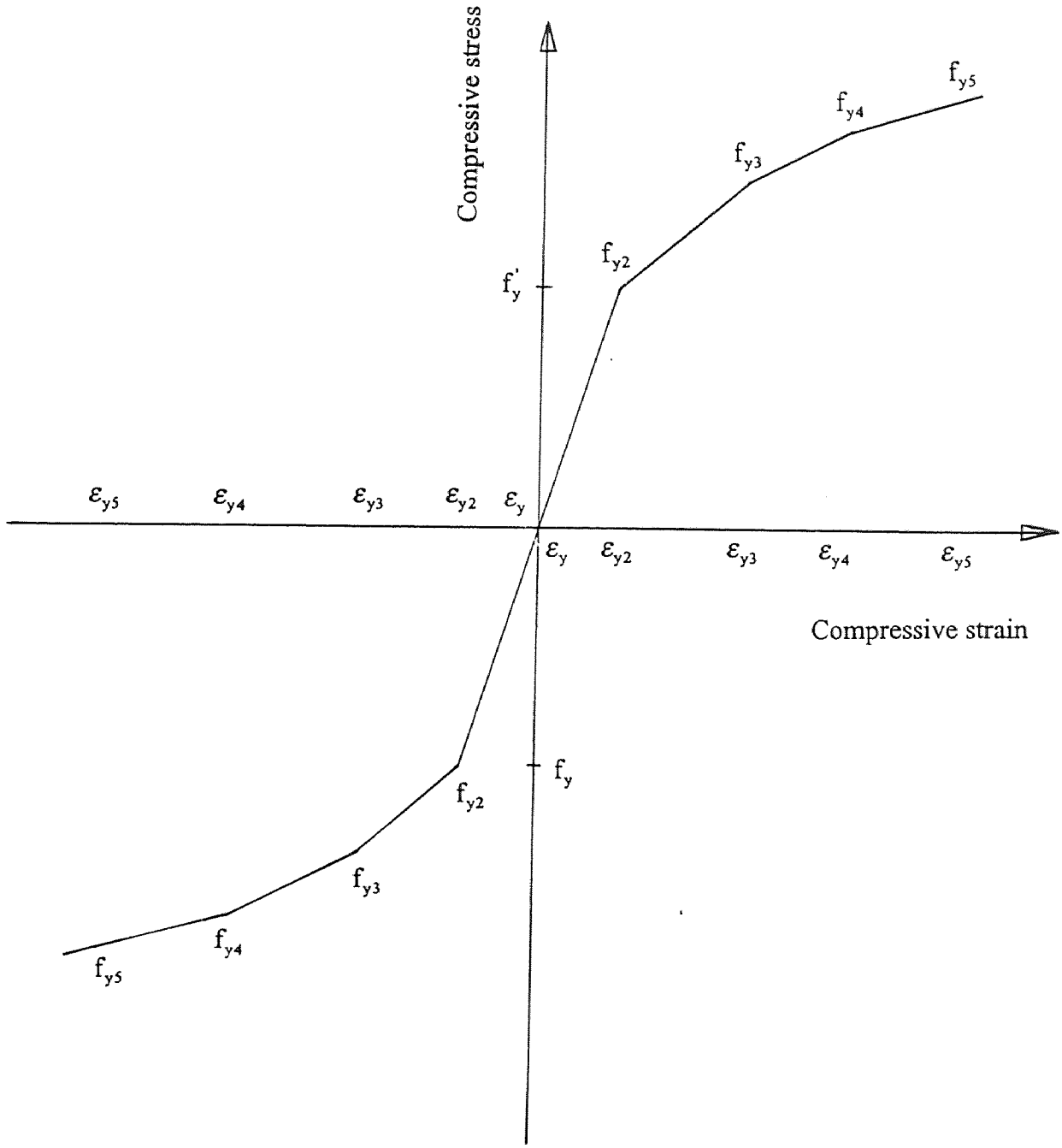

Figure 3.2 Idealized Piecewise Linear Stress-Strain Curve for Reinforcing Steel.

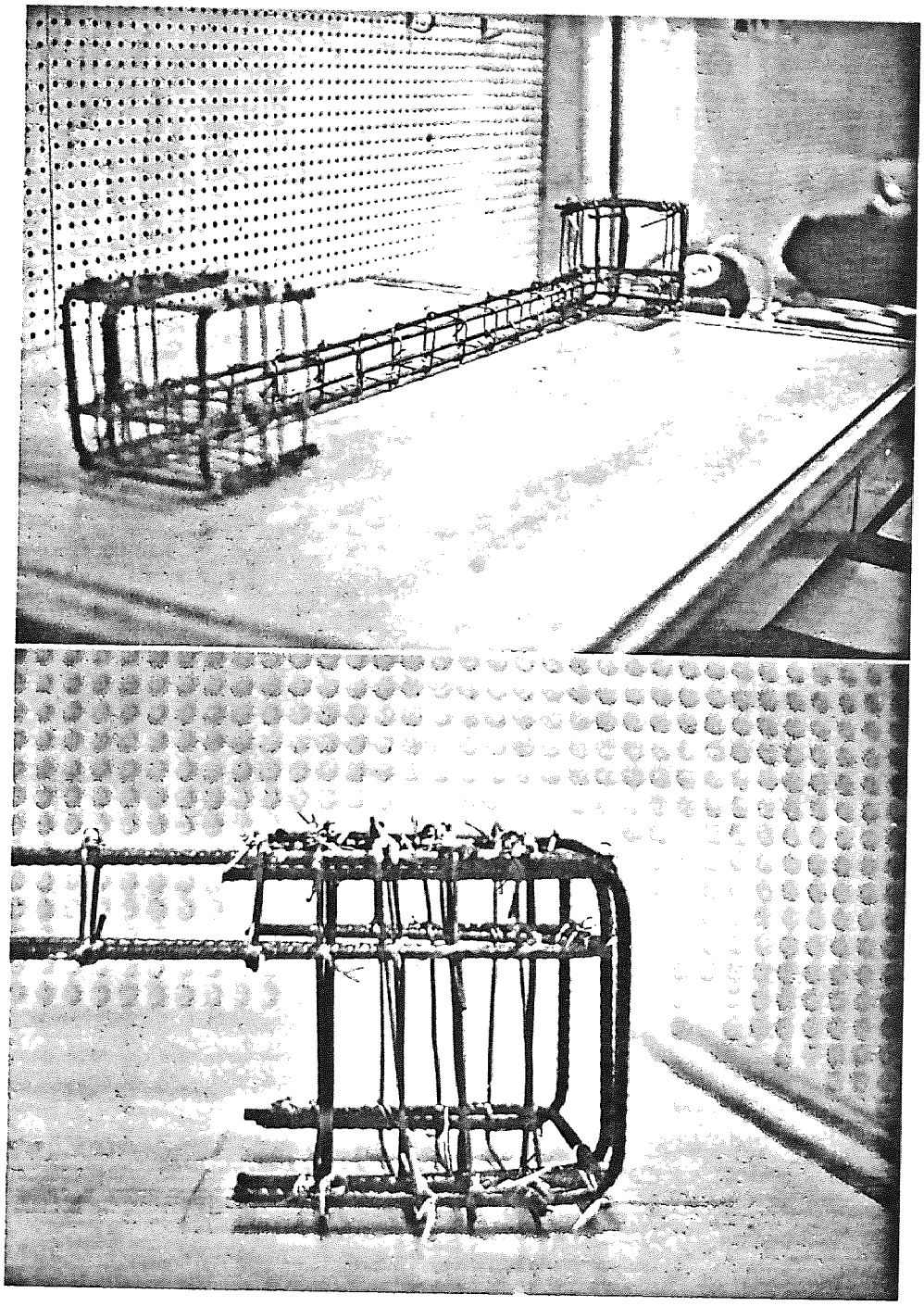

Figure 3.3 Reinforcement Details for Column Specimen.

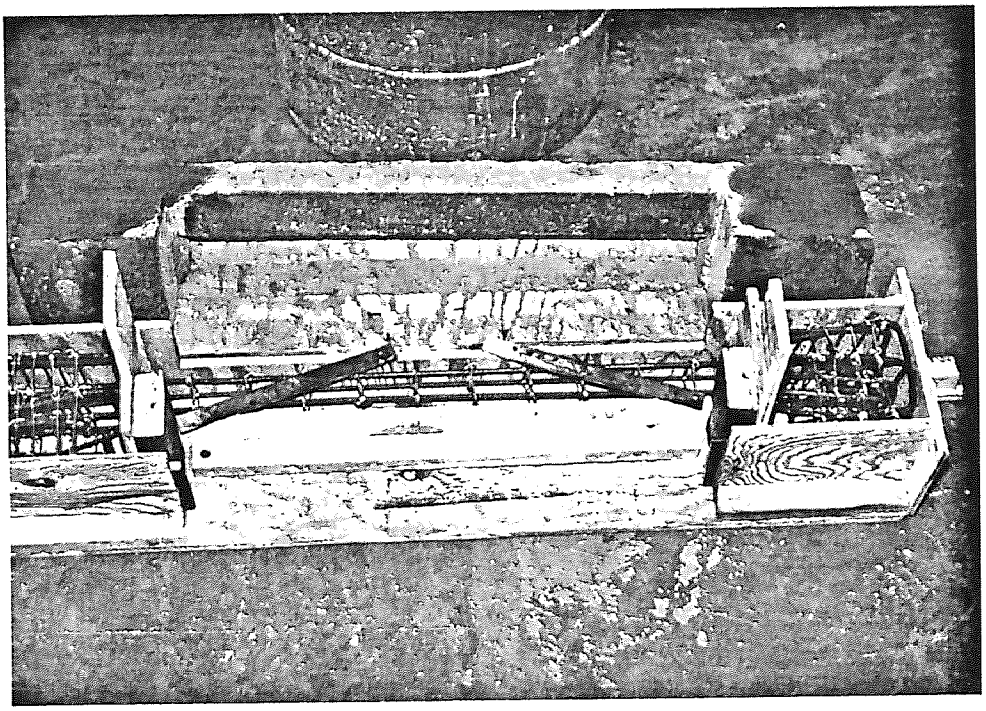

Figure 3.4 Details of Form Work.

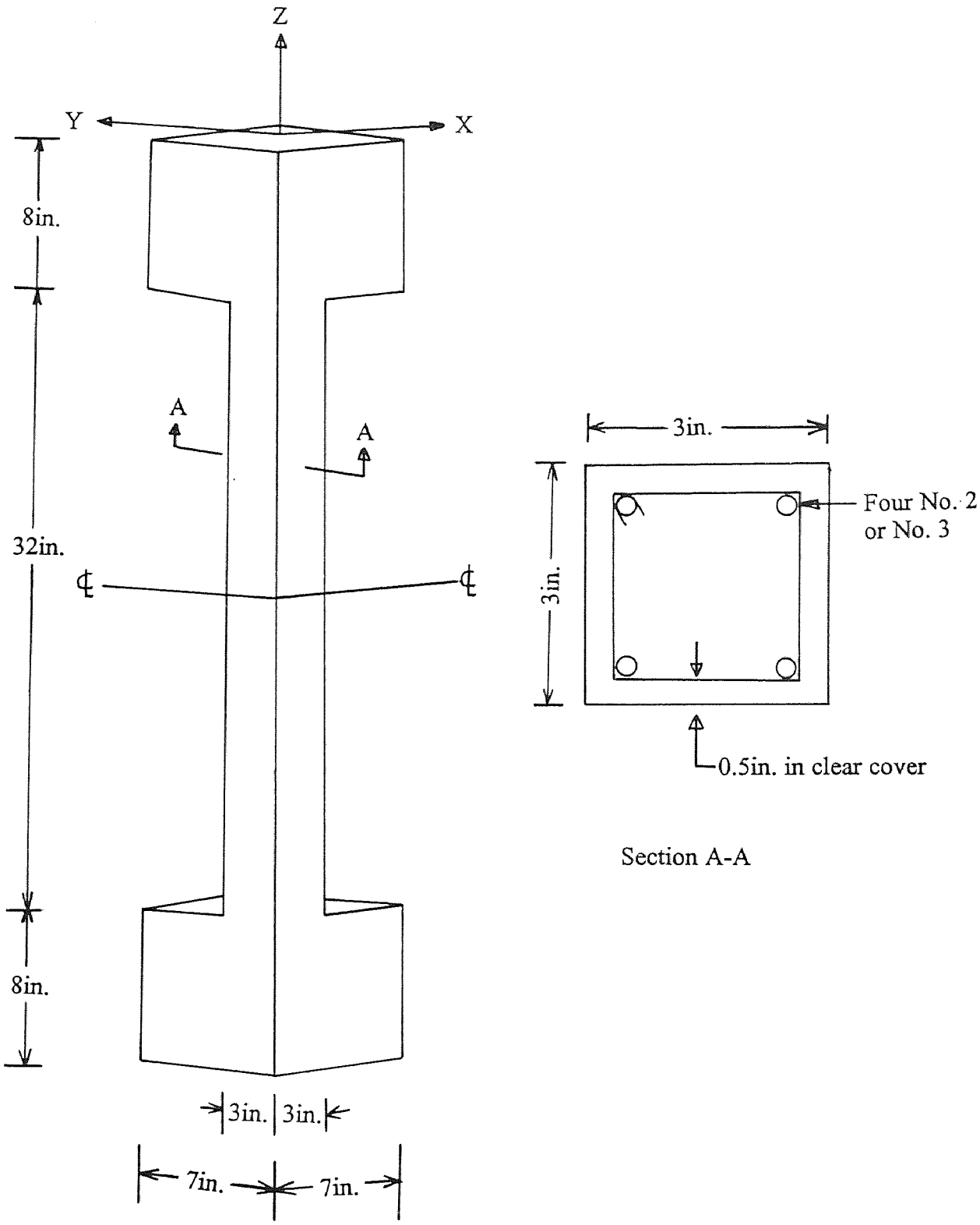

Figure 3.5 Details of Column Specimen.

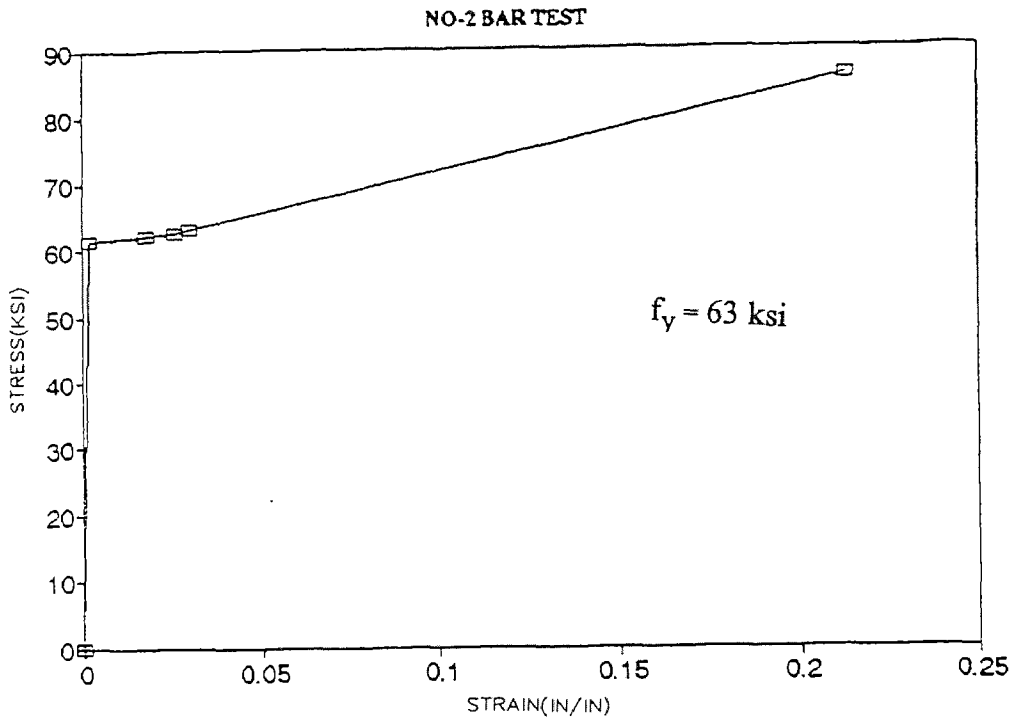

Figure 3.6 Stress-Strain Curve of No. 2 Reinforcing Bar.

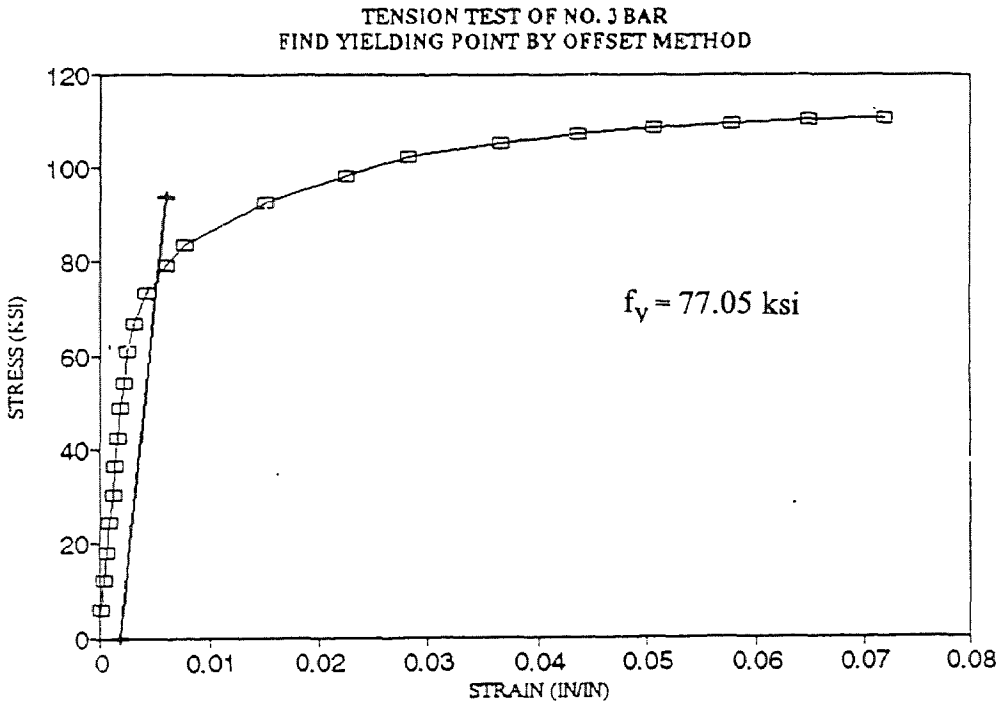

Figure 3.7 Stress-Strain Curve of No. 3 Reinforcing Bar.

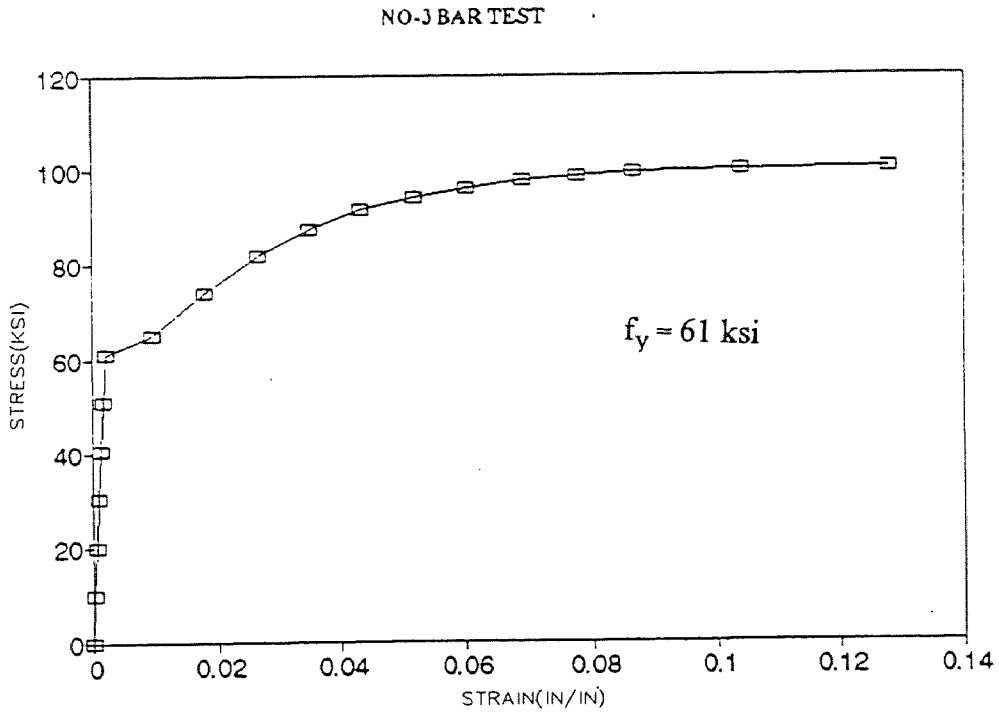

Figure 3.8 Stress-Strain Curve of No. 3 Reinforcing Bar.

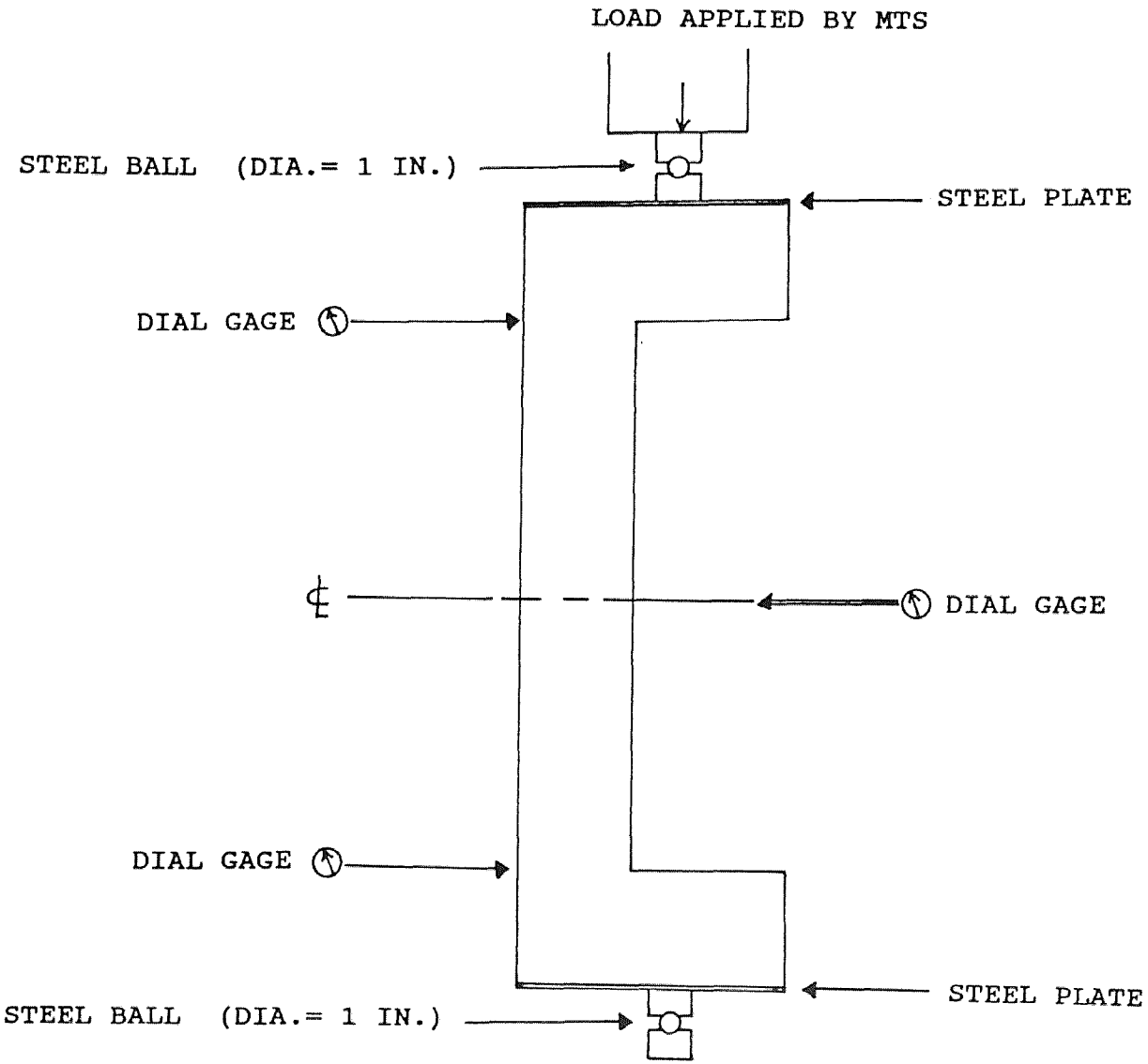

Figure 3.9 Loading and End Conditions for Pin-Ended Columns.

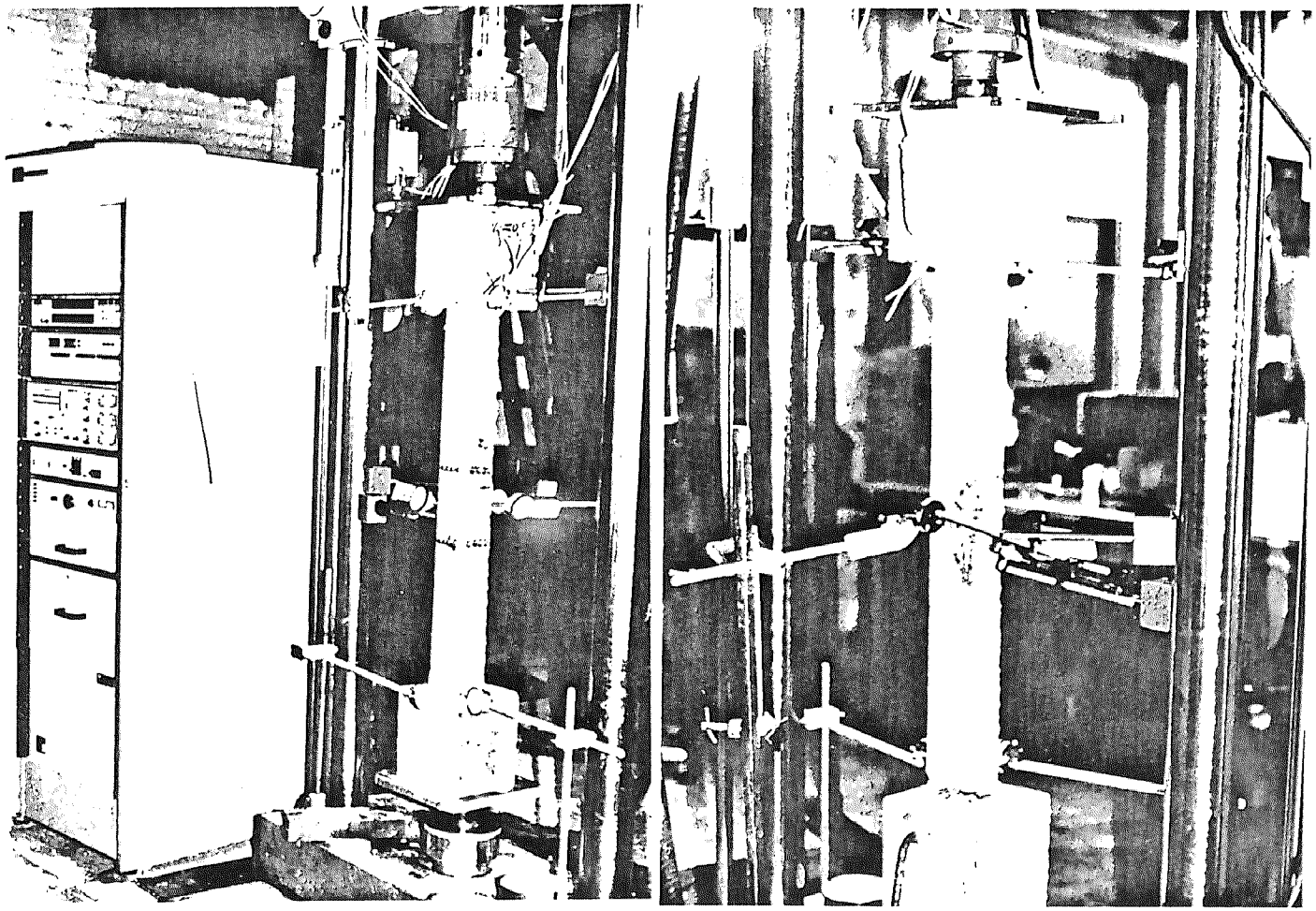

Figure 3.10 Experimental Setup for Column Test.

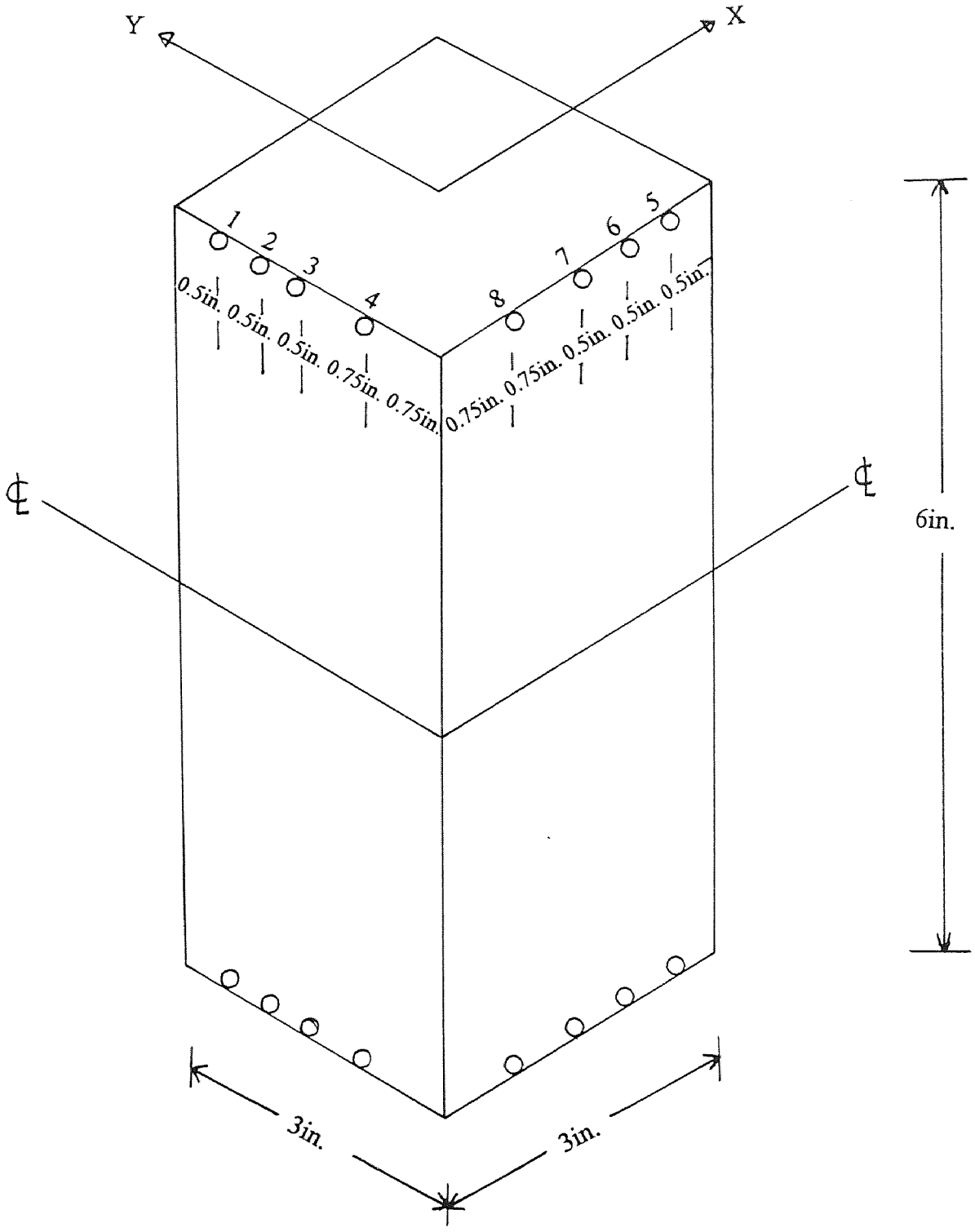

Figure 3.11 Arrangement of Mechanical Strain Gage Over the Segment of Column Member.

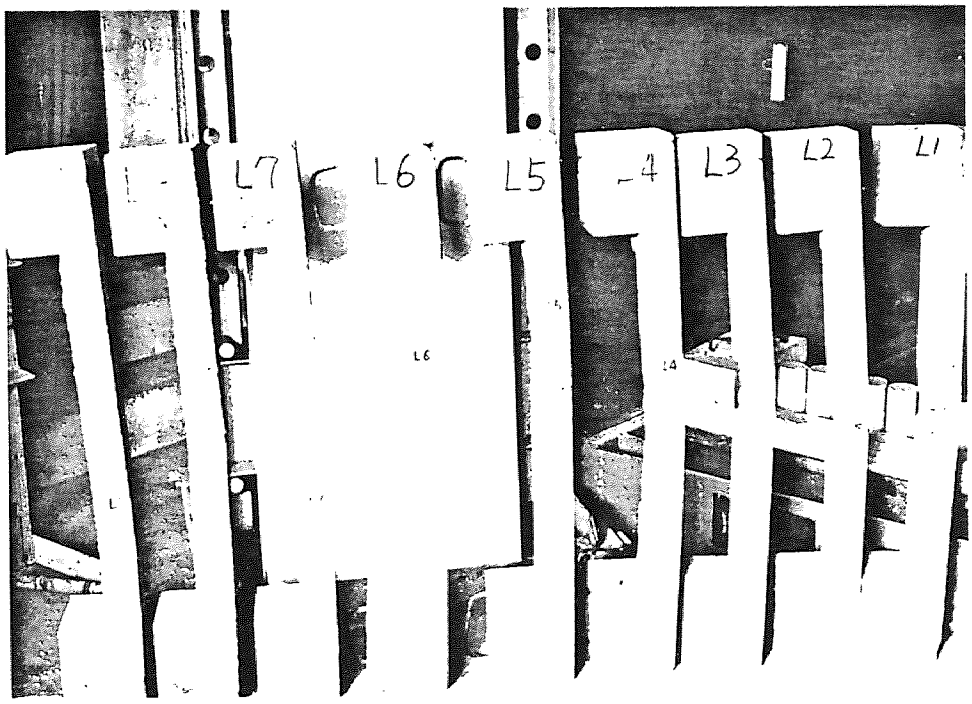

Figure 3.12 High Strength Columns after Failure.

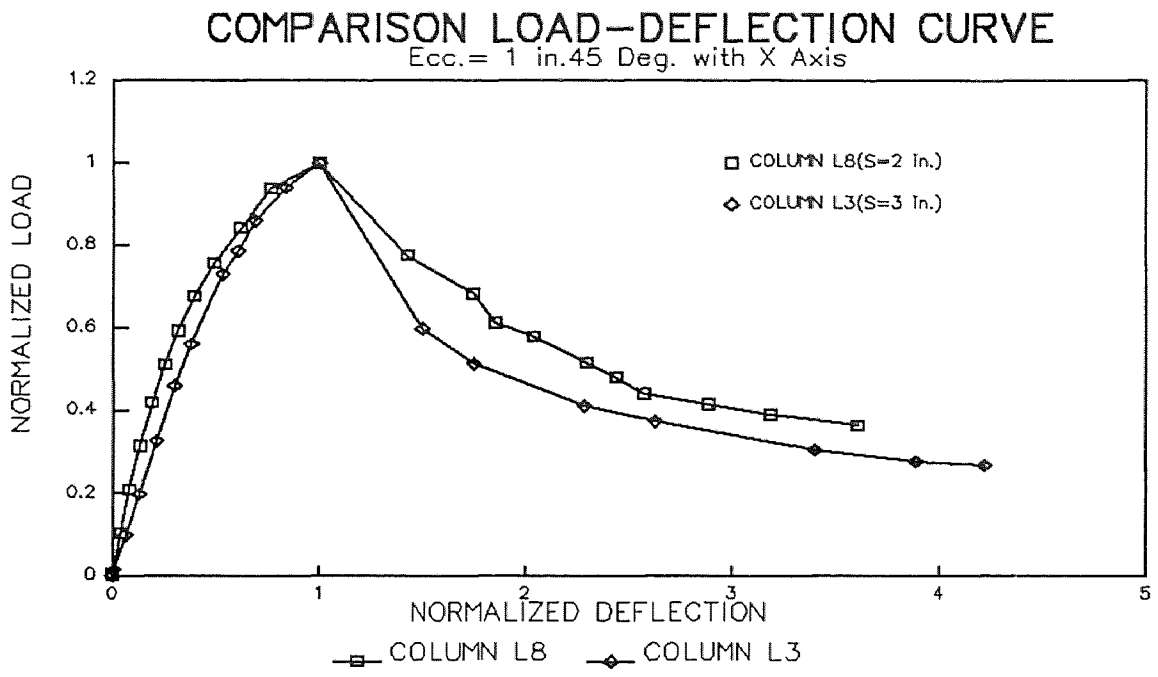

Figure 3.13 Effect of Tie Reinforcement on Ductility.

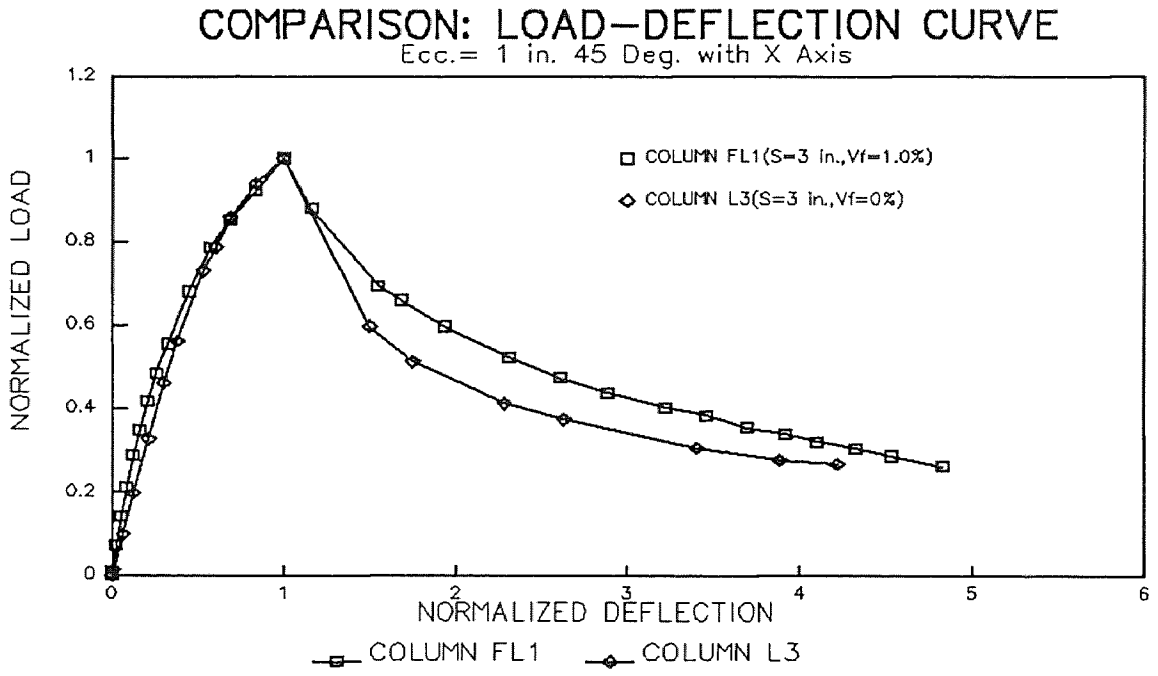

Figure 3.14 Effect of Steel Fiber on Ductility.

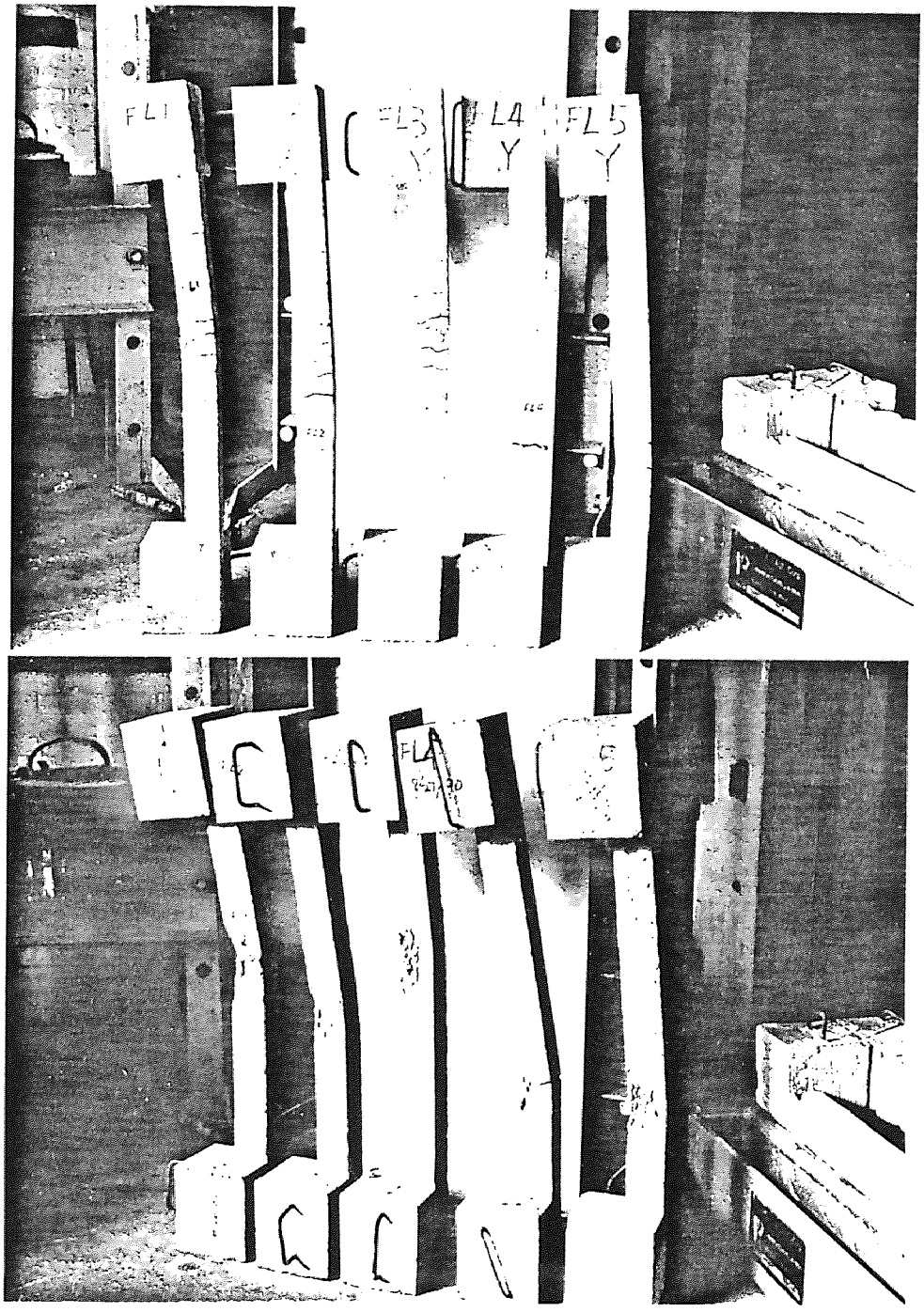

Figure 3.15 High Strength Fibrous Column after Failure

(a)

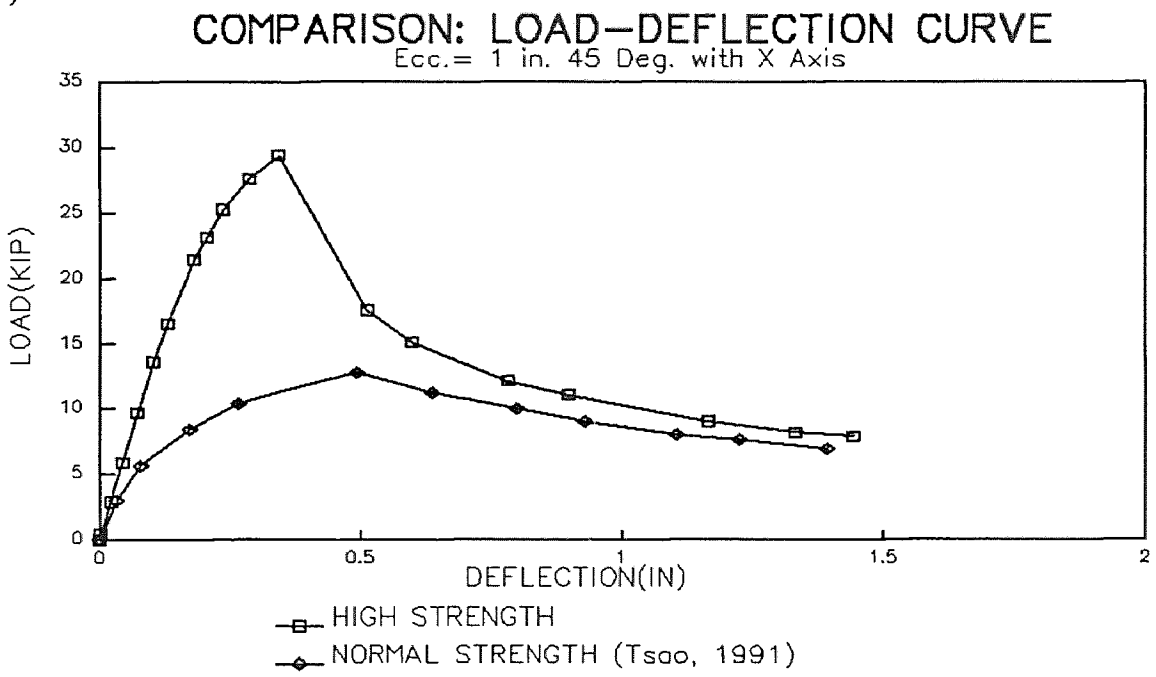

(b)

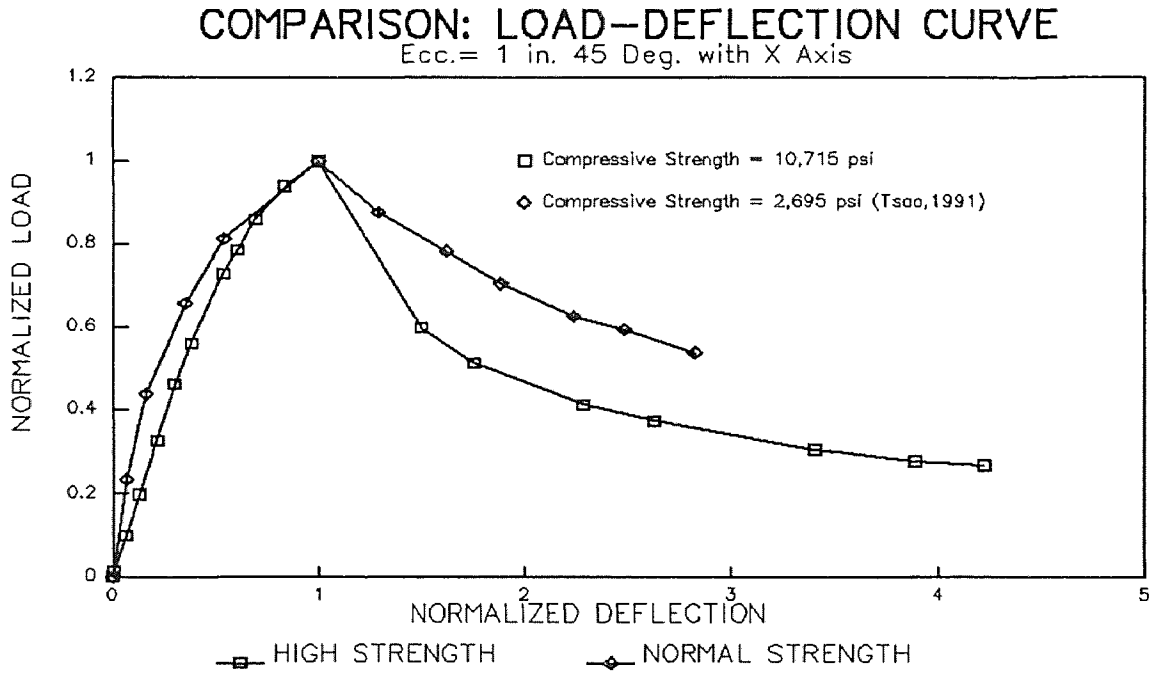

Figure 3.16 Effect of Concrete Strength on Ductility.

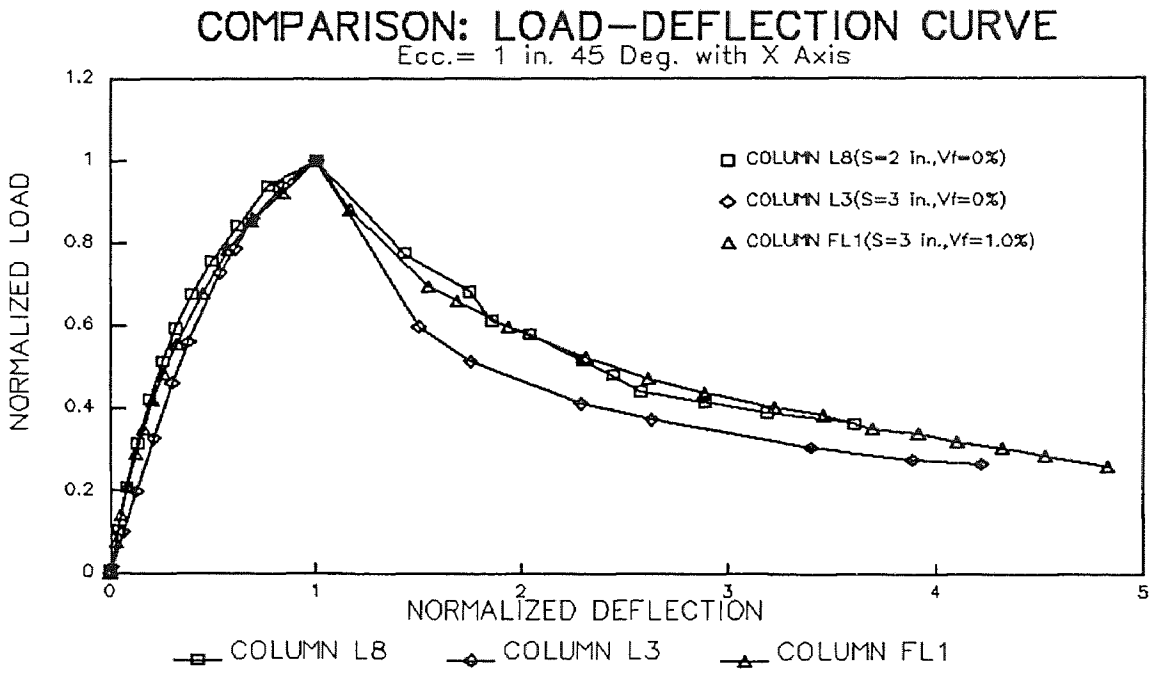

Figure 3.17 Effect of tie Confinement and Steel Fiber on Load-Deflection Curves.

CHAPTER FOUR

CONCLUSIONS

4.1 Conclusions on Behavior of Plain and Fibrous High Strength Concrete

4.1.1 Plain High Strength Concrete.

1. On an average, the strain corresponding to the peak stress for the high strength concrete is greater than that for the normal strength concrete. Therefore, the constant values of 0.002 and 0.003 for the strain corresponding to the peak stress and the ultimate strain, as specified by the ACI committee 318, are conservative.

2. The shape of the ascending part of the stress-strain curve for the high strength concrete behaves a more linear and steeper curve. The slope of the descending part also exhibits a steeper curve for the high strength concrete as compared to that of the normal concrete.

3. In this study, it shows that the ACI equation overestimates the modulus of elasticity for the high strength concrete.

4. The crack patterns for the high strength concrete show that the broken surface of the concrete cylinders exhibits a more smooth surface, and its surface passes through the aggregates.

5. Both the maximum compressive strength (peak stress) and the strain corresponding to the peak stress increase with increasing lateral tie confinements.

6. Analytical Eqs. (2.1) through (2.5) have been proposed herein to generate a complete stress-strain curve for plain unconfined concrete by a given single value of maximum compressive strength, f'_c. The parameters studied are shown in Eqs. (2.6) through (2.11).

7. Analytical Eqs. (2.1) through (2.4) have also been proposed to represent a complete stress-strain curve for confined concrete by a single value of maximum compressive strength, f'c. The parameters are included in Eqs. (2.6), (2.16), and (2.17), respectively.

8. A good agreement is achieved for the stress-strain curves between a various experimental results and the proposed analytical equations for both confined and unconfined concrete.

9. The proposed stress-strain equations also give an excellent result as compared to the experimental data from Wang and co-workers (Wang et al. 1978) and Shah co-workers (Shah et al. 1981) tests.

10. Base on present study, the modulus of elasticity for a confined concrete is essentially the same as that for the unconfined concrete.

4.1.2 High Strength Fiber-Reinforced Concrete

1. The addition of steel fibers to the high strength concrete usually increases the strain corresponding to the peak stress, however it does not yield any significant increase in the maximum compressive strength (peak stress).

2. The addition of steel fibers to the high strength concrete matrix changes its basic characteristics of the stress-strain behavior. As compared with the normal concrete, the ascending portion of the stress-strain curve changes slightly, but the descending portion of the stress-strain curve changes tremendously. The slope of the descending part increases with increasing the fiber content. With a reasonable amount of the fibers in the concrete, higher ductility and toughness of the concrete can be achieved.

3. Toughness index increases can be achieved with increasing fiber content.

4. During the tests, the fibrous concrete behaves a bulging phenomenon in the lateral direction. This phenomenon is due to the fibers which act as a crack arrestor.

5. Both the maximum compressive strength (peak stress) and strain corresponding to the peak stress increase with increasing tie confinements.

6. Analytical Eqs. (2.1) through (2.5) have been proposed to yield a complete stress-strain curve for an unconfined concrete of different fiber contents by the given values of

maximum compressive strength and fiber volume fraction. Their parameters can be predicted by Eq. (2.18) and Tables 2.10 and 2.11 .

7. Analytical Eqs. (2.1) through (2.4) have also been proposed to generate a complete stress-strain curve for a fibrous confined concrete at different fiber content by the given values of compressive strength and fiber volume fraction. Their parameters are shown in Eqs. (2.18) and (2.17), and Tables 2.10 and 2.18.

8. A good agreement is also achieved for the stress-strain curves between the present experimental results and the proposed analytical equations for both confined and unconfined fibrous concretes.

4.2 Conclusions on Behavior of Biaxially Loaded Plain and Fibrous High Strength Reinforced Concrete Slender Columns.

1. A computer analysis program is developed herein to analyze the complete load-deflection and moment-curvature relationships of biaxially loaded high strength slender reinforced concrete columns with and without fibers. This computer analysis program modifies an existing computer program of Wang and Hsu (Wang and Hsu 1990) and Tsao (Tsao 1991), by using the empirical stress-strain equations proposed in this study to characterize the behavior of both unconfined and confined concretes with and without steel fibers.

2. A total of nine high strength and five high strength steel fiber slender columns with square section were tested to failure. They were loaded by a biaxial-eccentric thrust in a MTS testing system. The end conditions are pinned-ended. The experimental load-deflection and moment-curvature curves were attained to compare with the theoretical ones to ensure that the theoretical model developed herein is valid.

3. The use of the proposed empirical stress-strain equations yields a reasonable accuracy in predicting an actual load-deformation behavior of the high strength column and high strength fibrous column subjected to combined biaxial bending and axial load.

4. The increase of lateral tie spacing and the addition of the steel fibers do not affect the ultimate load capacity, however they reduce significantly the cracked length and zone and also improve the ductility of the high strength columns.

5. Both the theoretical model and experimental results achieve not only the ascending branch, but also the descending branch of the load-deformation behavior of the high strength slender columns with and without steel fibers under combined biaxial flexure and axial compression.

APPENDIX A
STRESS-STRAIN RELATIONSHIPS FOR CONCRETE IN COMPRESSION

(A.1) Various empirical stress-strain relationships under compression for concrete have been propose by the following investigators, except as note, most of the equations are for use in normal concrete only.

(i) Unconfined Concrete:

1) Hognestad (1951)

$$f = f_o\left[2\left(\frac{\varepsilon}{\varepsilon_o}\right)-\left(\frac{\varepsilon}{\varepsilon_0}\right)^2\right] \qquad \text{for } \varepsilon \le \varepsilon_0$$

$$f = f_o\left[\frac{\varepsilon_u - 0.85\varepsilon_o - 0.15\varepsilon}{\varepsilon_u - \varepsilon_o}\right] \quad \text{for } \varepsilon > \varepsilon_0$$

where $\varepsilon_u = 0.0038$ in./in.

$\varepsilon_0 = 2f_0/ E_c$

$E_c=18000+0.4f_c^{'}$

$f_0 = 0.85\ f_c^{'}=k_3\ f_c^{'}$

where k_3 is a stress block parameter.

2) Lee (1955)

$$f = f_o\left[2\left(\frac{\varepsilon}{\varepsilon_o}\right)-\left(\frac{\varepsilon}{\varepsilon_0}\right)^2\right] \qquad \text{for } 0 \le \varepsilon \le 2\varepsilon_0$$

where $f_0 =k_3\ f_c^{'}$

k_3 is a stress block parameter.

ε_0 is a concrete strain corresponding to the maximum compressive stress.

Note that if $k_3 =1$, then $\eta = 2x - x^2$ (Ritter's parabola)

3) Sahlin (1955) and Smith and Young (1955)

$$f = f_o\left(\frac{\varepsilon}{\varepsilon_o}\right)\exp\left(1-\frac{\varepsilon}{\varepsilon_o}\right)$$

On the basis of experimental results, Smith and Young proposed,

ε_o 0.0017 to 0.002

$f_o = f'_c$

i.e. $\eta = x\exp(1-x)$

4) Rüsch (1960) and Rüsch, CEB recommendation (Levi (1961))

$$f = f_o\left[2\left(\frac{\varepsilon}{\varepsilon_o}\right)-\left(\frac{\varepsilon}{\varepsilon_0}\right)^2\right] \qquad \text{for } \varepsilon < \varepsilon_o$$

$$f = f_o \qquad \text{for } \varepsilon_o \le \varepsilon < \varepsilon_u$$

where $\varepsilon_o = 0.002$, $f_o = f'_c$, and $\varepsilon_u = 0.0035$

or

$\eta = 2x - x^2$ for $x < 1$ (Ritter's Parabola), and

$\eta = 1$ for $1 \le x \le 1.75$

5) Young (1960)

(a) $$f = \left(E_c\varepsilon_o - 2f'_c\right)\left(\frac{\varepsilon}{\varepsilon_o}\right)^3 - \left(2E_c\varepsilon_o - 3f'_c\right)\left(\frac{\varepsilon}{\varepsilon_o}\right)^2 + E_c\varepsilon$$

(b) $$f = f'_c \sin\left(\frac{\pi\varepsilon}{2\varepsilon_o}\right)$$

where $E_c = 1000f'_c$

$\varepsilon_o = 0.002$

6) Liebenberg (1962)

$$f = E_c\varepsilon - a\varepsilon^{n+1}$$

where $E_c = 67000\sqrt{f_c'}$

$\varepsilon_O = 0.002$

$f_O = 0.9\, f_c'$ or $2/3 f_{cu}$

where f_{cu} is a standard cube strength of concrete

$$a = \frac{1}{(n+1)\varepsilon_o^n}$$

$$n = \frac{f_o}{E_c\varepsilon - f_o}$$

$$\varepsilon_u = 0.001\left(0.4 - \frac{f_c'}{6.5\times 10^4}\right)$$

7) Saenz (1964)

$$f = E_c\left[\frac{\varepsilon}{1+\left(\frac{E_c}{E_o}-2\right)\frac{\varepsilon}{\varepsilon_o}+\left(\frac{\varepsilon}{\varepsilon_o}\right)^2}\right]$$ for the ascending branch.

where $E_o = \frac{f_o}{\varepsilon_o}$

$$E_c = \frac{\sqrt{f_o}\times 10^5}{1+0.006\sqrt{f_o}}$$

$$\varepsilon_o = 0.001\left[f_o^{\frac{1}{4}}\left(3.15 - f_o^{\frac{1}{4}}\right)\times 10^{-3}\right]$$

And

$$f = \frac{\varepsilon}{a + a_1\varepsilon + a_2\varepsilon^2 + a_3\varepsilon^3}$$ for the descending branch.

where a, a_1, a_2, and a_3 are determined by experiments.

8) Desayi and Krishnan (1964)

$$f = \frac{E_c\varepsilon}{\left[1+\left(\frac{\varepsilon}{\varepsilon_o}\right)^2\right]}$$

where $E_c = \frac{2f_o}{\varepsilon}$

$f_o = k_3 f'_c$

$\varepsilon_u = 0.003$

$k_3 = 7/8$

9) Sturman, Shah, and Winter (1965)

$$f = A\varepsilon + B\varepsilon^n$$

where A=4.0, B=-517.0, and n=1.6 for concentric loading, and A=4.13, B=-80.4, and n=1.6 for eccentric loading.

10) Hsu (1969)

$$\eta = \sin(\frac{\pi x}{2}) + 0.2x(x-1)(e^{1-x} - 1) \quad \text{for } 0 \le x \le 1$$

and

$$\eta = 0.226 + 2.157x - 1.907x^2 + 0.596x^3 + 0.063x^4 \quad \text{for } 1 \le x \le 4$$

where $\eta = \frac{f}{f_c'}$ and $x = \frac{\varepsilon}{\varepsilon_o}$

11) Ahmad and Shah (1971), Wang et al* (1978), Fanella and Naaman (1985)

$$Y = \frac{AX + BX^2}{1 + CX + DX^2}$$

where $Y = \frac{f}{f_o}$

$$X = \frac{\varepsilon}{\varepsilon_o}$$

f and ε = stress and strain in general

f_o and ε_o = peak stress and corresponding strain

A,B,C,D = are constant. Two different sets of constants were used for the ascending and the descending portions of the curve

$$E_o = \frac{f_o}{\varepsilon_o}$$

* Equations were proposed for high strength

12) Sargin (1971)

$$Y = \frac{AX + (D-1)X^2}{1 + (A-2)X + DX^2}$$

where $Y = \frac{f}{f_o}$

$$X = \frac{\varepsilon}{\varepsilon_o}$$

f and ε = the stress and strain at any point

f_0 and ε_0 = the stress and strain at peak

A = a constant which primarily determines the ascending portion

D = a constant which determines the descending portion. The value of D can be determined so as to fit the experimentally observed descending part.

13) Desayi et al (1978)

$$f = \frac{E_c \varepsilon}{g_2(\varepsilon)}$$

where

$$g_2 = 1 + (0.0638\frac{E_c}{E_c'} - 1.278)10^3\varepsilon + (0.528 - 0.138\frac{E_c}{E_c'})10^6\varepsilon^2 + (0.034\frac{E_c}{E_c'} - 0.069)10^9\varepsilon^3$$

where $E_c = 1{,}800{,}000 + 460f_c'$ (in psi)

$$E_c' = \frac{f_c'}{\varepsilon_o}$$

f is the compressive stress

f_c' is the ultimate stress

ε is the compressive strain

ε_o is the strain corresponding to the ultimate stress

14) Shah et al (1983)

a) for the ascending part

$$f = f_o\left[1-\left(1-\frac{\varepsilon}{\varepsilon_o}\right)^A\right]$$

where $A = \frac{E_c \varepsilon_o}{f_o^{'}}$

$$E_c = 27.55 w^{1.5}\sqrt{f_c^{'}}$$

where $f_o^{'}$ is the compressive strength in psi

w the density of concrete in pounds per cubic foot

b) for the descending part

$$f = f_o \exp\left[-k(\varepsilon-\varepsilon_o)^{1.15}\right]$$

where

k = a constant to be determined so as to fit the experimental data of the descending part

$$k = 0.17 f_o^{'}$$

$$\varepsilon_o = 0.001648 + 1.14 x 10^{-7}\left(f_o^{'}\right)$$

15) Carreira and Chu (1985)

$$\frac{f_c}{f_c^{'}} = \frac{\beta\left(\frac{\varepsilon}{\varepsilon_c^{'}}\right)}{\beta - 1 + \left(\frac{\varepsilon}{\varepsilon_c^{'}}\right)^{\beta}}$$

and $$\beta = \frac{1}{1 - \frac{f_c'}{\varepsilon_c' E_{it}}}$$

for $\beta \geq 1.0$ and $\varepsilon \leq \varepsilon_u$

where β is a material parmeter that depends on the shape of the stress-strain diagram.

(ii) Confined Concrete:

1) Sargin and Handa (1969) and Sargin (1971):

$$\eta = k_3 \left[\frac{Ax + (D-1)x^2}{1 + (A-2)x + Dx^2} \right]$$

where $k_3 = 1$ for concrete cylinder tests.

These parameters, A, D, and k_3 depend on the following factors: concrete strength, confinement due to lateral reinforcement, creep, strain gradient, cyclic loading, size of specimen and type of loading, etc.

2) Szulczynski and Sozen (1963) and Roy and Sozen (1963)

Peak point is given by $f=f_o$ and $\varepsilon = 0.002$

Termination point is given by $f = 0.5\ f_o$ and $\varepsilon = 0.75\rho \frac{h_e}{s}$

where $f_o = h_3 f_c'$

ρ is a volumetric ratio

s is the spacing of the stirrups

h_e is the distance inside-to-inside of the ties (see Fig. A.1)

3) Baker and Amarakone (1965)

$$f_o = f_c^{'}\left(0.8+\frac{1}{k}\right)$$

$$\varepsilon_u = 0.0015\left\{1+1.5\rho+\left[\frac{0.7-0.1\rho}{k}\right]-0.1f_c^{'}\right\}$$

where k is an experimental parameter and ρ is volumetric ratio

4) Kent and Park (1969)

Kent and Park used the tests results from Soliman and Yu (1967), Roy and Sozen (1963) and Bertero and Felippa (1965) to derive the stress-strain curves shown in Fig. A.2.

For confined concrete

(a) If $f \le f'_C$, then $f = f_o\left[2\frac{\varepsilon}{\varepsilon_o}-\left(\frac{\varepsilon}{\varepsilon_o}\right)^2\right]$ (Ritter's Parabola)

If $f > f_c^{'}$, then $f = f_c^{'}\left[1-z(\varepsilon-\varepsilon_o)\right]$

where $\varepsilon_o = 0.002$

$$z = \frac{0.5}{\varepsilon_{50c}+\varepsilon_{50u}-\varepsilon_o}$$

$$\varepsilon_{50u} = \frac{3+0.002f_c^{'}}{f_c^{'}-1000}$$

$$\varepsilon_{50c} = \frac{3}{4}\rho\sqrt{\frac{b}{s}}$$

$$\rho = \frac{2(b+d)A_s}{bds}$$

where s, b, d, and A_S are shown in Fig. A.2.

5) Chan (1955) (Fig. A.3.)

(a) If $f \le f_o$, $f_o = E\,\varepsilon_o$ (Straight line)

and $\varepsilon_o = 0.002$, E is the module of elasticity in concrete

(b) If $f > f_o$, $f_{ucp} = f_o + f_o \frac{\sqrt{\rho}}{0.238}$

$$\varepsilon_{u2p} = 0.002 + \frac{\sqrt[3]{\rho}}{24.5}$$

$$f_{u4p} = f_o + f_o \frac{\sqrt{\rho + 0.05}}{0.238}$$

$$\varepsilon_{u4p} = 0.002 + \frac{\sqrt[3]{\rho + 0.05}}{24.5}$$

$$\rho = \frac{2(b+d)A_s}{bds}$$

6) Soliman and Yu (1967) (See Fig. A.4)

(a) If $f \le f_o$ (Ritter's Parabola)

$\eta = 2x - x^2$

ε=0.002, and

f_o can be related to f'_c for unconfined concrete.

(b) $f > f_o$

$f = f_o$

$$\varepsilon_{u2p} = 0.002 + \frac{\sqrt[3]{\rho}}{24.5}$$

$$\varepsilon_{u3p} = 0.012 + \frac{\sqrt[3]{\rho}}{4.9}$$

$$\rho = \frac{2(b+d)A_s}{bds}$$

7) Cranston and Chatterji (1970)

Cranston and Chatterji referred to the stress-strain curves developed by Chan (1955) and Szulczynski and Sozen (1961) and obtained three different stress-strain relations for unconfined, confined by stirrups and concrete at hinges and lying over 0.5 in. inside stirrups, respectively as shown in Fig. A.5. The equations used in Fig. A.5 are:

$$f = f_o\left[2\frac{\varepsilon}{\varepsilon_o} - \left(\frac{\varepsilon}{\varepsilon_o}\right)^2\right] \text{ or } \eta = 2x - x^2$$

$$f_{u2p} = f_o + f_o\frac{\sqrt{\rho}}{0.238}$$

$$\varepsilon_{u2p} = 0.002 + \frac{\sqrt[3]{\rho}}{24.5}$$

$$f_{u3p} = f_o\frac{\sqrt{\rho+0.05}}{0.238}$$

$$\varepsilon_{u3p} = 0.002\frac{\sqrt[3]{\rho+0.05}}{24.5}$$

8) Sargin et al (1971)

$$Y = K_3 f_c' \frac{AX + (D-1)X^2}{1 + (A-2)X + DX^2}$$

where $A = \frac{E_c \varepsilon_o}{K_3 f_c'}$

$$X = \frac{\varepsilon}{\varepsilon_o}$$

f_c' = Cylinder strength of concrete

E_c = Initial modulus of elasticity

K_3 = Ratio of maximum stress to cylinder strength

ε_o = Strain corresponding to maximum stress

D.= a parameter mainly affecting the slope of the descending branch

9) Desay et al (1978)

$$f = \frac{E_c \varepsilon}{g_1(\varepsilon)}$$

where

$$g_1(\varepsilon) = 1 + [\frac{1 - 2k\beta + k\beta^2}{k(\beta-1)^2} \frac{E_c}{E_c'} - \frac{2\beta+1}{\beta}] \frac{\varepsilon}{\varepsilon_c} + [\frac{\beta+2}{\beta} \frac{2(1-k)}{k(\beta-1)^2} \frac{E_c}{E_c'}] (\frac{\varepsilon}{\varepsilon_c})^2 + [\frac{1-k}{k(\beta-1)^2} \frac{E_c}{E_c'} - \frac{1}{\beta}] (\frac{\varepsilon}{\varepsilon_c})^3$$

where $E_c' = \frac{\bar{f}_c'}{\varepsilon_c}$

$$E_c = 1{,}800{,}800 + 460 f_c' \qquad \text{(in psi)}$$

k=0.85

$$\beta = \frac{\bar{\varepsilon}_{0.85}}{\bar{\varepsilon}_c} = \frac{1.8 + 46.5C_i}{1.0 + 23.0C_i}$$

where E_c= initial slope of the stress-strain curve

$$E_c' = \frac{\bar{f}_c'}{\bar{\varepsilon}_c}$$

$\bar{f}_c'$= is the ultimate stress of a confined concrete

$\bar{\varepsilon}_c$= is the strain corresponding to the ultimate stress of a confined concrete

C_i= confinement index=$(\rho_b - \bar{\rho}_b)\frac{f_y}{f_c'}$

where ρ_b= volumetric ratio, i.e. ratio of the volume of spiral to the volume of confined concrete

$\bar{\rho}_b$= value of ρ_b when the pitch of spiral is equal to the least lateral dimension of the specimen

f_y= yield strength or 0.2% proof stress of steel spiral

f_c'= is the ultimate stress of plain concrete

10) Shah et al (1983)

$$f = f_o\left[1-\left(1-\frac{\varepsilon}{\varepsilon_o}\right)^A\right]$$ for the ascending branch

where $A = \frac{E_c\varepsilon_c}{f_o}$

$$E_c = 33w^{1.5}\sqrt{f_c'} \qquad \text{(Customary U.S. unit, psi)}$$

where w = the density of concrete in pounds per cubic foot

f_c' = maximum concrete strength

$$f = f_o \exp\left[-k(\varepsilon - \varepsilon_o)^{1.15}\right] \qquad \text{for the descending branch}$$

where

k = a constant to be determined so as to fit the experimental data of the descending part

$$k = 0.17f_c' \exp(-0.01f_r) \qquad \text{(Customary U.S. unit, psi)}$$

$$f_o = f_c' + (1.15 + \frac{3048}{f_c'})f_r \qquad \text{(Customary U.S. unit, psi)}$$

$$\varepsilon_o = 1.027x10^{-7} f_c' + 0.0296\frac{f_r}{f_c'} + 0.00195 \qquad \text{(Customary U.S. unit, psi)}$$

$$f_r = \frac{2A_s f_y}{sd}$$

where A_S = the cross section area of the spiral wire

s = the spacing or the patch of the spiral.

d = the diameter of the confine core

11) Yong et al (1988)*

a) for the ascending part

$$Y = \frac{AX + BX^2}{1 + (A-2)X + (B+1)X^2} \qquad \varepsilon_c \le \varepsilon_o$$

where $Y = \frac{f_c}{f_o}$

$$X = \frac{\varepsilon_c}{\varepsilon_o}$$

$$A = \frac{E_c \varepsilon_c}{f_o}$$

$$B = \left[\frac{(A-1)^2}{0.55}\right]^{-1}$$

$$E_c = 27.55 W^{1.5} \sqrt{f_c'}$$

f_c and ε_c = the concrete stress and strain

f_o and ε_o = the peak stress and strain

* Equations were proposed for high strength concrete

b) for the descending part

$$Y = \frac{CX + DX^2}{1 + (C-2)X + (D+1)X^2} \qquad \varepsilon_c \geq \varepsilon_o$$

where $$C = \left[\frac{\varepsilon_{2i} - \varepsilon_i}{\varepsilon_o}\right]\left\{\left[\frac{\varepsilon_{2i} E_{2i}}{(f_o - f_i)}\right] - \left[\frac{4\varepsilon_i E_{2i}}{(f_o - f_{2i})}\right]\right\}$$

$$D = (\varepsilon_i - \varepsilon_{2i})\left\{\left[\frac{E_i}{(f_o - f_i)}\right] - \left[\frac{4E_{2i}}{(f_o - f_i)}\right]\right\}$$

$$E_i = \frac{f_i}{\varepsilon_i}$$

$$E_{2i} = \frac{f_{2i}}{\varepsilon_{2i}}$$

f_c and ε_c = the concrete stress and strain

f_o and ε_o = the peak stress and strain

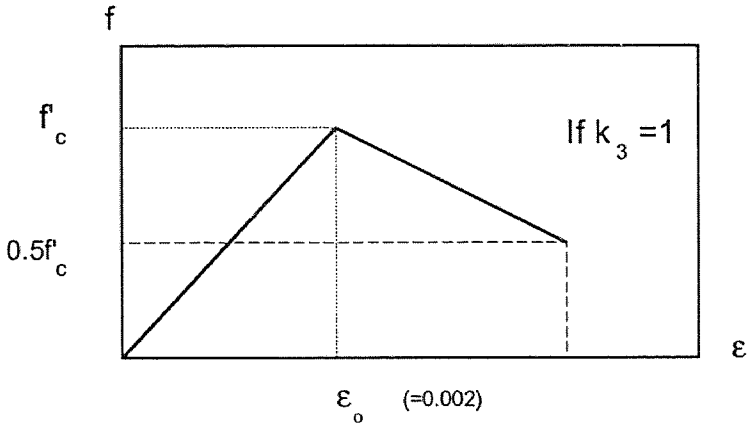

Fig. A.1 Concrete Stress-Strain Curve by Szulczynski, Sozen, Roy, and Sozen

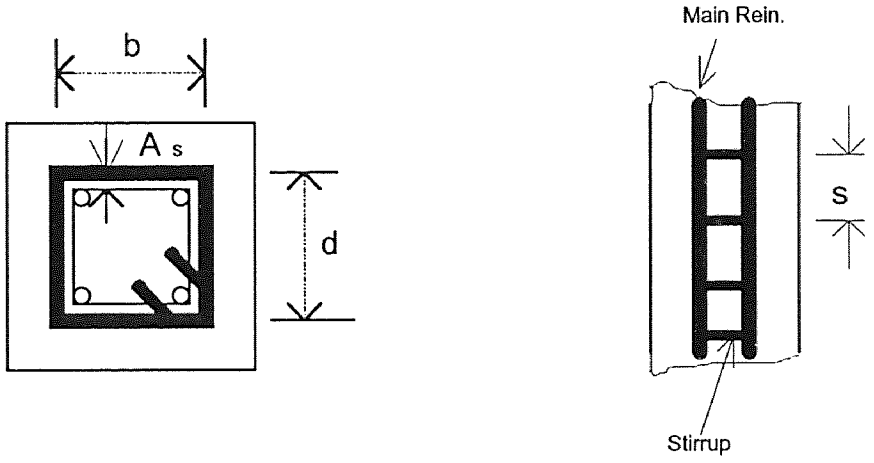

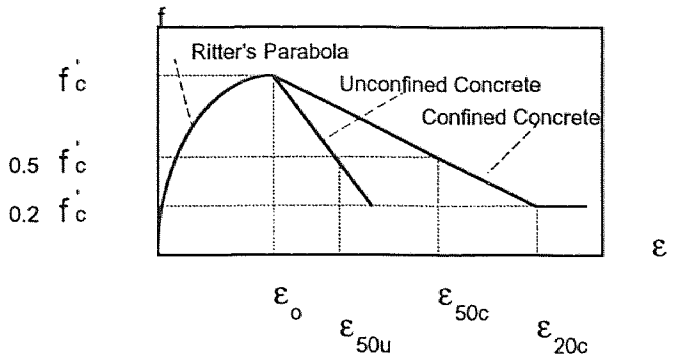

Fig. A.2 Concrete Stress-Strain Curve by Kent and Park.

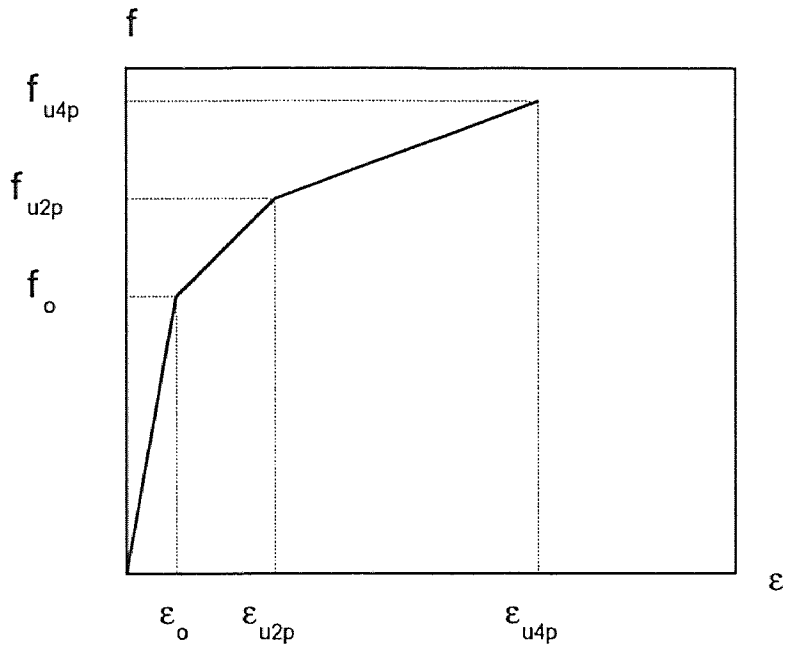

Fig. A.3 Concrete Stress-Strain Curve by Chan.

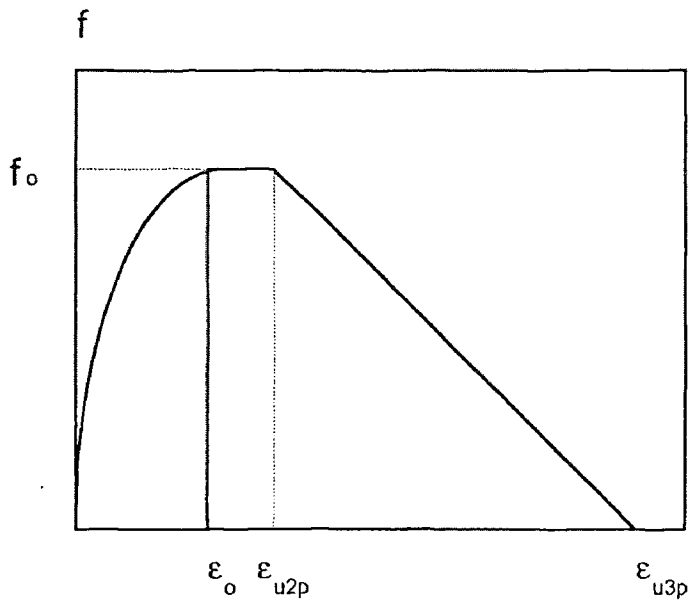

Fig. A.4 Concrete Stress-Strain Curve by Soliman and Yu.

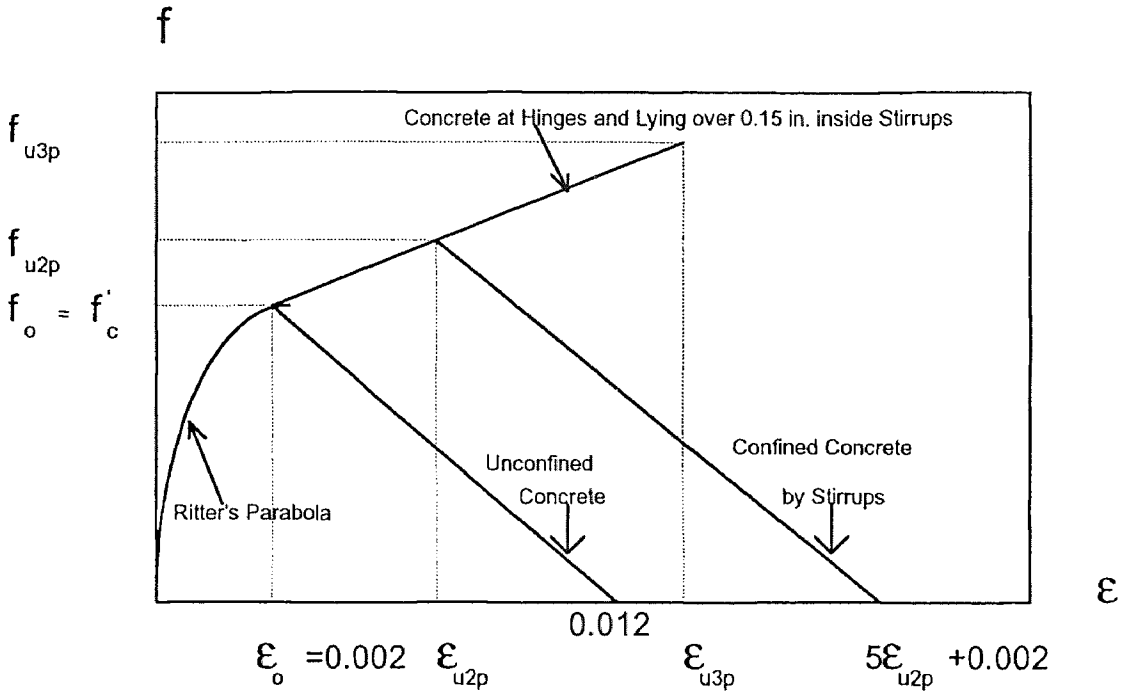

Fig. A5 .Concrete Stress-Strain Curve by Cranston and Chatterzi.

(A.2) Various empirical stress-strain relationships for unconfined fiber-reinforced normal concrete have been proposed by the following investigators. No one has proposed any empirical equations for either confined fiber-reinforced normal concrete or both unconfined and confined fibrous high strength concrete.

1) Fanella and Naaman (1985)

$$Y = \frac{AX + BX^2}{1 + CX + DX^2}$$

where $Y = \frac{f_c}{f'_{cf}}$ = normalized stress

$X = \frac{\varepsilon}{\varepsilon_p}$ = normalized strain

ε = strain in general

ε_p = strain at peak stress

f_c = stress in general

f'_{cf} = peak stress of fiber reinforced matrix

A,B,C,D = constants to be determined from the boundary conditions of the curves

2) Ezeldin (1989)

$$\frac{f_c}{f'_{cf}} = \frac{\beta(\frac{\varepsilon}{\varepsilon_{of}})}{\beta - 1 + (\frac{\varepsilon}{\varepsilon_{of}})^{\beta}}$$

f'_{cf} = compressive strength of fiber concrete

ε_{of} = strain corresponding to the compressive strength

f_c, ε = stress and strain values on the curve

β =a material parameter which can be calculated by using the follows equations:

$\beta = 1.093 + 0.7132(\text{R.I.})^{-0.926}$ for hooked steel fibers

$\beta = 1.093 + 7.4818(\text{r.i.})^{-1.387}$ for straight steel fibers

where R.I.: the reinforcing index of hooked steel fiber related to the weight fraction,

$\text{R.I.} = W_f x \ell / d$

W_f = weight fraction of steel fibers with respect to concrete

ℓ / d = aspect ratio of steel fiber (length/diameter)

r.i. = the reinforcing index of smooth steel fiber related to the weight fraction

APPENDIX B
FITTING PROPOSED EQUATIONS TO EXPERIMENTAL DATA FOR HSC

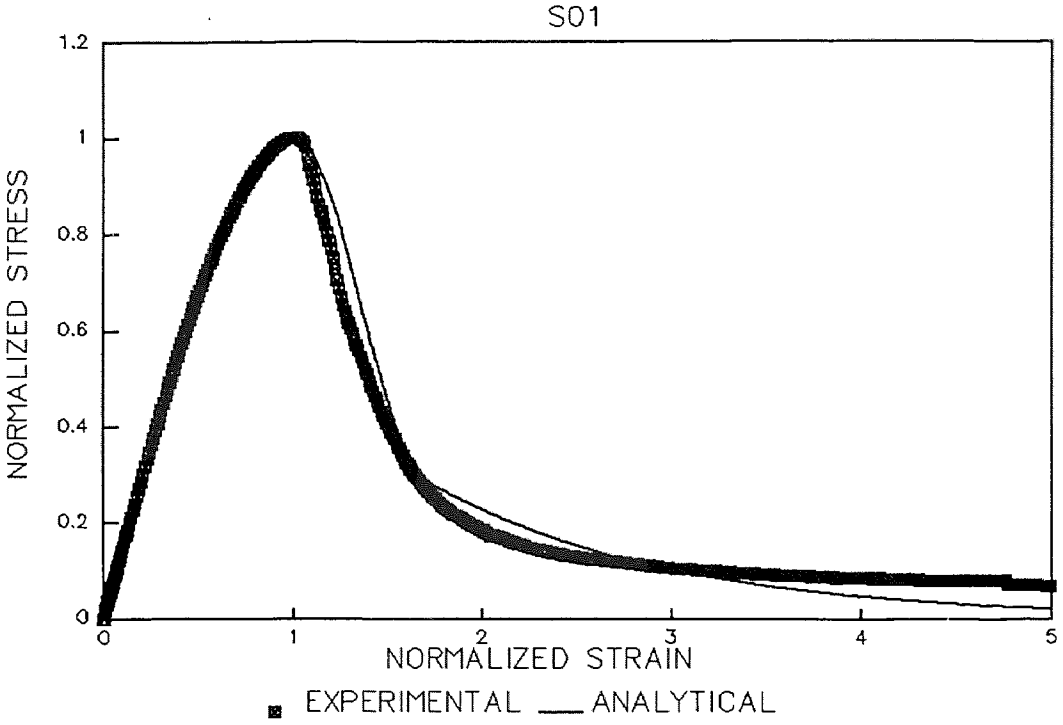

Figure B.1 Fitting Proposed Equations to Experimental Data for HSC.

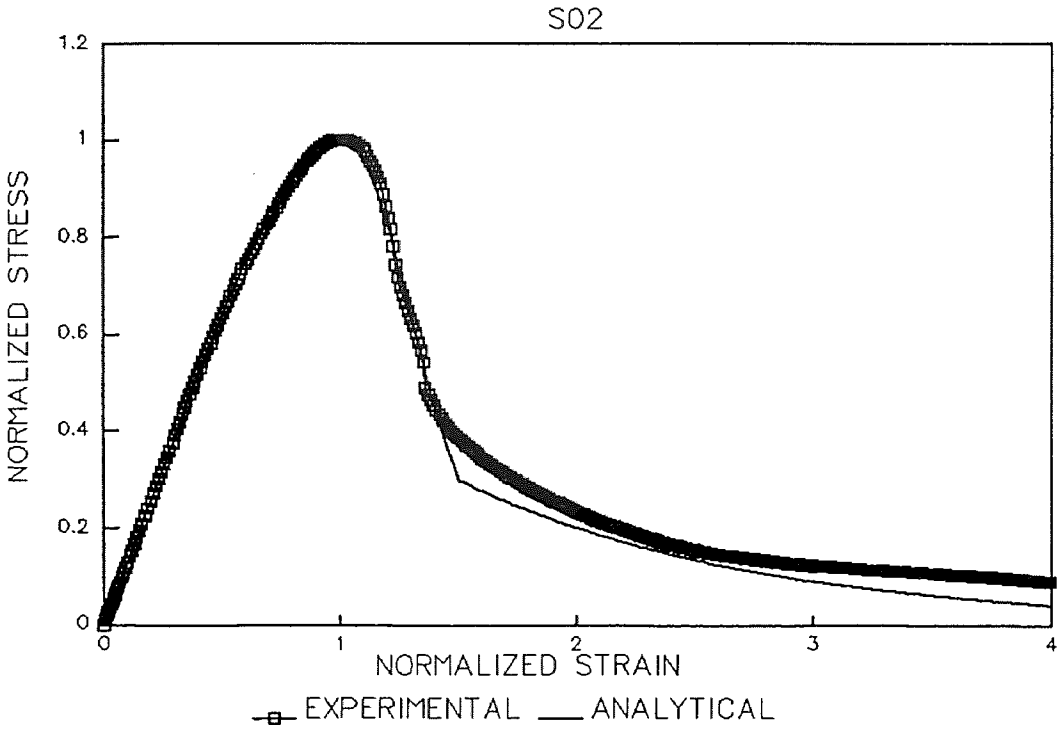

Figure B.2 Fitting Proposed Equations to Experimental Data for HSC.

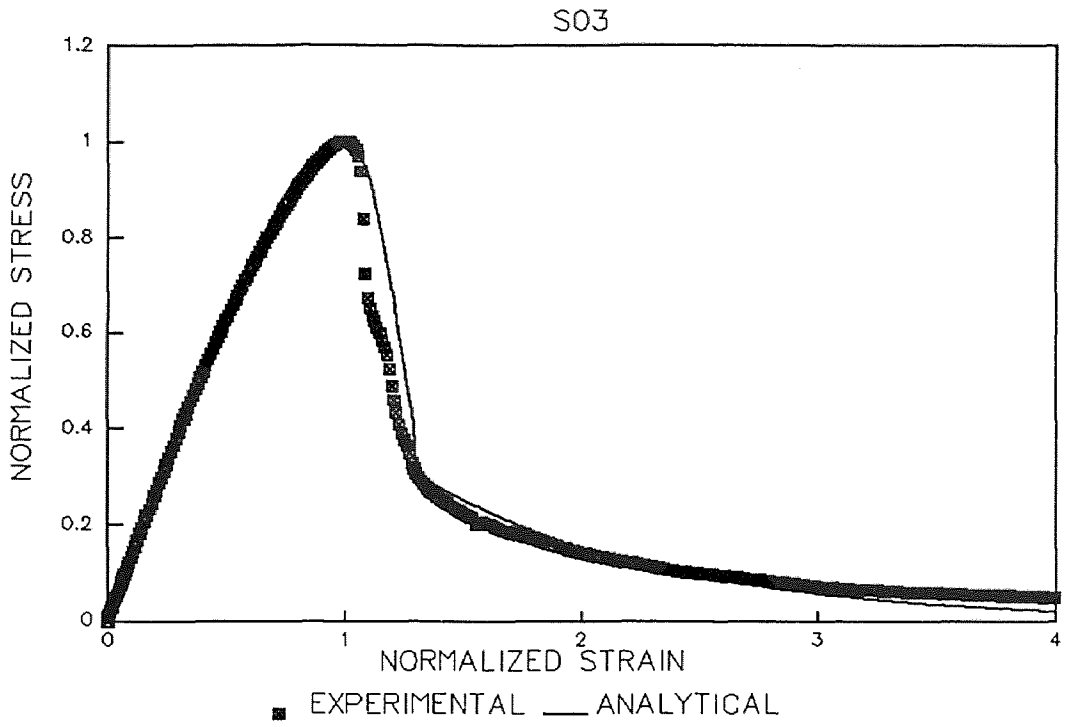

Figure B.3 Fitting Proposed Equations to Experimental Data for HSC.

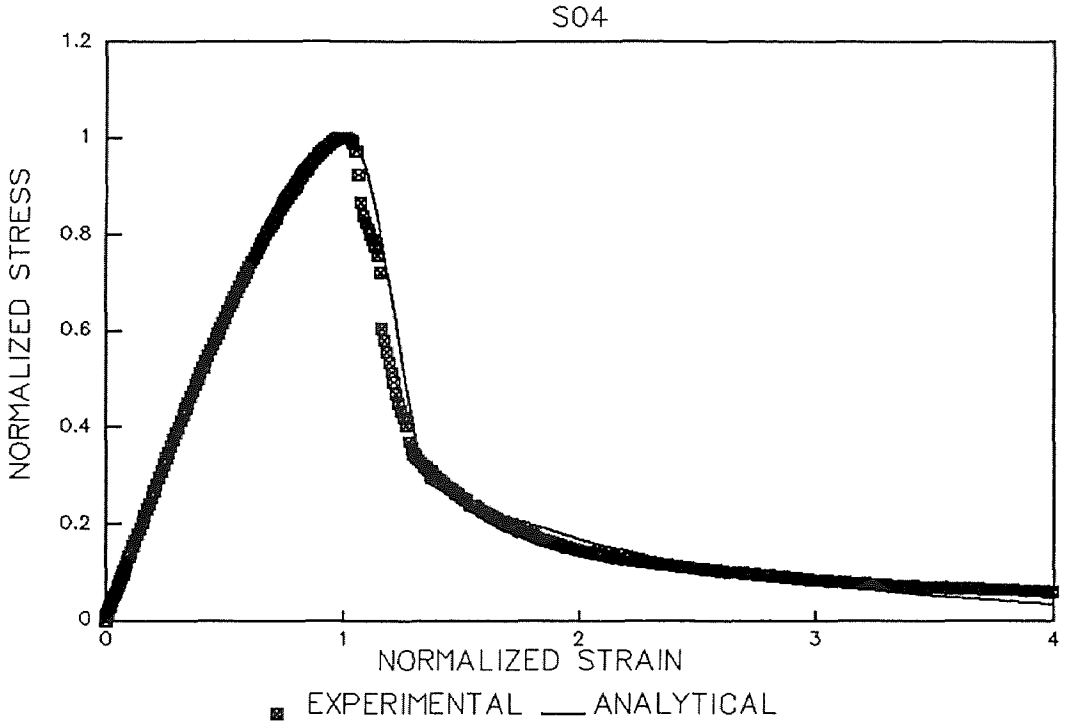

Figure B.4 Fitting Proposed Equations to Experimental Data for HSC.

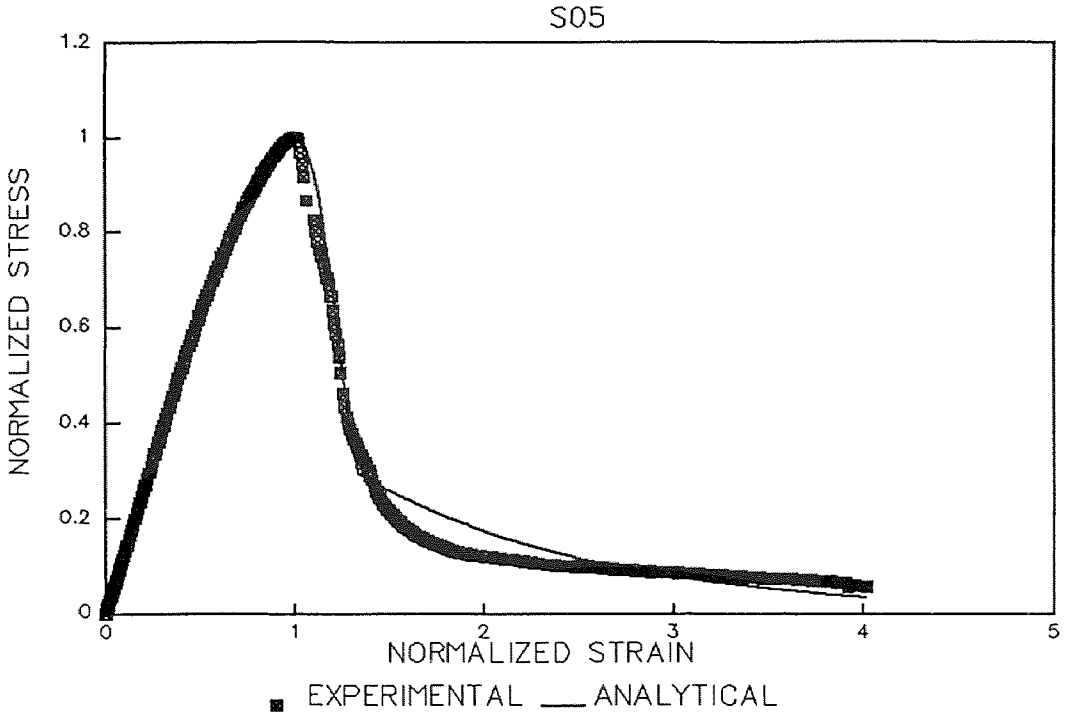

Figure B.5 Fitting Proposed Equations to Experimental Data for HSC.

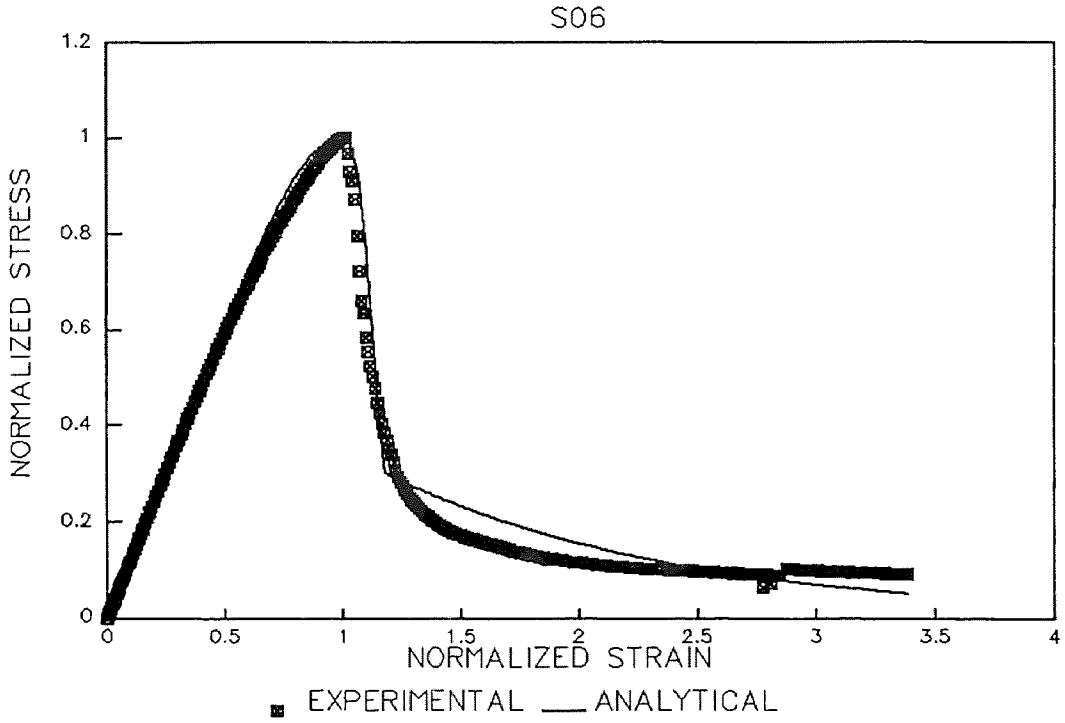

Figure B.6 Fitting Proposed Equations to Experimental Data for HSC.

APPENDIX C
FITTING PROPOSED EQUATIONS TO EXPERIMENTAL DATA AT DIFFERENT TIE SPACING

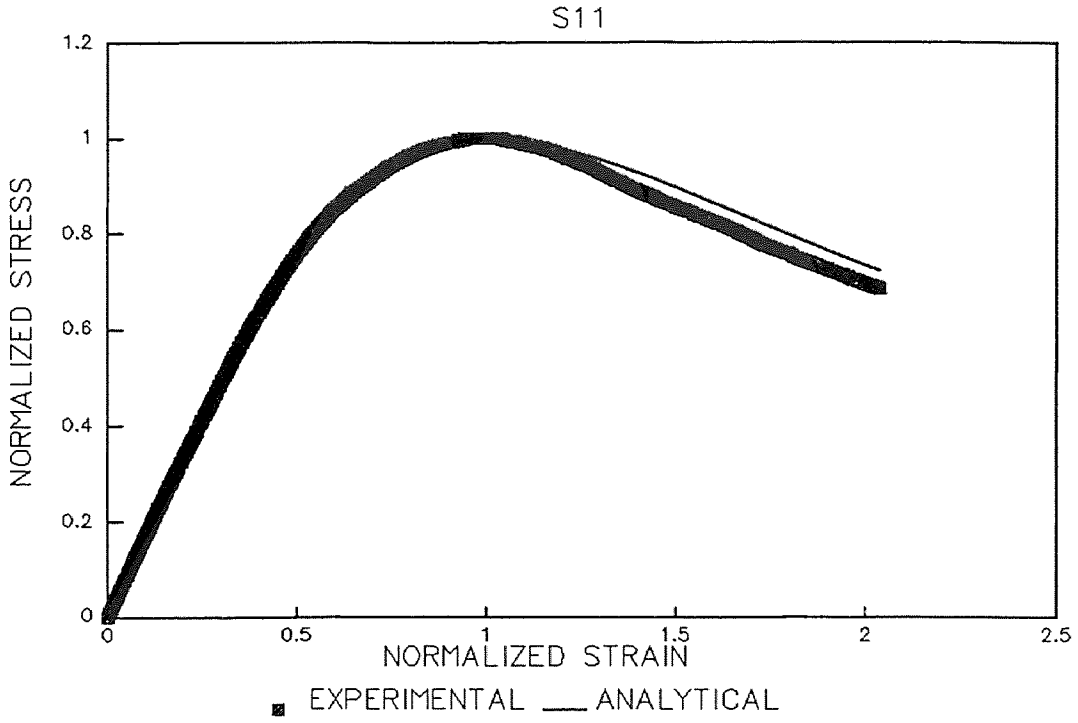

Figure C.1 Fitting Proposed Equations to Experimental Data at Tie Spacing of 1 in.

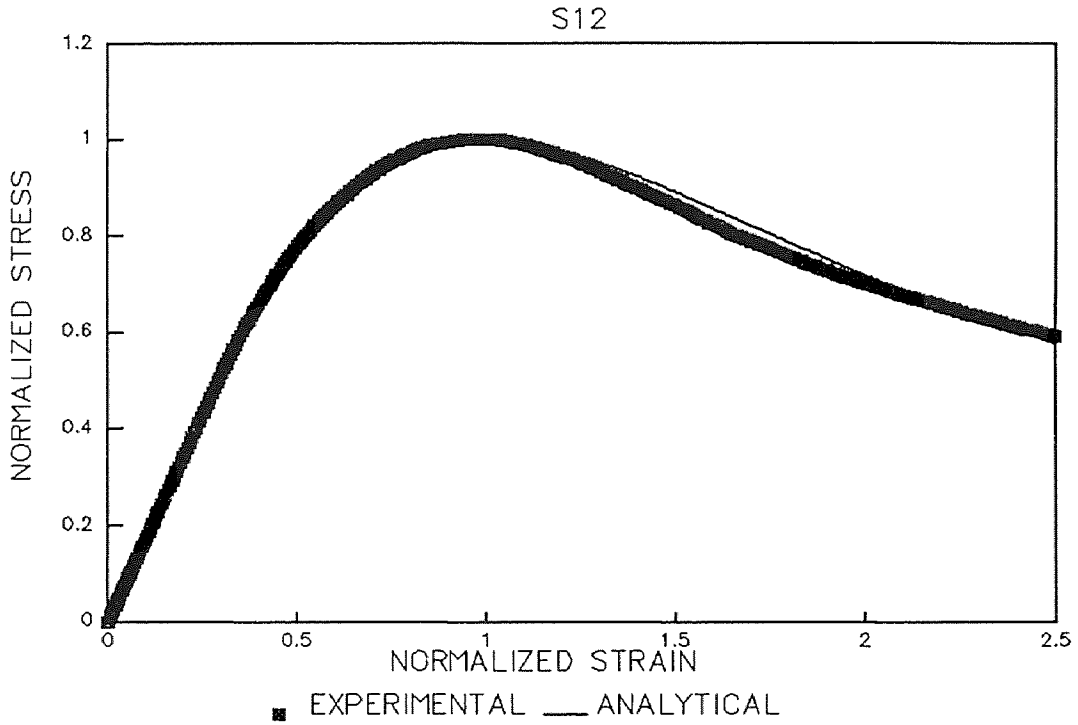

Figure C.2 Fitting Proposed Equations to Experimental Data at Tie Spacing of 1 in.

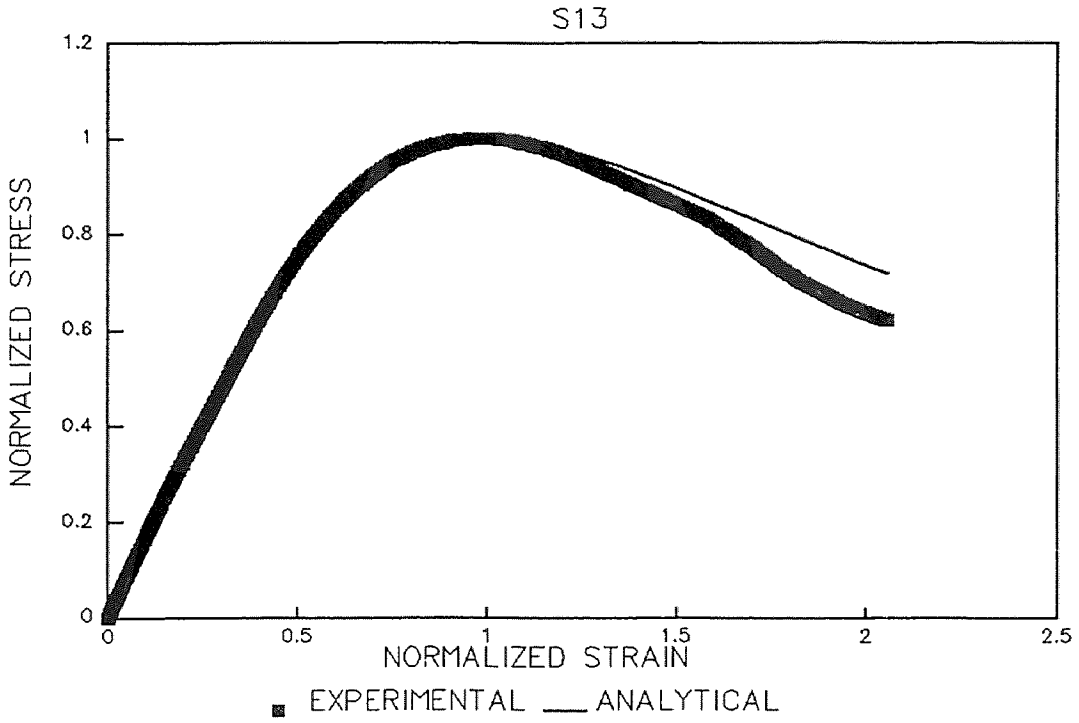

Figure C.3 Fitting Proposed Equations to Experimental Data at Tie Spacing of 1 in.

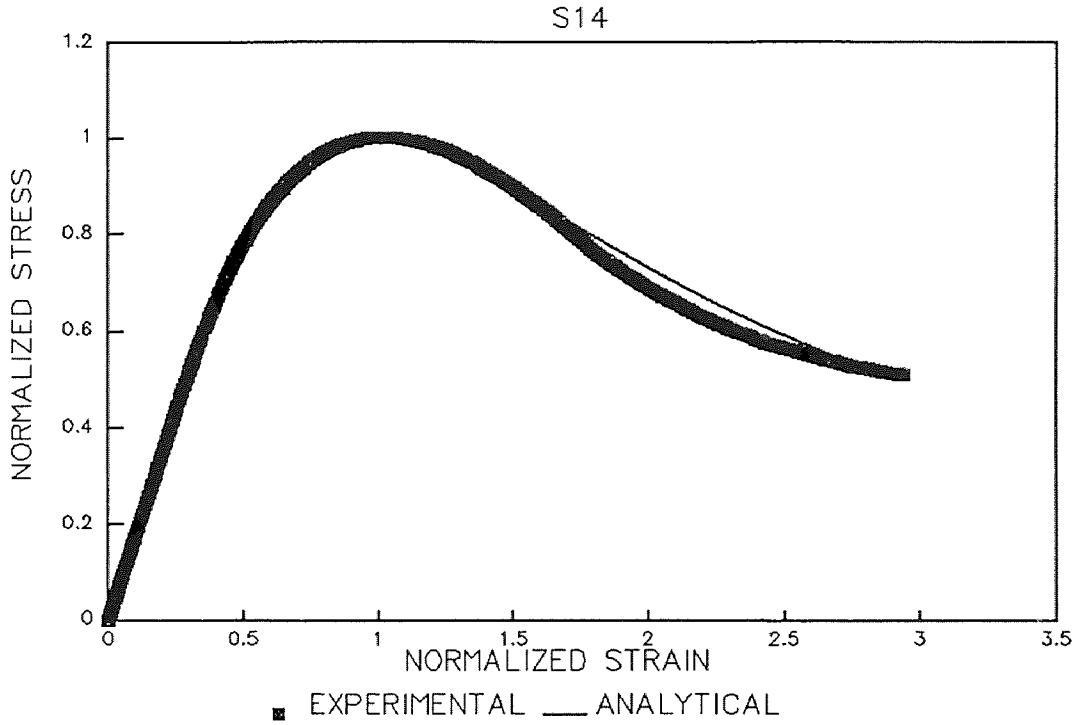

Figure C.4 Fitting Proposed Equations to Experimental Data at Tie Spacing of 1 in.

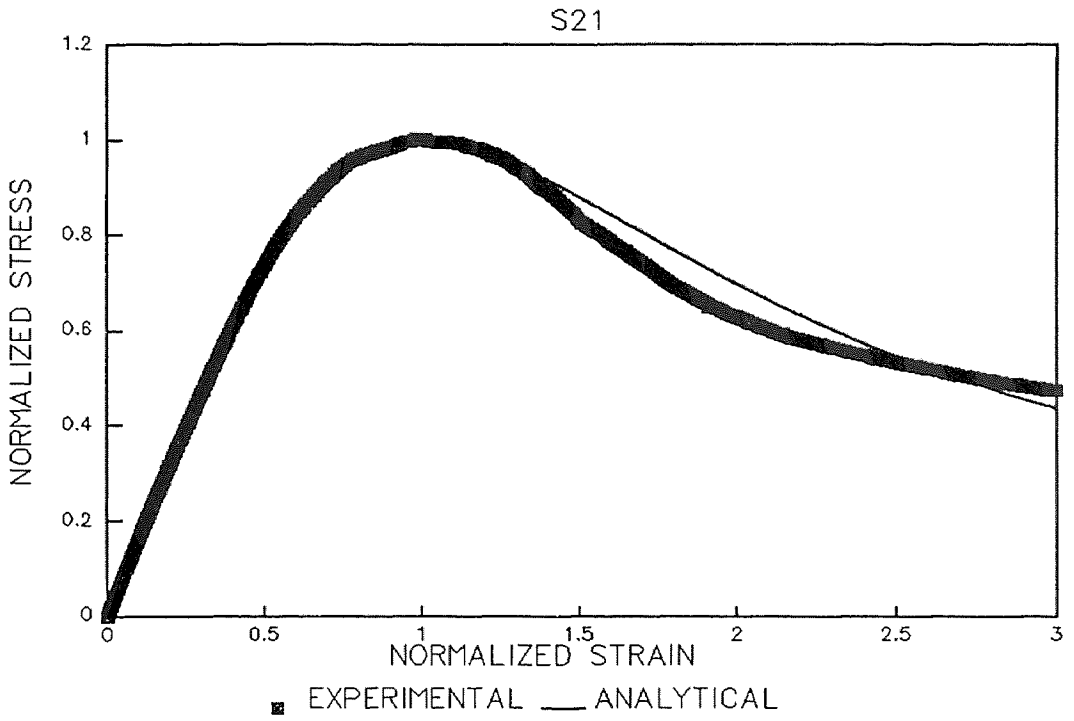

Figure C.5 Fitting Proposed Equations to Experimental Data at Tie Spacing of 2 in.

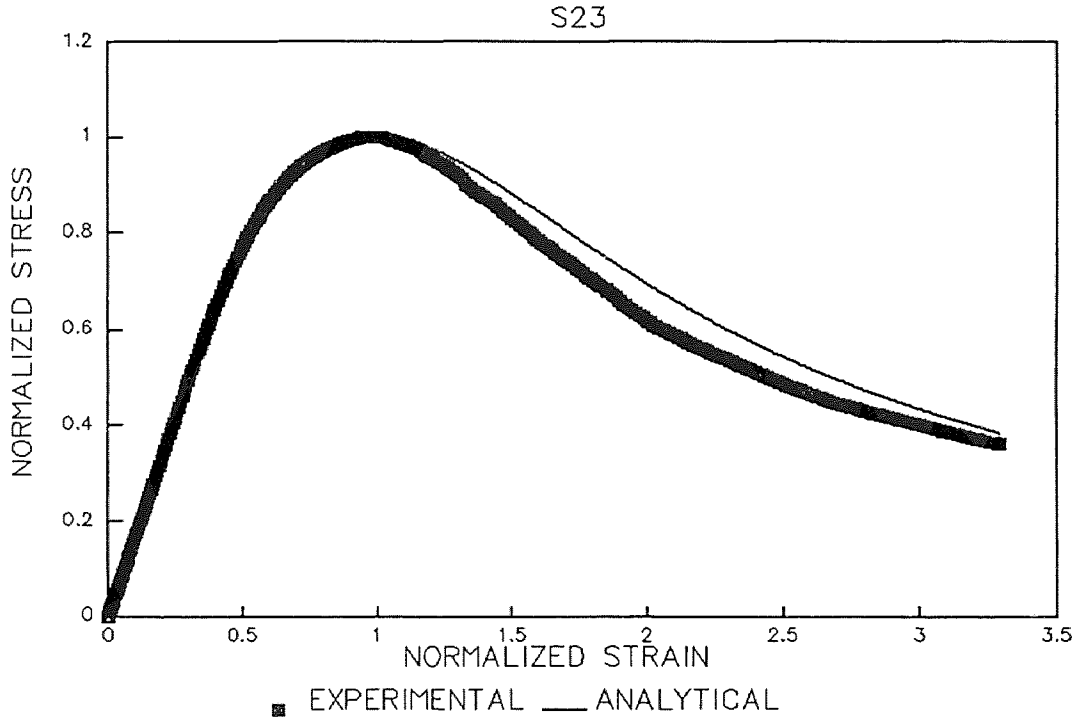

Figure C.6 Fitting Proposed Equations to Experimental Data at Tie Spacing of 2 in.

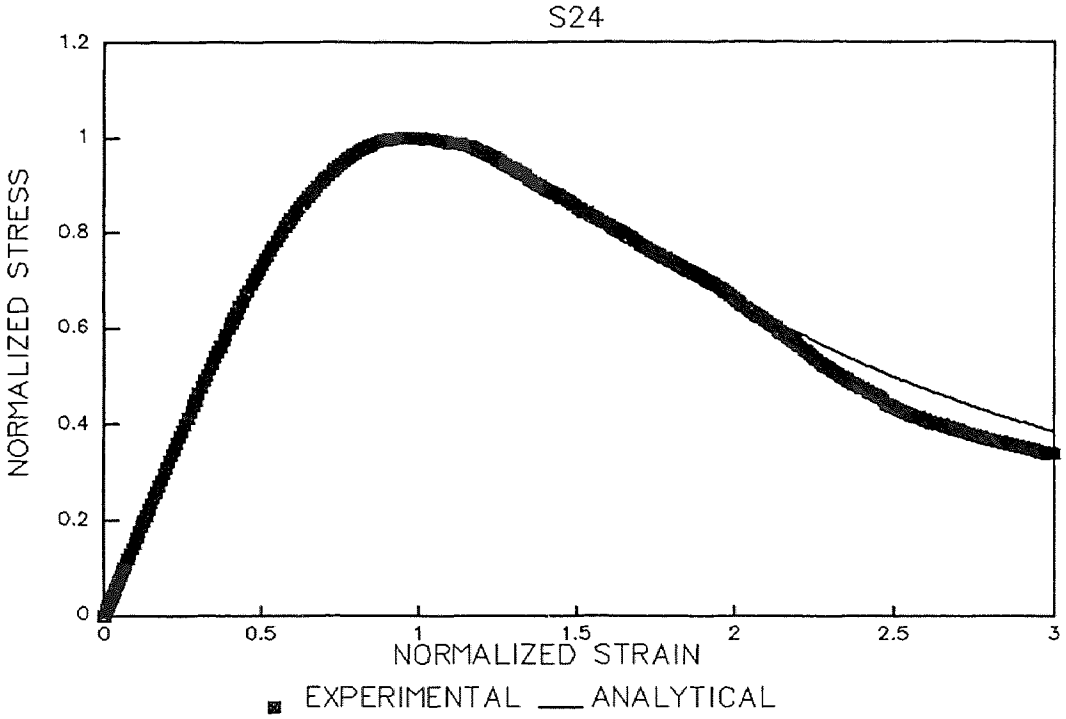

Figure C.7 Fitting Proposed Equations to Experimental Data at Tie Spacing of 2 in.

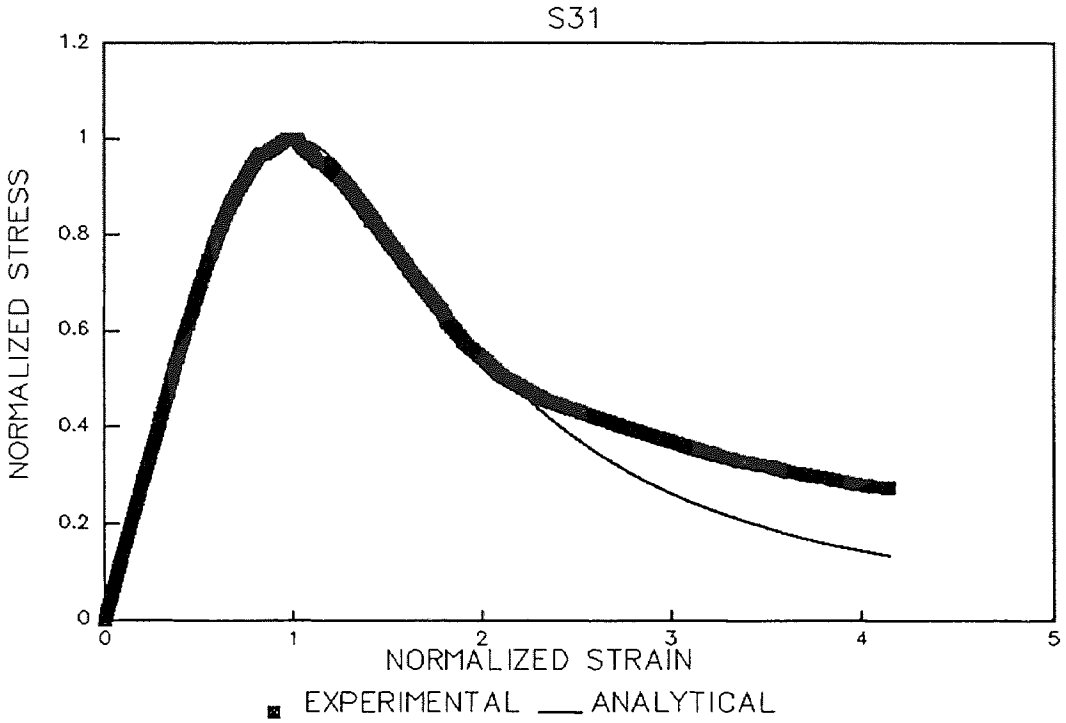

Figure C.8 Fitting Proposed Equations to Experimental Data at Tie Spacing of 3 in.

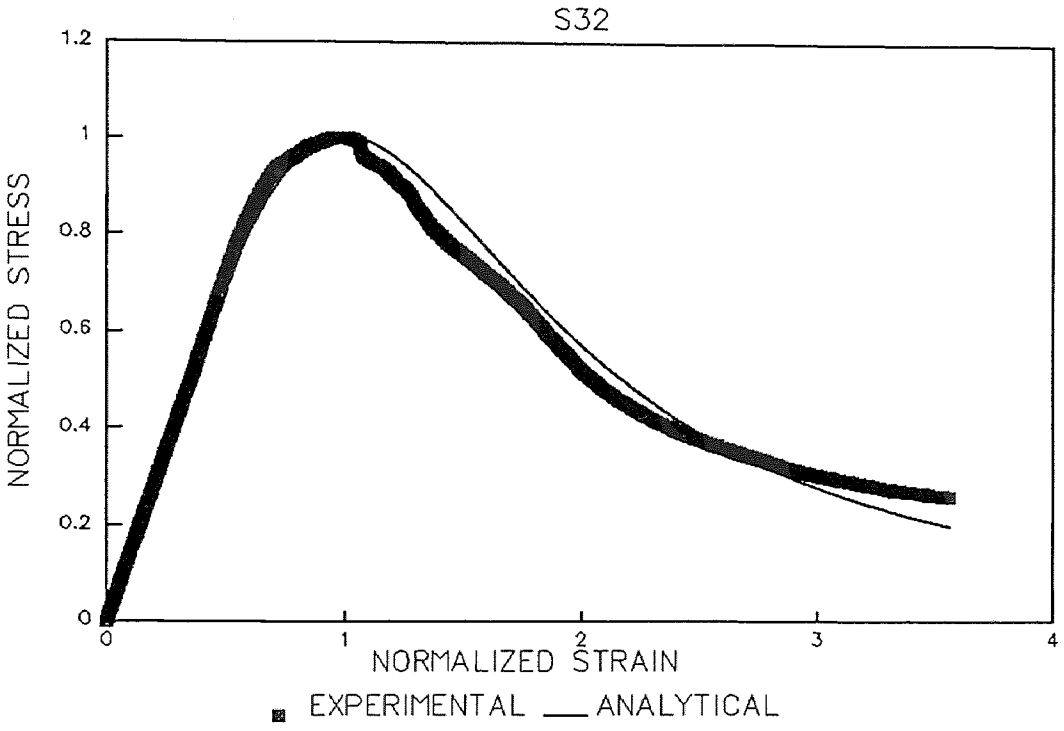

Figure C.9 Fitting Proposed Equations to Experimental Data at Tie Spacing of 3 in.

APPENDIX D
FITTING PROPOSED EQUATIONS TO EXPERIMENT DATA AT DIFFERENT FIBER VOLUME FRACTION

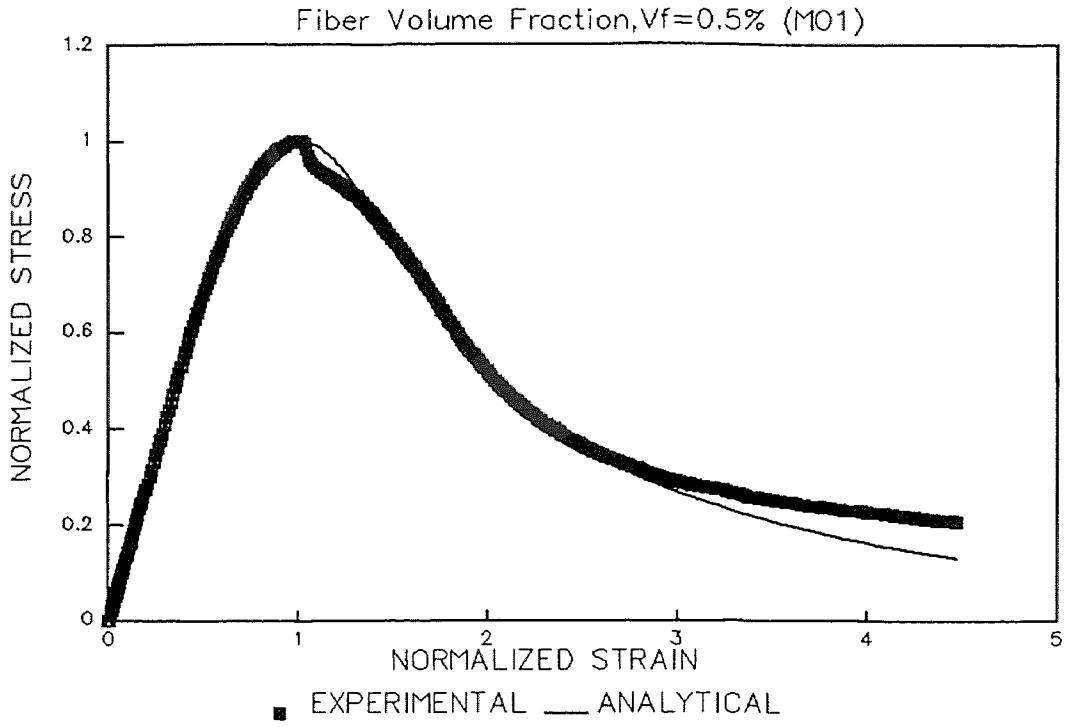

Figure D.1 Fitting Proposed Equations to Experimental Data for HSC at 0.5% Fiber Volume Fraction.

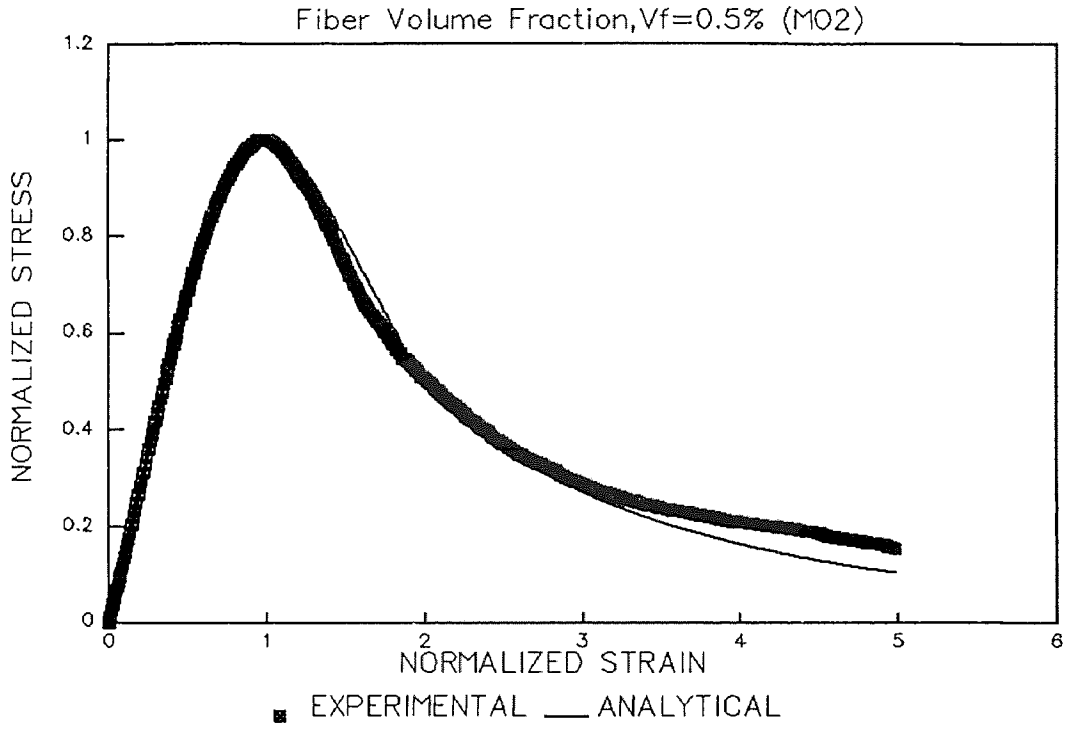

Figure D.2 Fitting Proposed Equations to Experimental Data for HSC at 0.5% Fiber Volume Fraction.

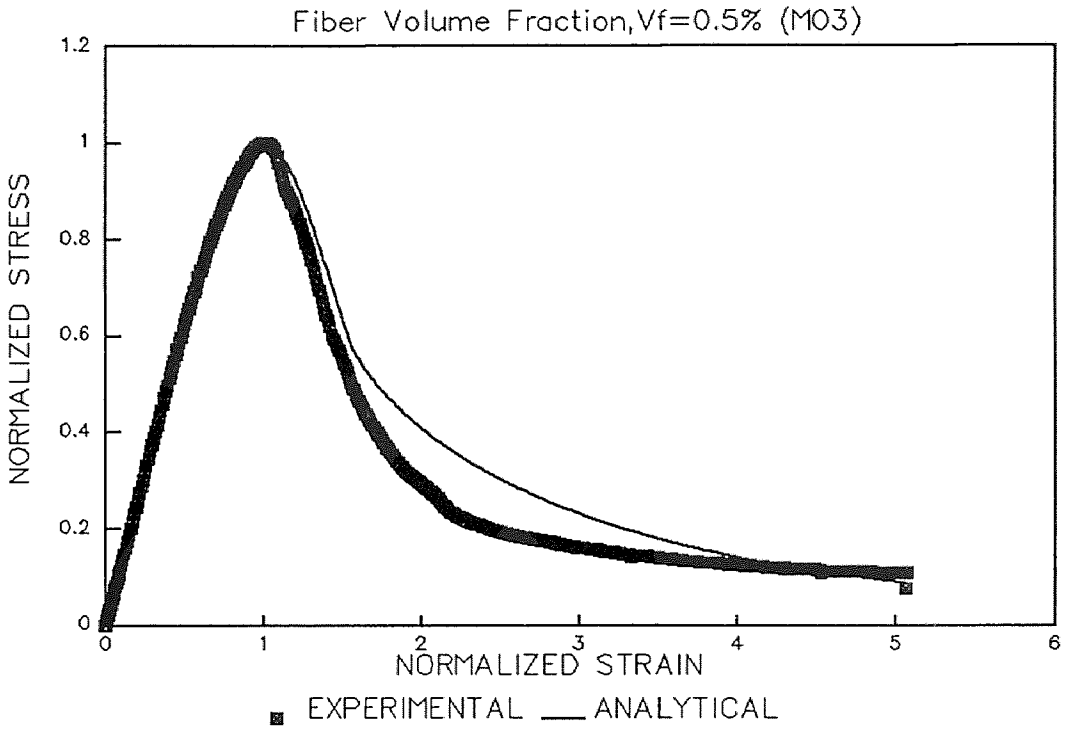

Figure D.3 Fitting Proposed Equations to Experimental Data for HSC at 0.5% Fiber Volume Fraction.

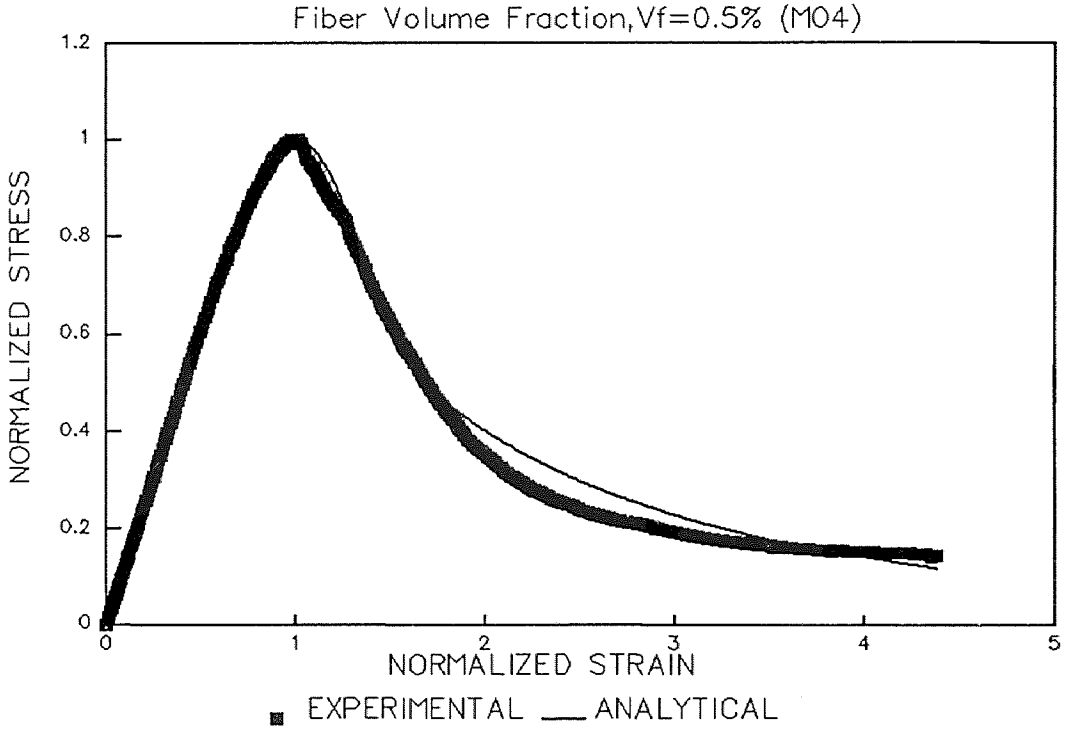

Figure D.4 Fitting Proposed Equations to Experimental Data for HSC at 0.5% Fiber Volume Fraction.

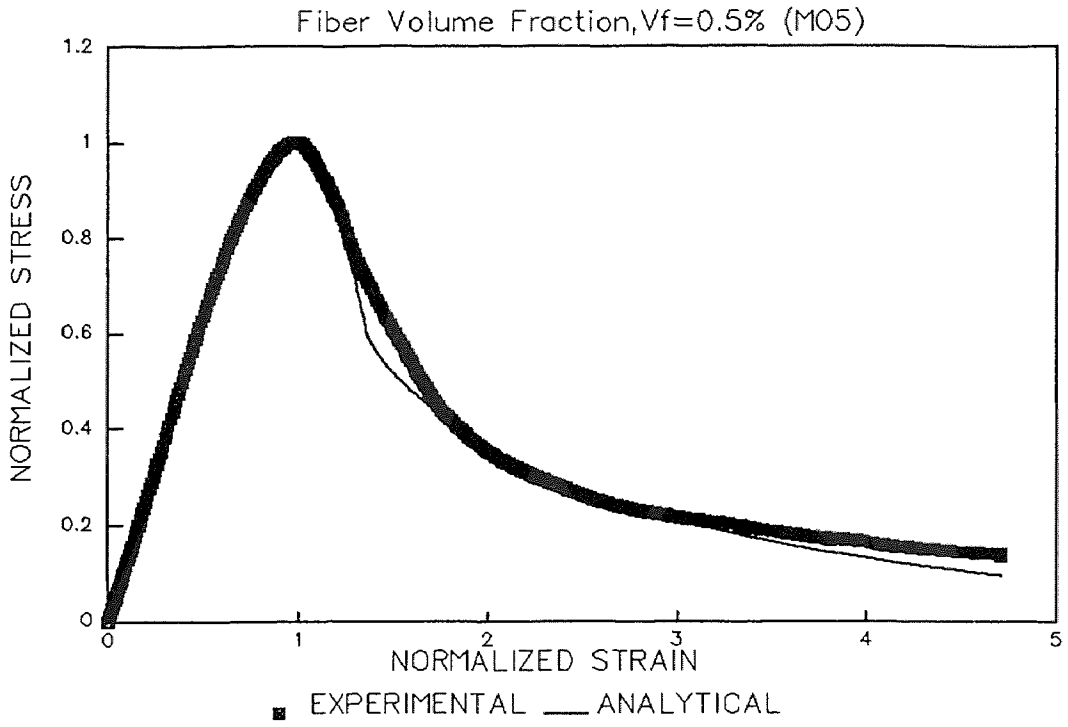

Figure D.5 Fitting Proposed Equations to Experimental Data for HSC at 0.5% Fiber Volume Fraction.

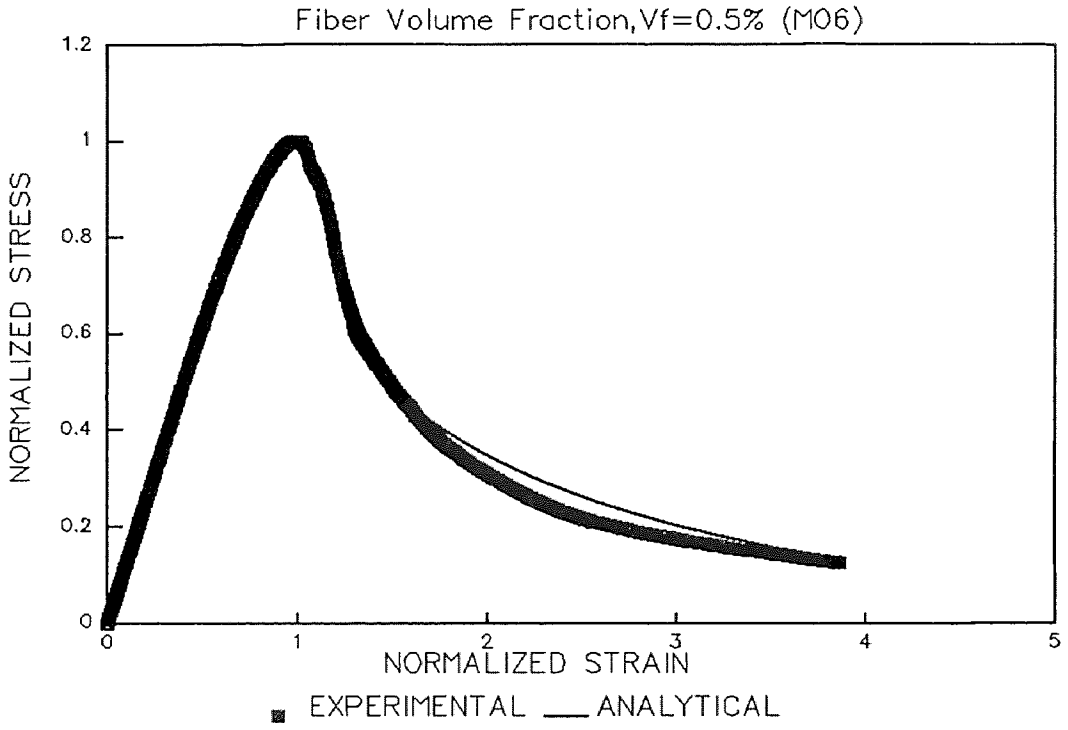

Figure D.6 Fitting Proposed Equations to Experimental Data for HSC at 0.5% Fiber Volume Fraction.

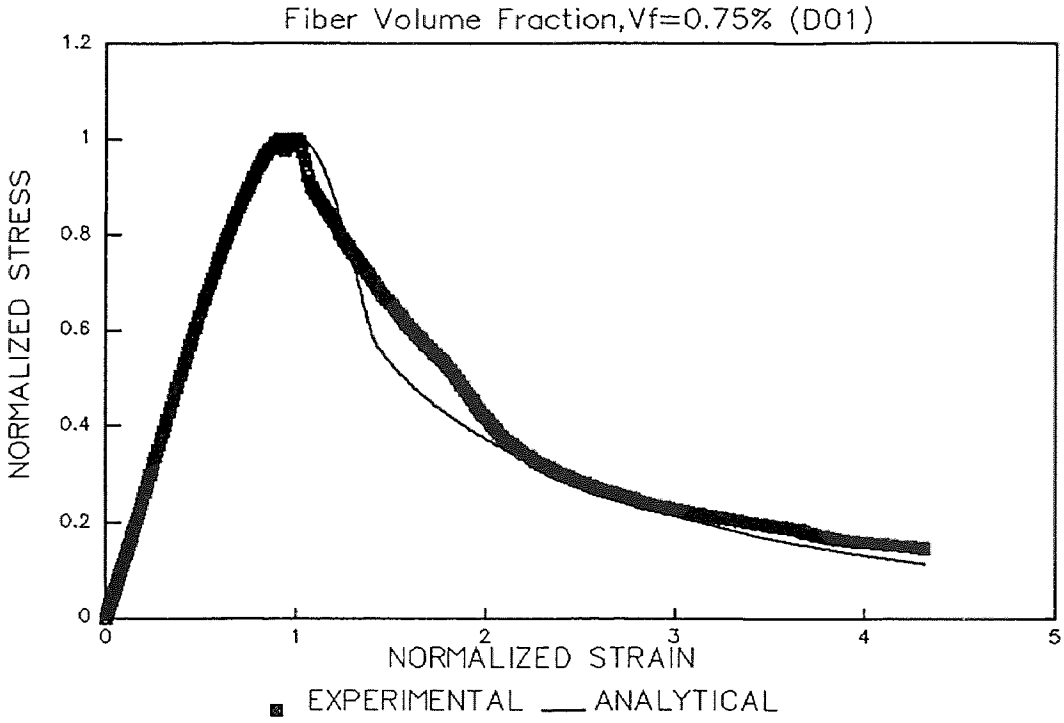

Figure D.7 Fitting Proposed Equations to Experimental Data for HSC at 0.75% Fiber Volume Fraction.

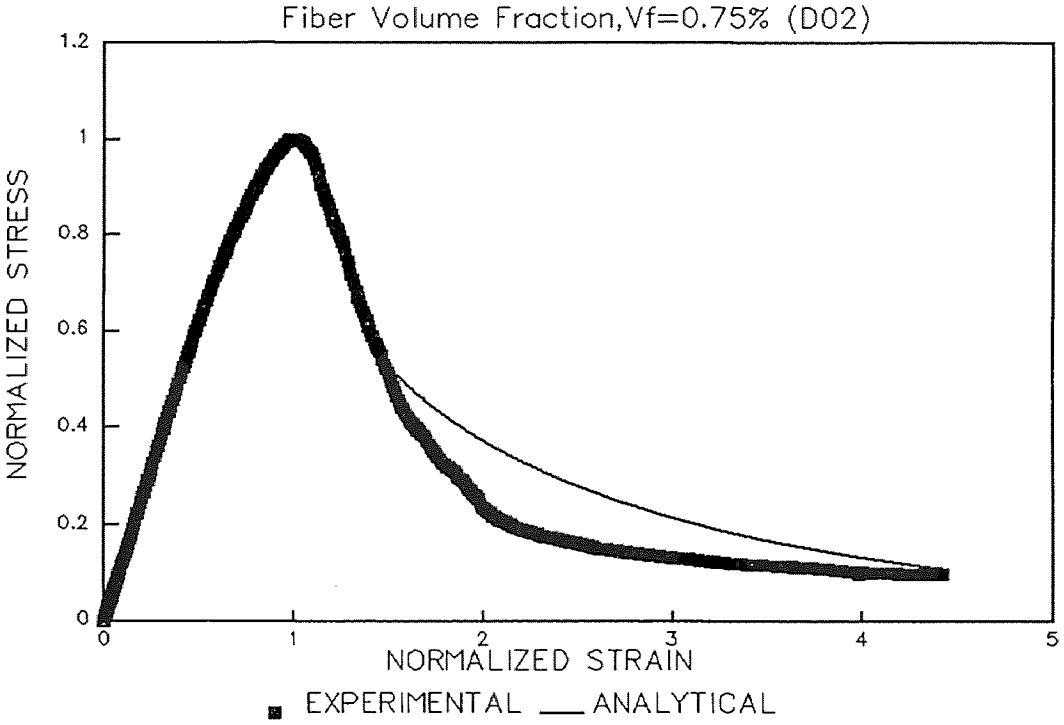

Figure D.8 Fitting Proposed Equations to Experimental Data for HSC at 0.75% Fiber Volume Fraction.

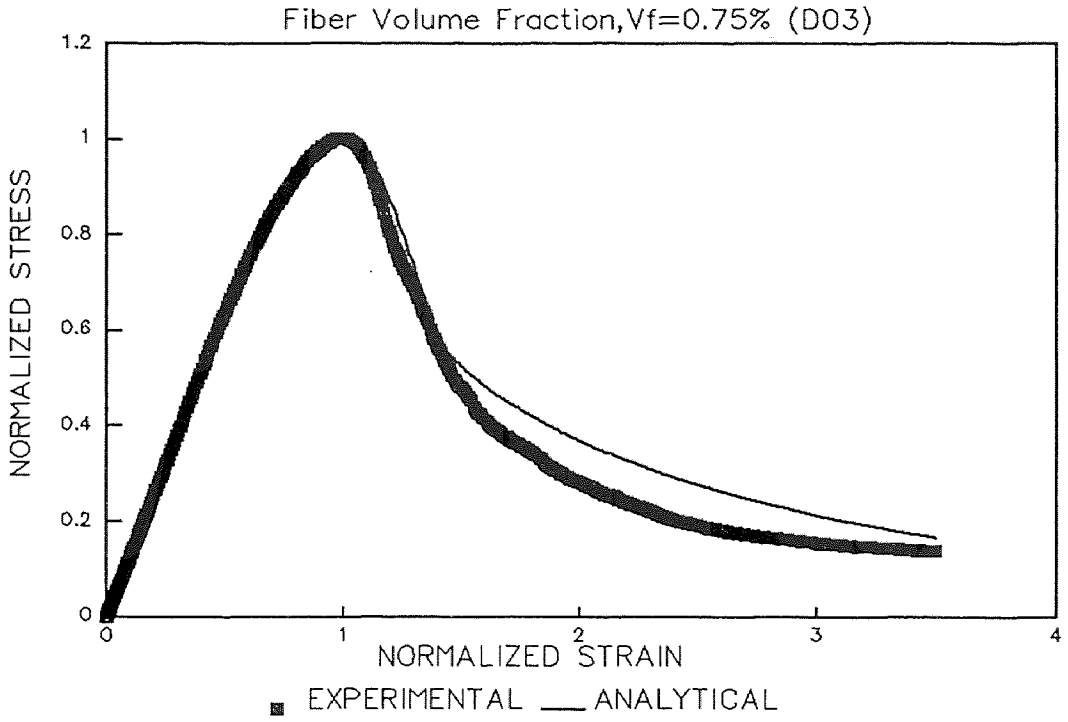

Figure D.9 Fitting Proposed Equations to Experimental Data for HSC at 0.75% FiberVvolume Fraction.

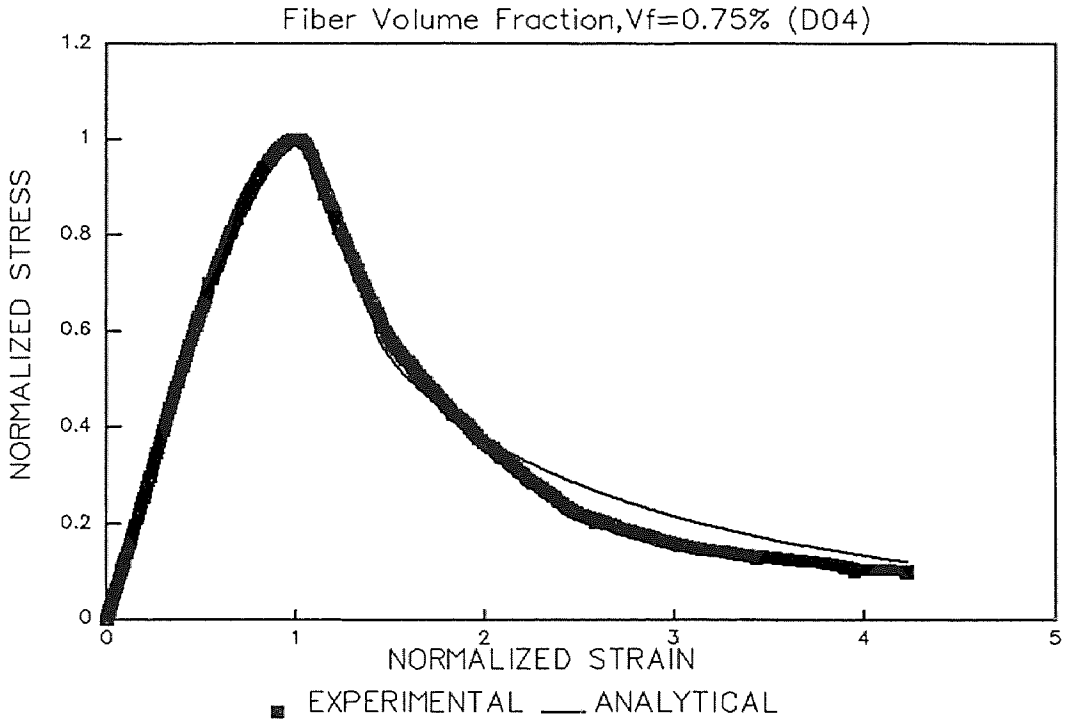

Figure D.10 Fitting Proposed Equations to Experimental Data for HSC at 0.75% Fiber Volume Fraction.

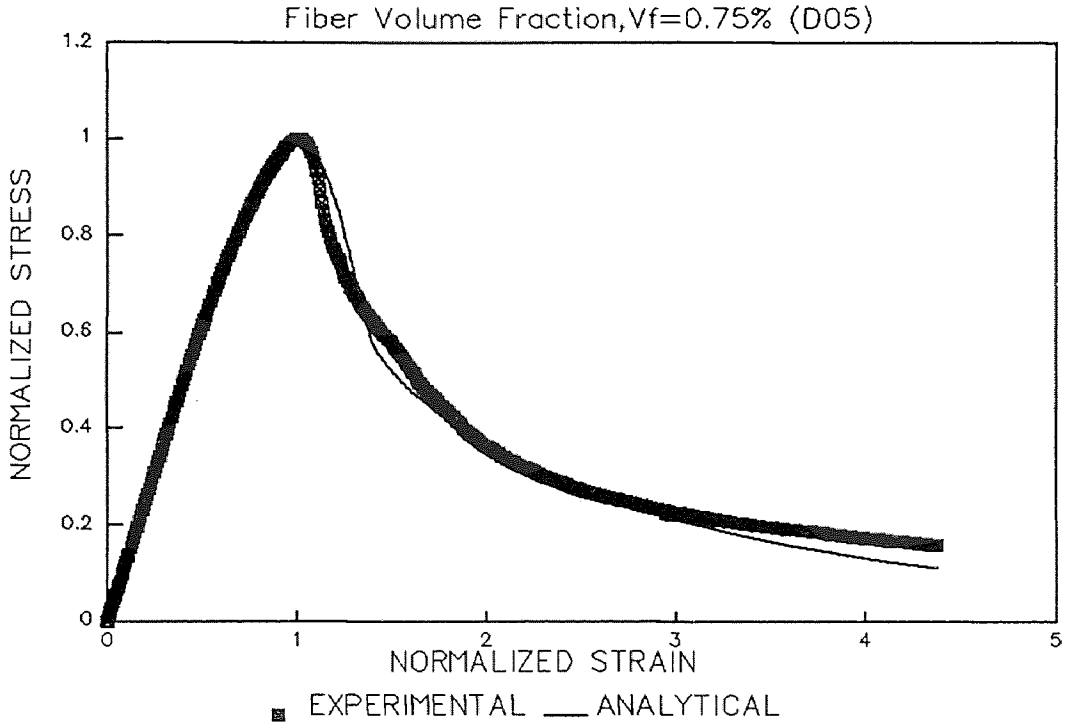

Figure D.11 Fitting Proposed Equations to Experimental Data for HSC at 0.75% Fiber Volume Fraction.

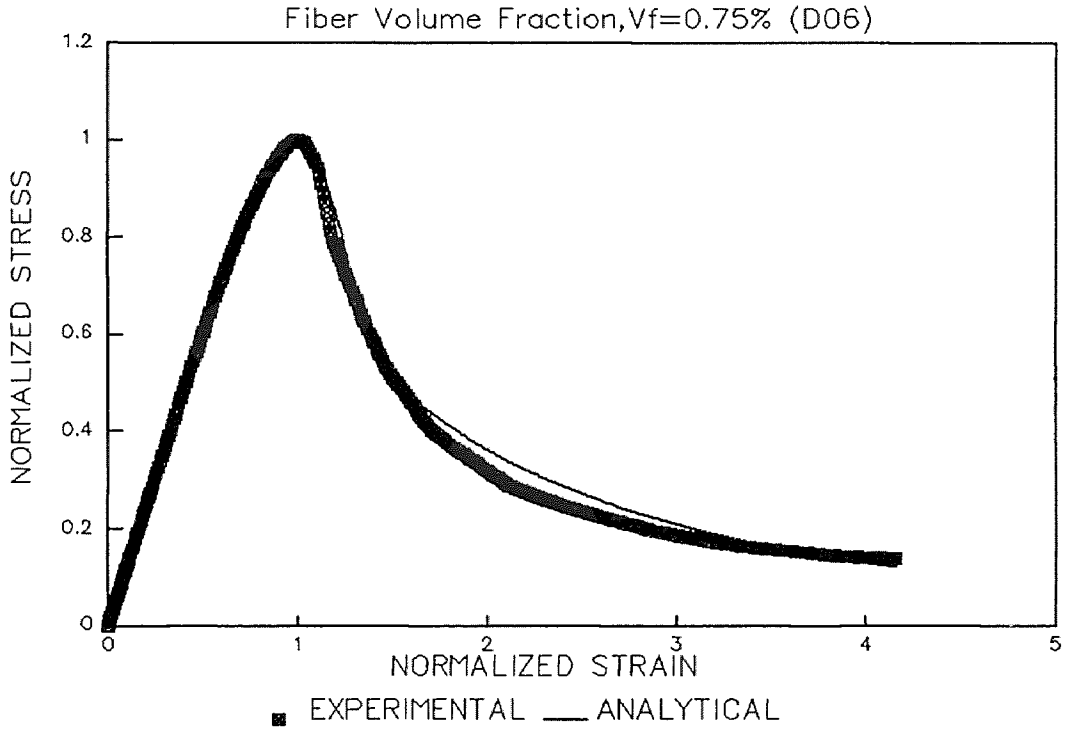

Figure D.12 Fitting Proposed Equations to Experimental Data for HSC at 0.75% Fiber Volume Fraction.

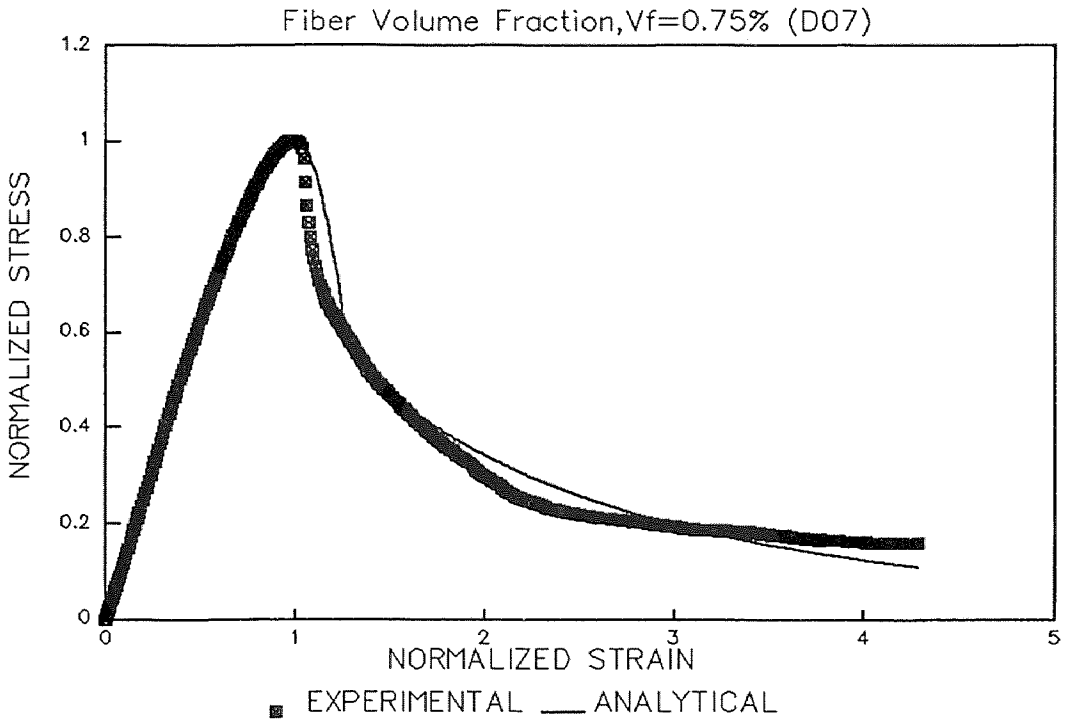

Figure D.13 Fitting Proposed Equations to Experimental Data for HSC at 0.75% Fiber Volume Fraction.

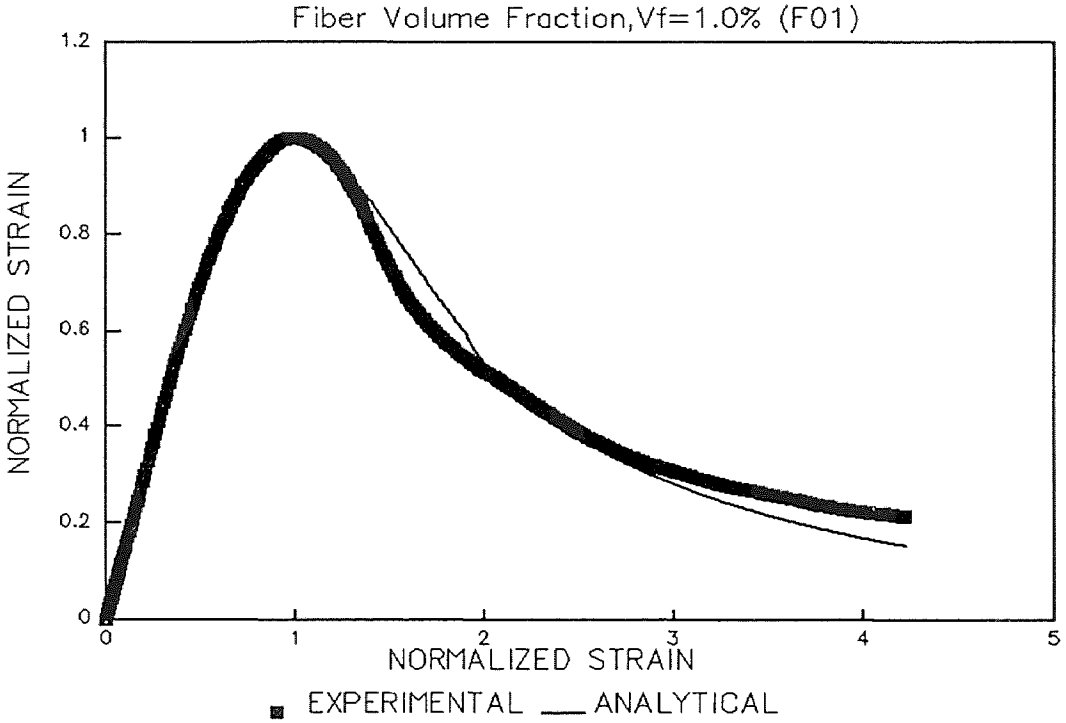

Figure D.14 Fitting Proposed Equations to Experimental Data for HSC at 1.0% Fiber Volume Fraction.

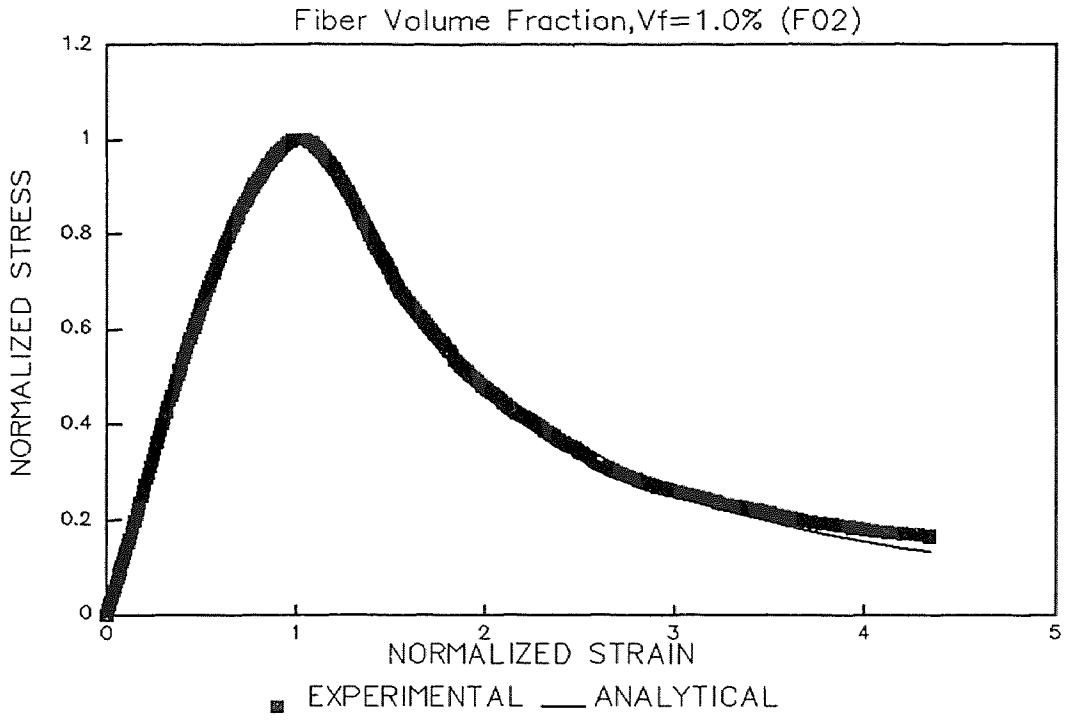

Figure D.15 Fitting Proposed Equations to Experimental Data for HSC at 1.0% Fiber Volume Fraction.

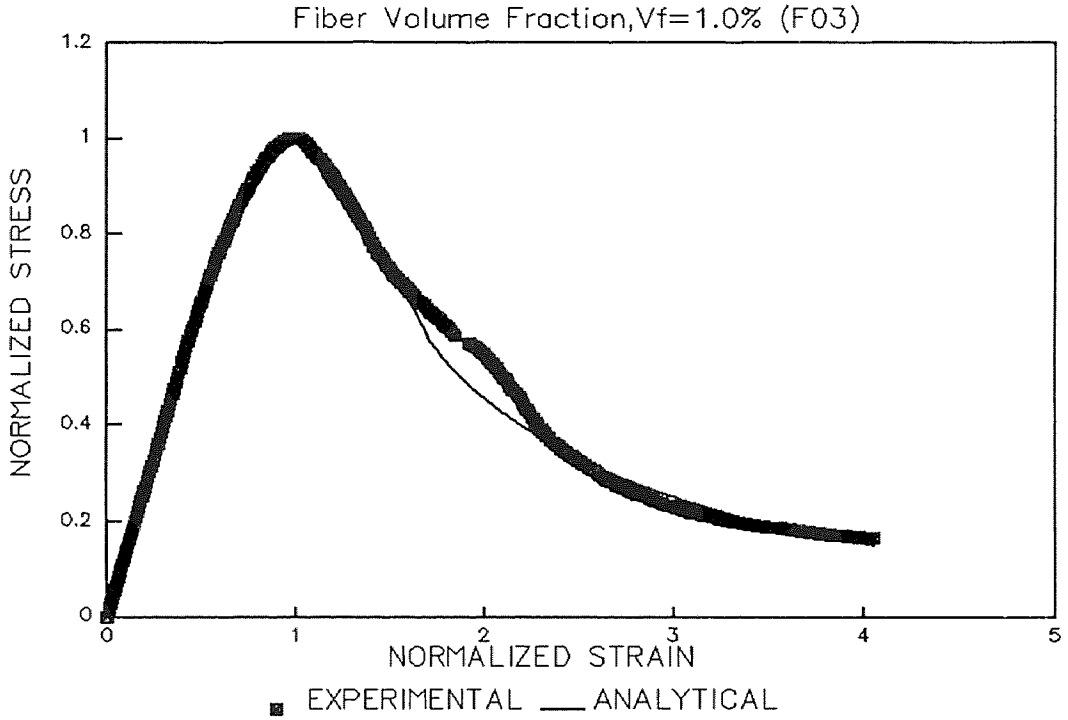

Figure D.16 Fitting Proposed Equations to Experimental Data for HSC at 1.0% Fiber Volume Fraction.

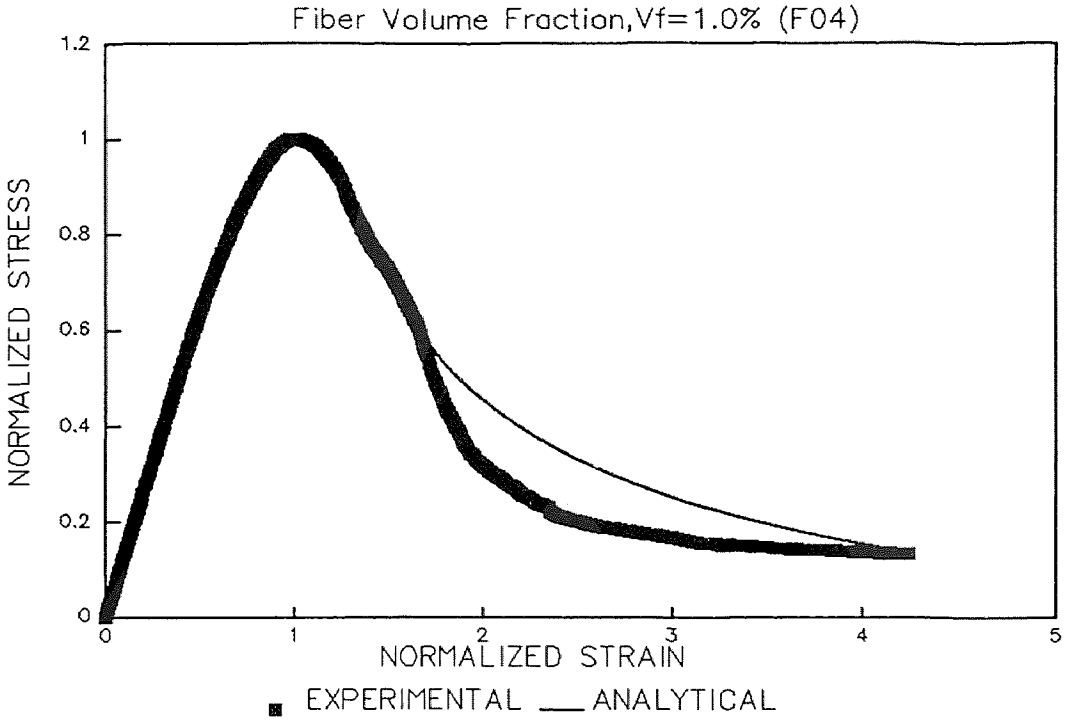

Figure D.17 Fitting Proposed Equations to Experimental Data for HSC at 1.0% Fiber Volume Fraction.

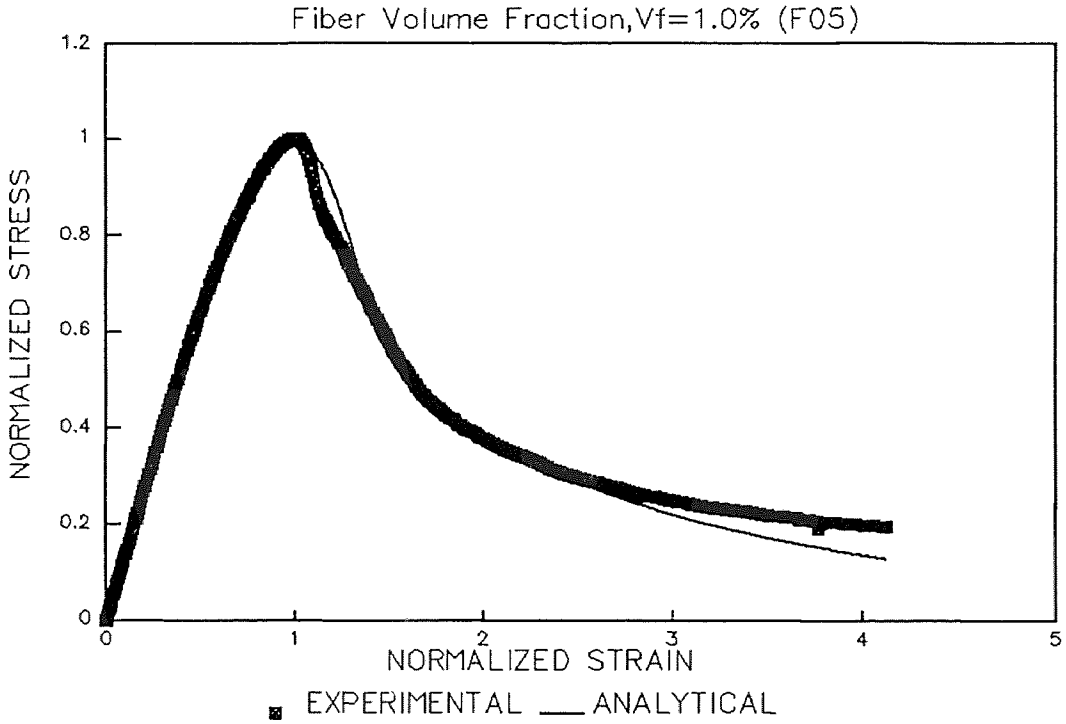

Figure D.18 Fitting Proposed Equations to Experimental Data for HSC at 1.0% Fiber Volume Fraction.

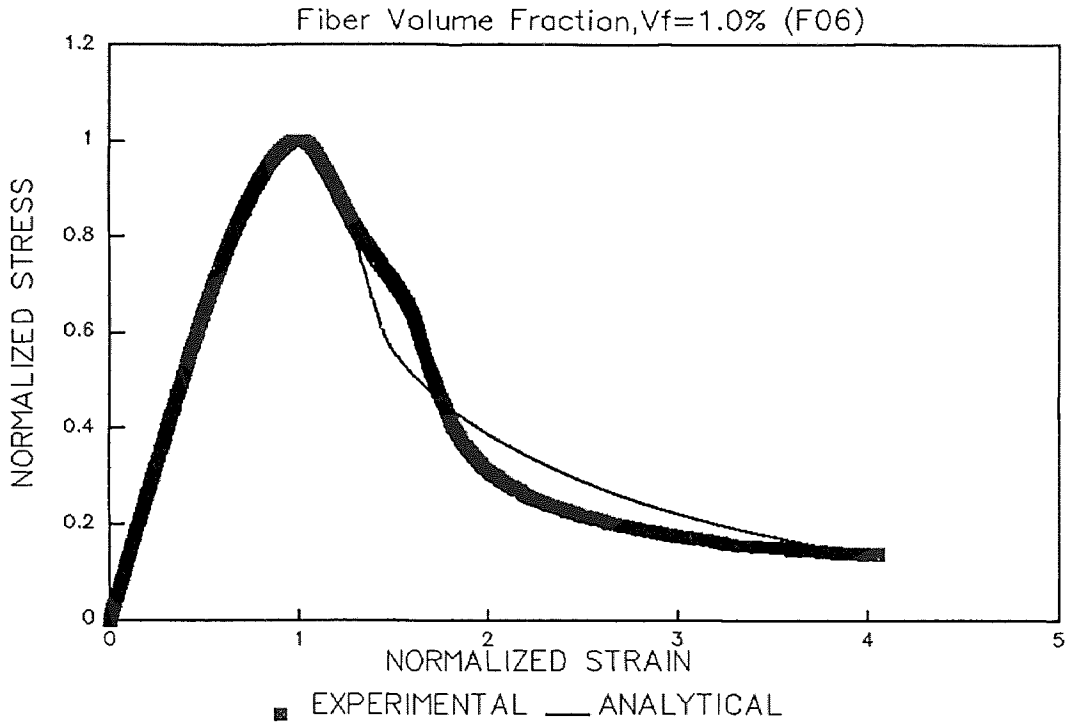

Figure D.19 Fitting Proposed Equations to Experimental Data for HSC at 1.0% Fiber Volume Fraction.

APPENDIX E
FITTING PROPOSED EQUATIONS TO EXPERIMENT DATA AT DIFFERENT FIBER VOLUME FRACTION AND TIE SPACING

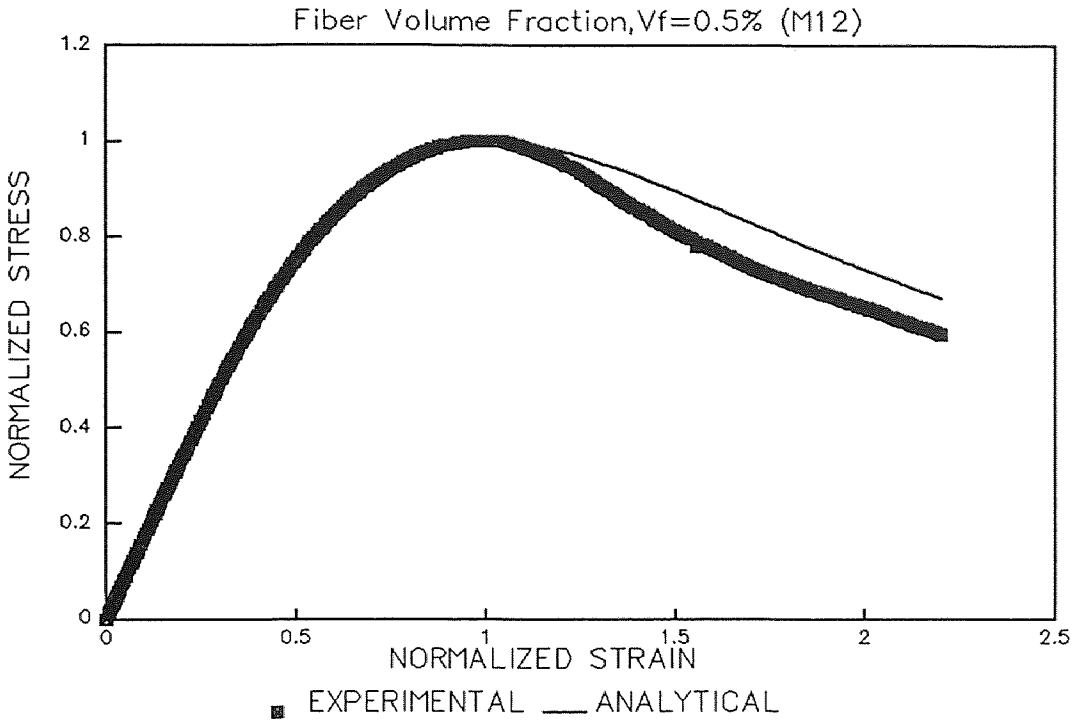

Figure E.1 Fitting Proposed Equations to Experimental Data for HSC at Tie Spacing of 1 in. and 0.5% Fiber Volume Fraction.

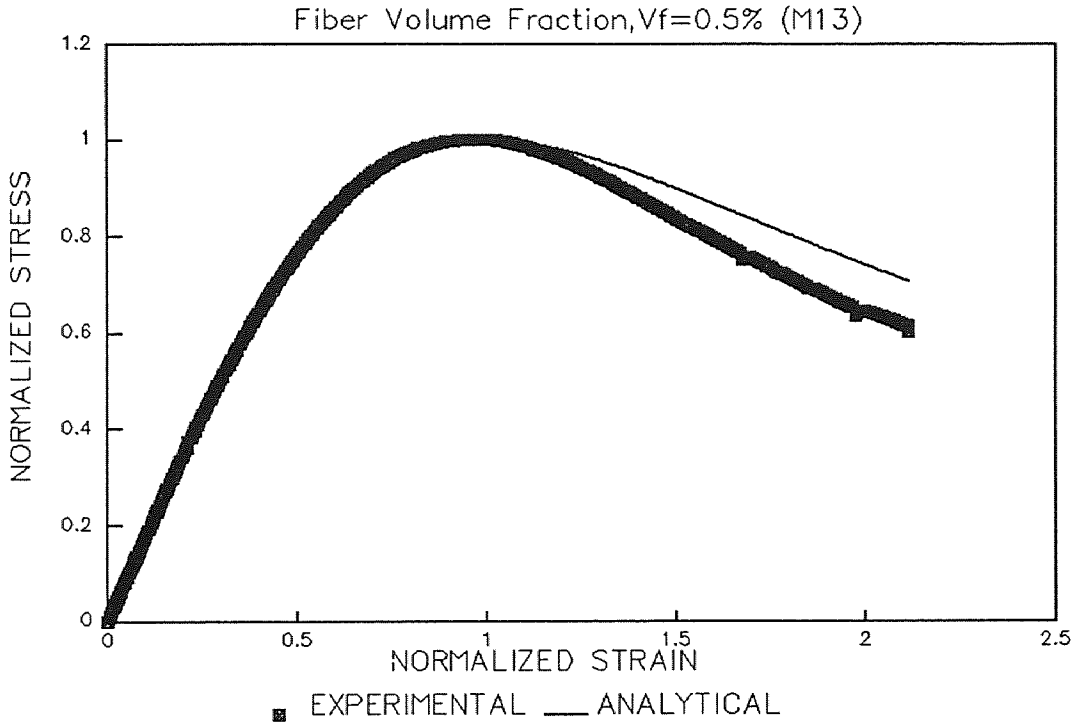

Figure E.2 Fitting Proposed Equations to Experimental Data for HSC at Tie Spacing of 1 in. and 0.5% Fiber Volume Fraction.

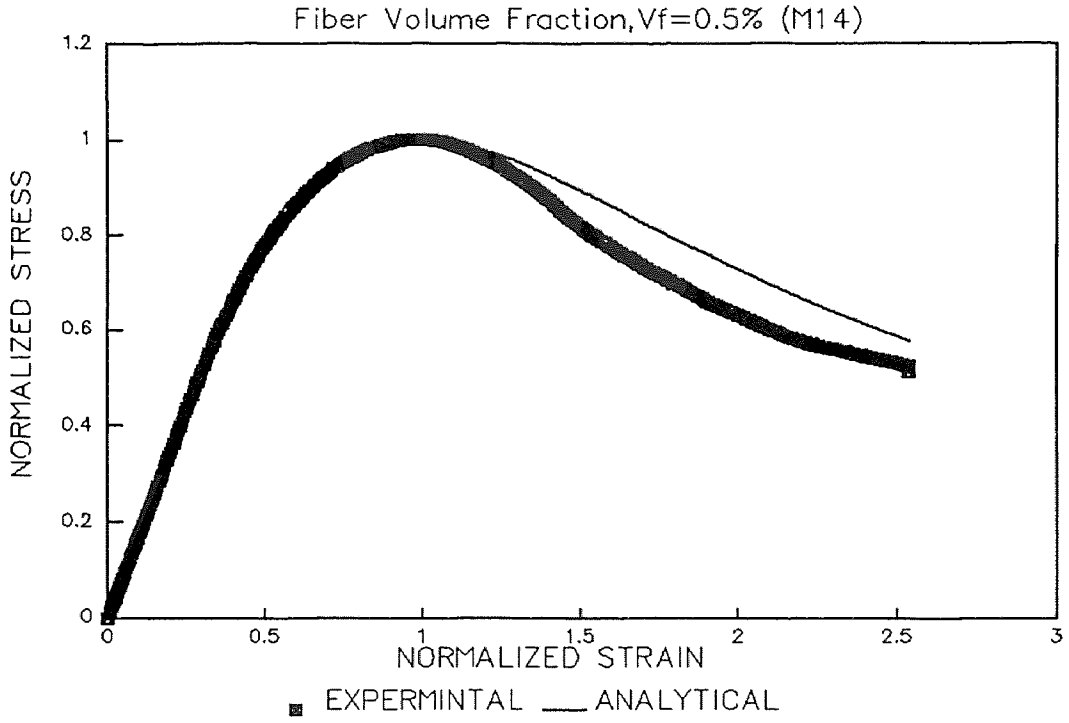

Figure E.3 Fitting Proposed Equations to Experimental Data for HSC at Tie Spacing of 1 in. and 0.5% Fiber Volume Fraction.

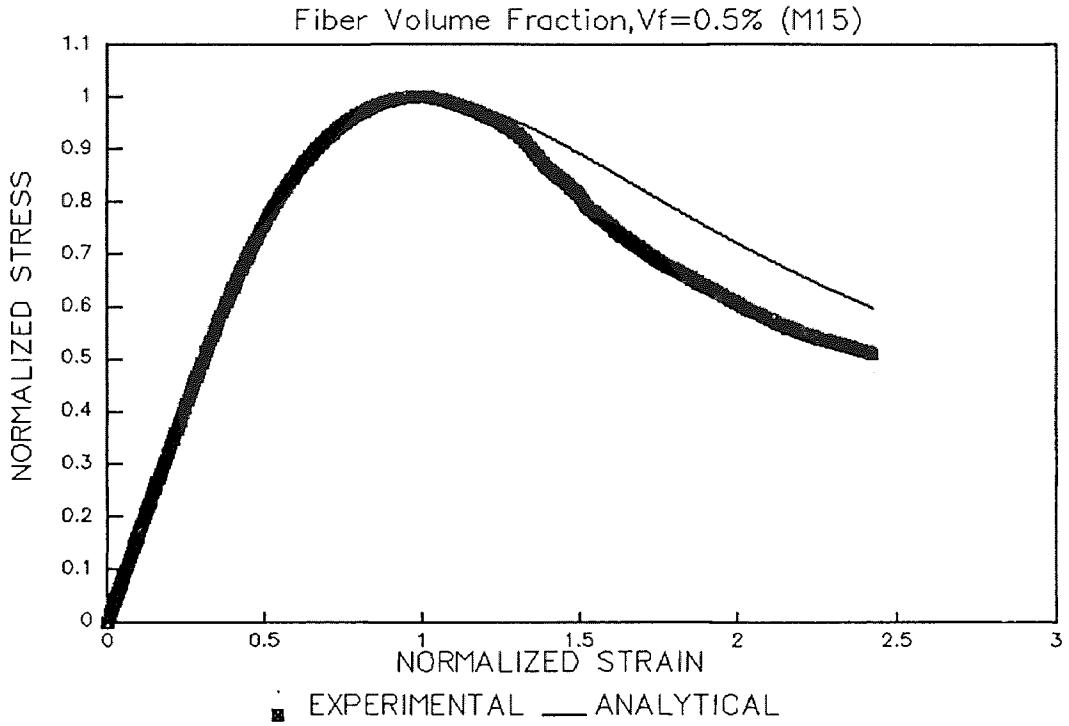

Figure E.4 Fitting Proposed Equations to Experimental Data for HSC at Tie Spacing of 1 in. and 0.5% Fiber Volume Fraction.

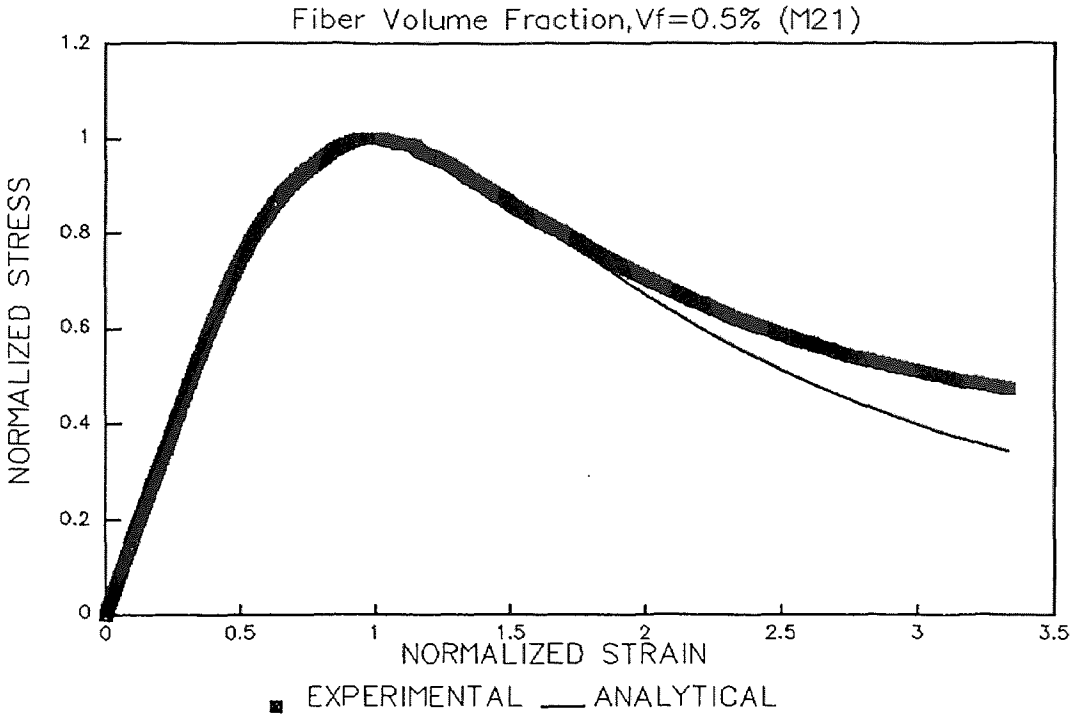

Figure E.5 Fitting Proposed Equations to Experimental Data for HSC at Tie Spacing of 2 in. and 0.5% Fiber Volume Fraction.

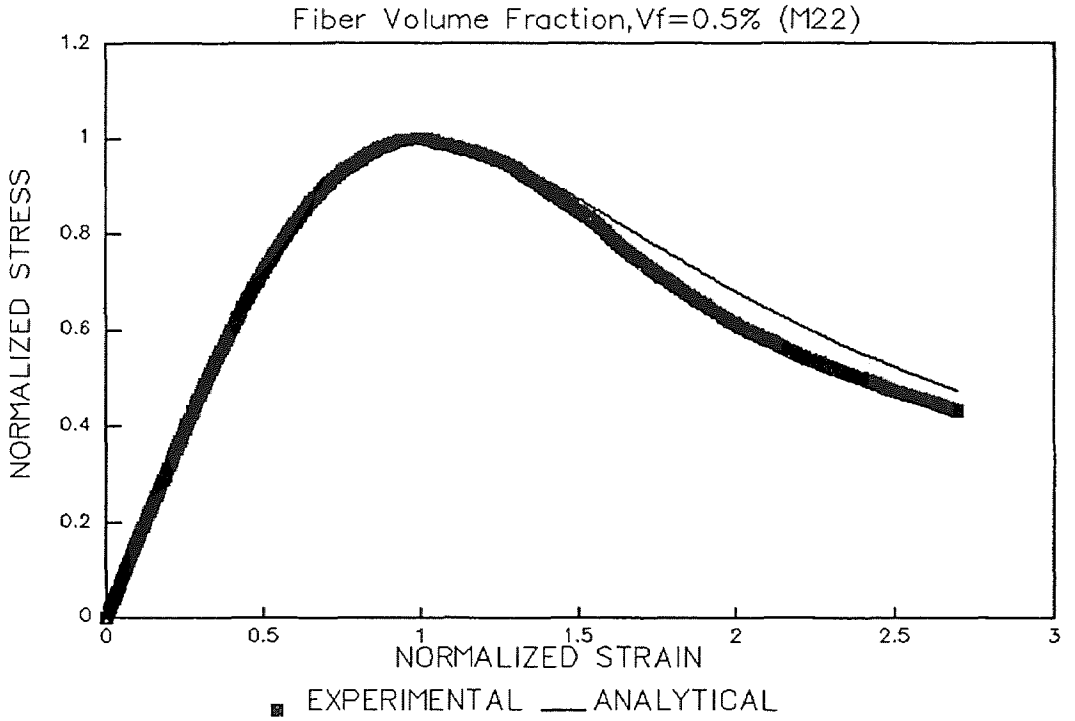

Figure E.6 Fitting Proposed Equations to Experimental Data for HSC at Tie Spacing of 2 in. and 0.5% Fiber Volume Fraction.

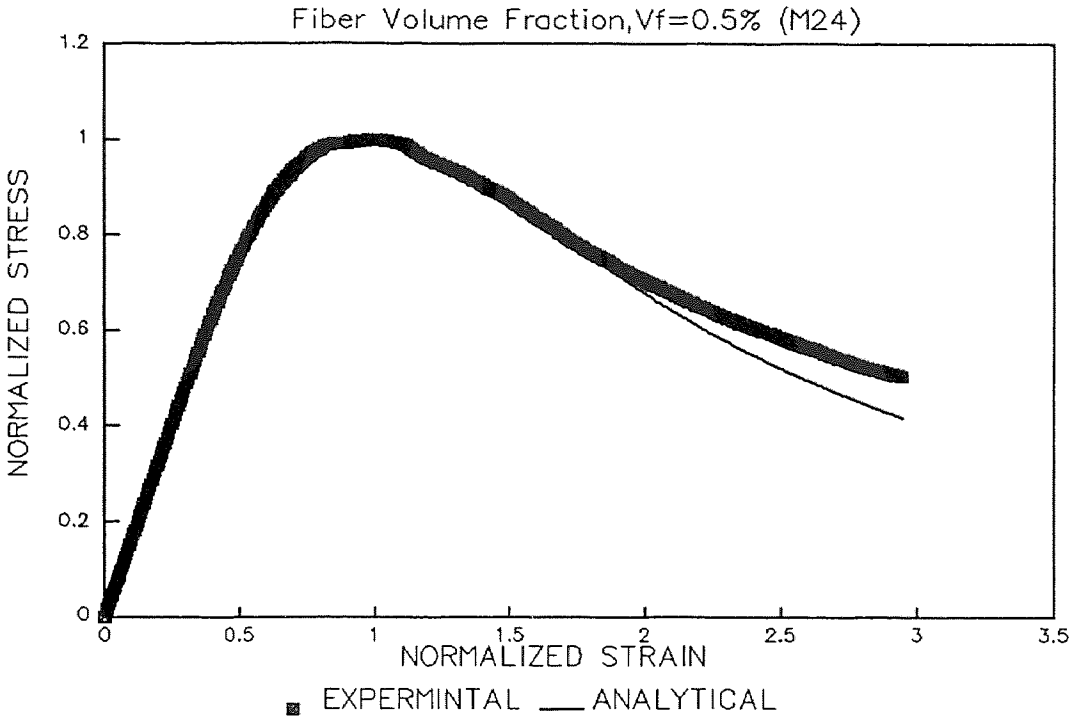

Figure E.7 Fitting Proposed Equations to Experimental Data for HSC at Tie Spacing of 2 in. and 0.5% Fiber Volume Fraction.

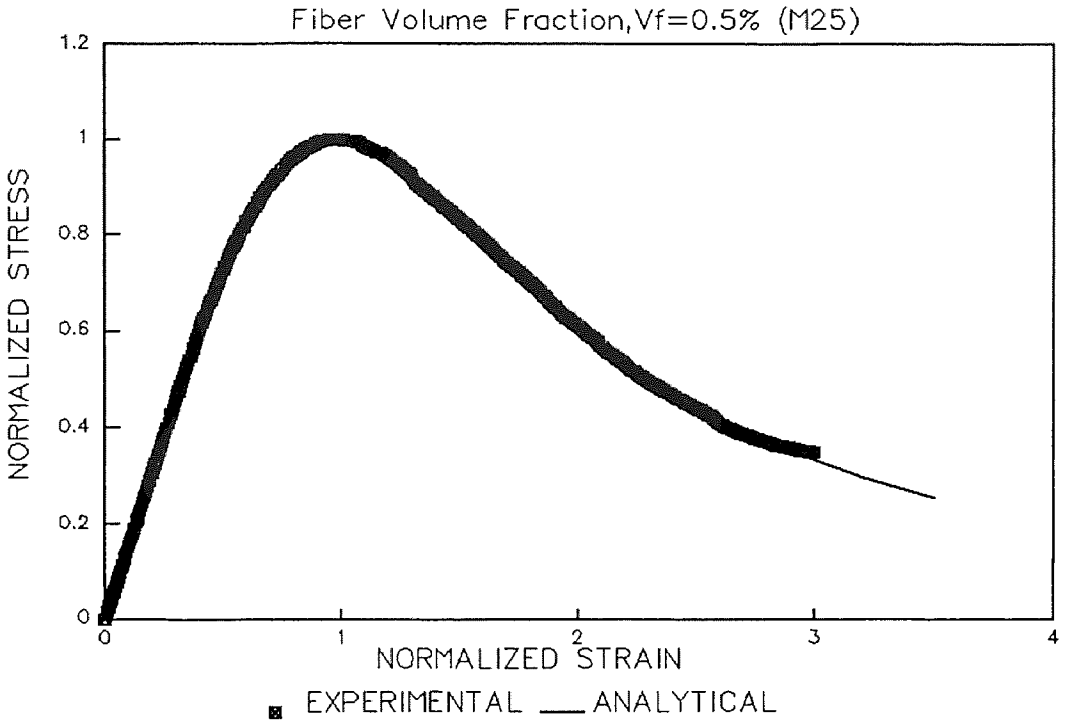

Figure E.8 Fitting Proposed Equations to Experimental Data for HSC at Tie Spacing of 2 in. and 0.5% Fiber Volume Fraction.

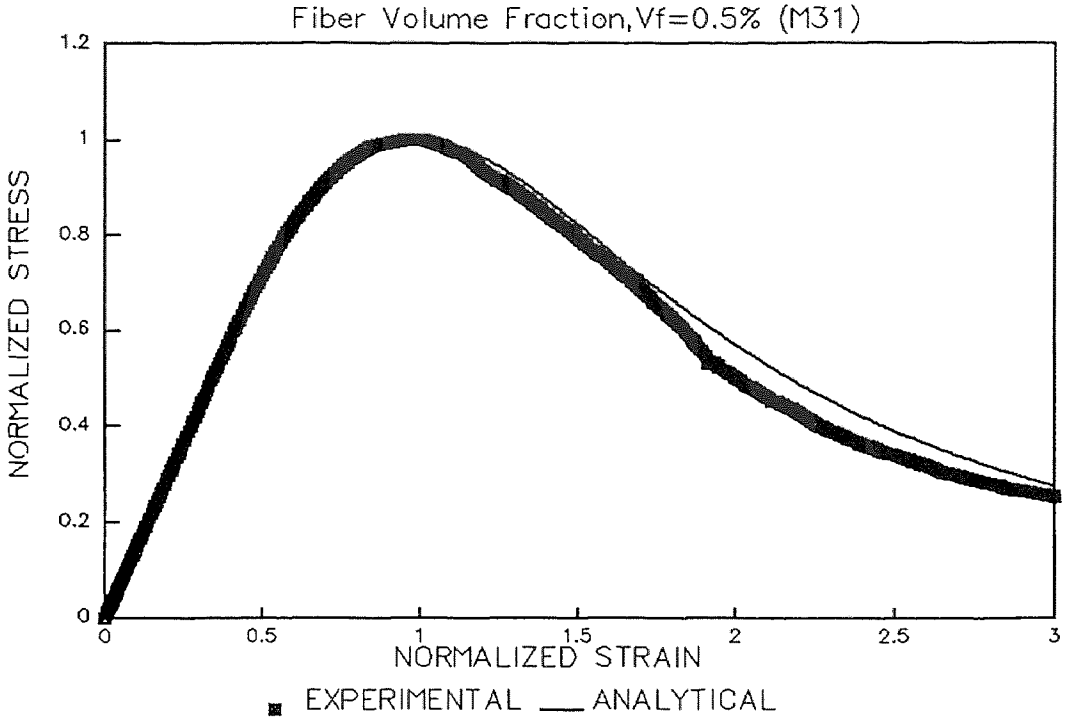

Figure E.9 Fitting Proposed Equations to Experimental Data for HSC at Tie Spacing of 3 in. and 0.5% Fiber Volume Fraction.

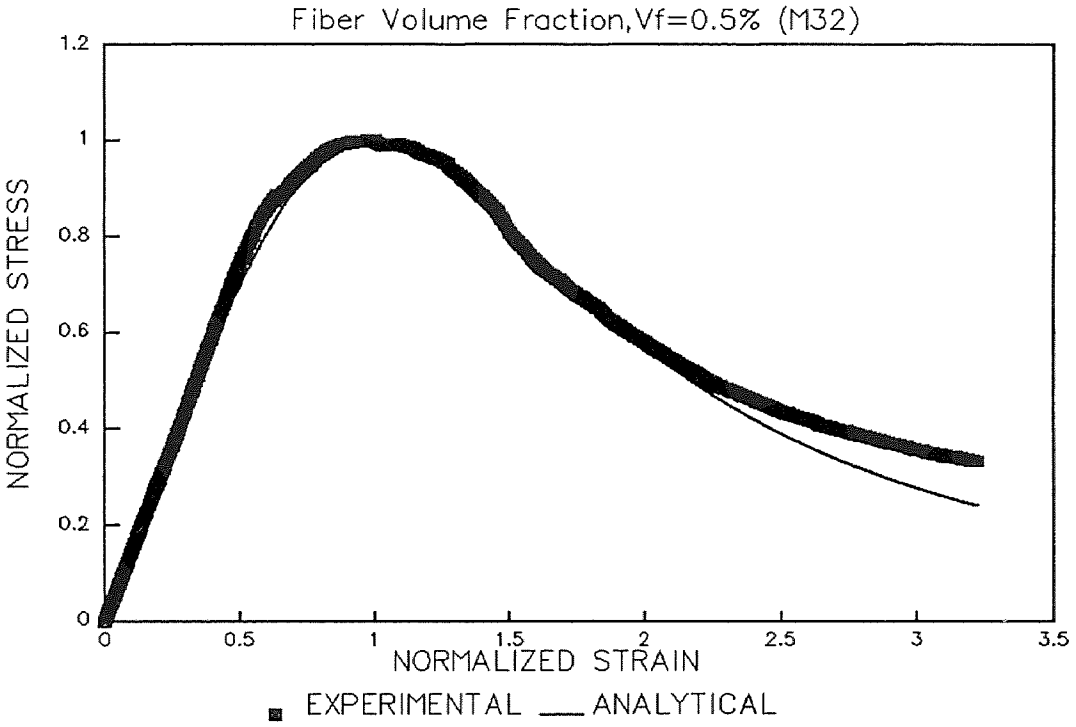

Figure E.10 Fitting Proposed Equations to Experimental Data for HSC at Tie Spacing of 3 in. and 0.5% Fiber Volume Fraction.

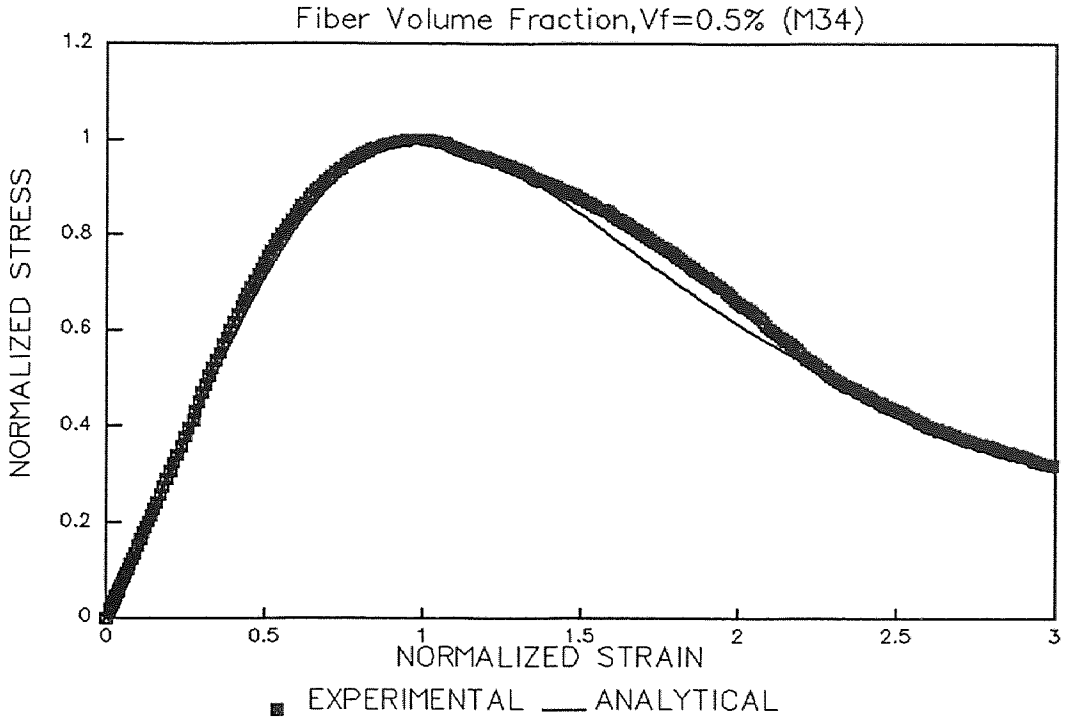

Figure E.11 Fitting Proposed Equations to Experimental Data for HSC at Tie Spacing of 3 in. and 0.5% Fiber Volume Fraction.

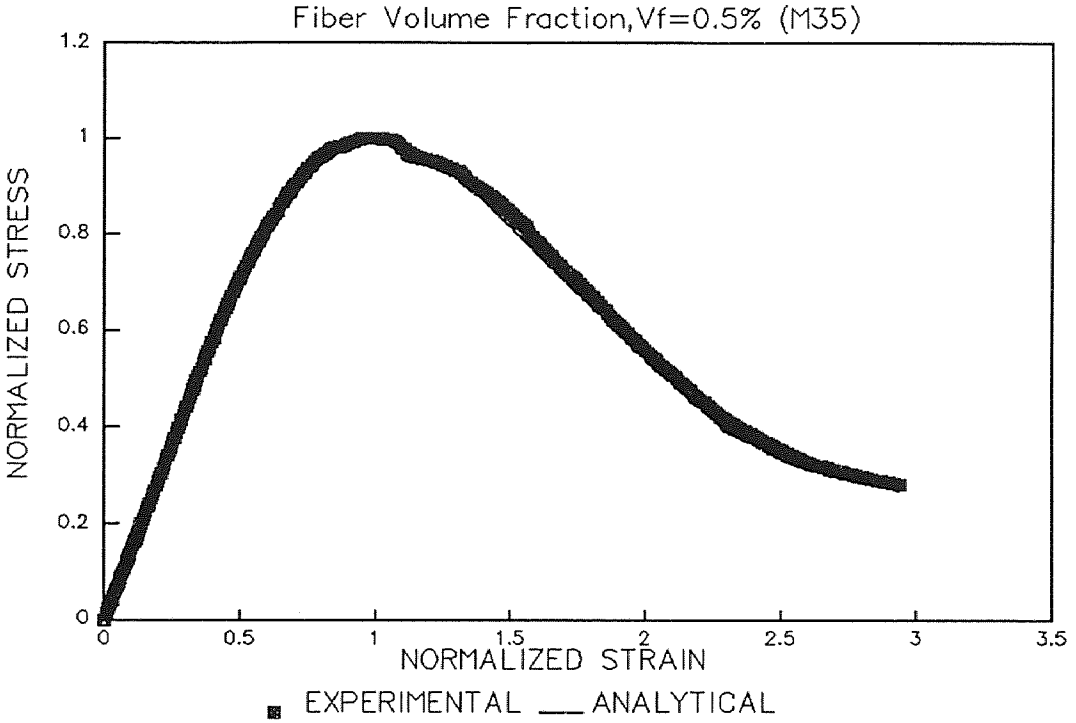

Figure E.12 Fitting Proposed Equations to Experimental Data for HSC at Tie Spacing of 3 in. and 0.5% Fiber Volume Fraction.

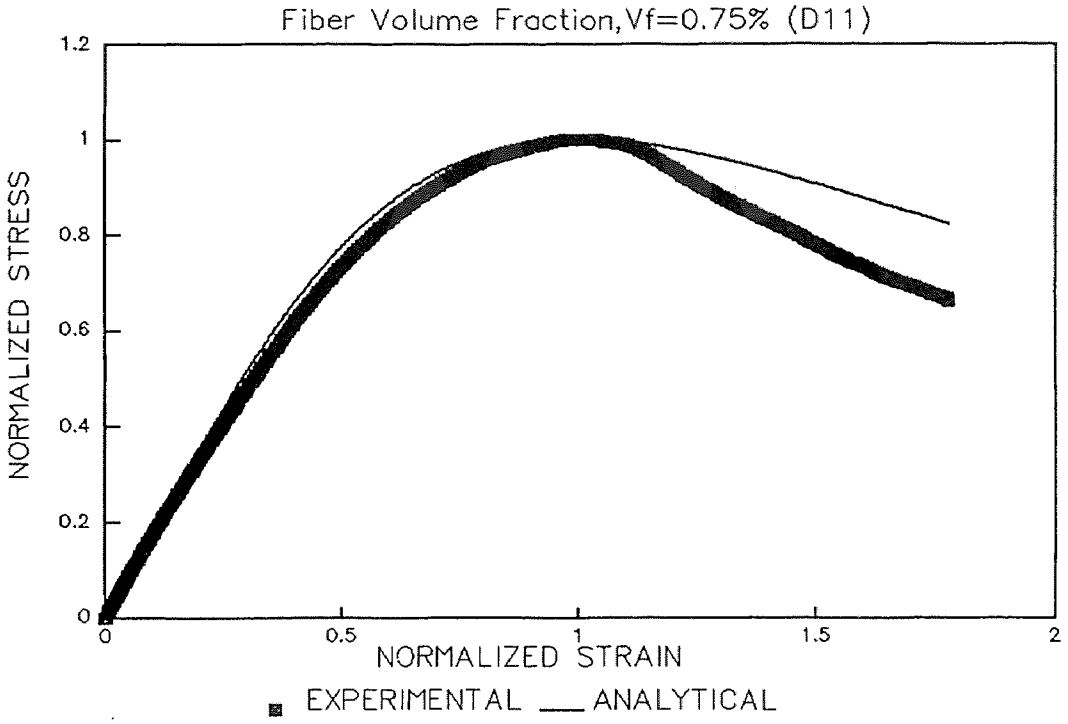

Figure E.13 Fitting Proposed Equations to Experimental Data for HSC at Tie Spacing of 1 in. and 0.75% Fiber Volume Fraction.

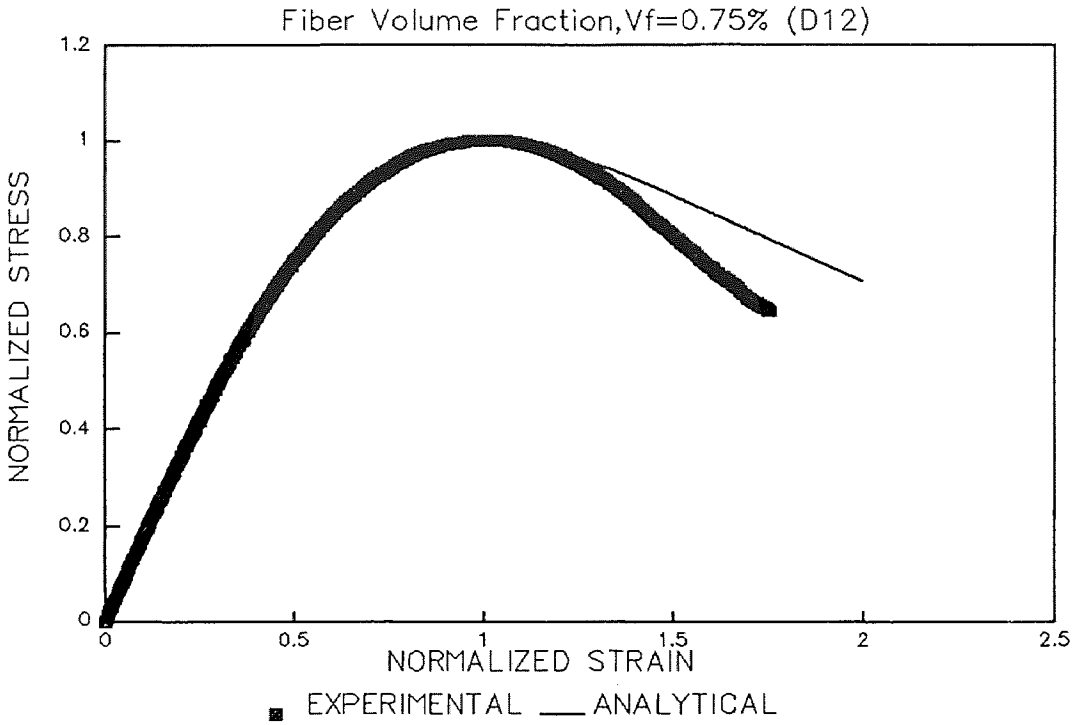

Figure E.14 Fitting Proposed Equations to Experimental Data for HSC at Tie Spacing of 1 in. and 0.75% Fiber Volume Fraction.

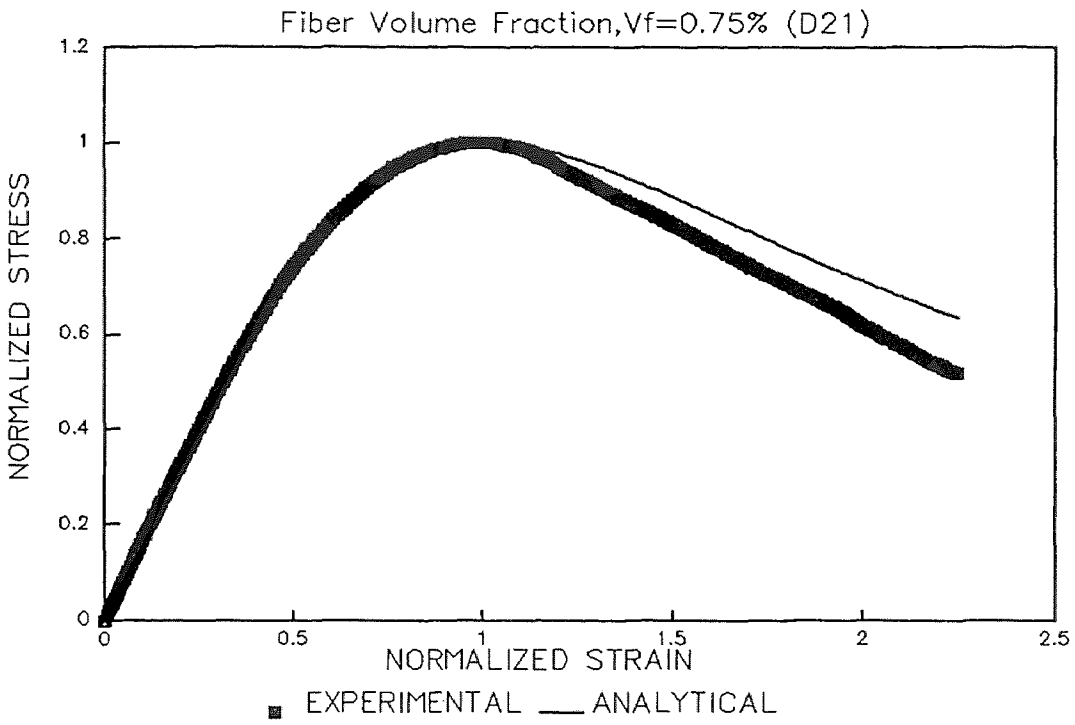

Figure E.15 Fitting Proposed Equations to Experimental Data for HSC at Tie Spacing of 2 in. and 0.75% Fiber Volume Fraction.

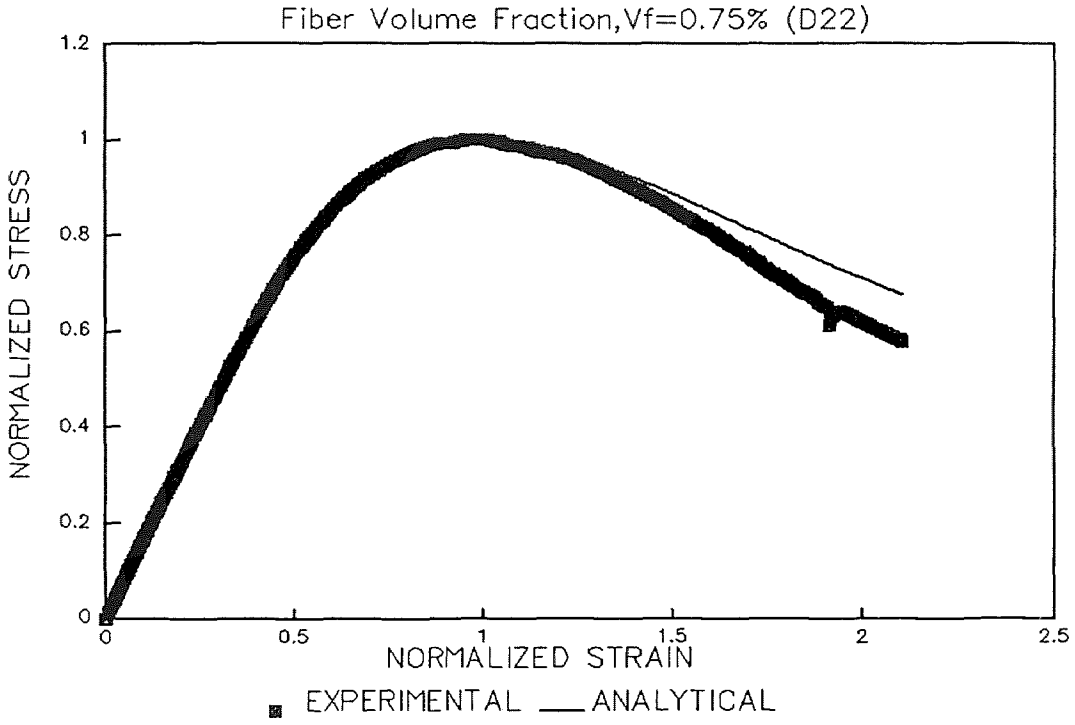

Figure E.16 Fitting Proposed Equations to Experimental Data for HSC at Tie Spacing of 2 in. and 0.75% Fiber Volume Fraction.

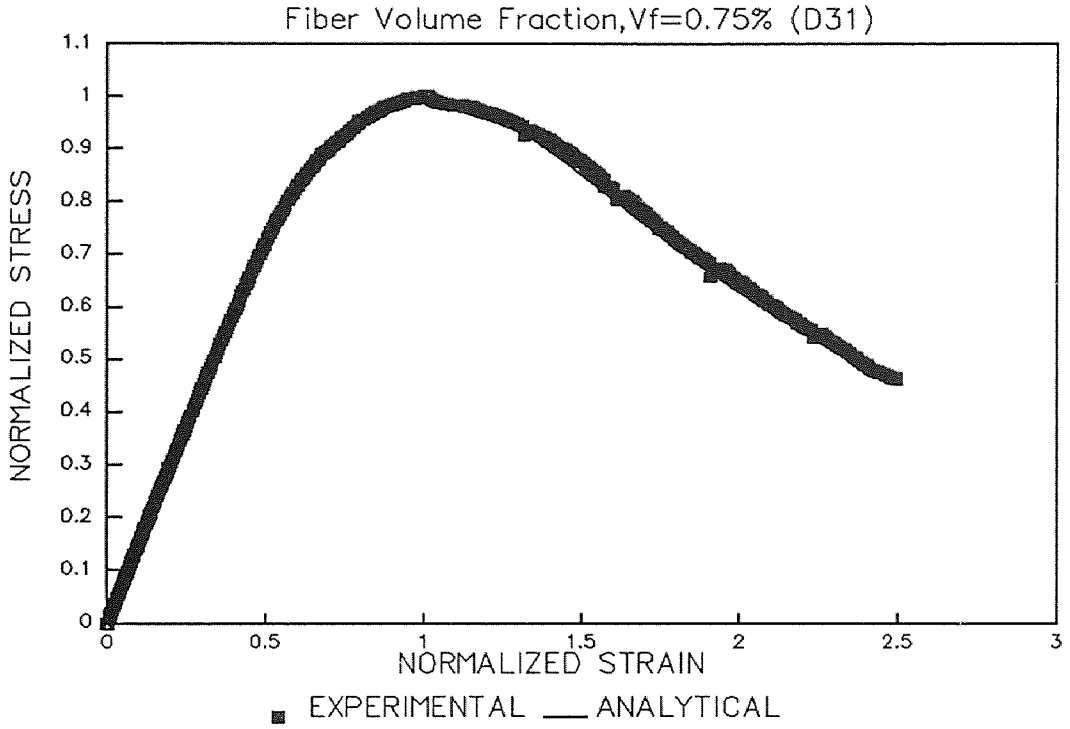

Figure E.17 Fitting Proposed Equations to Experimental Data for HSC at Tie Spacing of 3 in. and 0.75% Fiber Volume Fraction.

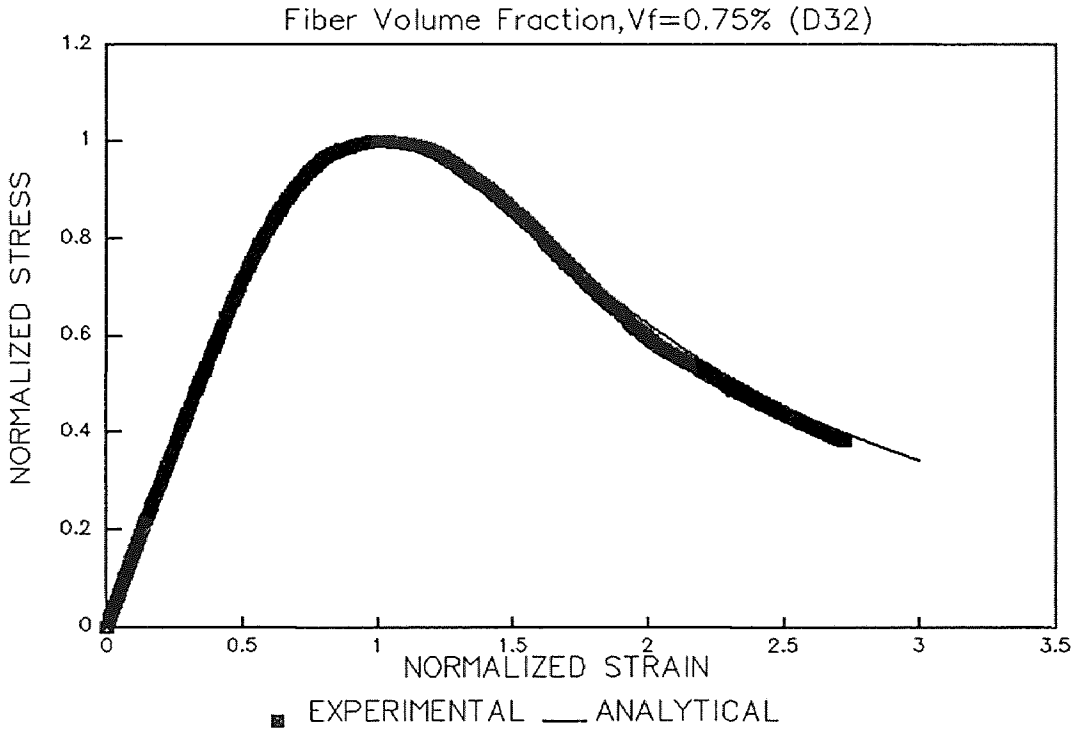

Figure E.18 Fitting Proposed Equations to Experimental Data for HSC at Tie Spacing of 3 in. and 0.75% Fiber Volume Fraction.

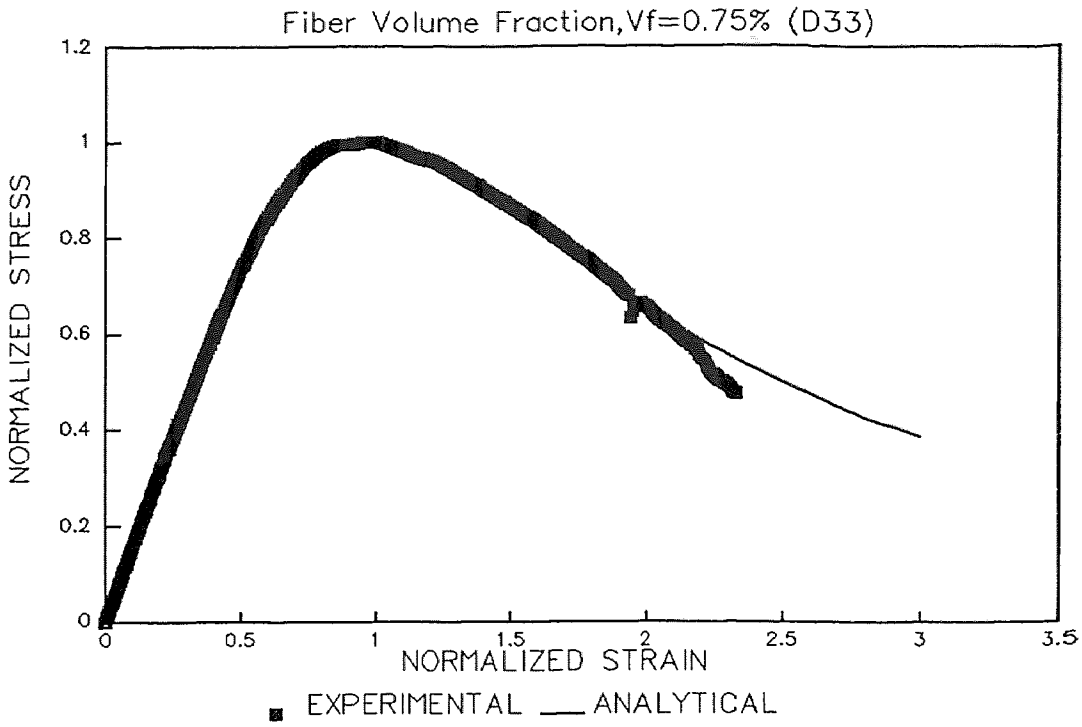

Figure E.19 Fitting Proposed Equations to Experimental Data for HSC at Tie Spacing of 3 in. and 0.75% Fiber Volume Fraction.

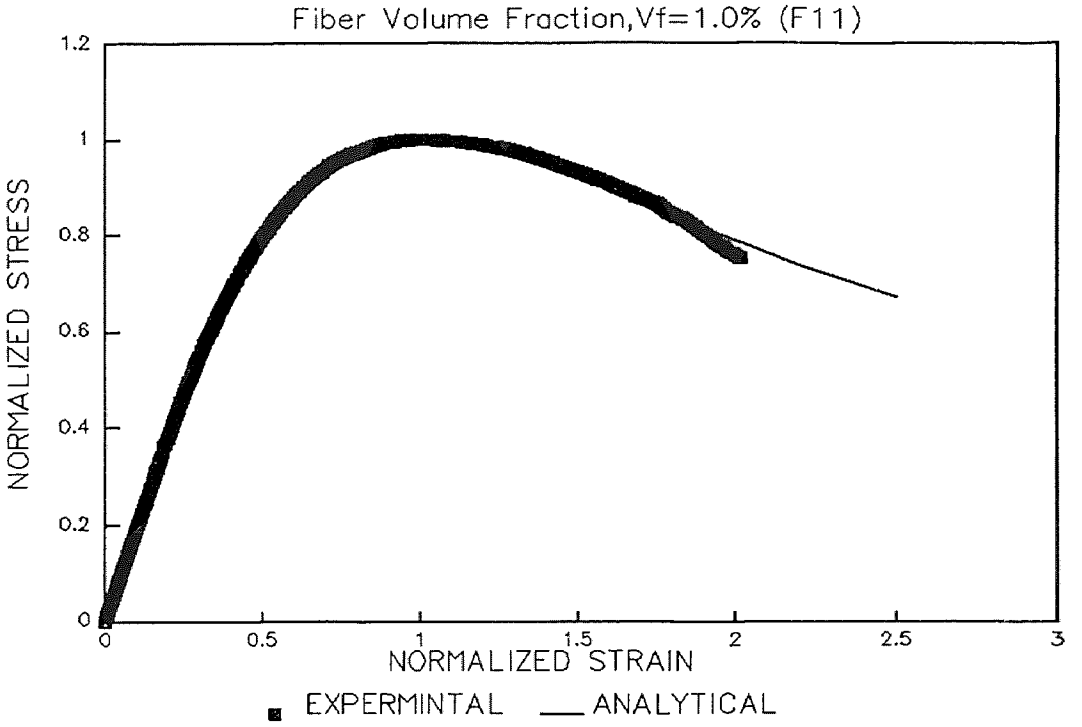

Figure E.20 Fitting Proposed Equations to Experimental Data for HSC at Tie Spacing of 1 in. and 1.0% Fiber Volume Fraction.

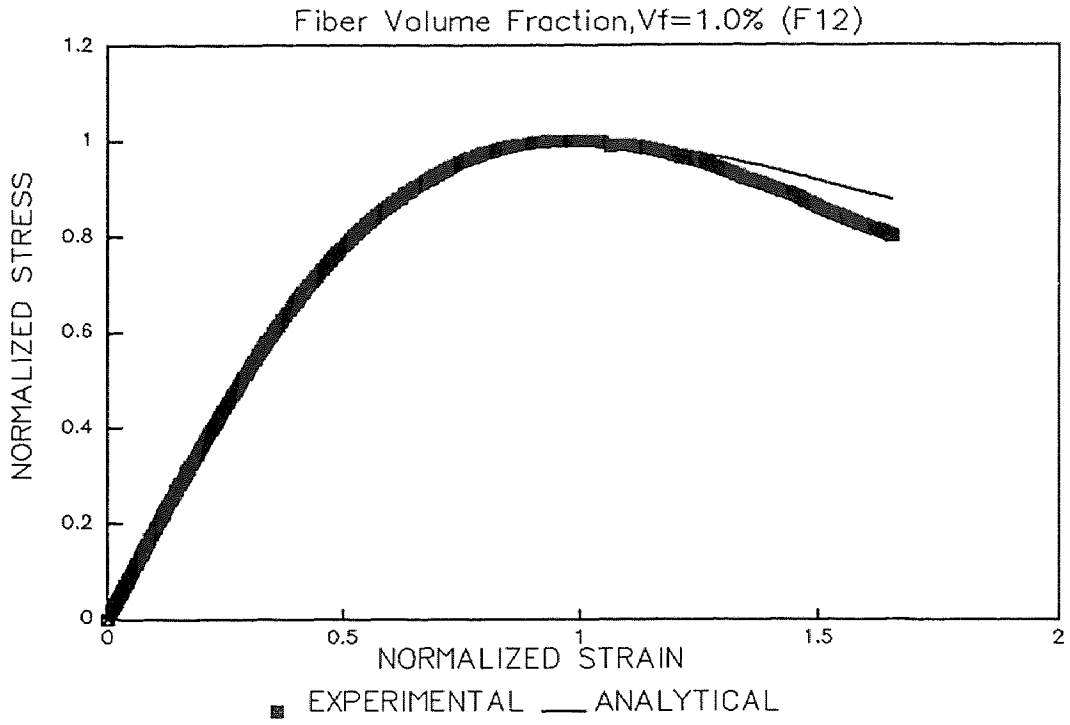

Figure E.21 Fitting Proposed Equations to Experimental Data for HSC at Tie Spacing of 1 in. and 1.0% Fiber Volume Fraction.

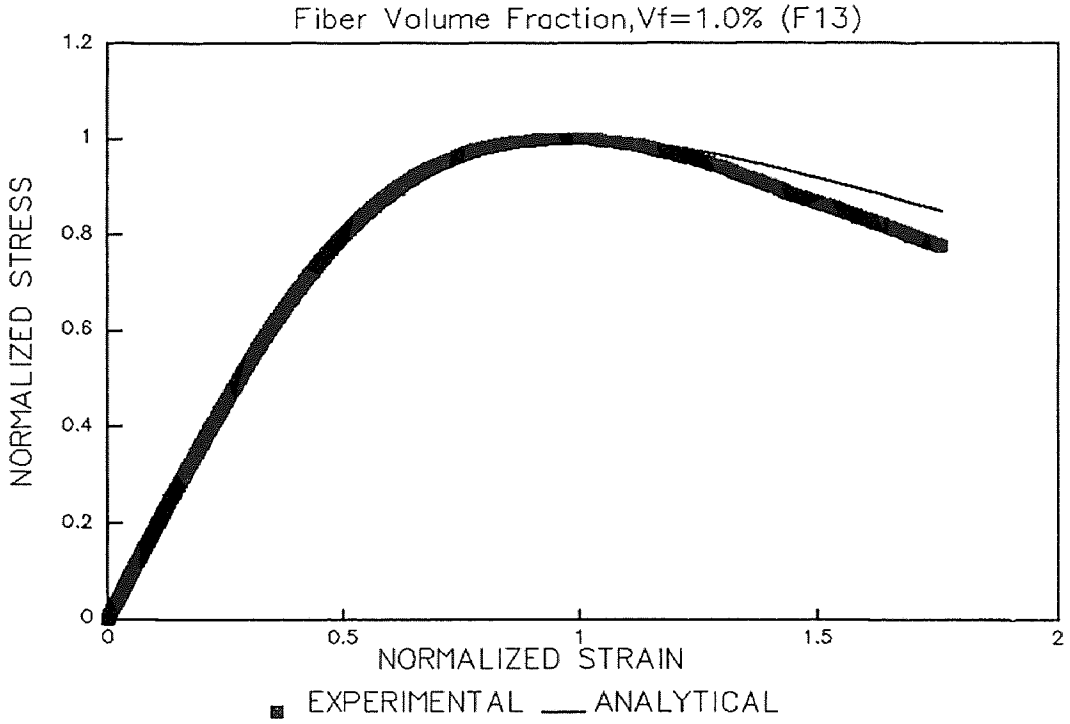

Figure E.22 Fitting Proposed Equations to Experimental Data for HSC at Tie Spacing of 1 in. and 1.0% Fiber Volume Fraction.

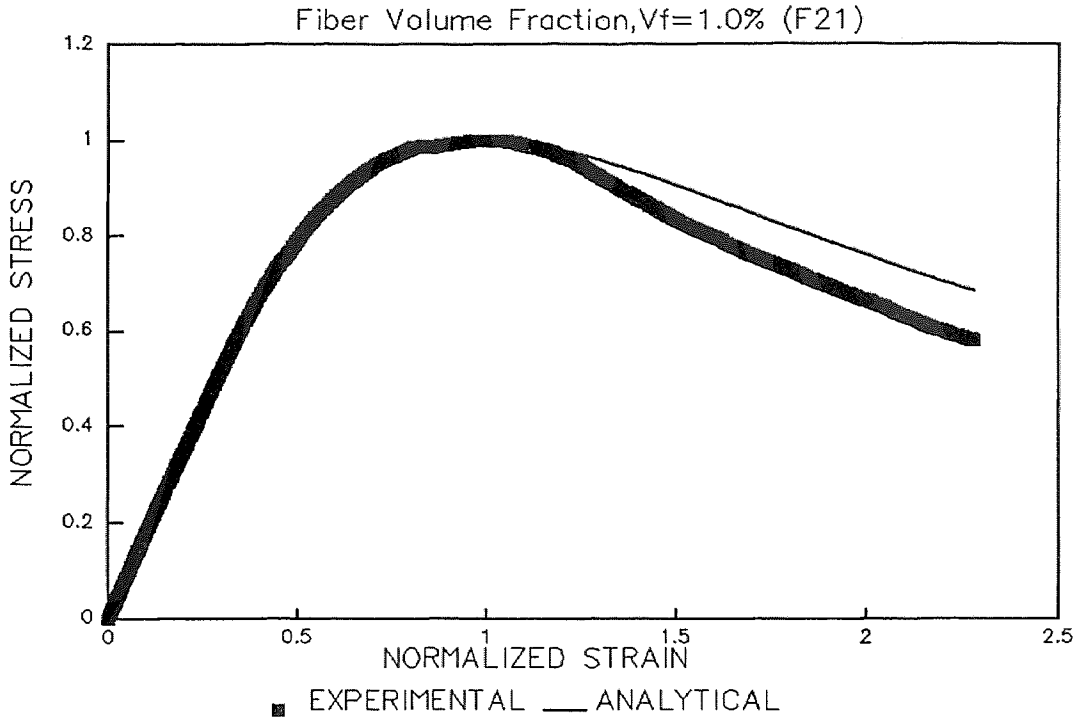

Figure E.23 Fitting Proposed Equations to Experimental Data for HSC at Tie Spacing of 2 in. and 1.0% Fiber Volume Fraction.

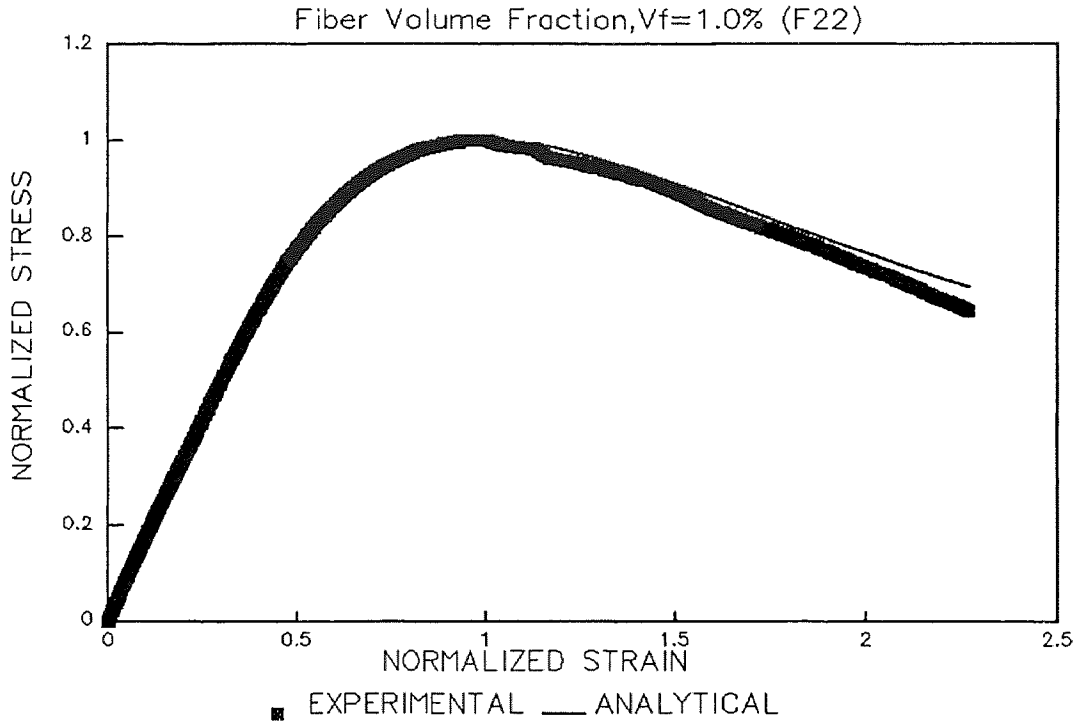

Figure E.24 Fitting Proposed Equations to Experimental Data for HSC at Tie Spacing of 2 in. and 1.0% Fiber Volume Fraction.

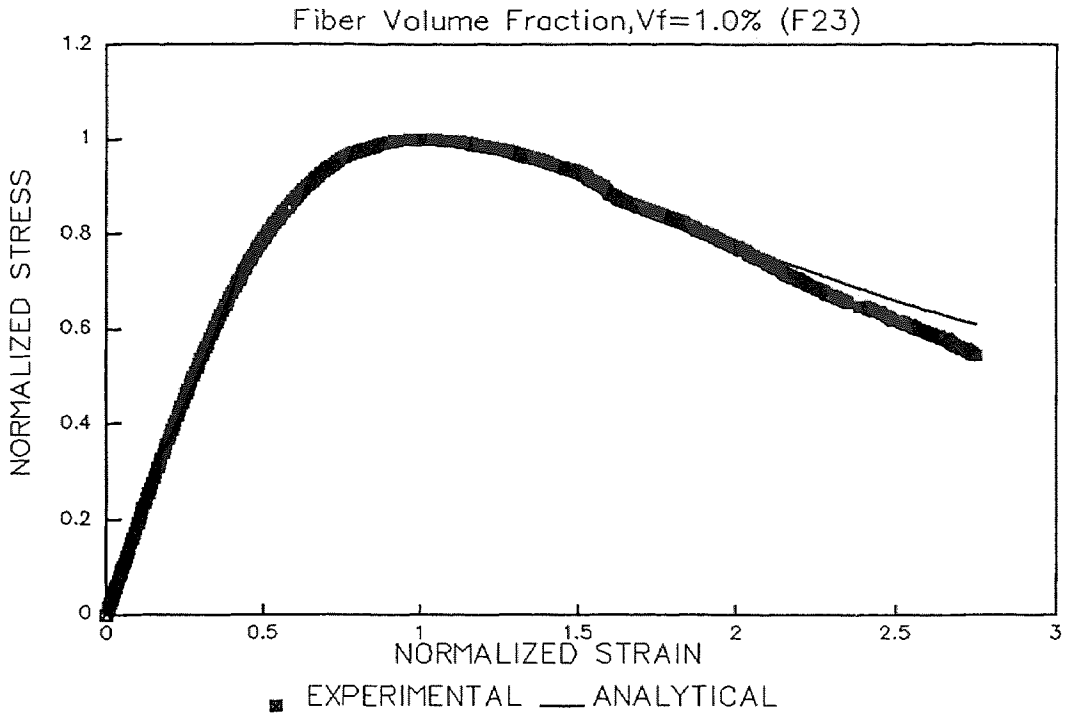

Figure E.25 Fitting Proposed Equations to Experimental Data for HSC at Tie Spacing of 2 in. and 1.0% Fiber Volume Fraction.

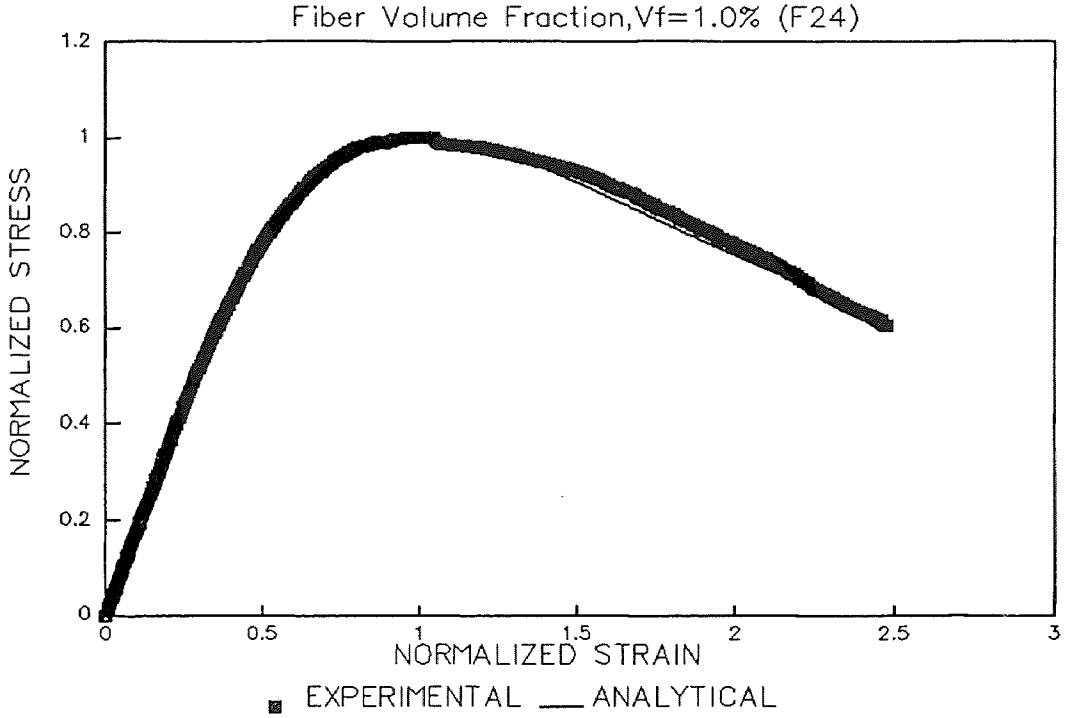

Figure E.26 Fitting proposed equations to experimental data for HSC at tie spacing of 2 in. and 1.0% fiber volume fraction.

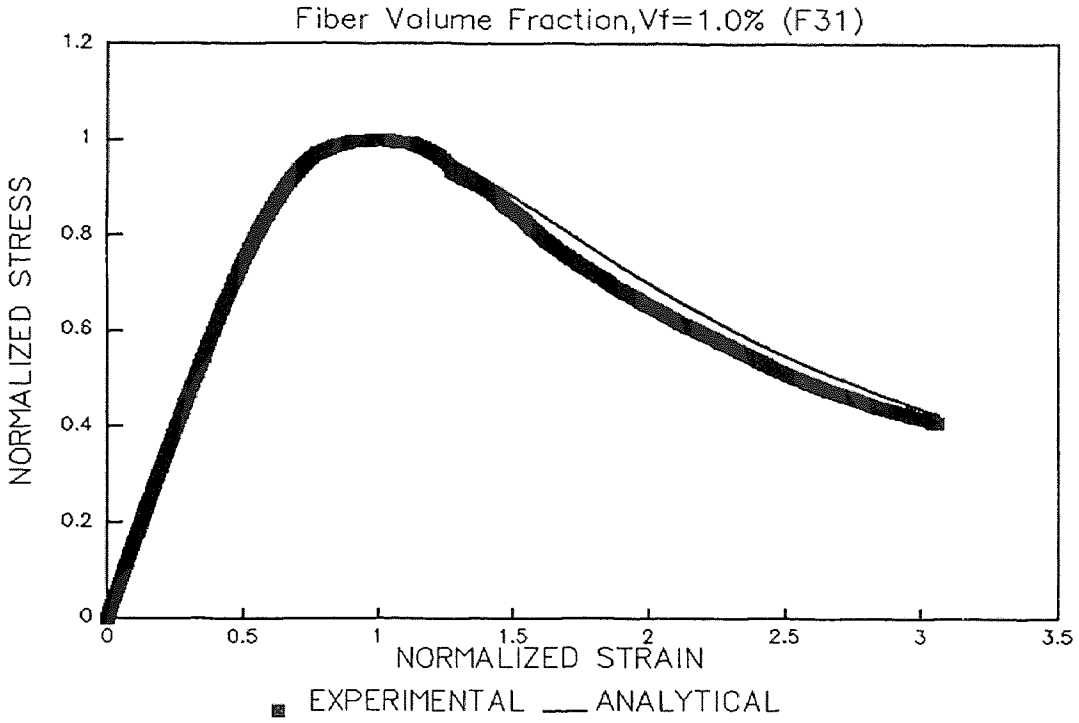

Figure E.27 Fitting Proposed Equations to Experimental Data for HSC at Tie spacing of 3 in. and 1.0% Fiber Volume Fraction.

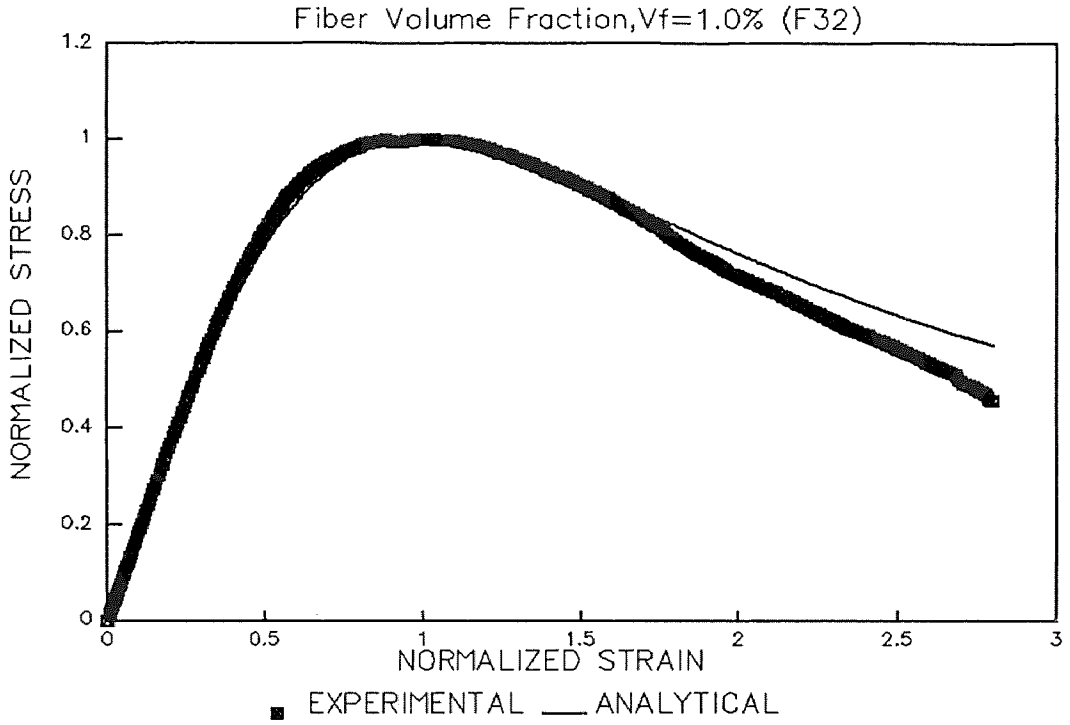

Figure E.28 Fitting Proposed Equations to Experimental Data for HSC at Tie Spacing of 3 in. and 1.0% Fiber Volume Fraction.

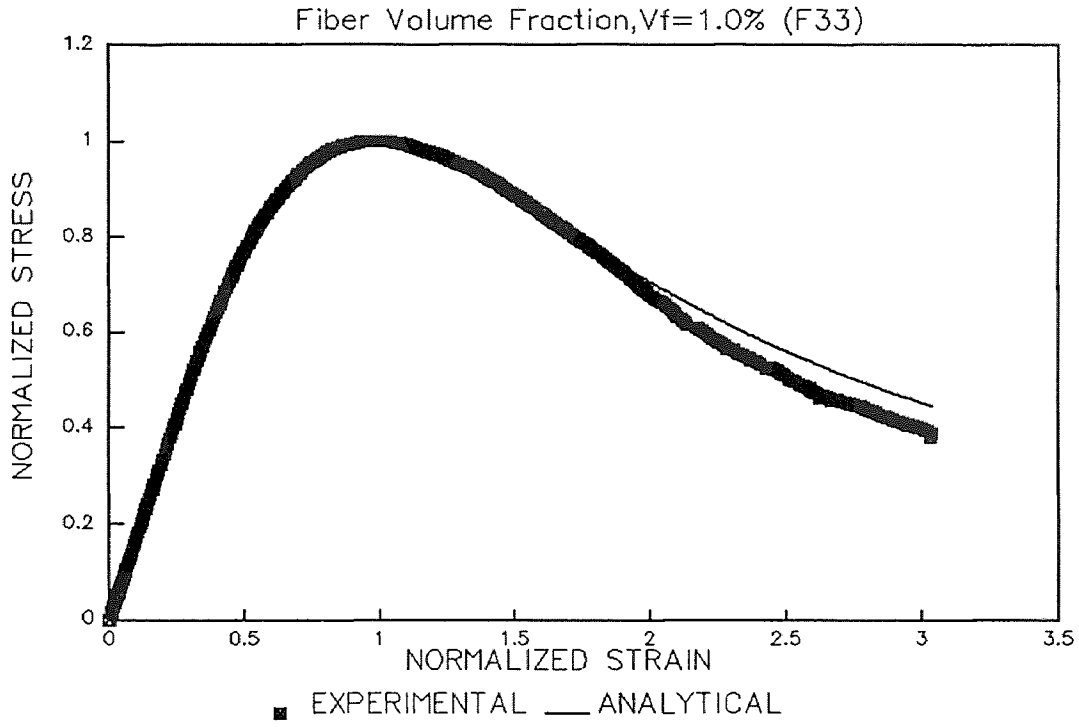

Figure E.29 Fitting Proposed Equations to Experimental Data for HSC at Tie Spacing of 3 in. and 1.0% Fiber Volume Fraction.

APPENDIX F
COMPARISON ANALYTICAL EQUATIONS AND EXPERIMENTAL RESULTS FOR HSC

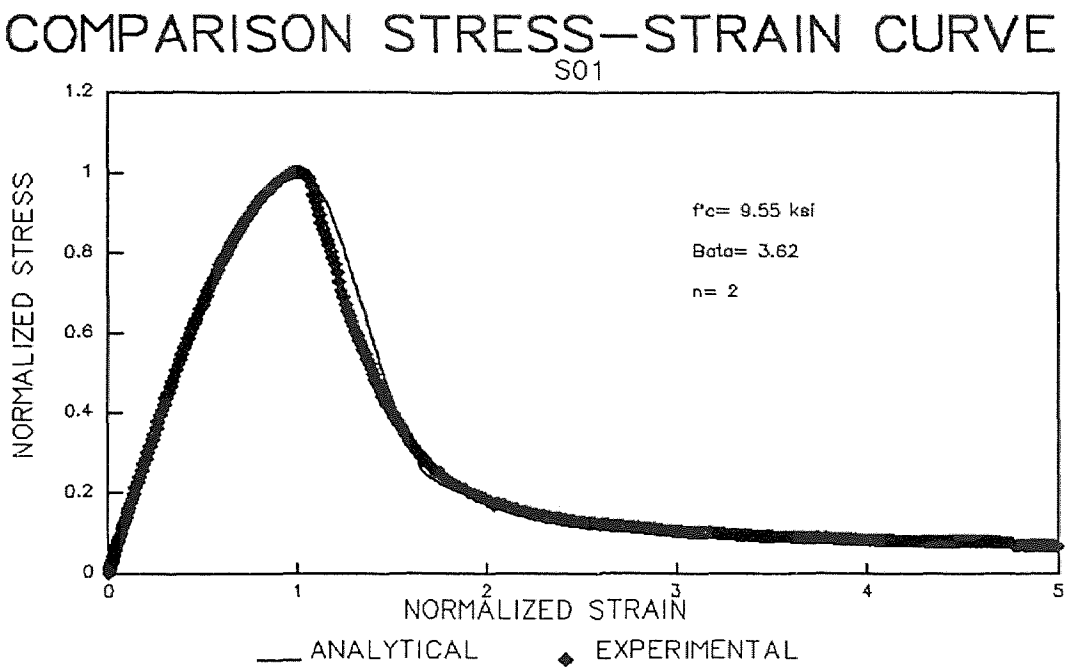

Figure F.1 Experimental Vs. Proposed Model Results; S= 0 in. and V ≠ 0%.

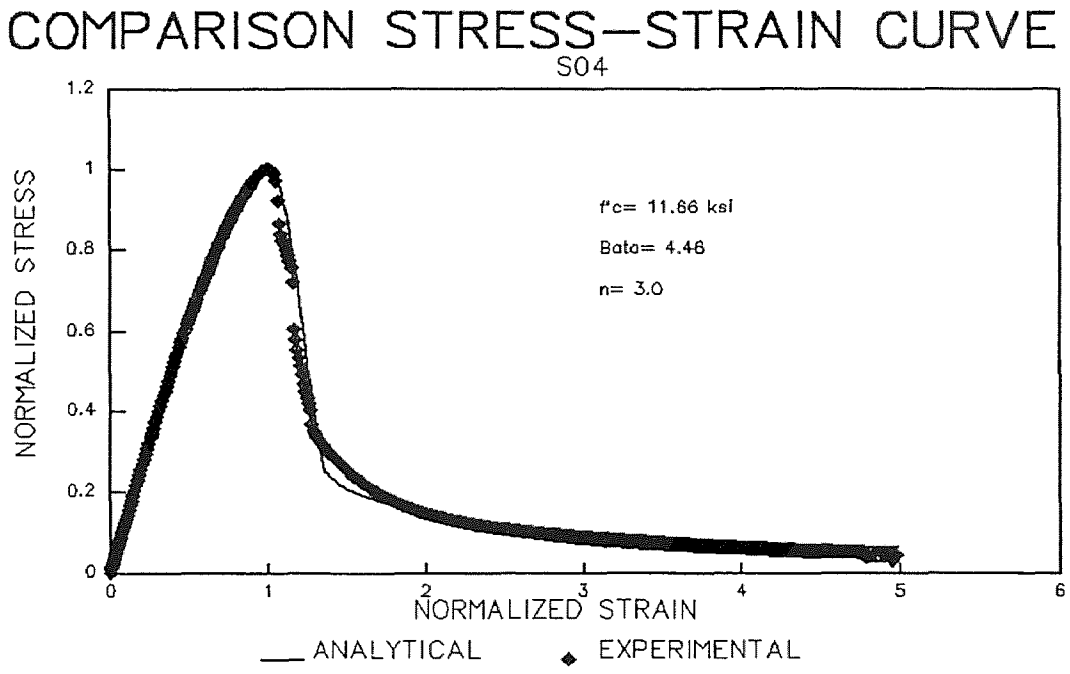

Figure F.2 Experimental Vs. Proposed Model Results; S= 0 in. and V ≠ 0%.

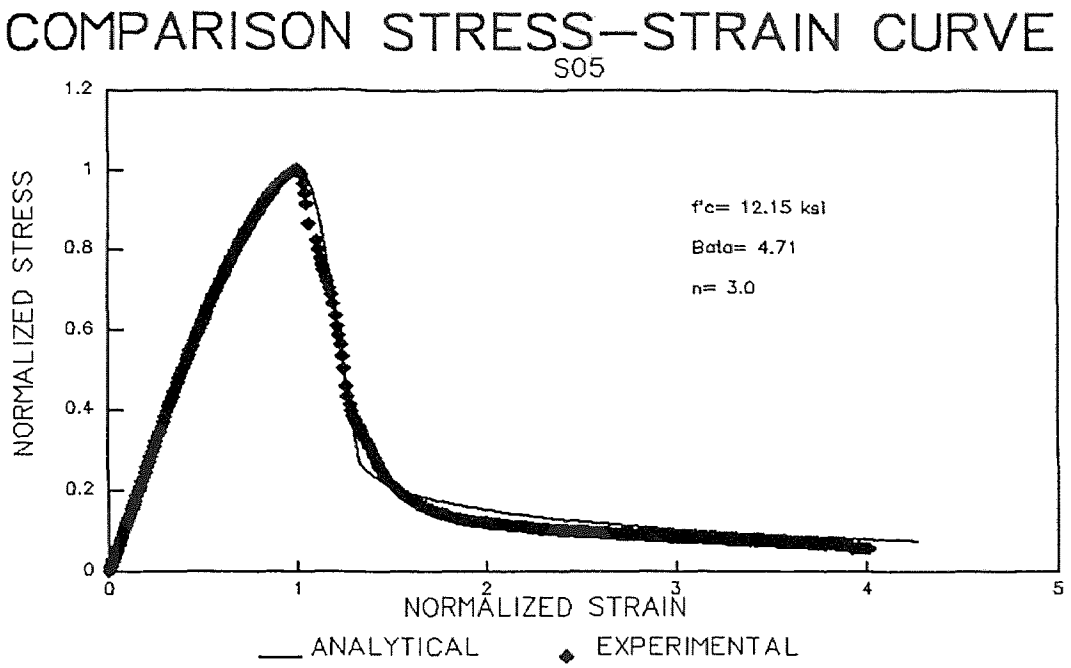

Figure F.3 Experimental Vs. Proposed Model Results; S= 0 in. and V ≠ 0%.

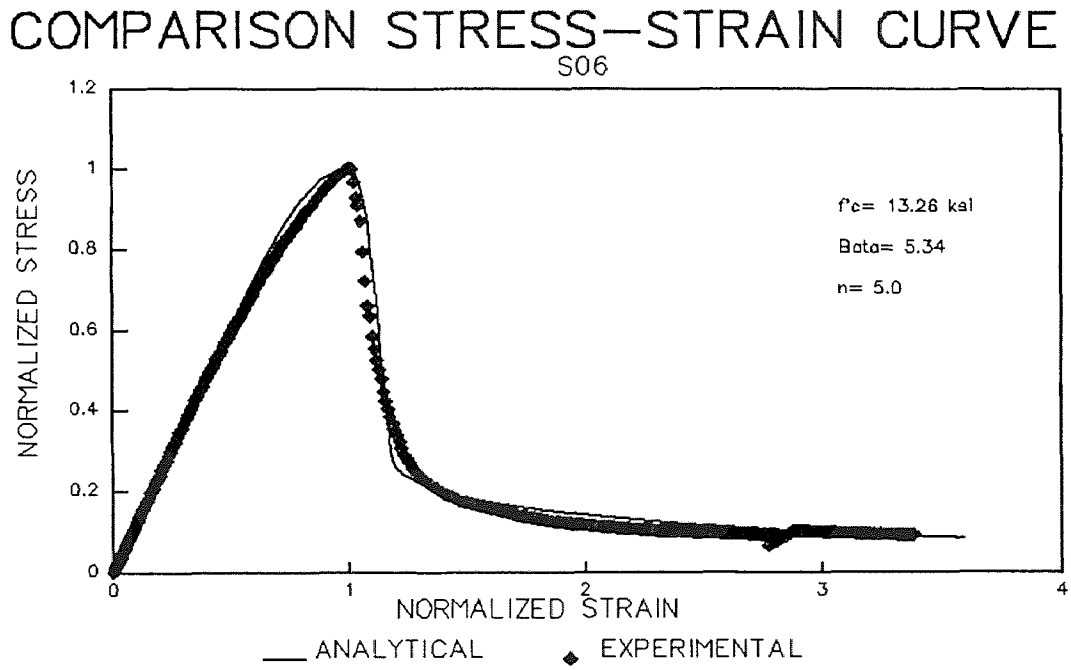

Figure F.4 Experimental Vs. Proposed Model Results; S= 0 in. and V ≠ 0%.

APPENDIX G
COMPARISON ANALYTICAL EQUATIONS AND EXPERIMENTAL RESULTS AT DIFFERENT TIE SPACING

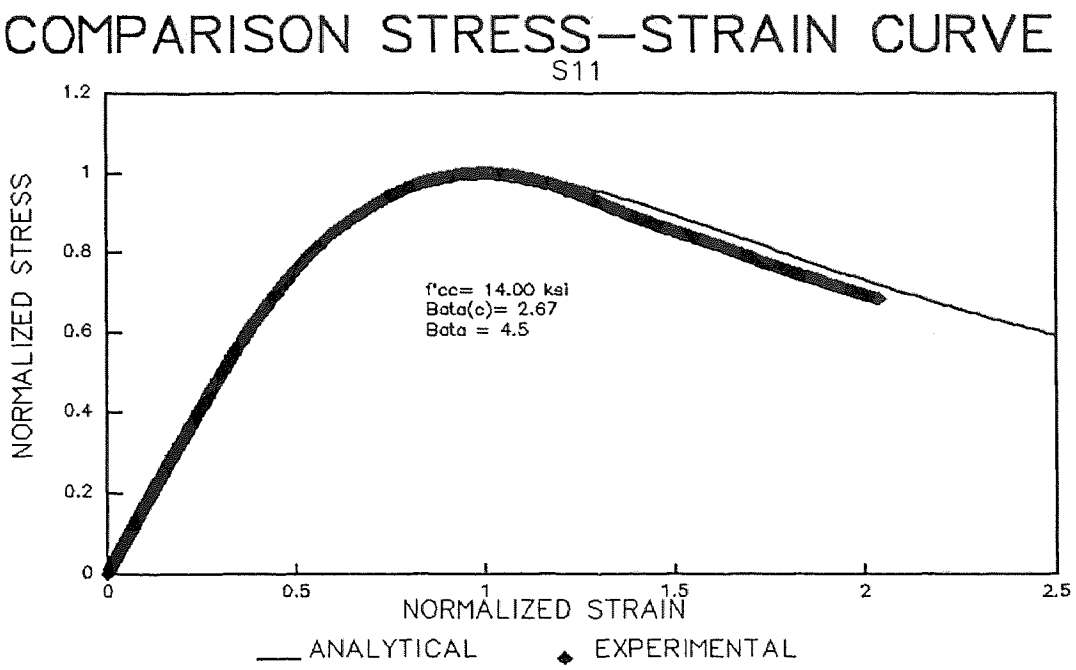

Figure G.1 Experimental Vs. Proposed Model Results; S= 1 in. and V ≠ 0%.

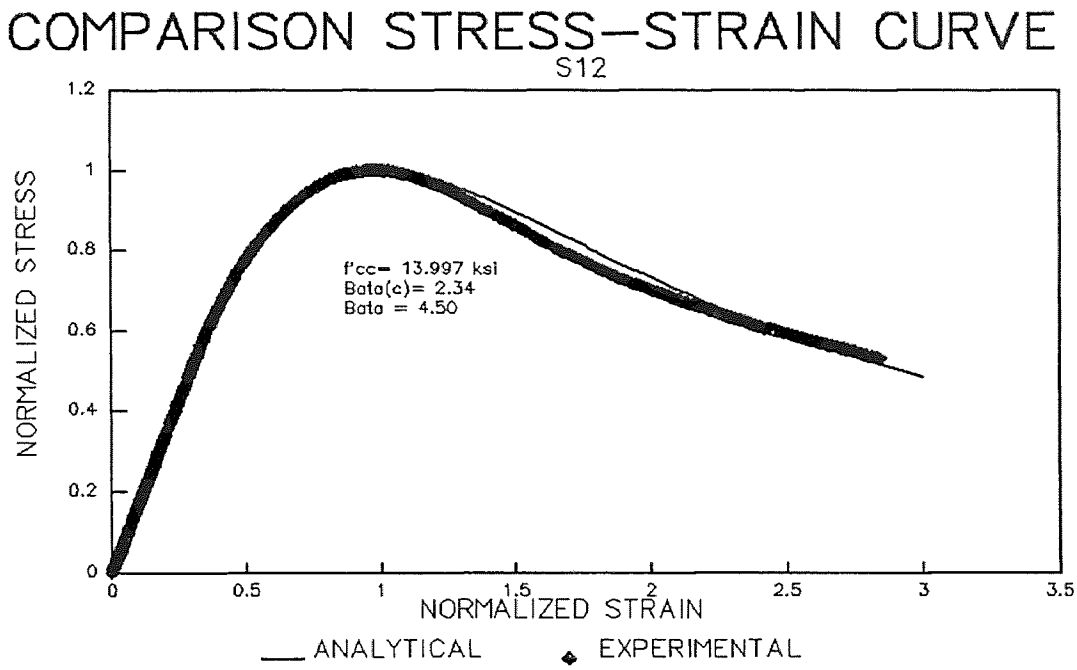

Figure G.2 Experimental Vs. Proposed Model Results; S= 1 in. and V ≠ 0%.

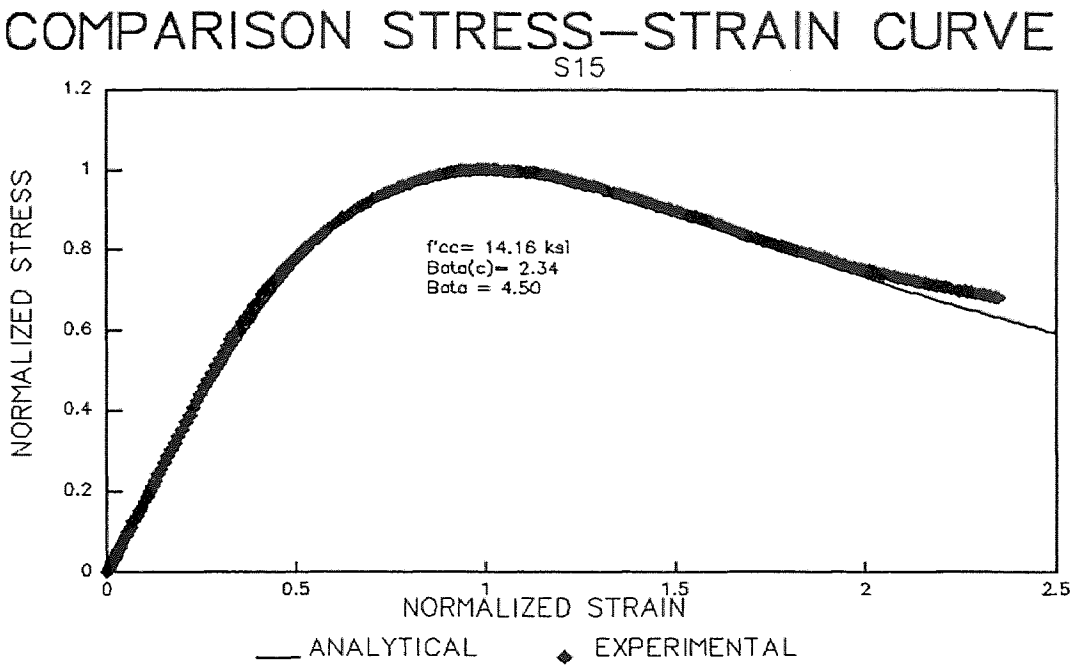

Figure G.3 Experimental Vs. Proposed Model Results; S= 1 in. and V ≠ 0%.

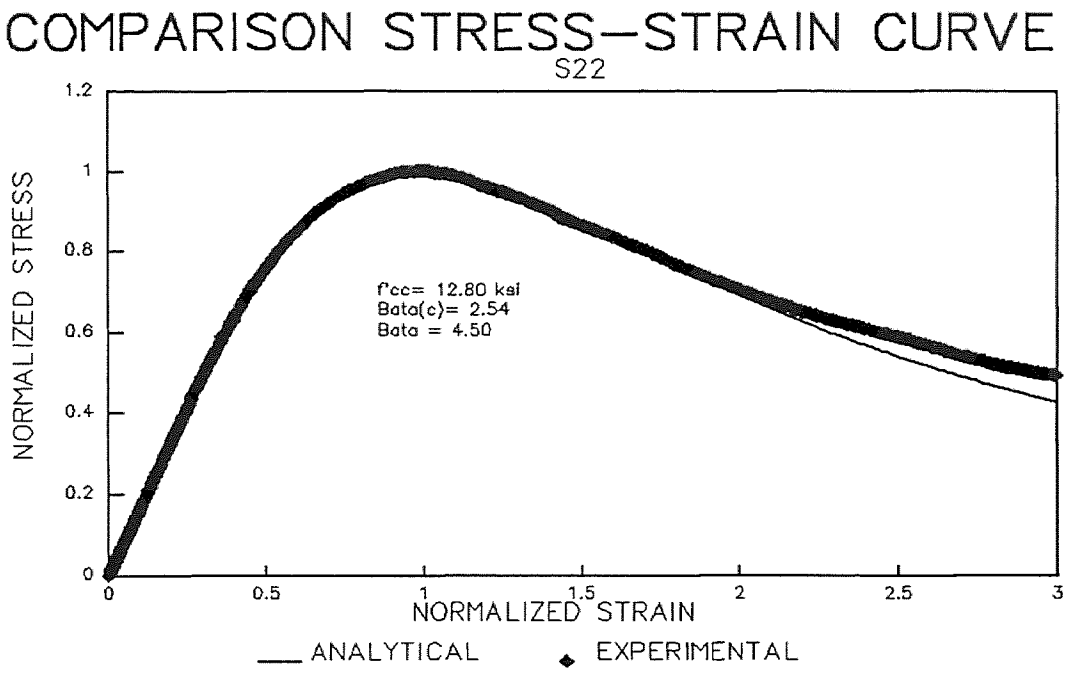

Figure G.4 Experimental Vs. Proposed Model Results; S= 2 in. and V ≠ 0%.

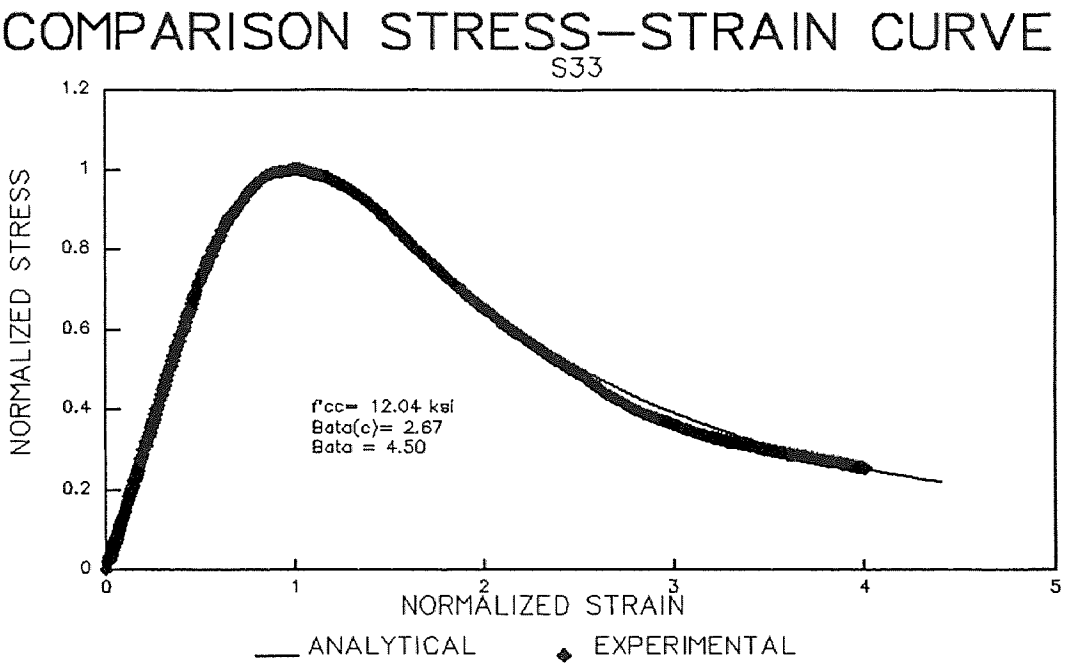

Figure G.5 Experimental Vs. Proposed Model Results; S= 3 in. and V $_f$= 0%.

APPENDIX H
COMPARISON ANALYTICAL EQUATIONS AND EXPERIMENTAL RESULTS AT DIFFERENT FIBER VOLUME FRACTION

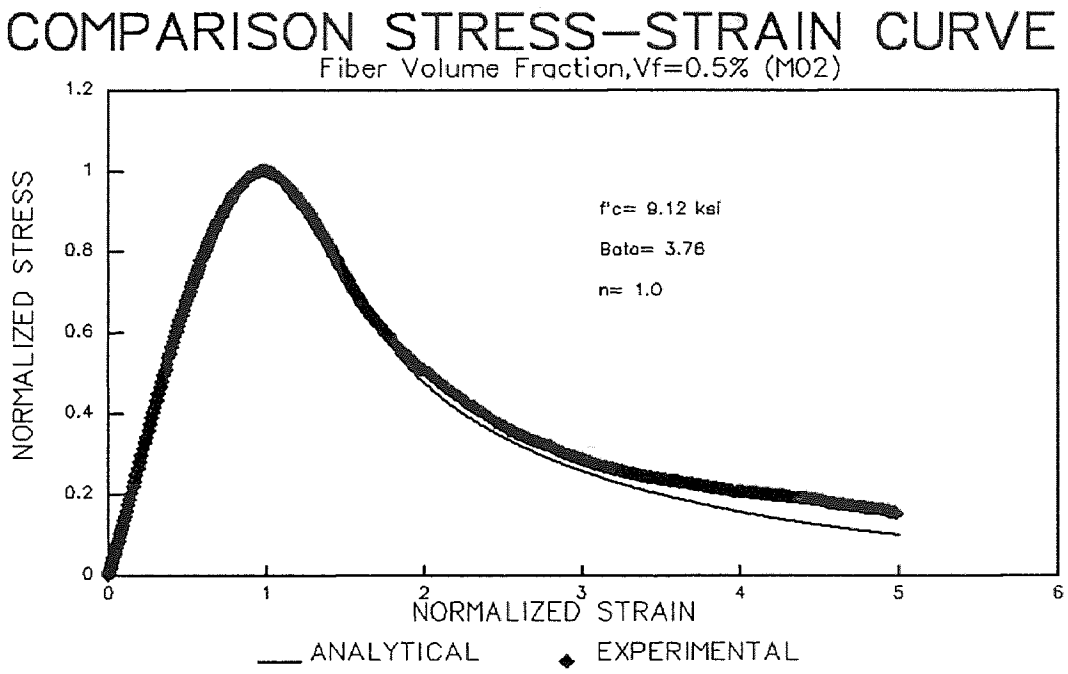

Figure H.1 Experimental Vs. Proposed Model Results; S= 0 in. and V $_F$=0.5%.

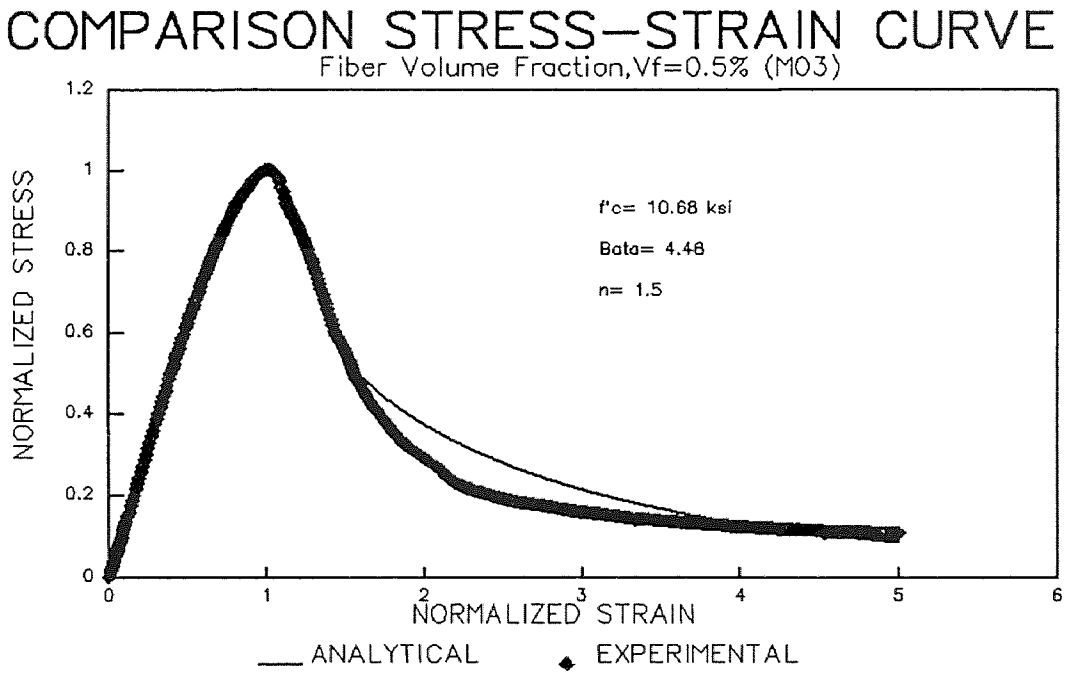

Figure H.2 Experimental Vs. Proposed Model Results; S= 0 in. and V $_F$=0.5%.

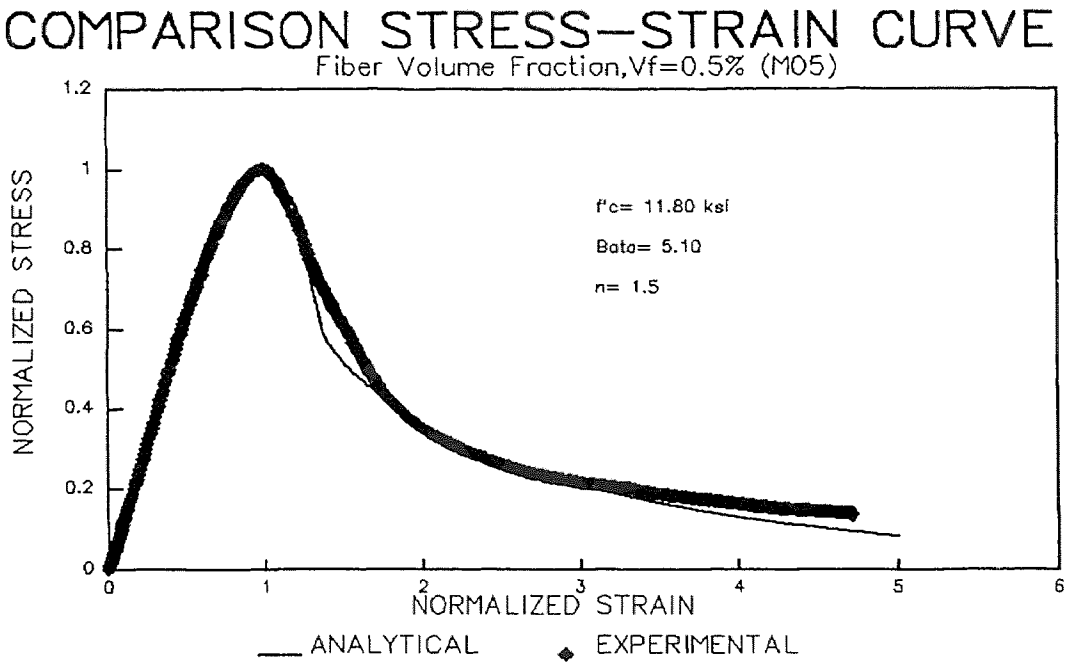

Figure H.3 Experimental Vs. Proposed Model Results; S= 0 in. and V $_f$=0.5%.

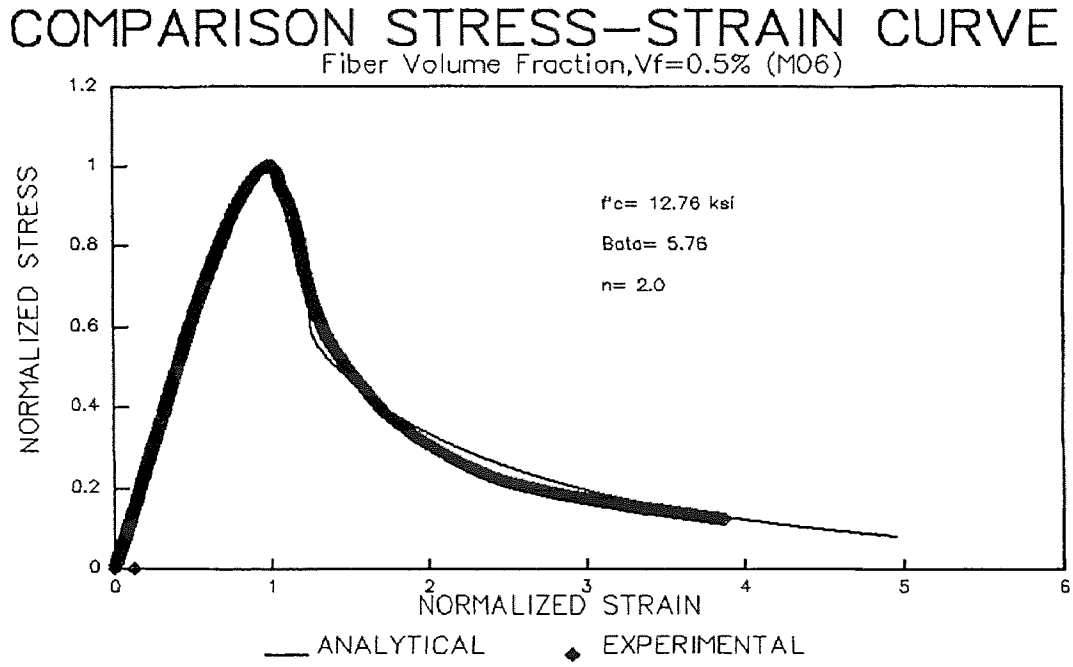

Figure H.4 Experimental Vs. Proposed Model Results; S= 0 in. and V $_f$=0.5%.

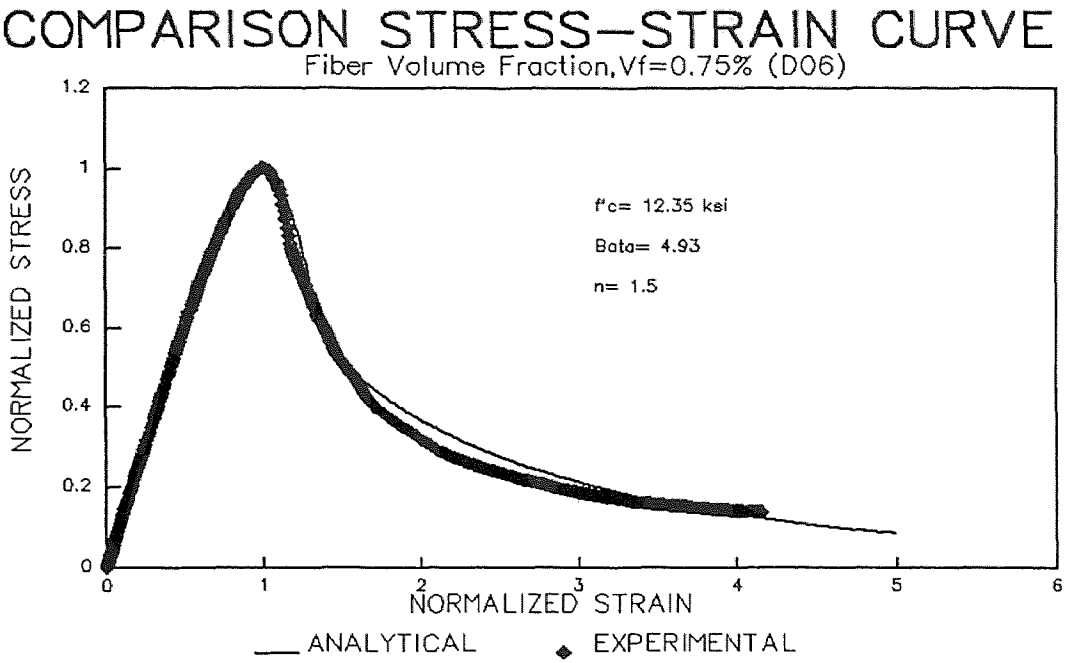

Figure H.5 Experimental Vs. Proposed Model Results; S= 0 in. and V $_f$=0.75%.

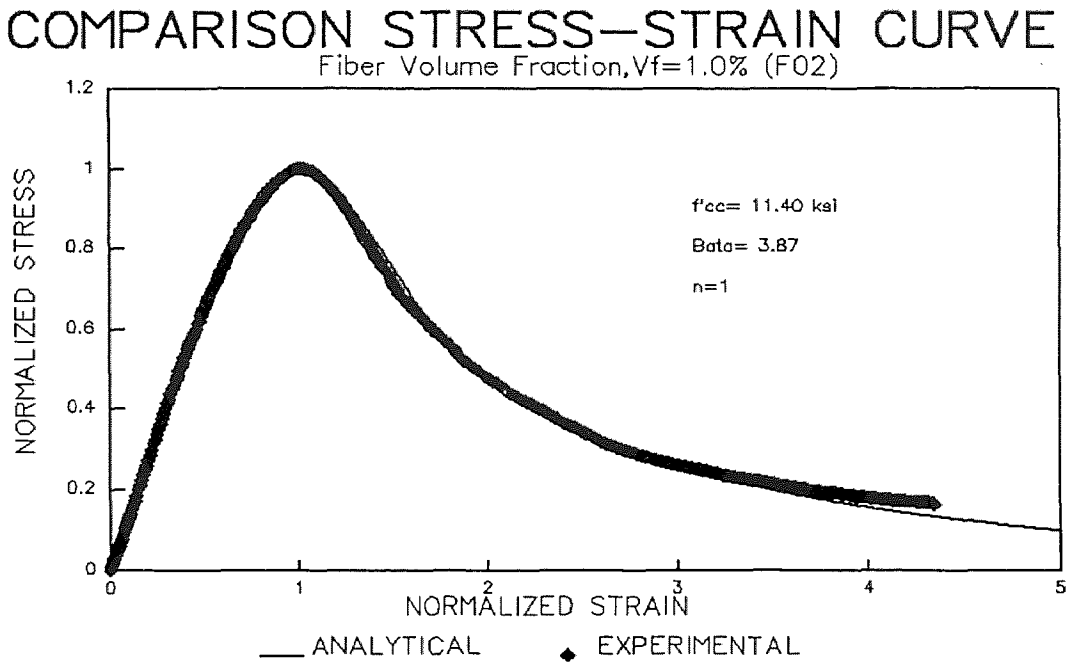

Figure H.6 Experimental Vs. Proposed Model Results; S= 0 in. and V $_f$=1.0%.

APPENDIX I
COMPARISON ANALYTICAL EQUATIONS AND EXPERIMENTAL RESULTS AT DIFFERENT FIBER VOLUME FRACTION AND TIE SPACING

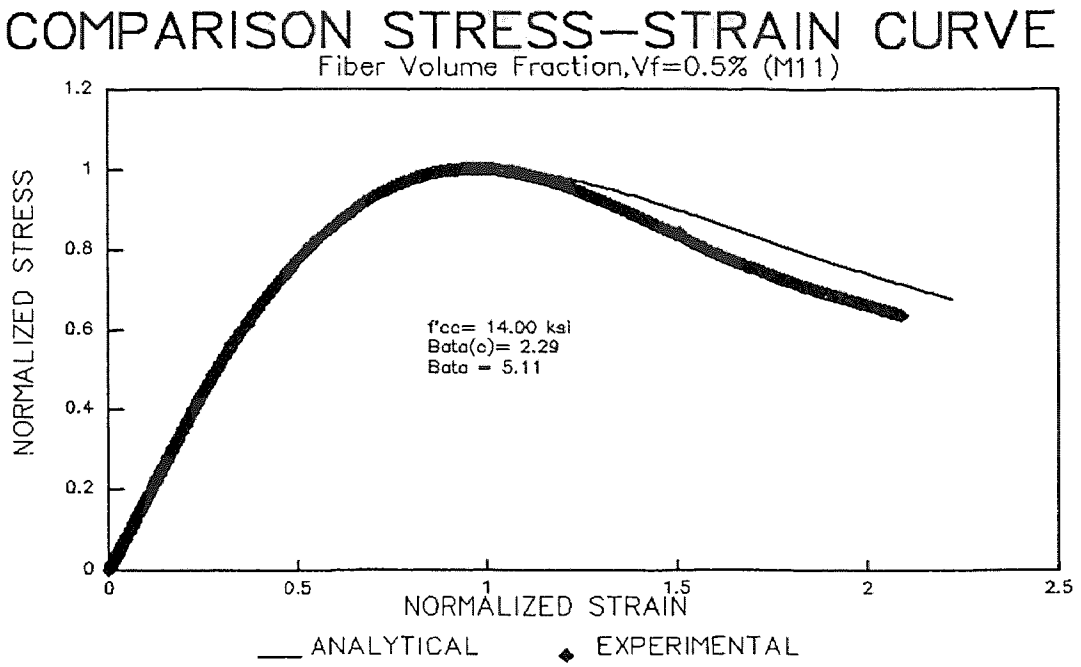

Figure I.1 Experimental Vs. Proposed Model Results; S= 1 in. and V $_f$=0.5%.

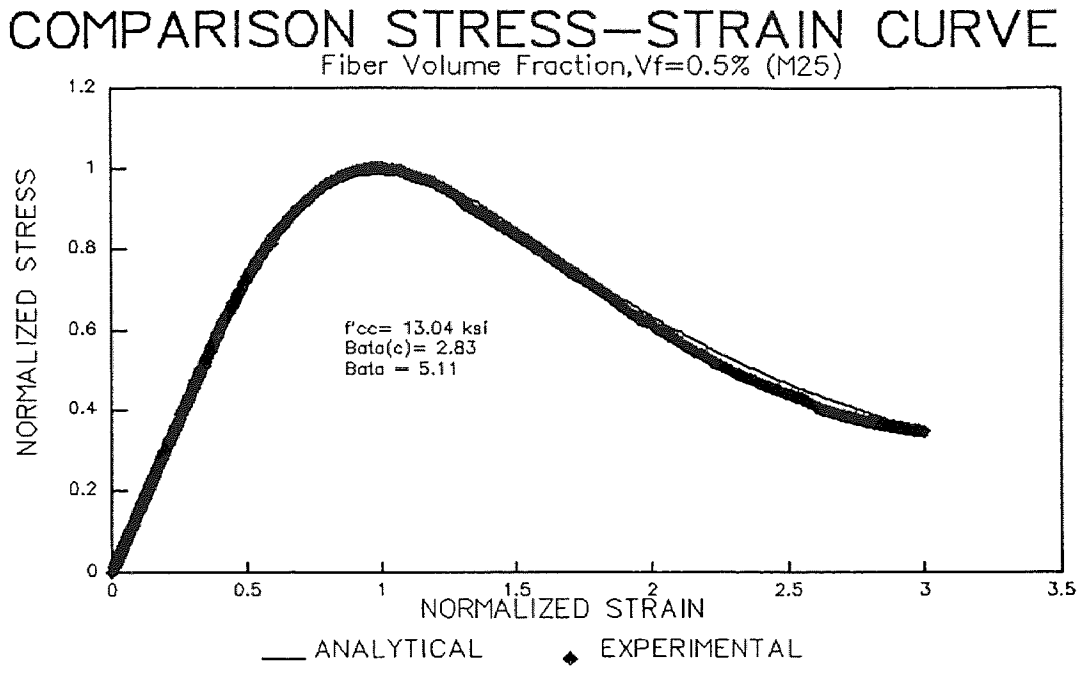

Figure I.2 Experimental Vs. Proposed Model Results; S= 2 in. and V $_f$=0.5%.

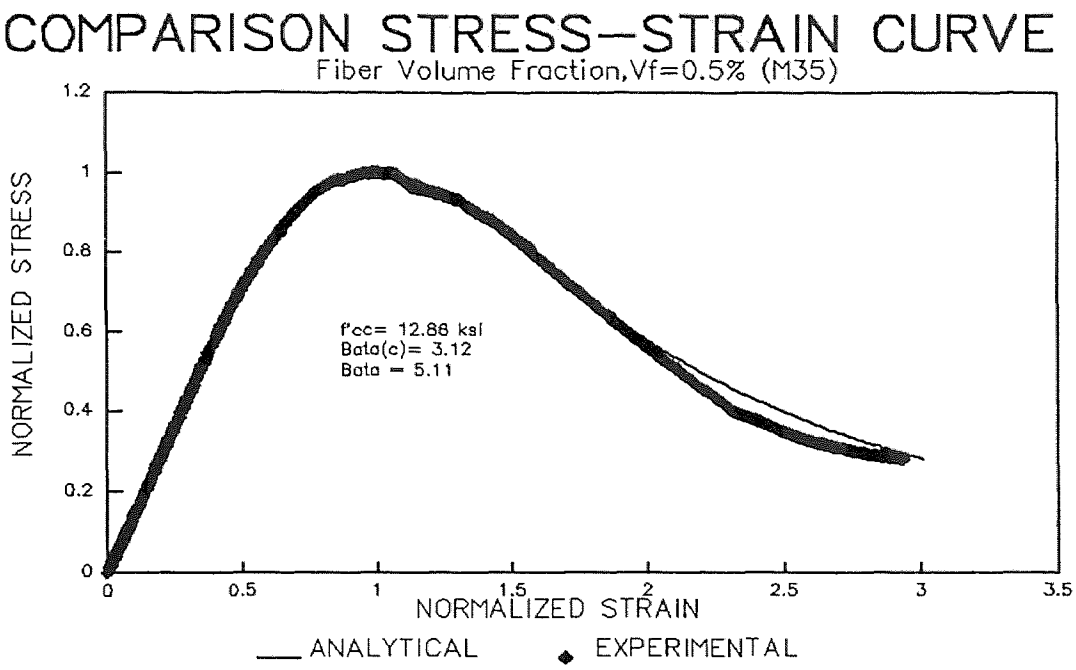

Figure I.3 Experimental Vs. Proposed Model Results; S= 3 in. and V $_f$=0.5%.

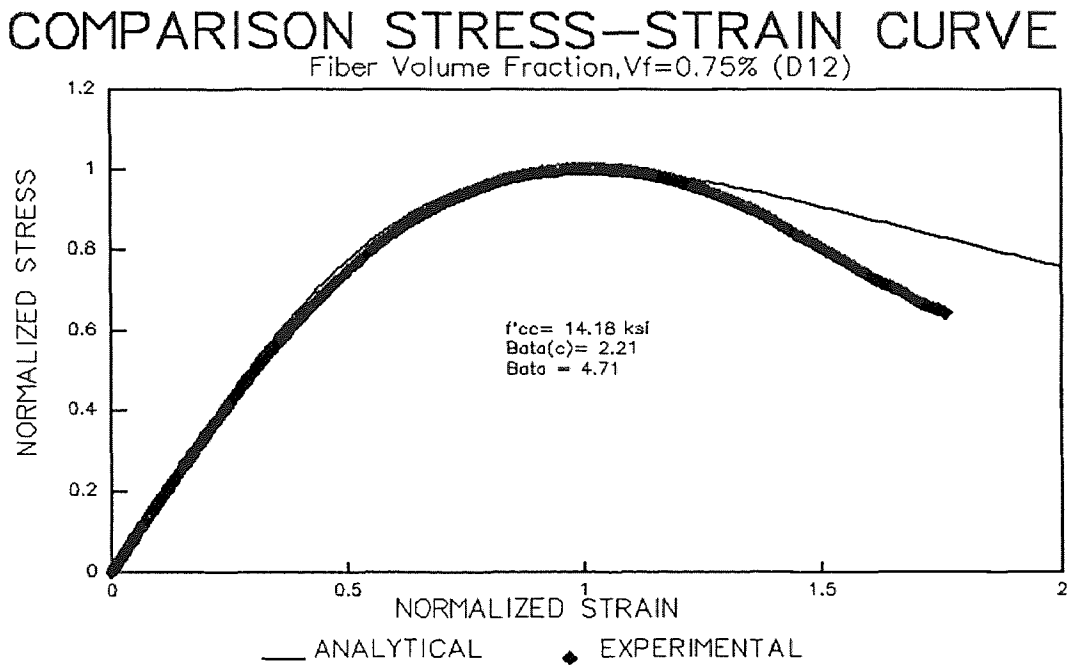

Figure I.4 Experimental Vs. Proposed Model Results; S= 1 in. and V $_f$=0.75%.

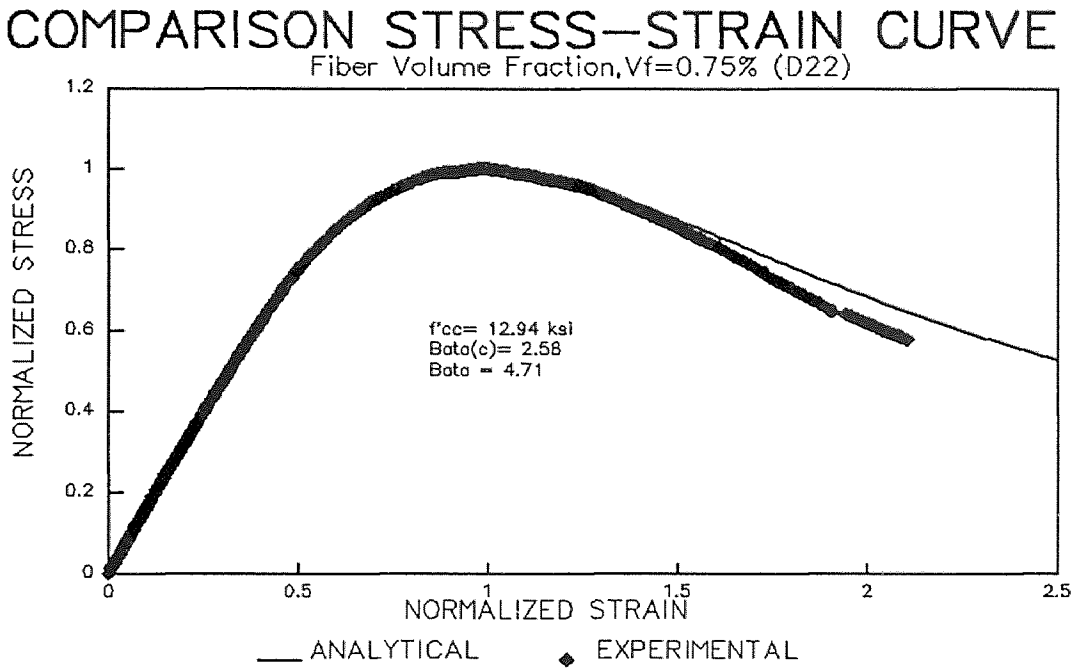

Figure I.5 Experimental Vs. Proposed Model Results; S= 2 in. and V $_f$=0.75%.

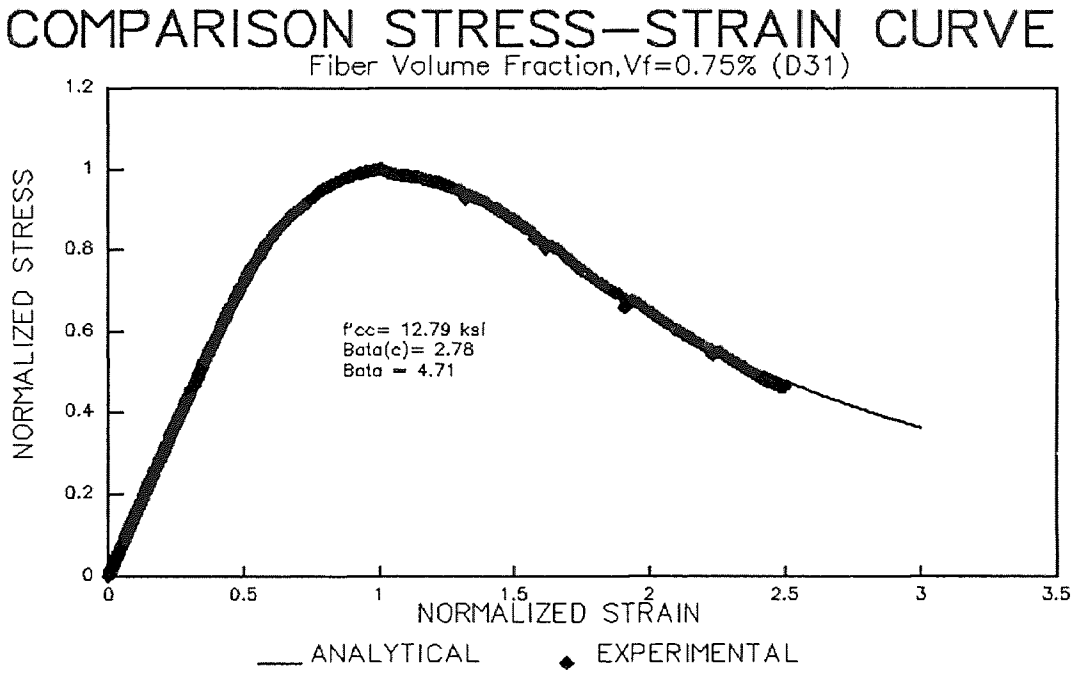

Figure I.6 Experimental Vs. Proposed Model Results; S= 3 in. and V $_f$=0.75%.

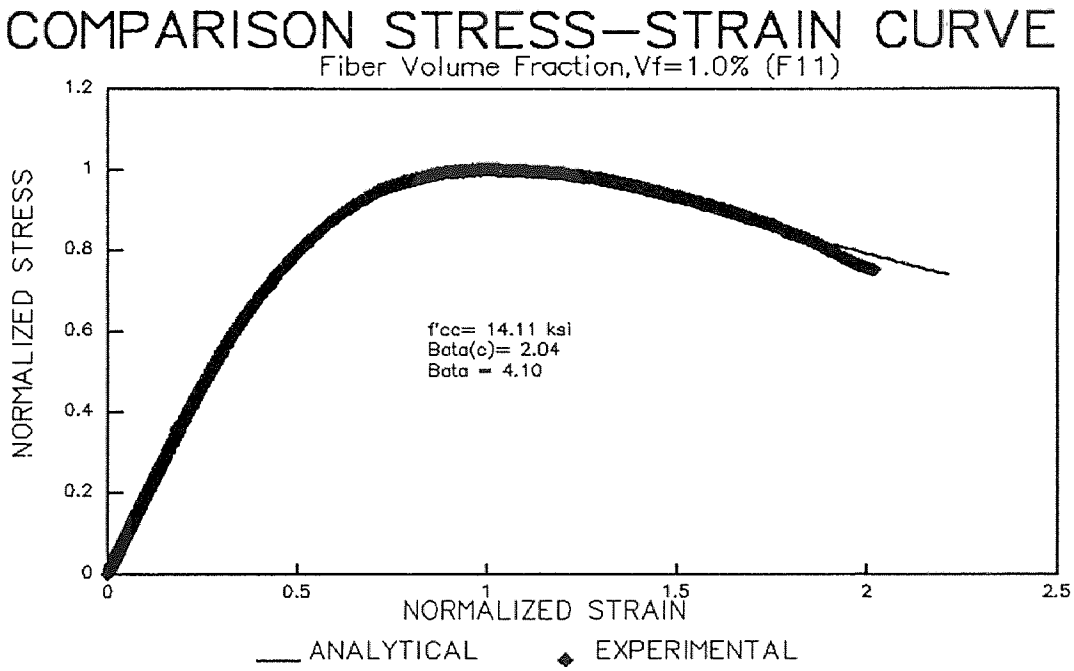

Figure I.7 Experimental Vs. Proposed Model Results; S= 1 in. and V $_f$=1.0%.

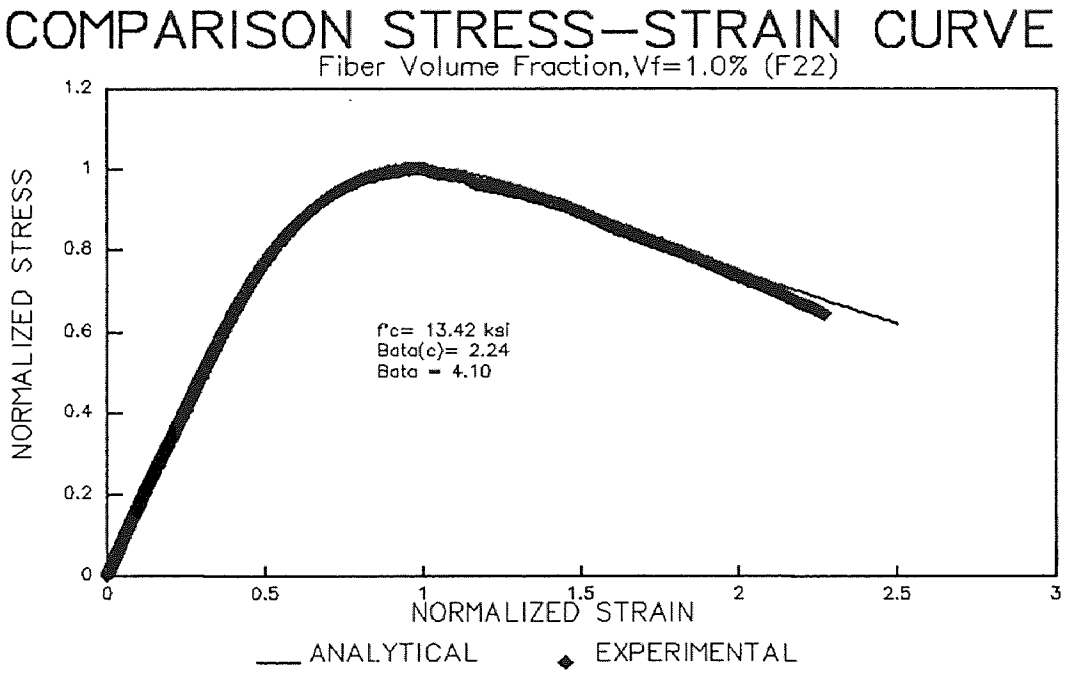

Figure I.8 Experimental Vs. Proposed Model Results; S= 2 in. and V $_f$=1.0%.

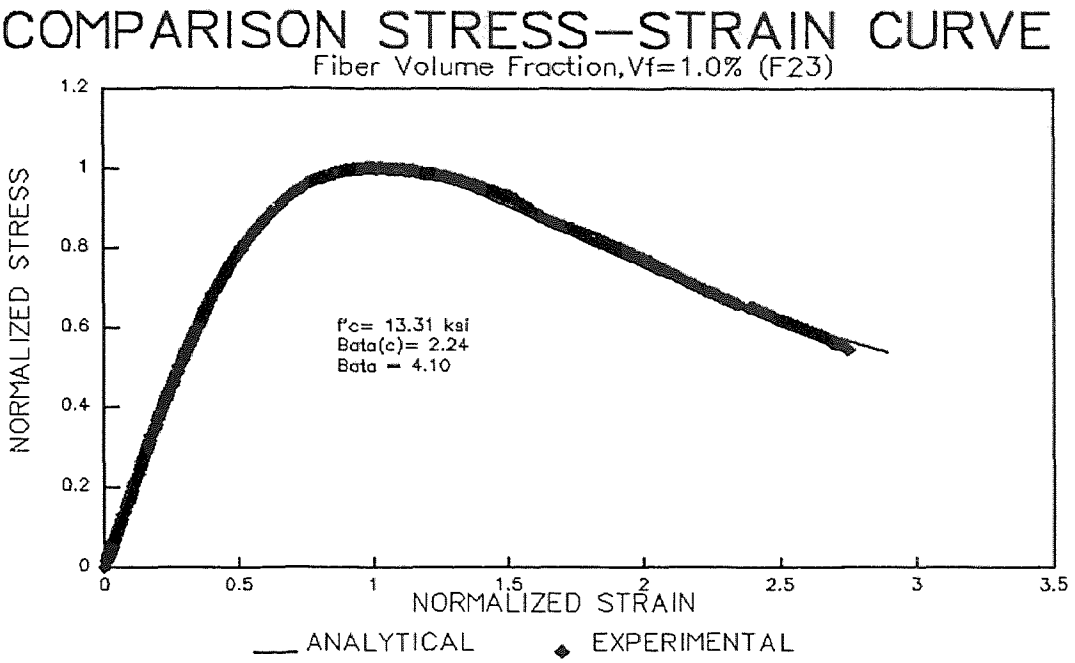

Figure I.9 Experimental Vs. Proposed Model Results; S= 2 in. and V $_{f}$=1.0%.

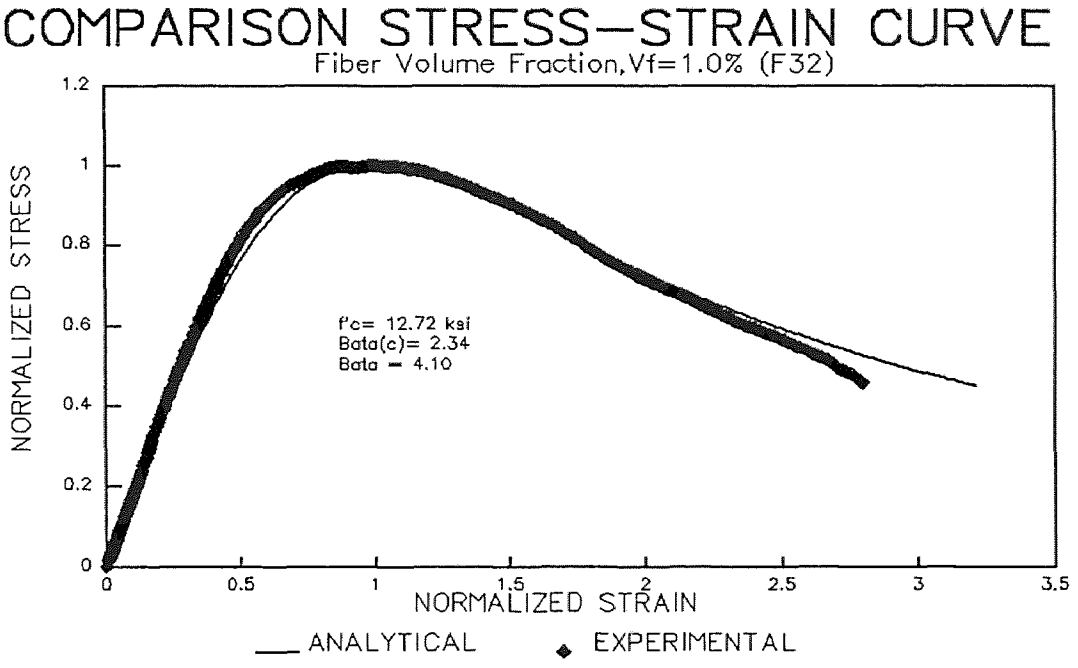

Figure I.10 Experimental Vs. Proposed Model Results; S= 3 in. and V $_{f}$=1.0%.

APPENDIX J
STRAIN-POSITION CURVES FOR HSC COLUMNS

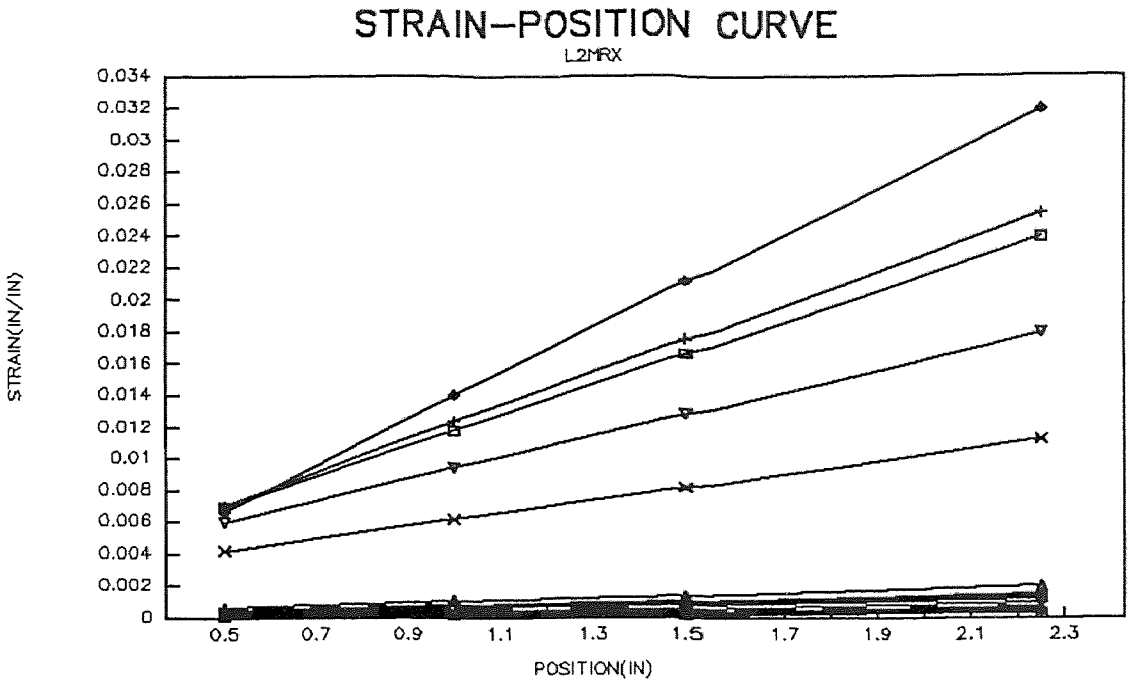

Figure J.1 Strain-Position Curves for High Strength Column L2 in X-Direction.

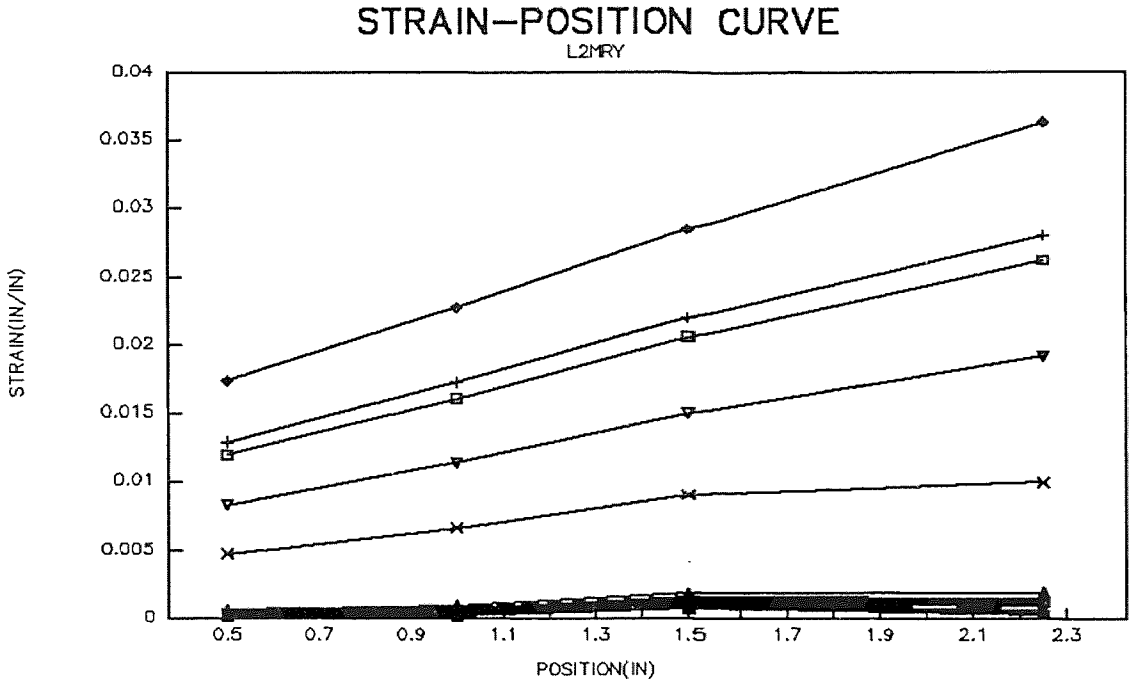

Figure J.2 Strain-Position Curves for High Strength Column L2 in Y-Direction.

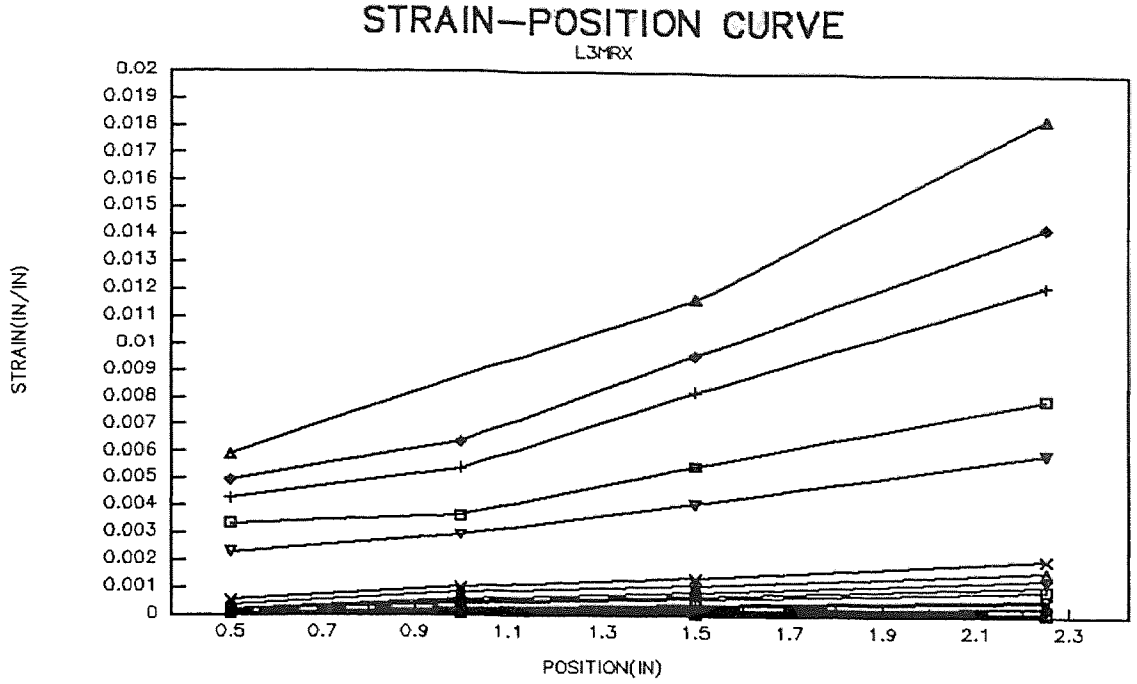

Figure J.3 Strain-Position Curves for High Strength Column L3 in X-Direction.

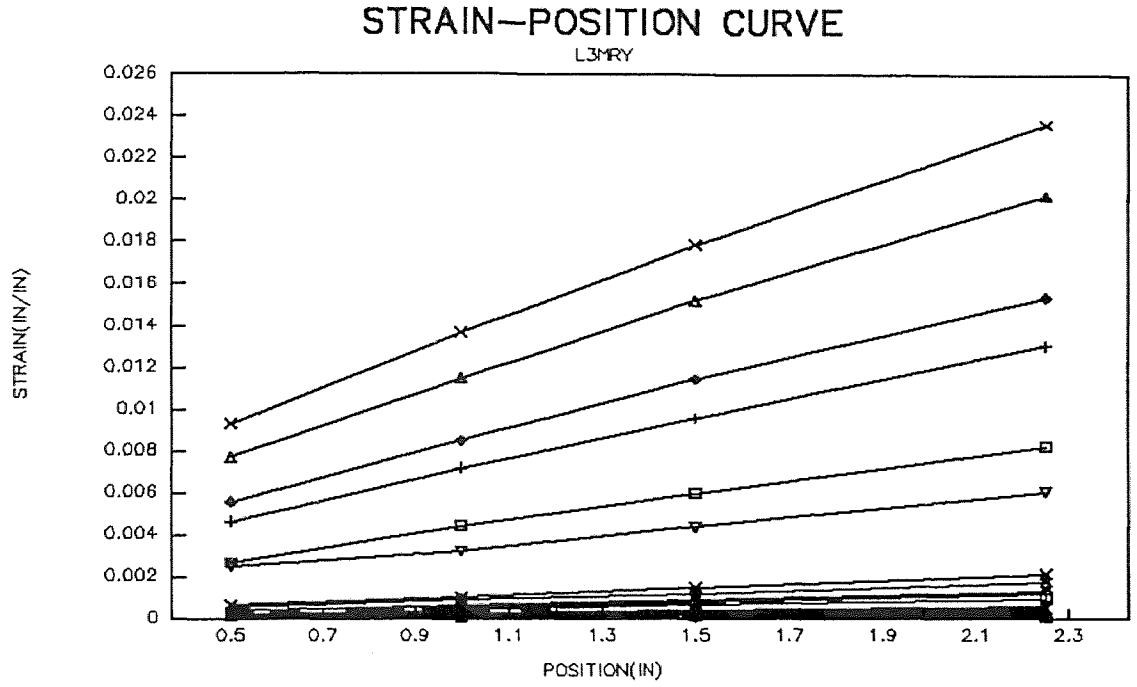

Figure J.4 Strain-Position Curves for High Strength Column L3 in Y-Direction.

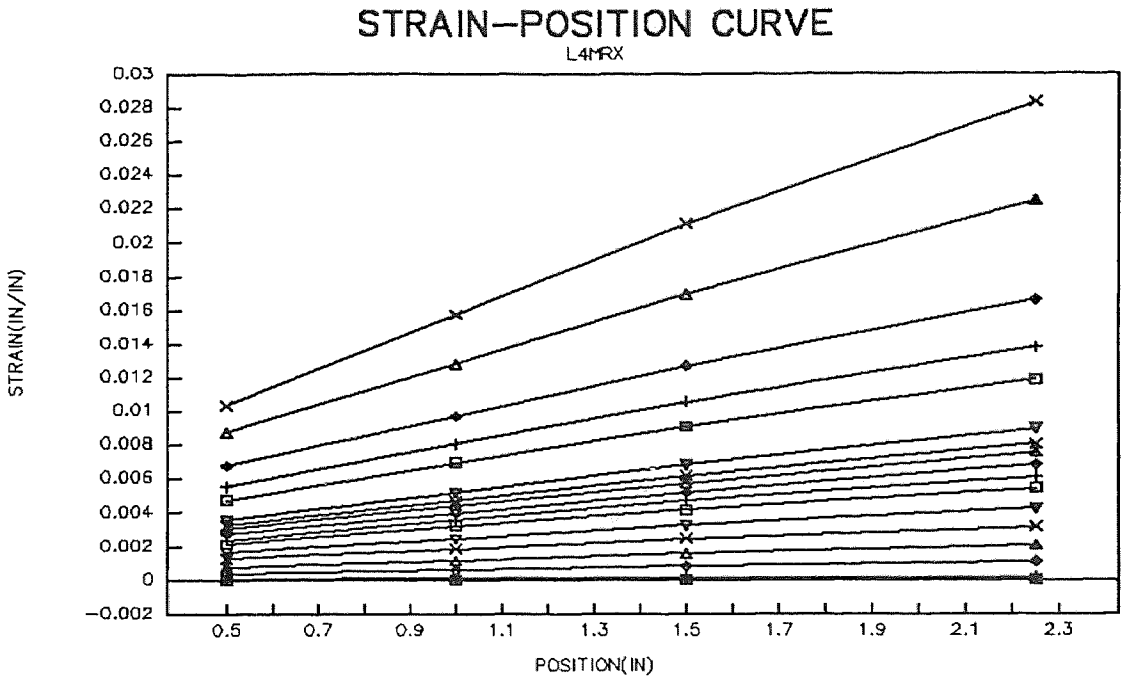

Figure J.5 Strain-Position Curves for High Strength Column L4 in X-Direction.

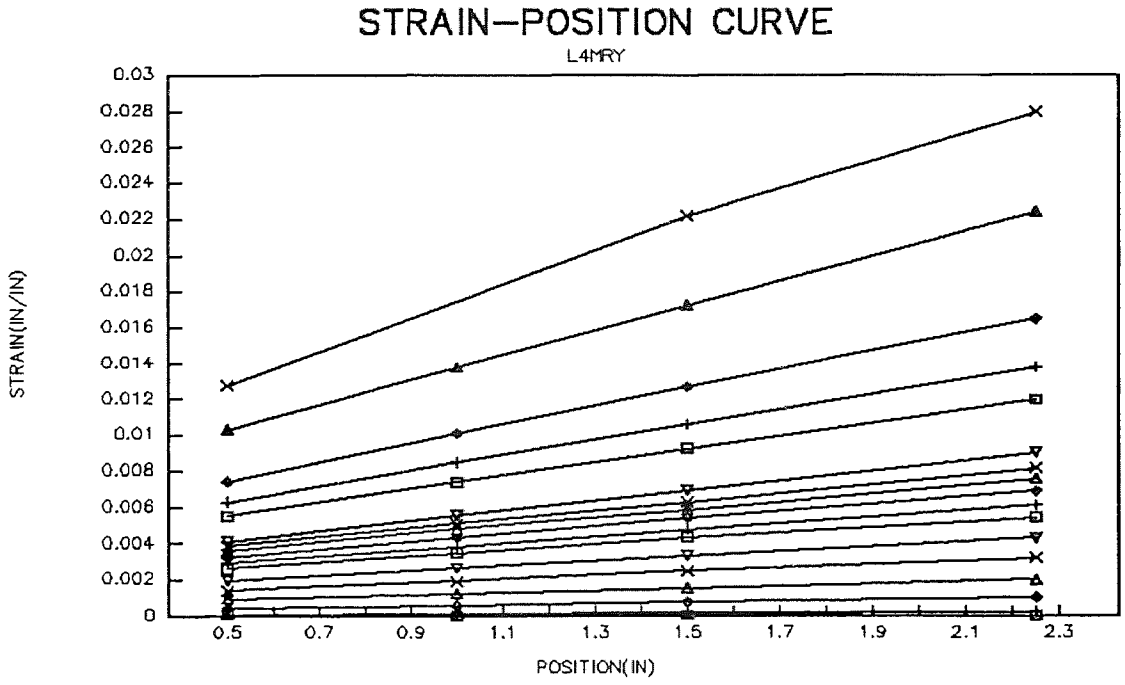

Figure J.6 Strain-Position Curves for High Strength Column L4 in Y-Direction.

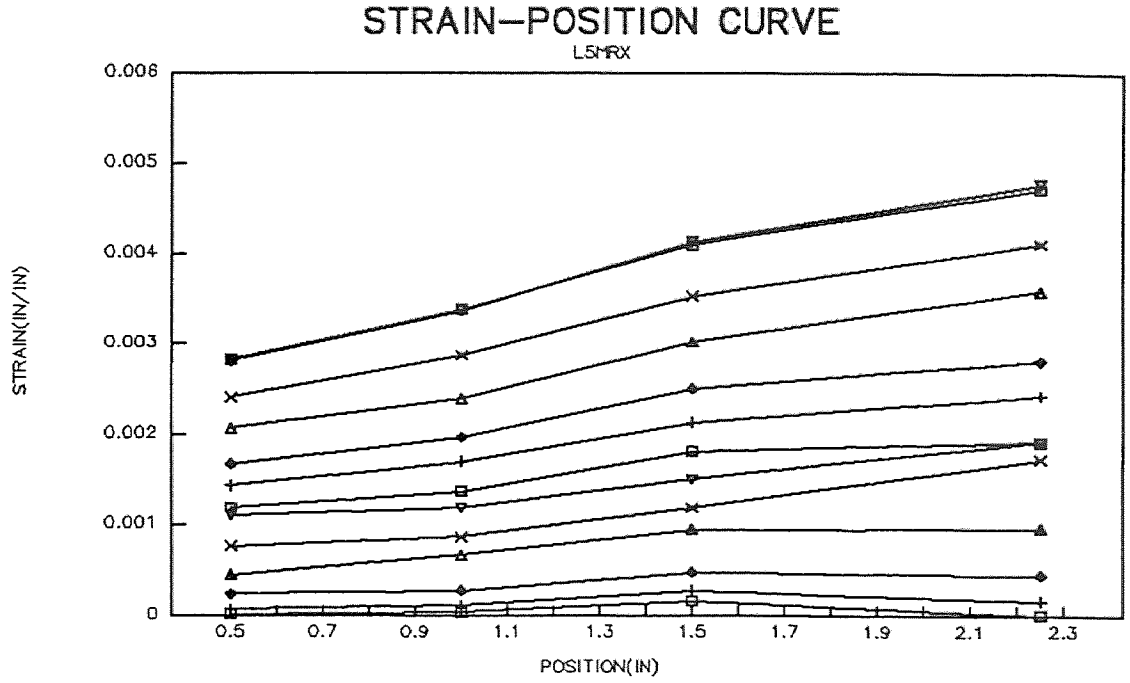

Figure J.7 Strain-Position Curves for High Strength Column L5 in X-Direction.

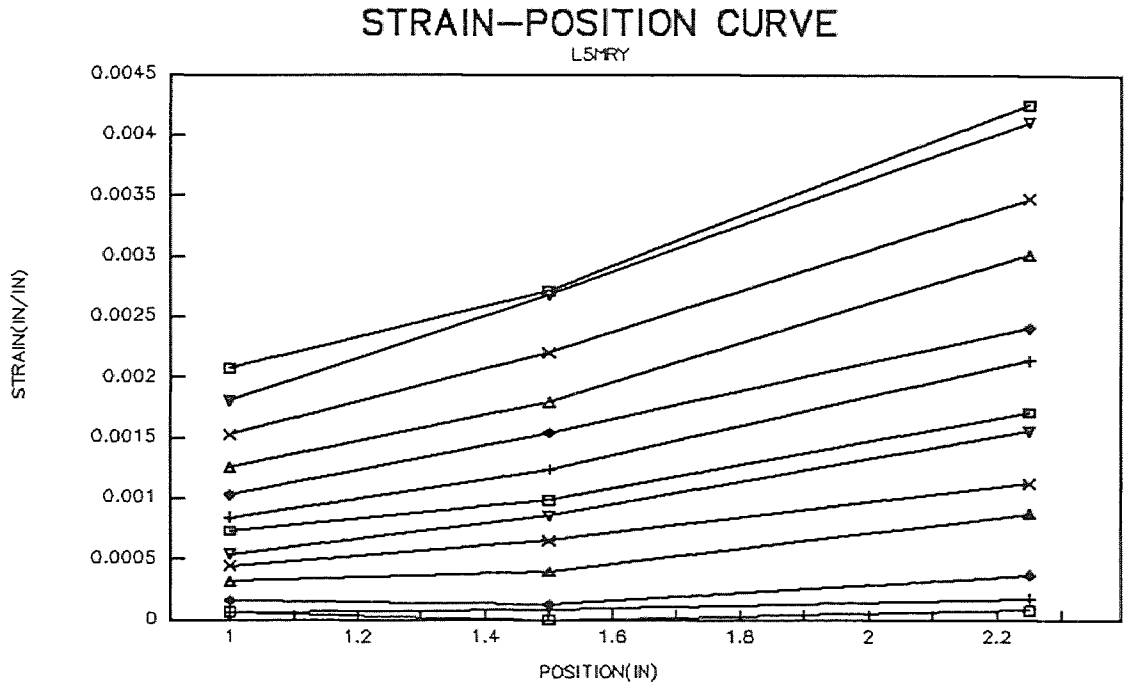

Figure J.8 Strain-Position Curves for High Strength Column L5 in Y-Direction.

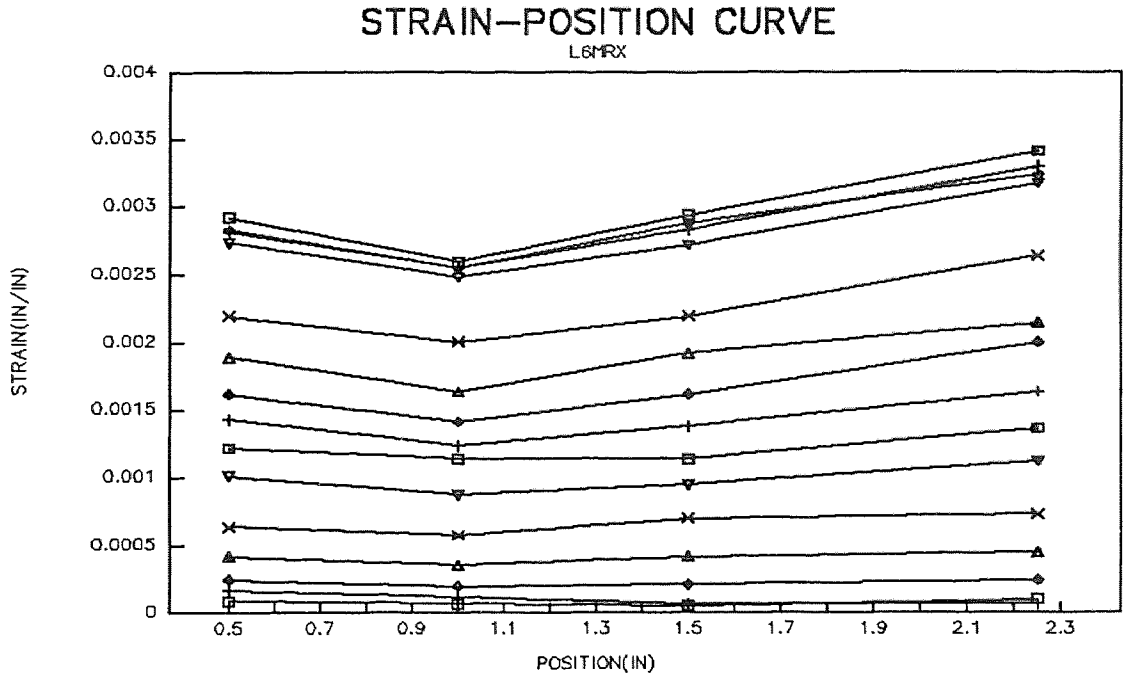

Figure J.9 Strain-Position Curves for High Strength Column L6 in X-Direction.

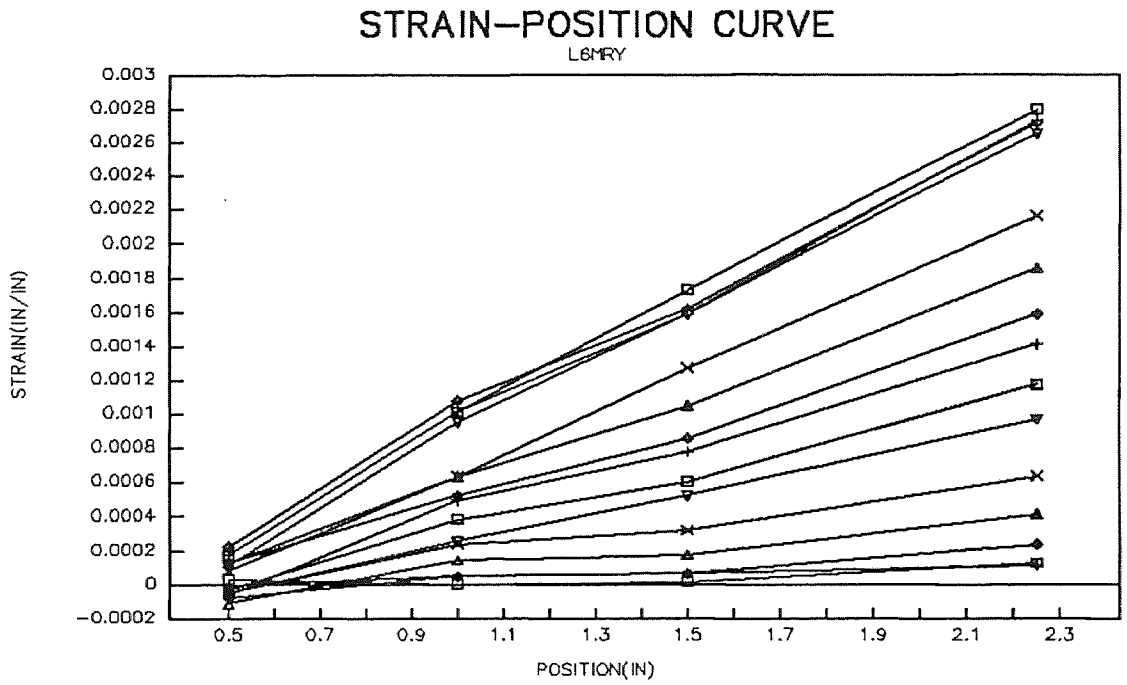

Figure J.10 Strain-Position Curves for High Strength Column L6 in Y-Direction.

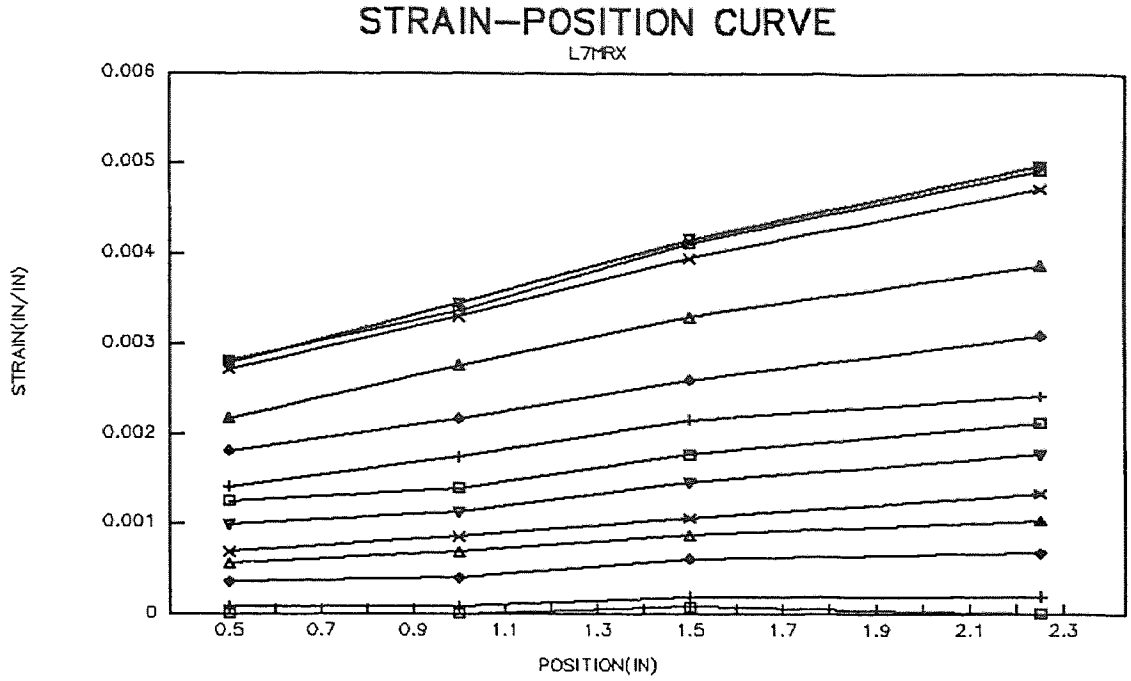

Figure J.11 Strain-Position Curves for High Strength Column L7 in X-Direction.

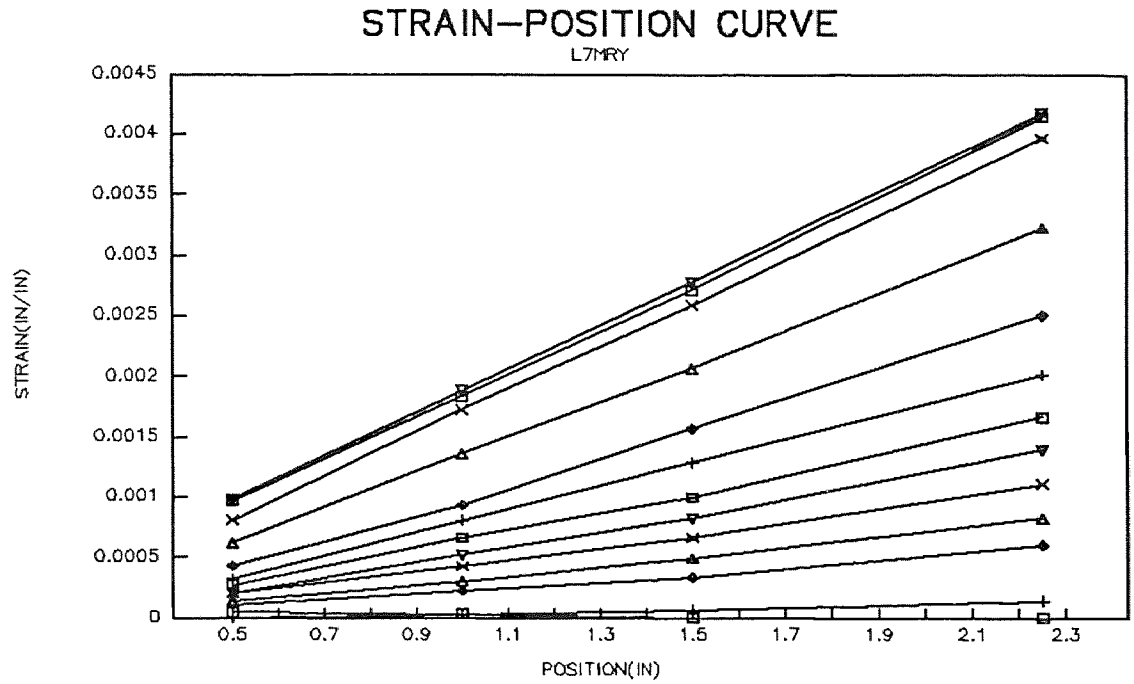

Figure J.12 Strain-Position Curves for High Strength Column L7 in Y-Direction.

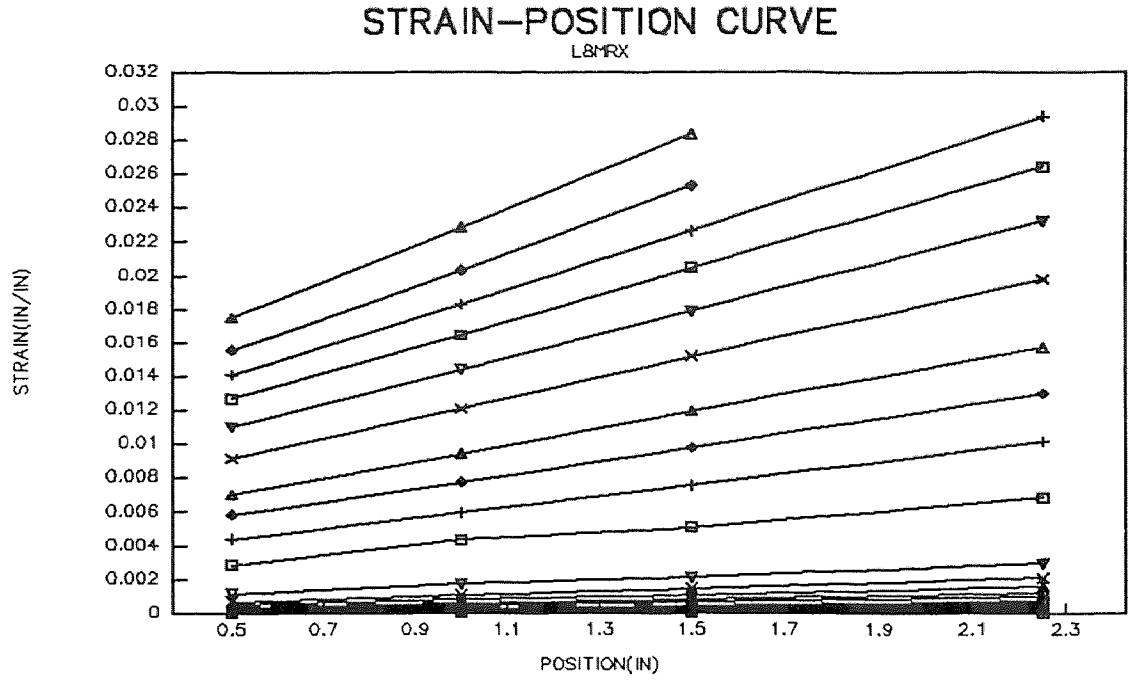

Figure J.13 Strain-Position Curves for High Strength Column L8 in X-Direction.

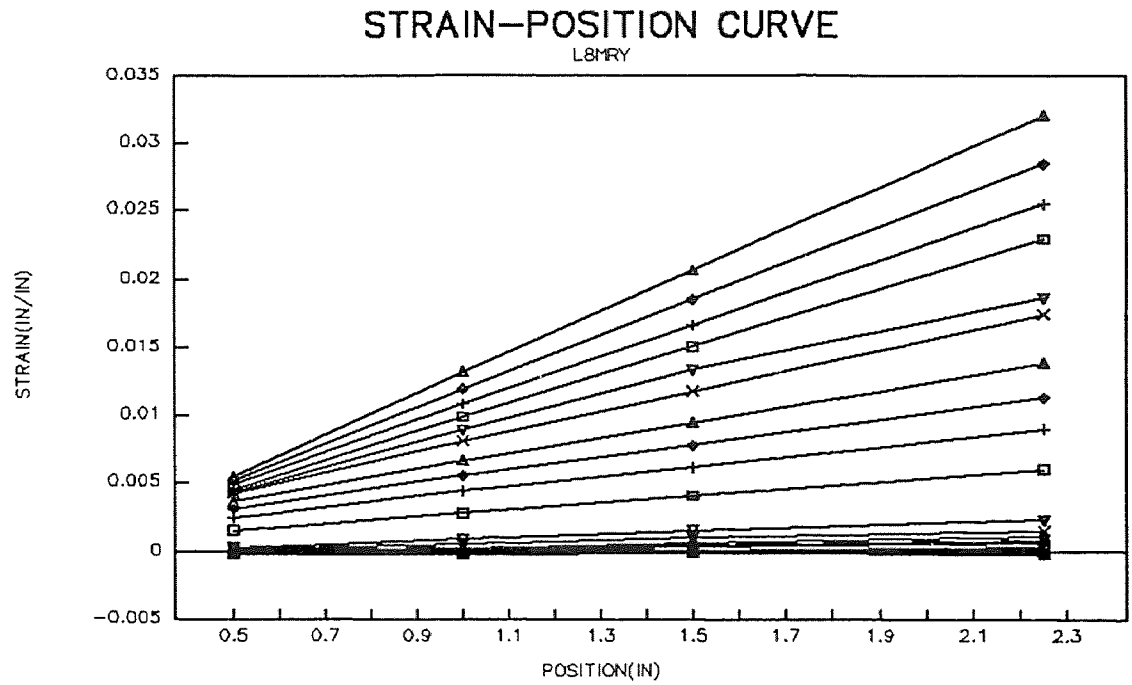

Figure J.14 Strain-Position Curves for High Strength Column L8 in Y-Direction.

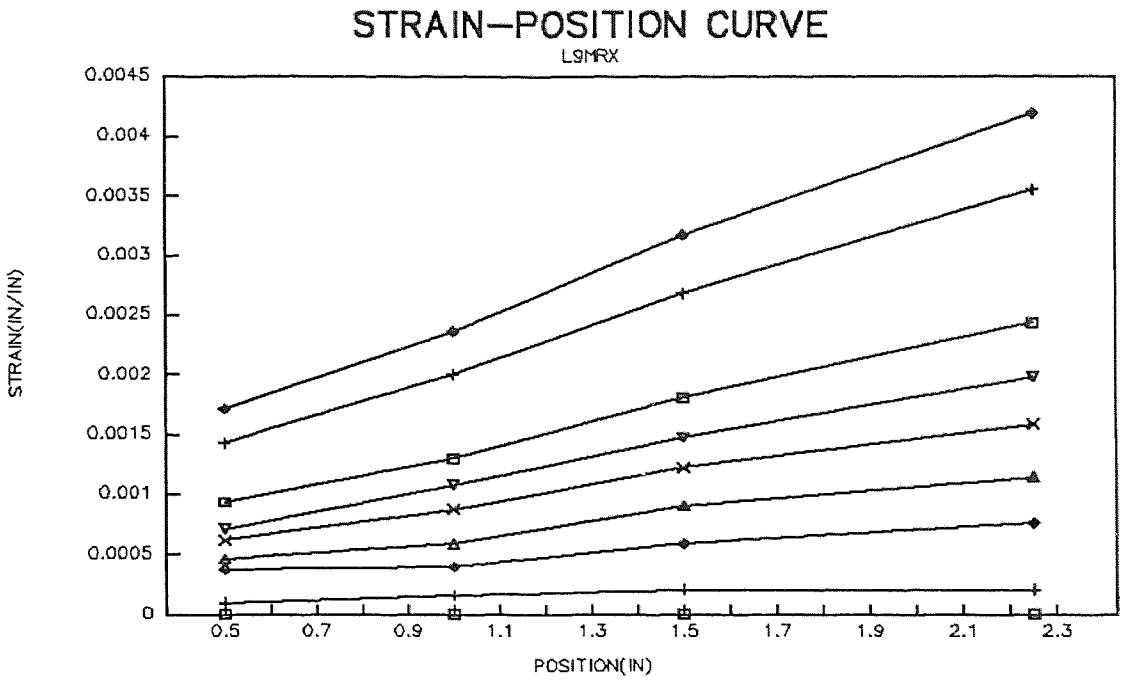

Figure J.15 Strain-Position Curves for High Strength Column L9 in X-Direction.

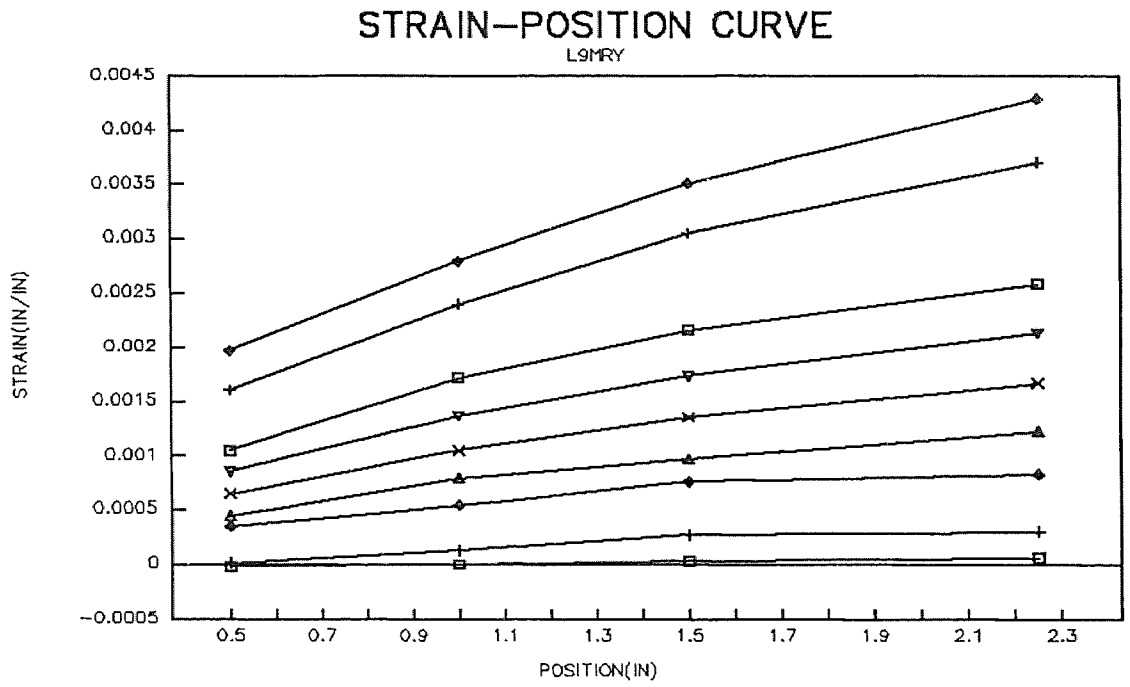

Figure J.16 Strain-Position Curves for High Strength Column L9 in Y-Direction.

APPENDIX K
STRAIN-POSITION CURVES FOR HIGH STRENGTH FIBROUS COLUMNS

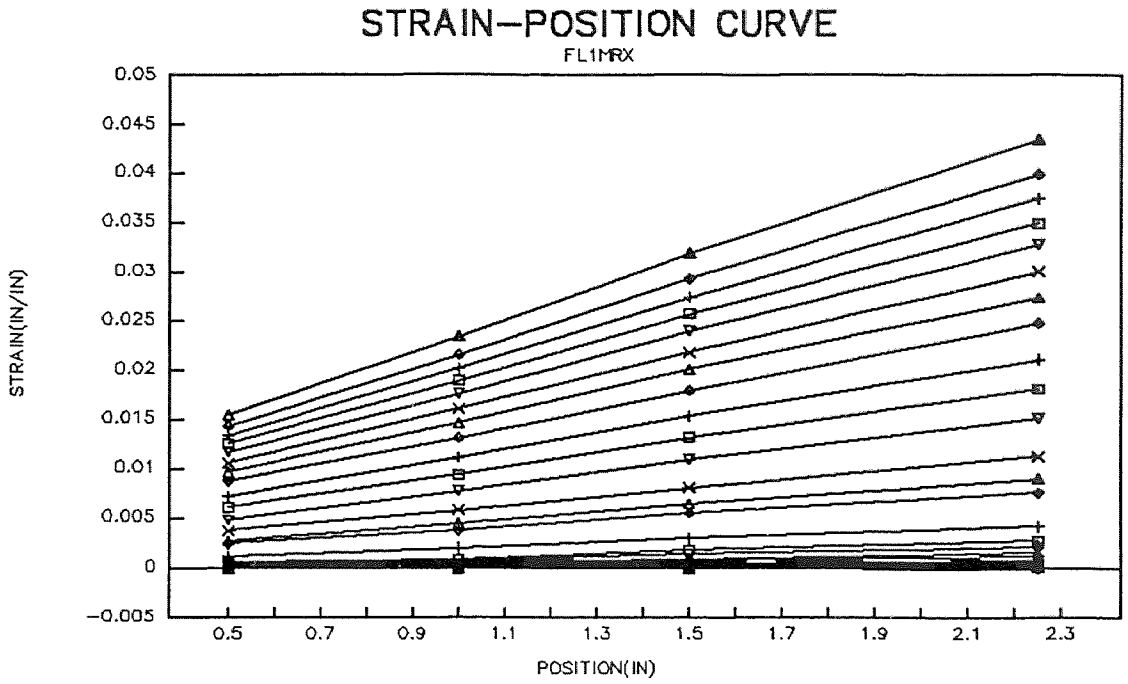

Figure K.1 Strain-Position Curves for High Strength Fibrous Column FL1 in X-Direction.

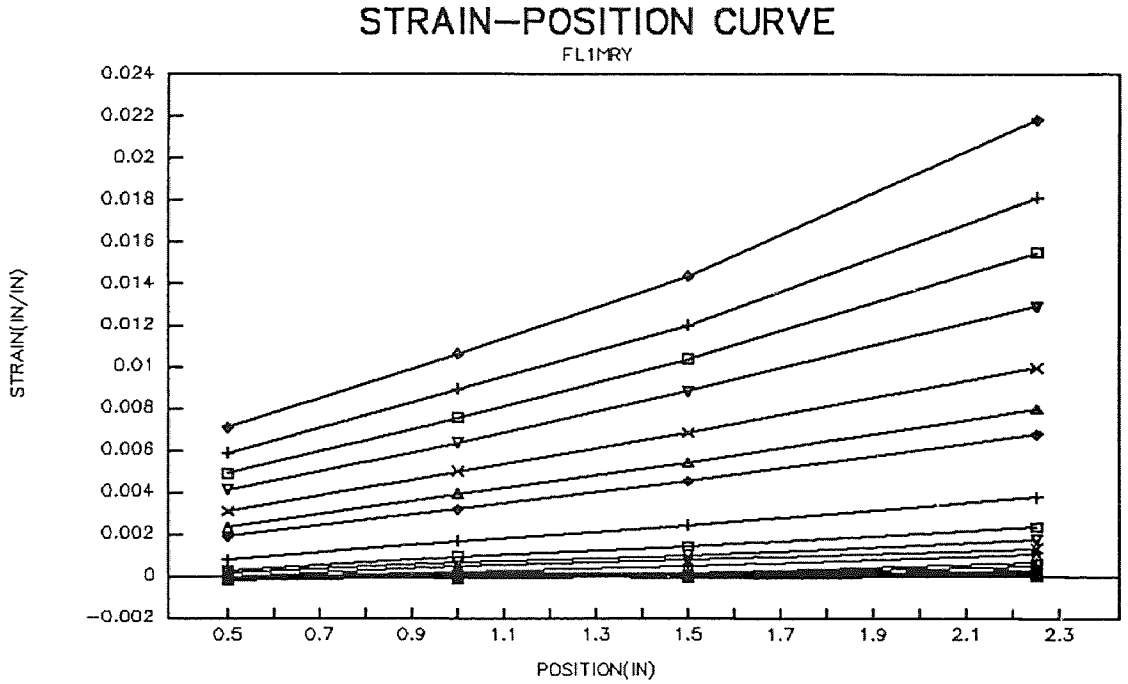

Figure K.2 Strain-Position Curves for High Strength Fibrous Column FL1 in Y-Direction.

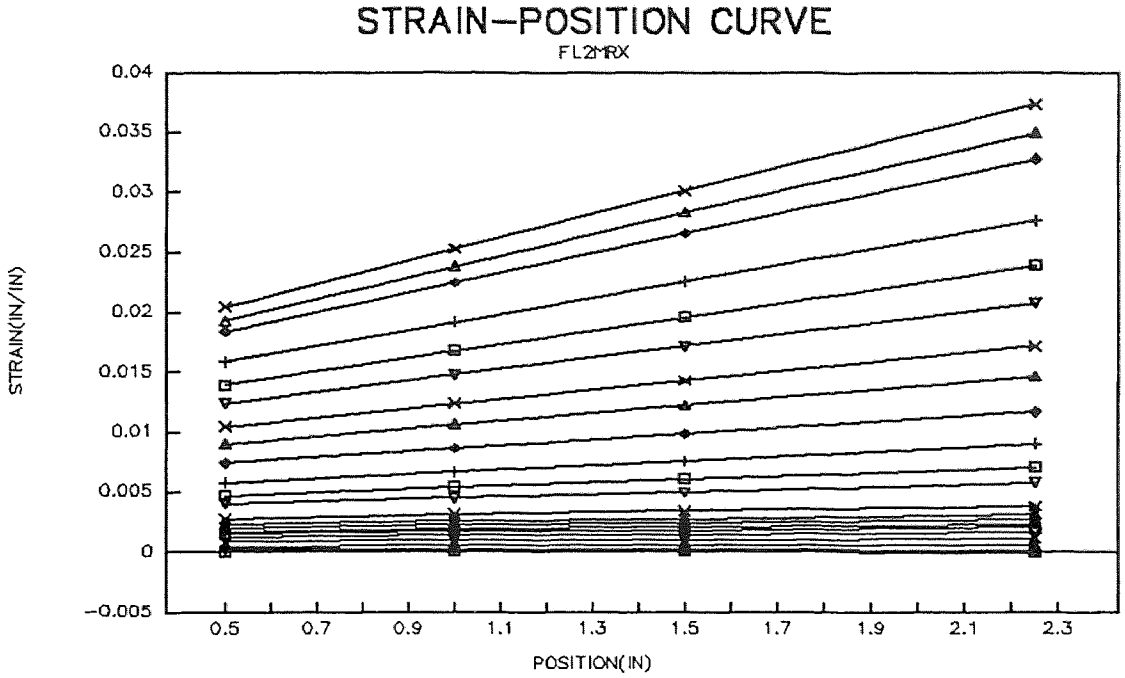

Figure K.3 Strain-Position Curves for High Strength Fibrous Column FL2 in X-Direction.

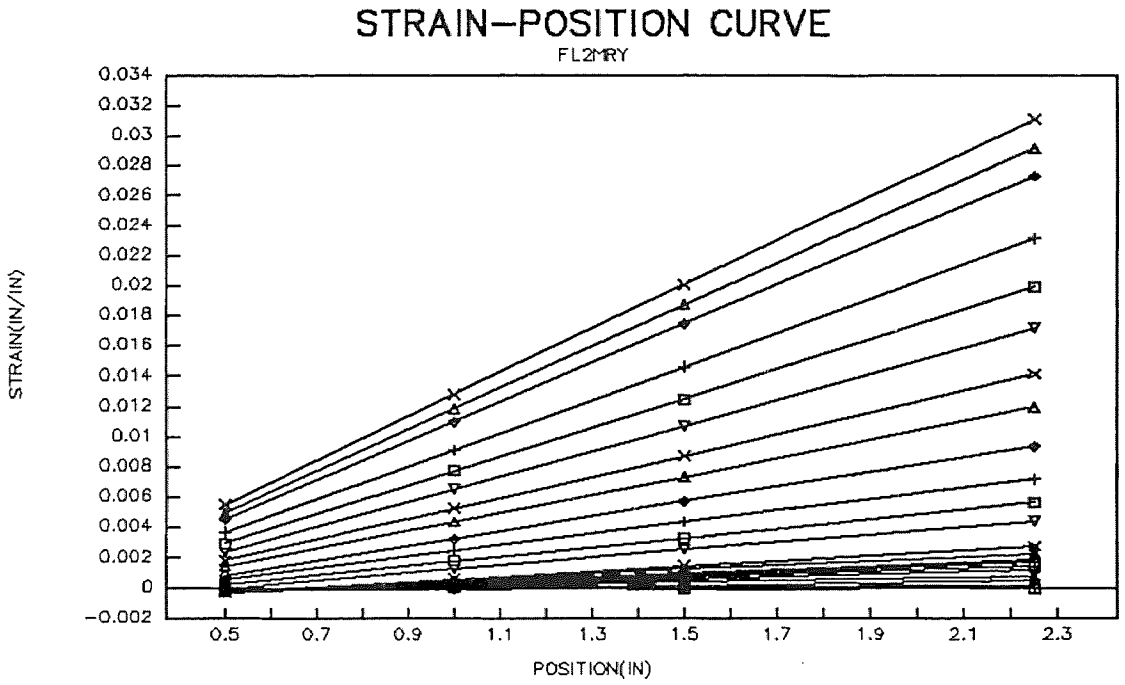

Figure K.4 Strain-Position Curves for High Strength Fibrous Column FL2 in Y-Direction.

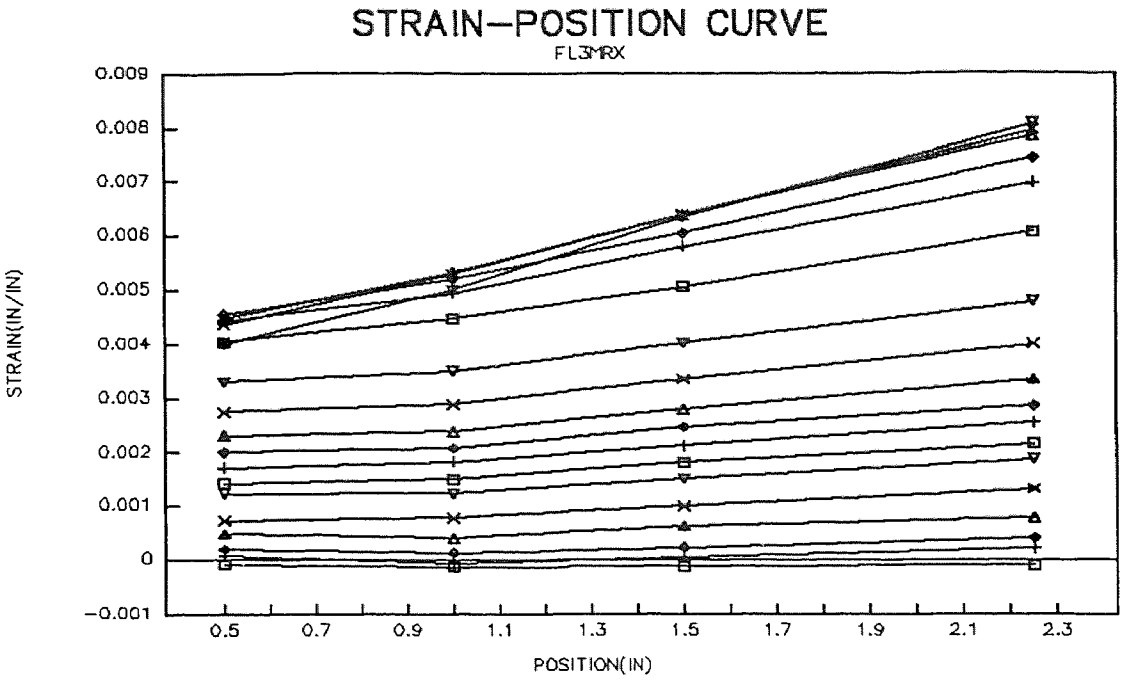

Figure K.5 Strain-Position Curves for High Strength Fibrous Column FL3 in X-Direction.

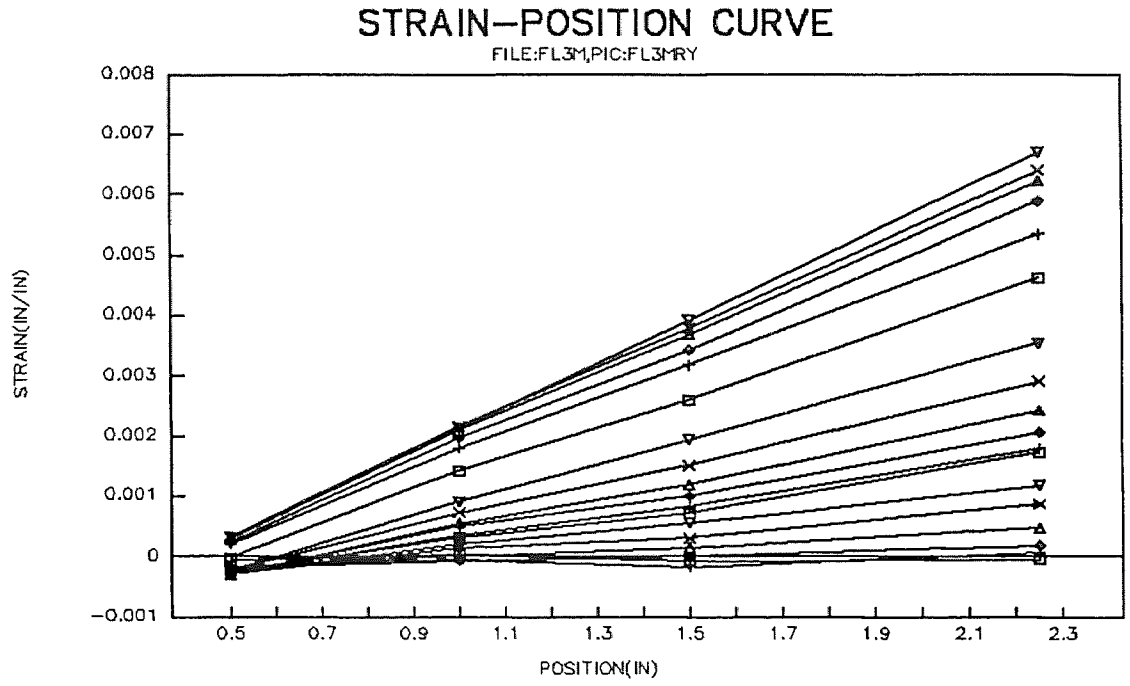

Figure K.6 Strain-Position Curves for High Strength Fibrous Column FL3 in Y-Direction.

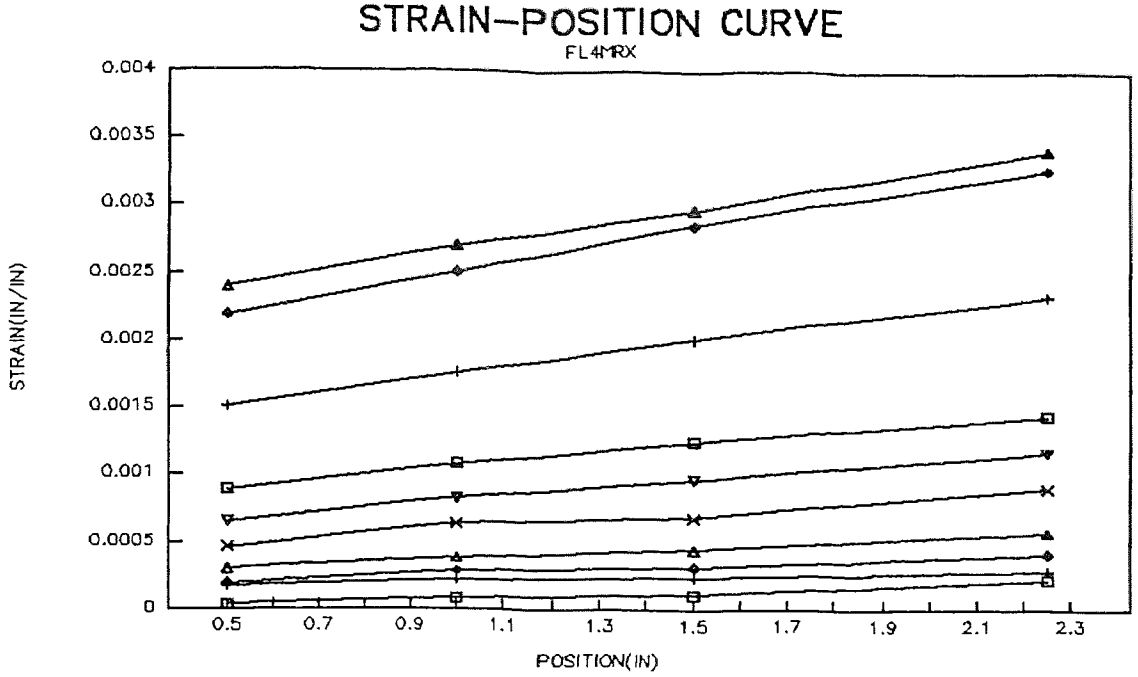

Figure K.7 Strain-Position Curves for High Strength Fibrous Column FL4 in X-Direction.

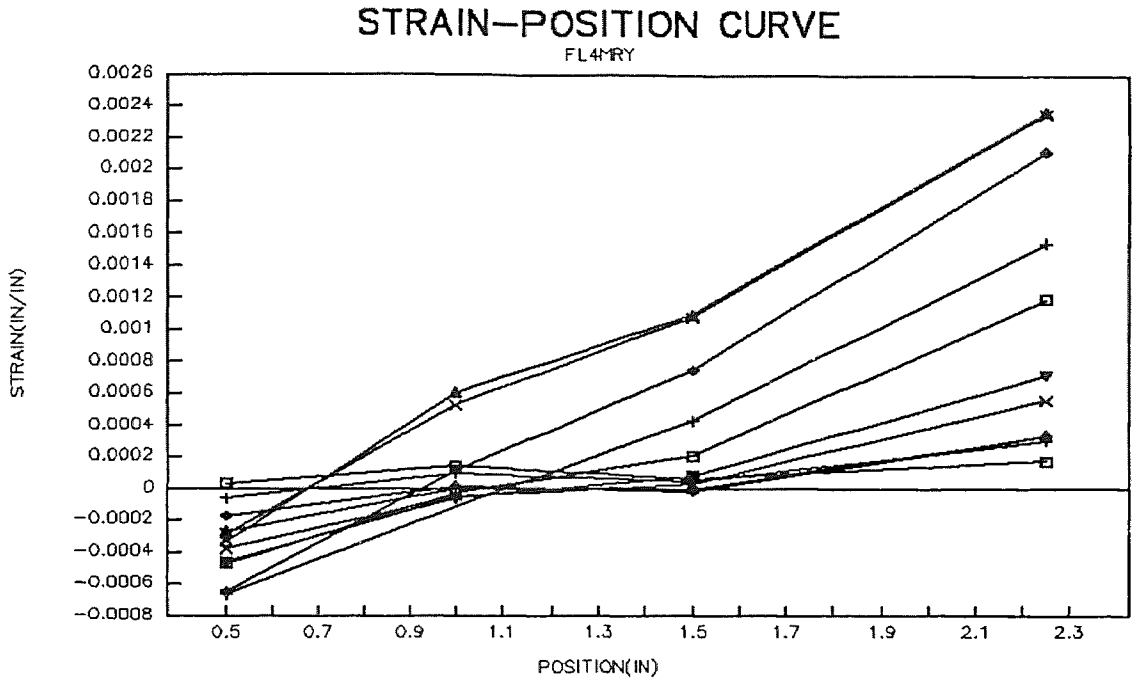

Figure K.8 Strain-Position Curves for High Strength Fibrous Column FL4 in Y-Direction.

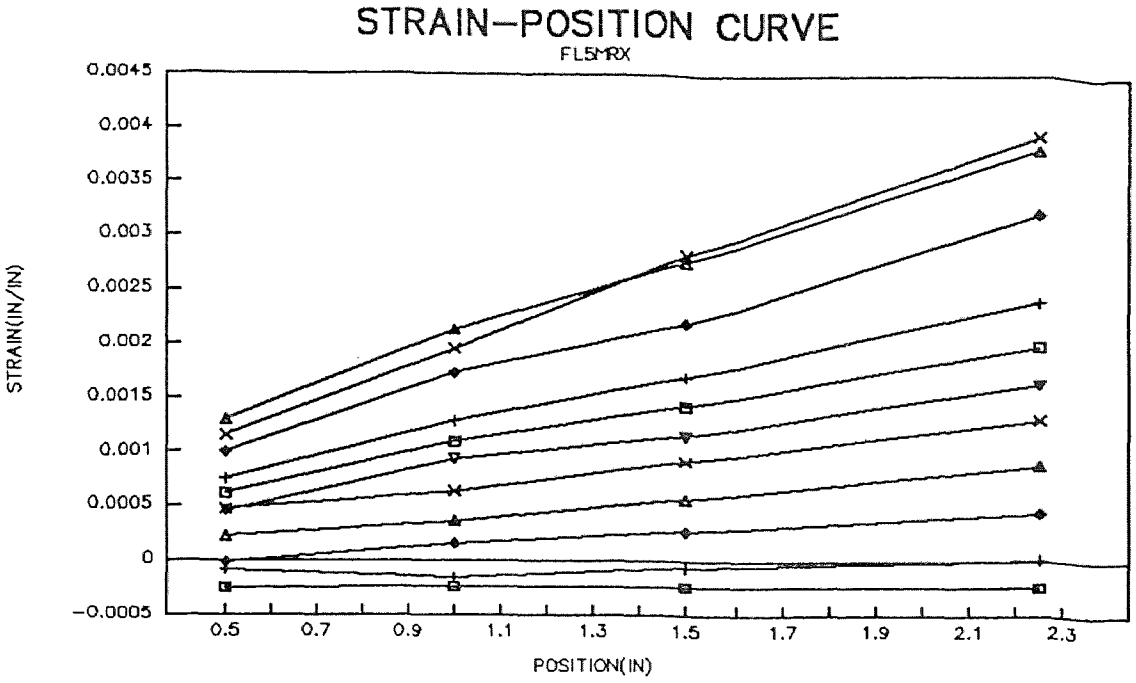

Figure K.9 Strain-Position Curves for High Strength Fibrous Column FL5 in X-Direction.

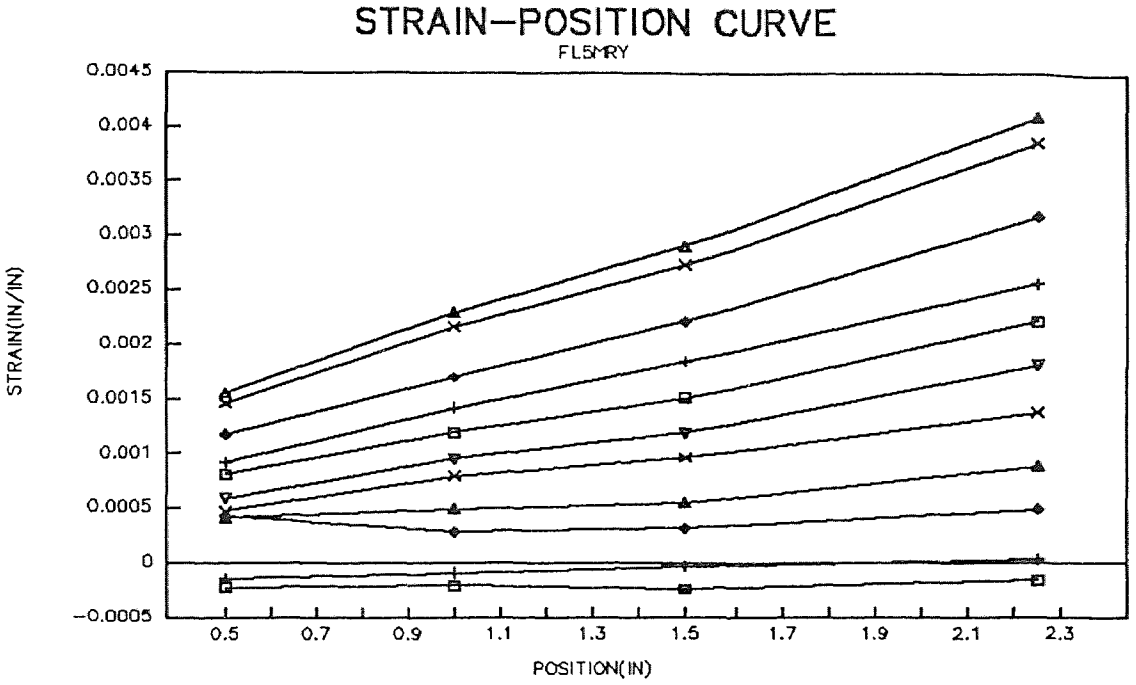

Figure K.10 Strain-Position Curves for High Strength Fibrous Column FL5 in Y-Direction.

APPENDIX L
CRACK AND CRUSH PATTERN FOR HSC COLUMNS

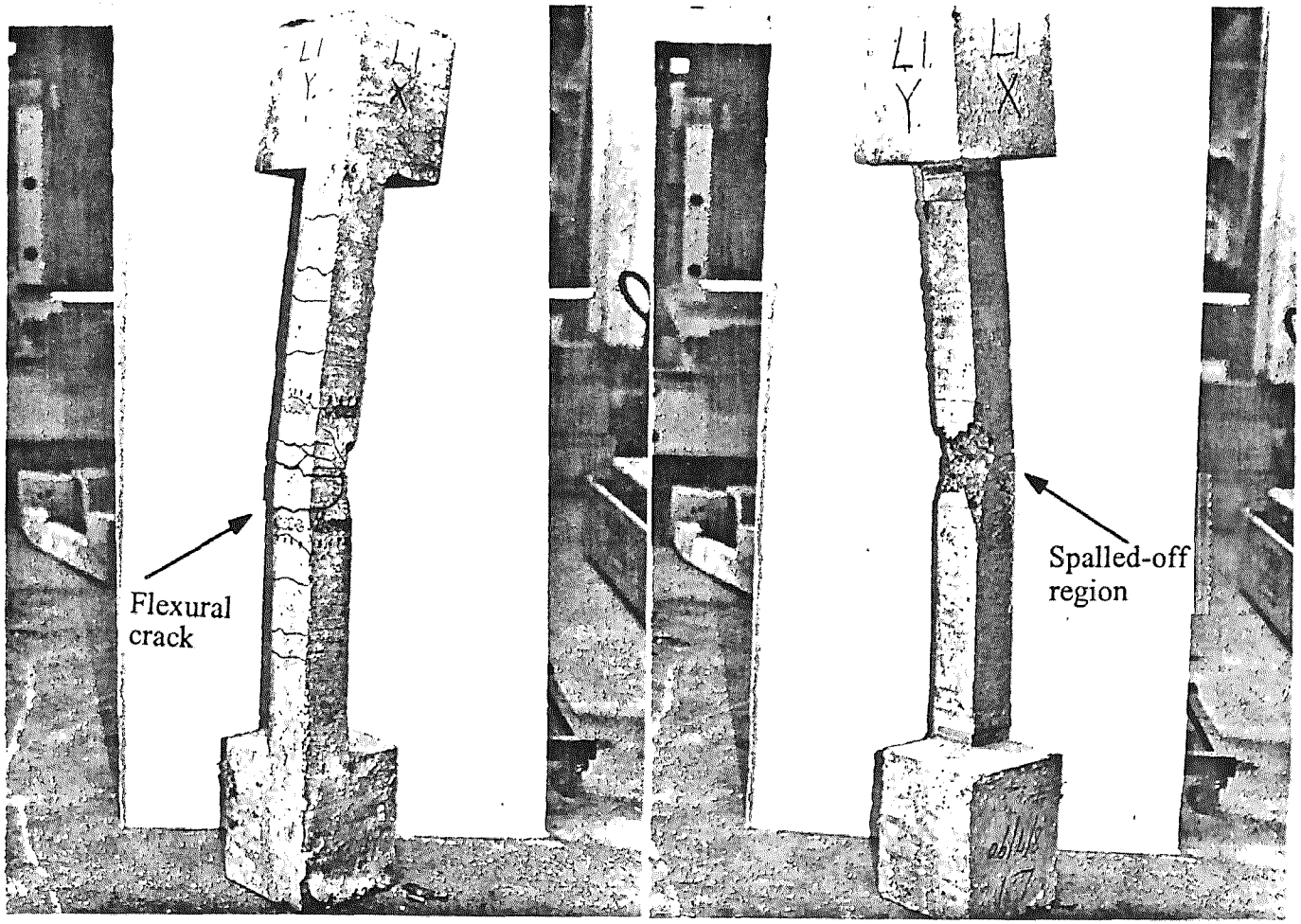

Figure L.1 Crack and crush pattern for specimen L1

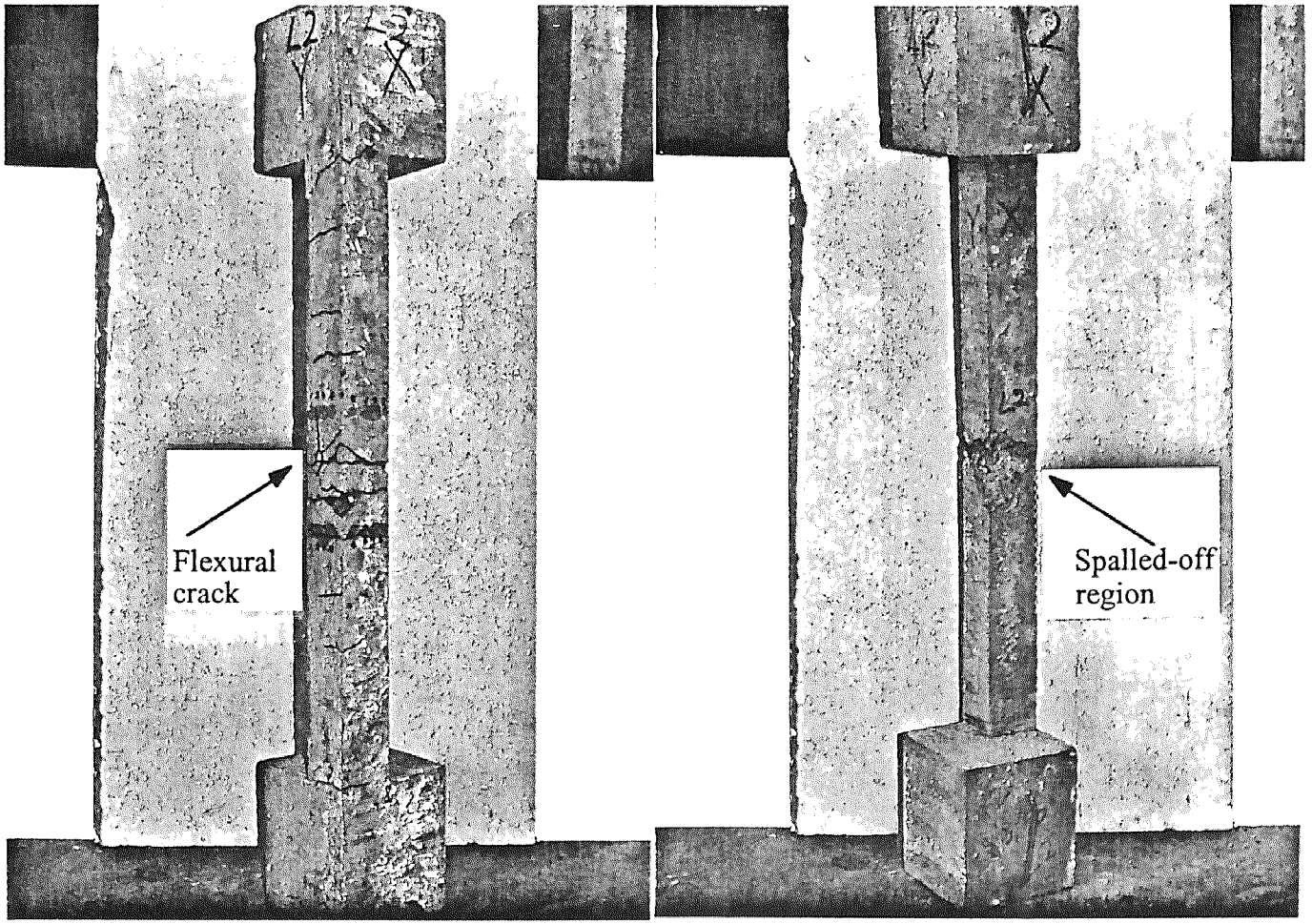

Figure L.2 Crack and crush pattern for specimen L2

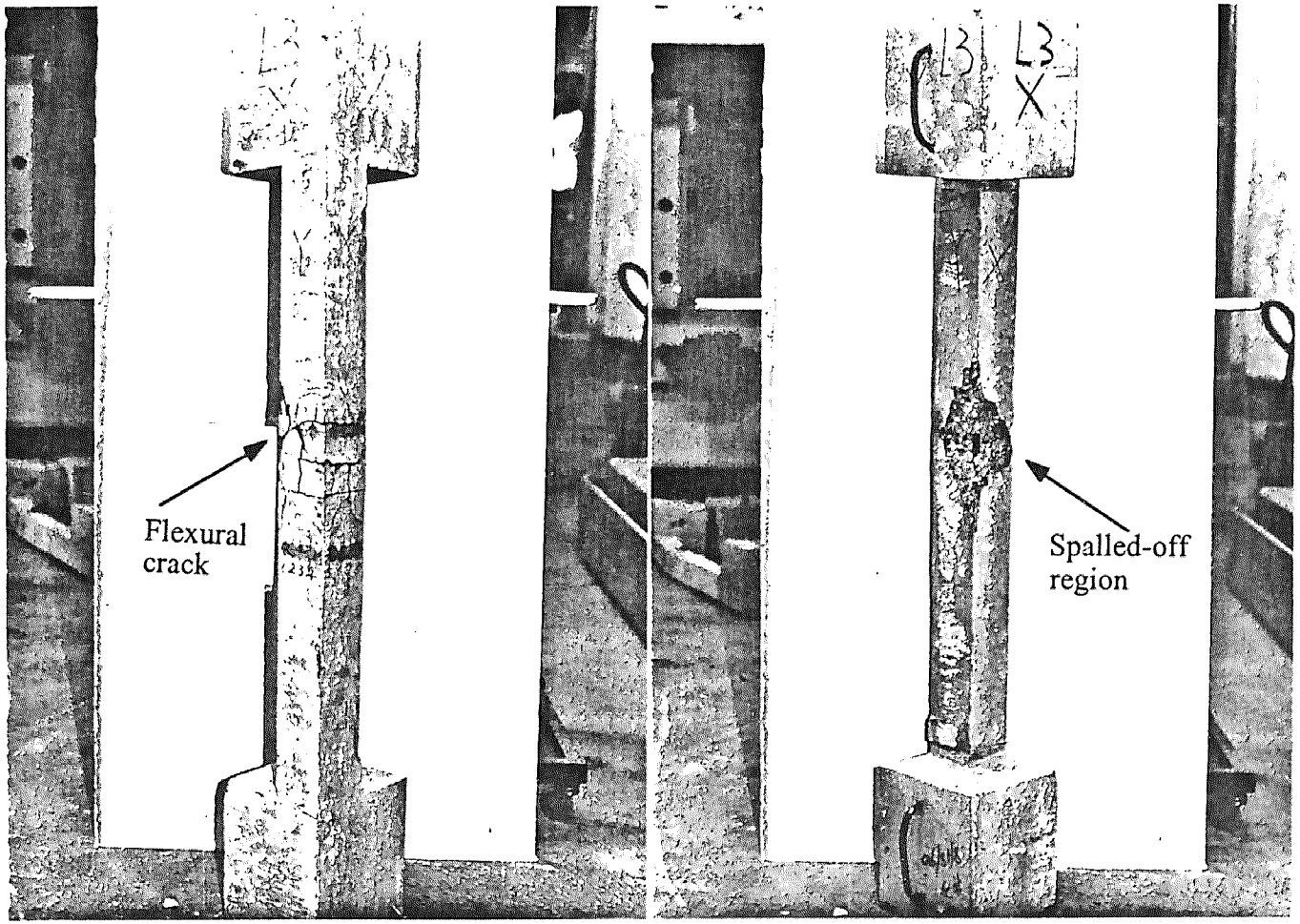

Figure L.3 Crack and crush pattern for specimen L3

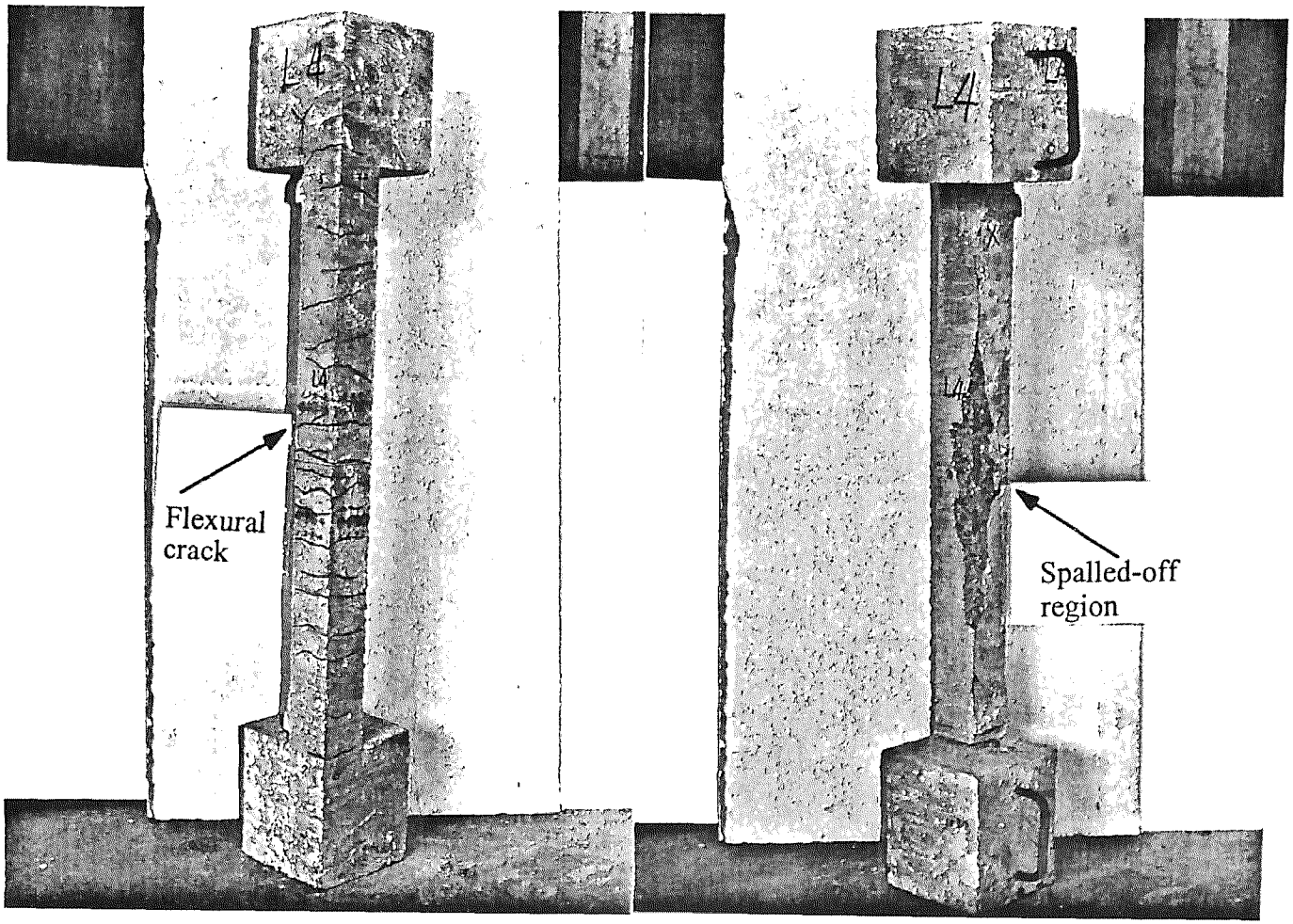

Figure L.4 Crack and crush pattern for specimen L4

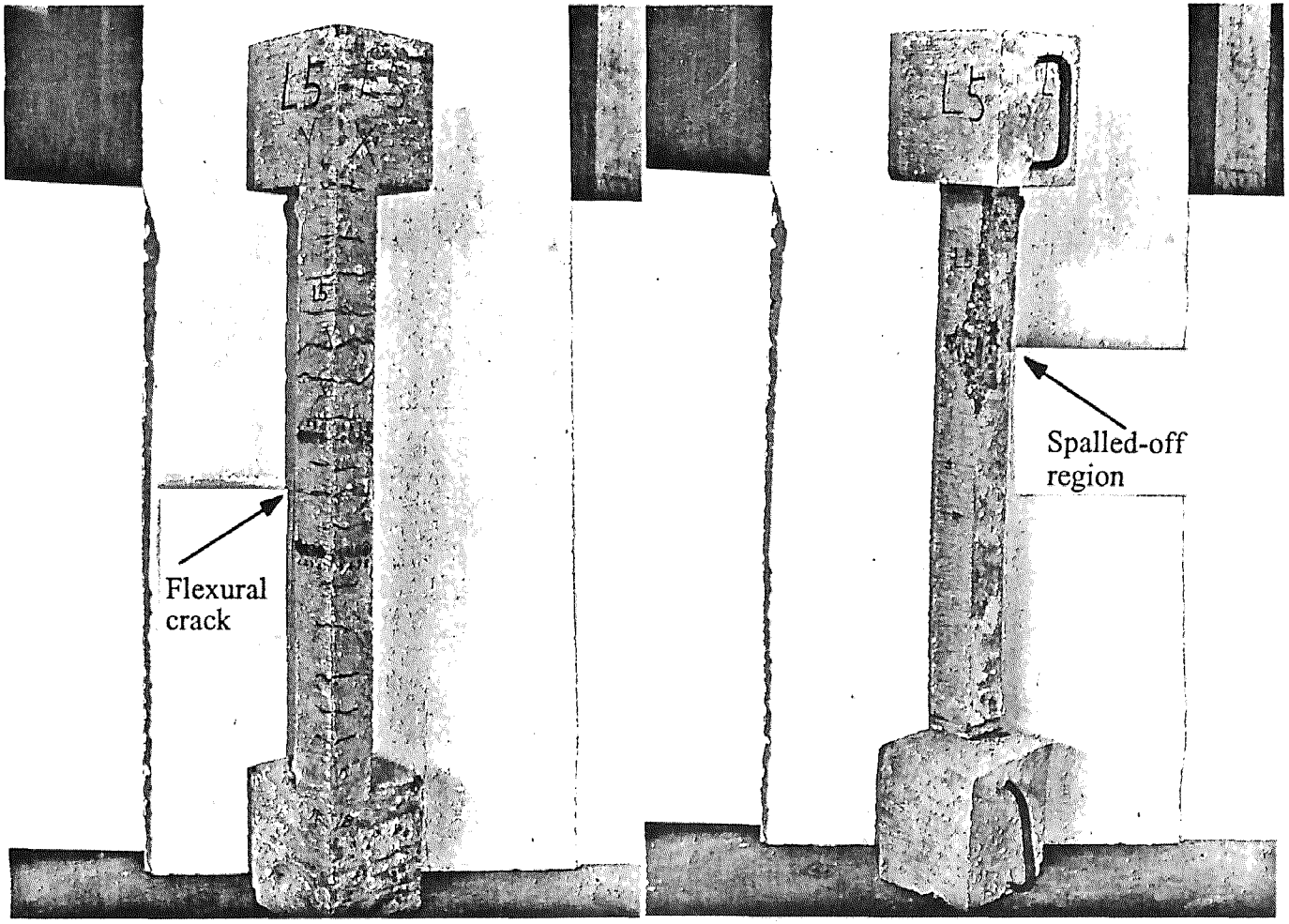

Figure L.5 Crack and crush pattern for specimen L5

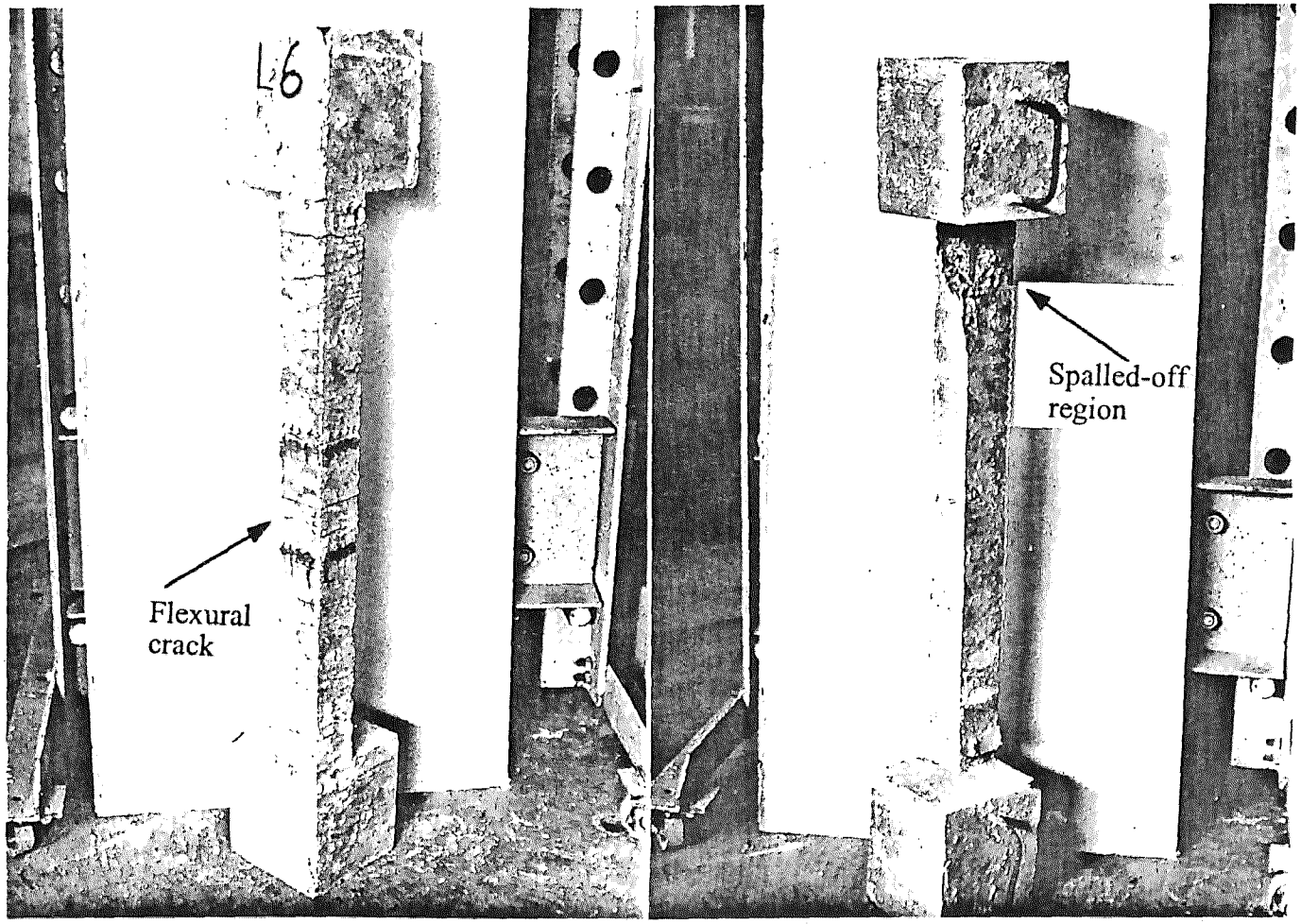

Figure L.6 Crack and crush pattern for specimen L6

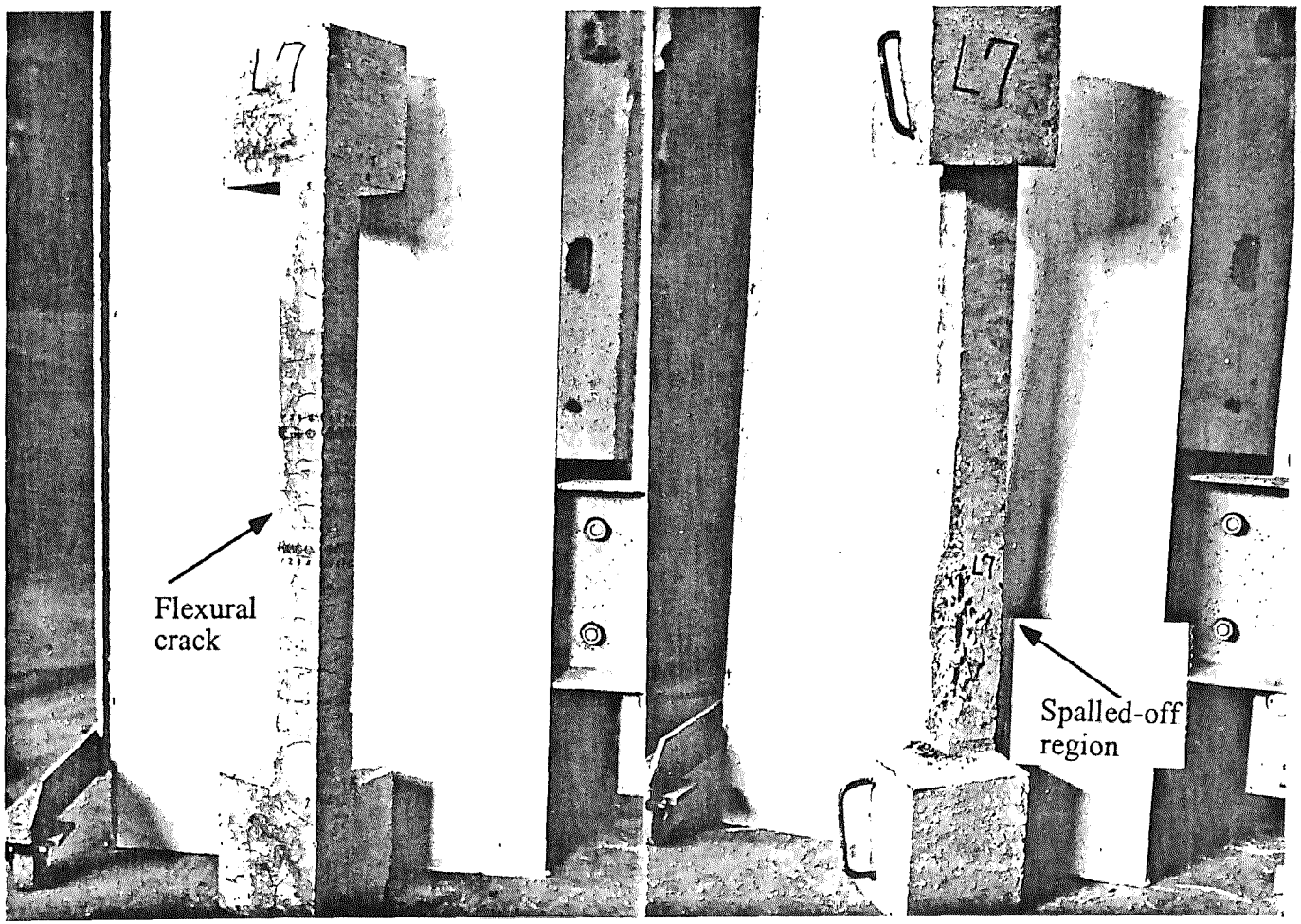

Figure L.7 Crack and crush pattern for specimen L7

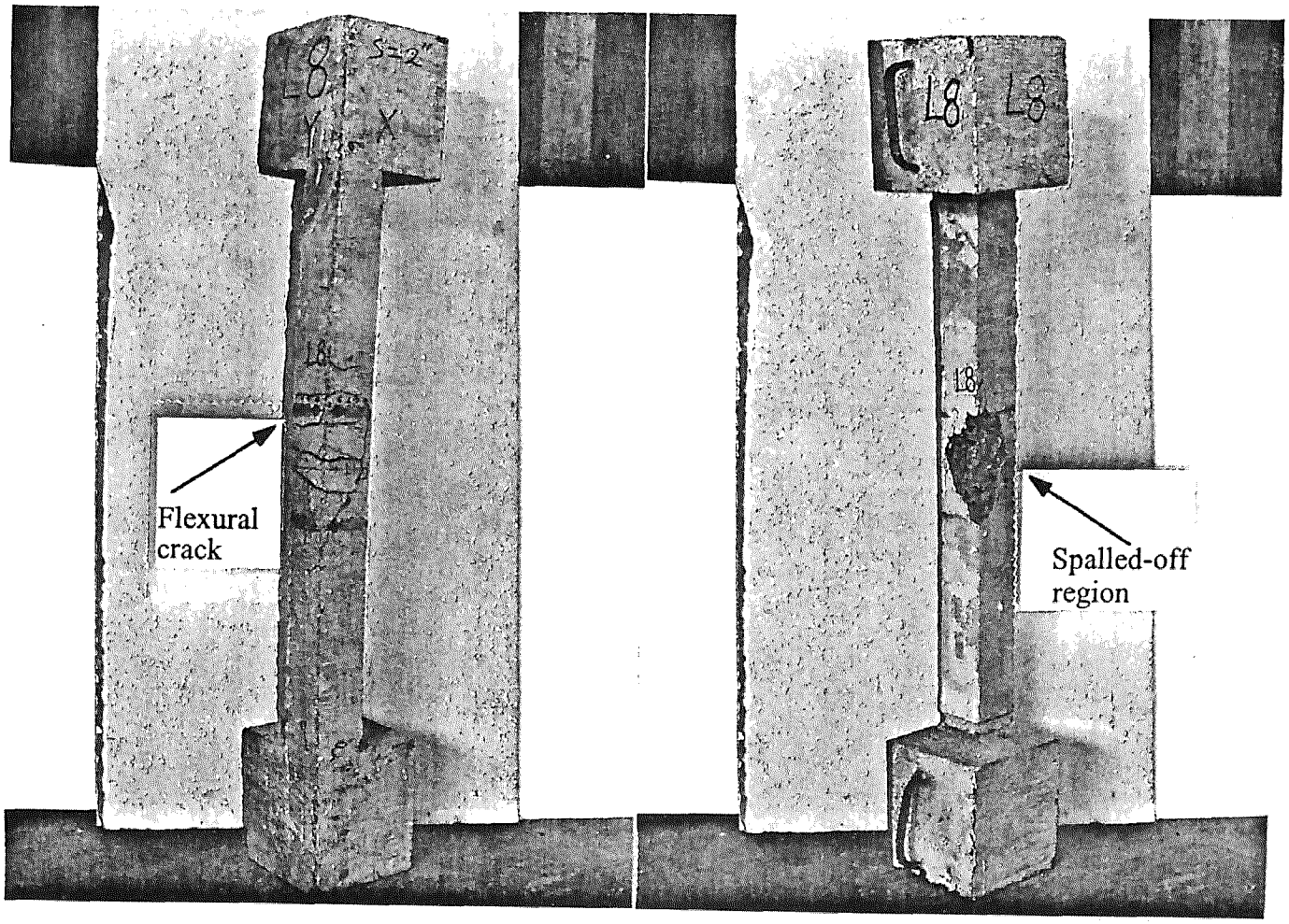

Figure L.8 Crack and crush pattern for specimen L8

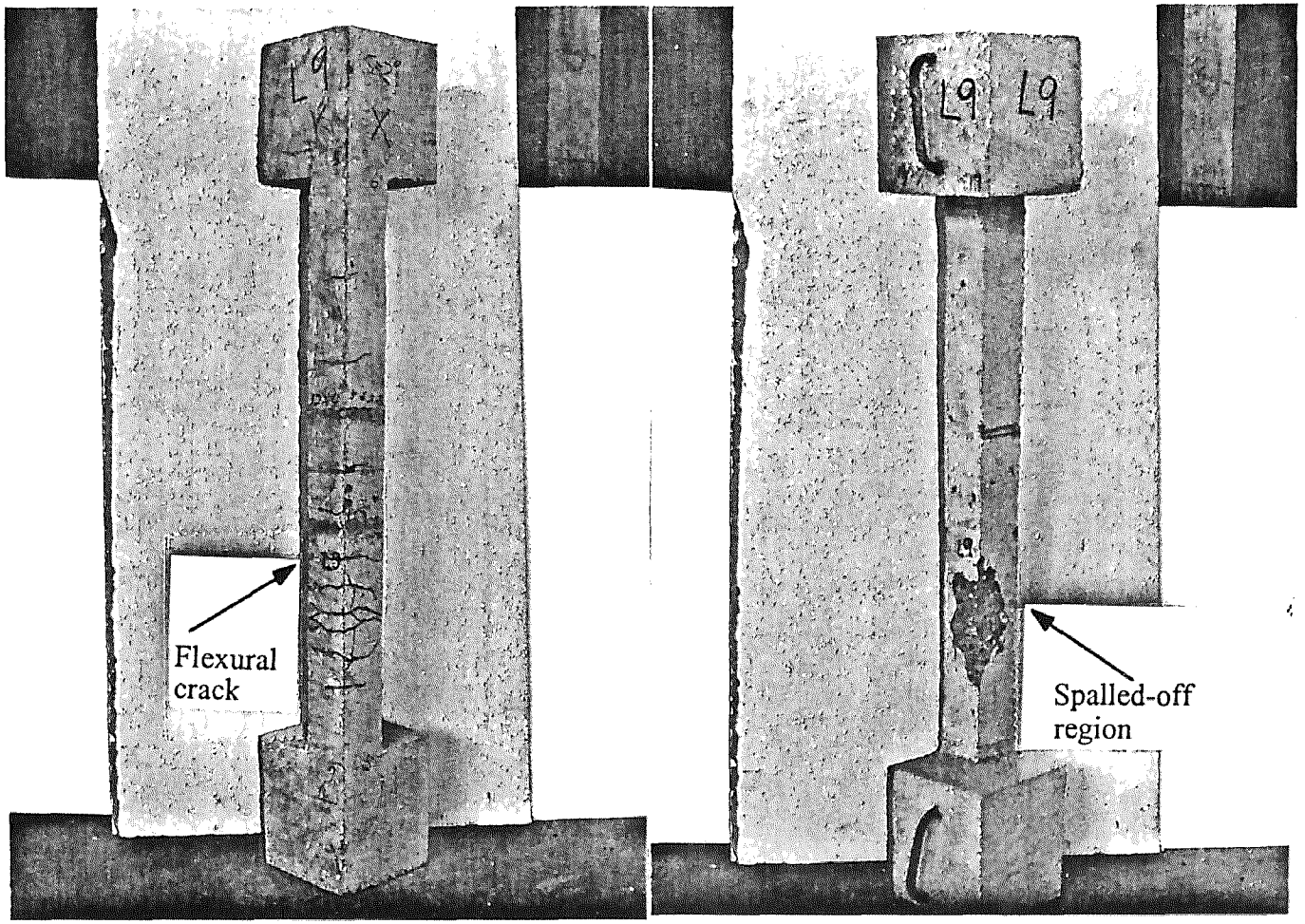

Figure L.9 Crack and crush pattern for specimen L9

APPENDIX M
CRACK AND CRUSH PATTERN FOR HIGH STRENGTH FIBROUS COLUMNS

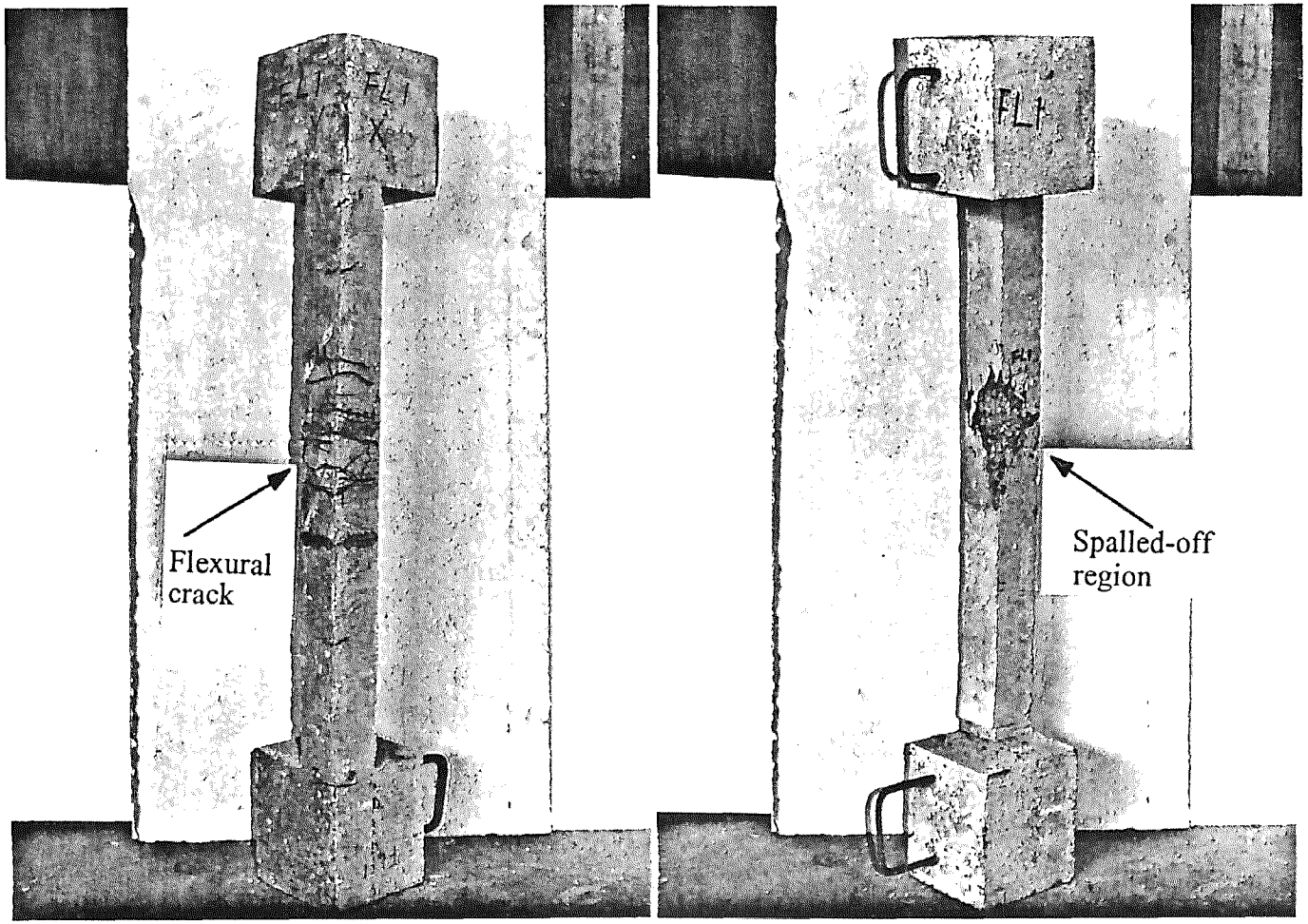

Figure M.1 Crack and crush pattern for specimen FL1

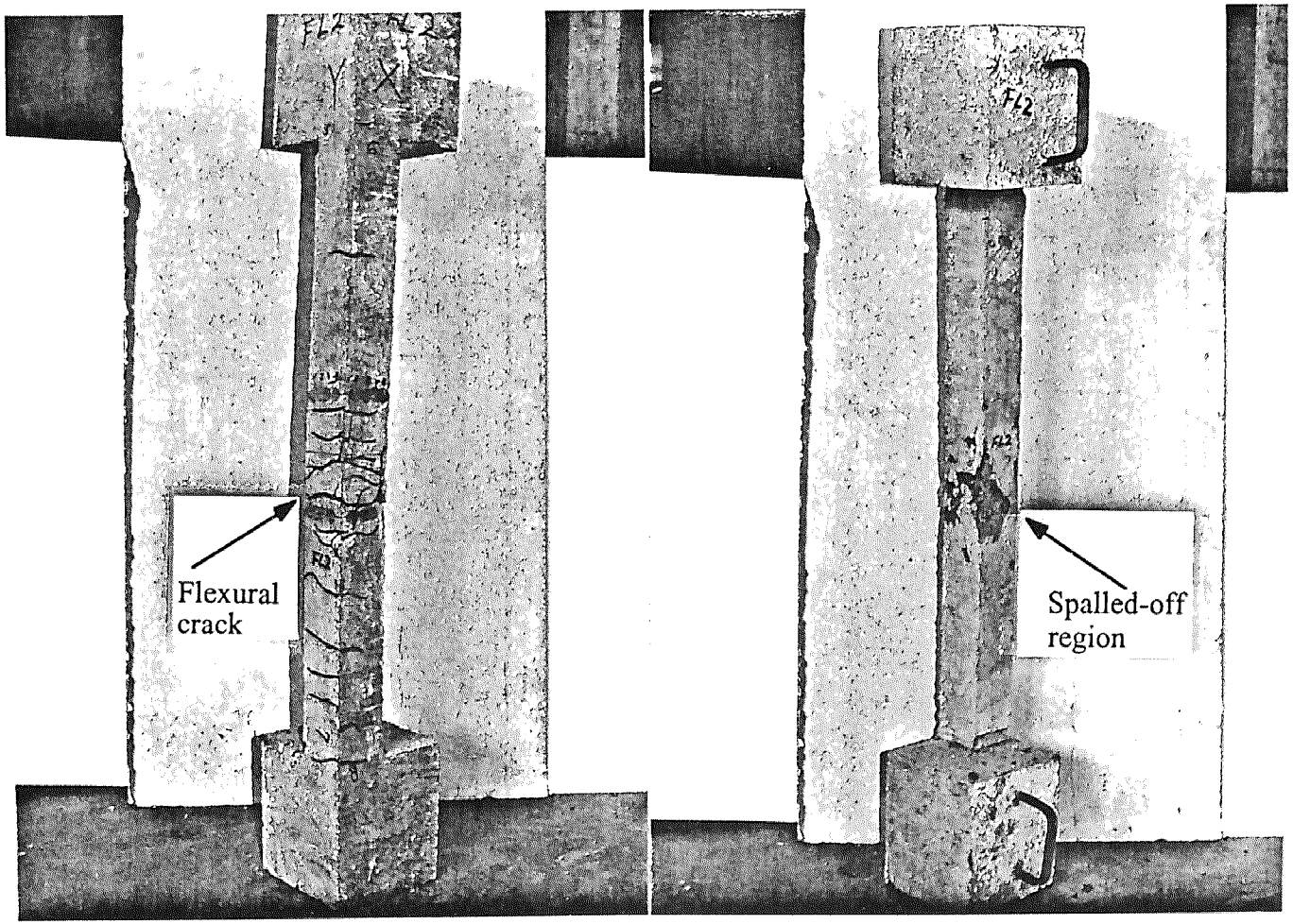

Figure M.2 Crack and crush pattern for specimen FL2

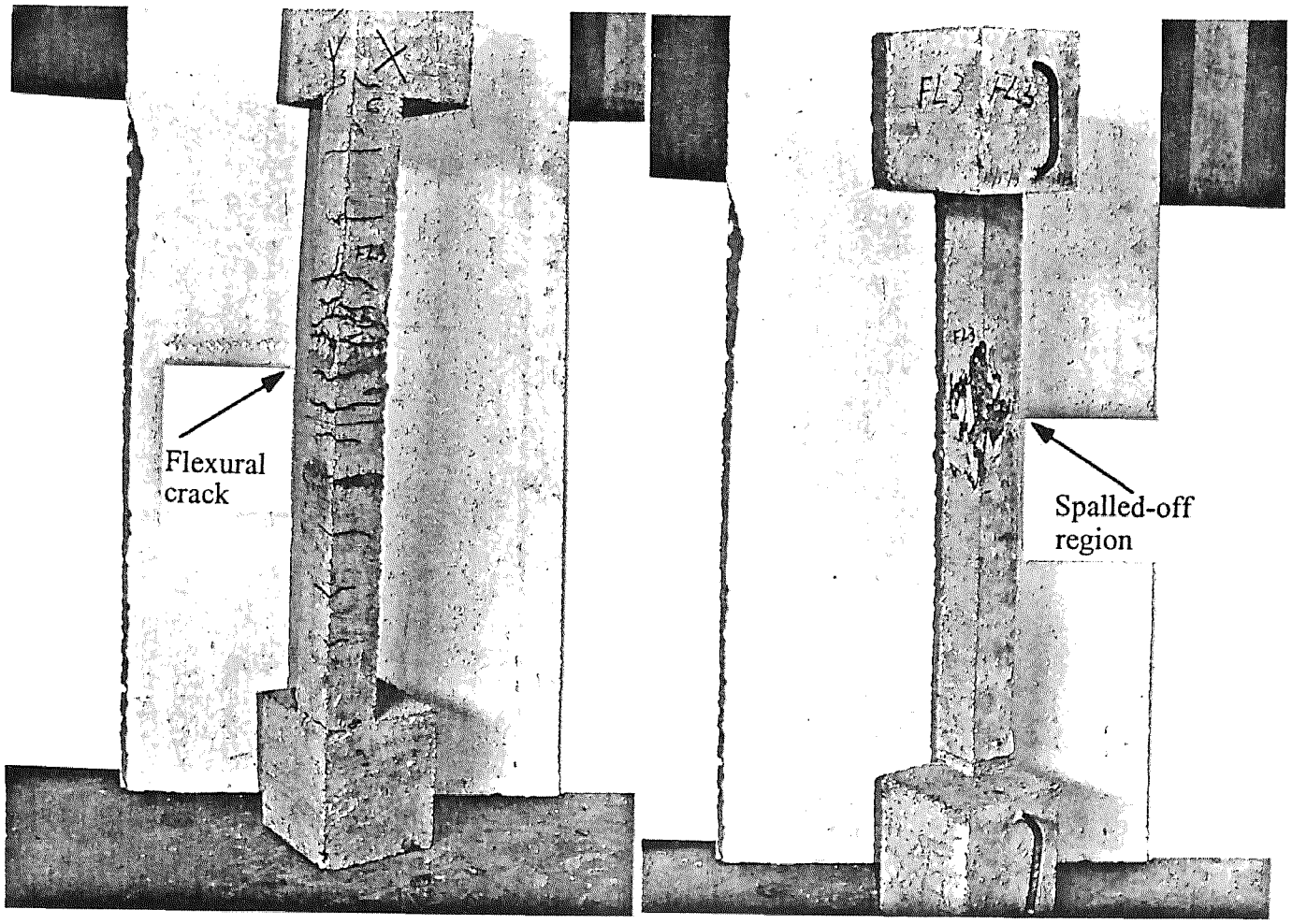

Figure M.3 Crack and crush pattern for specimen FL3

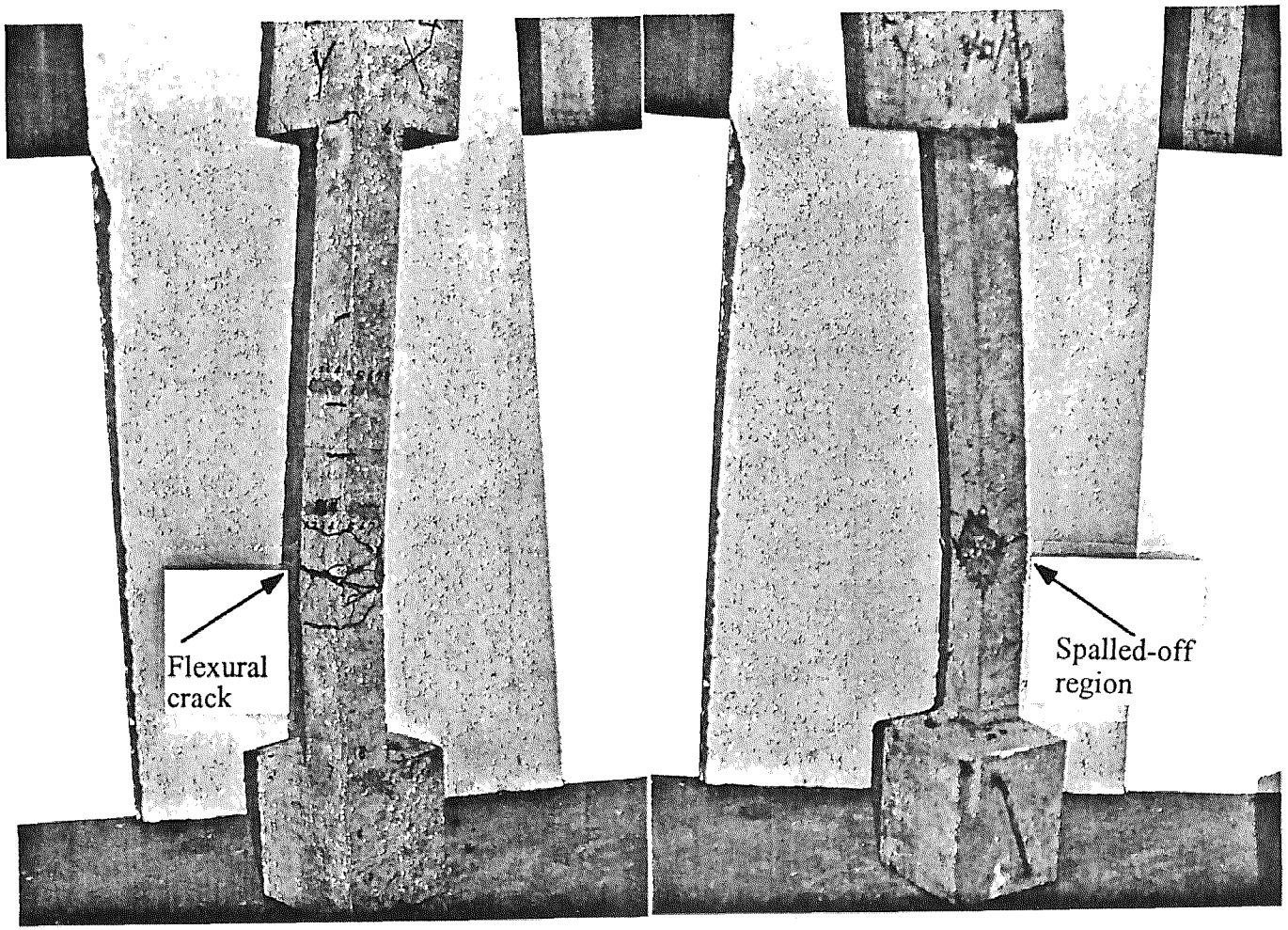

Figure M.4 Crack and crush pattern for specimen FL4

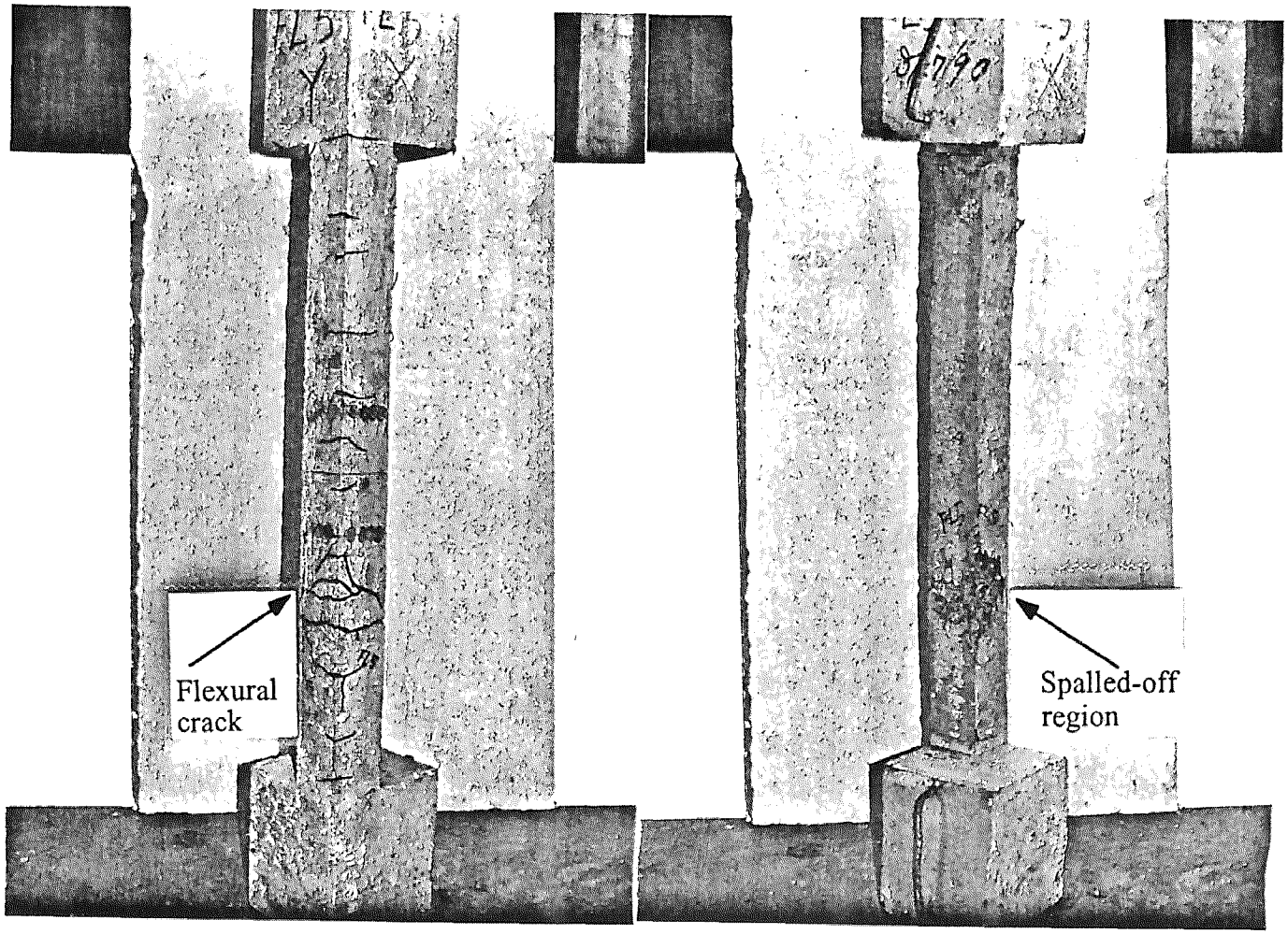

Figure M.5 Crack and crush pattern for specimen FL5

APPENDIX N
COMPARISON OF LOAD-DEFLECTION AND MOMENT-CURVATURE CURVES FOR HSC COLUMNS

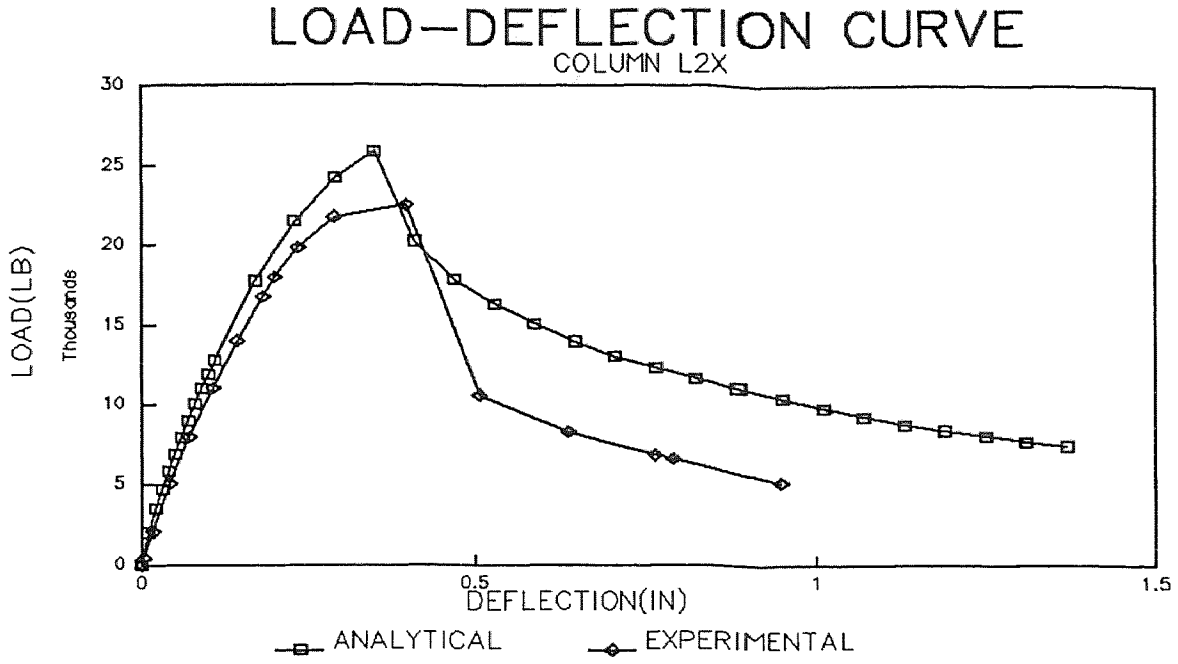

Figure N.1 Comparison of Load-Deflection Curve for High Strength Column L2 in X-Direction.

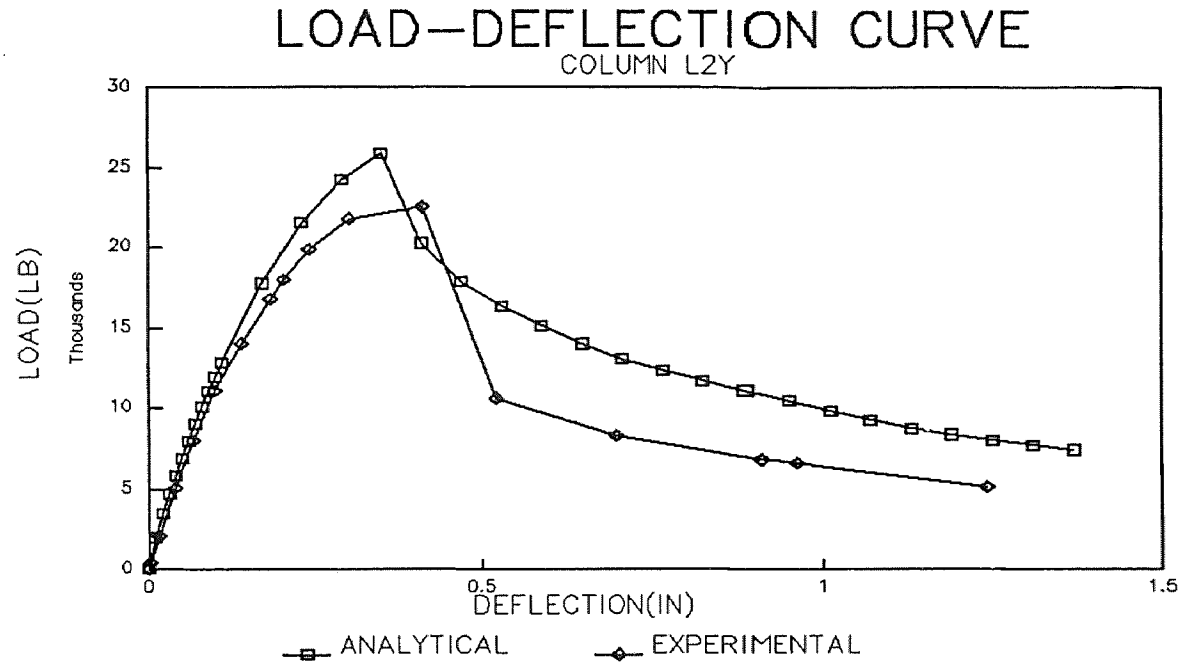

Figure N.2 Comparison of Load-Deflection Curve for High Strength Column L2 in Y-Direction.

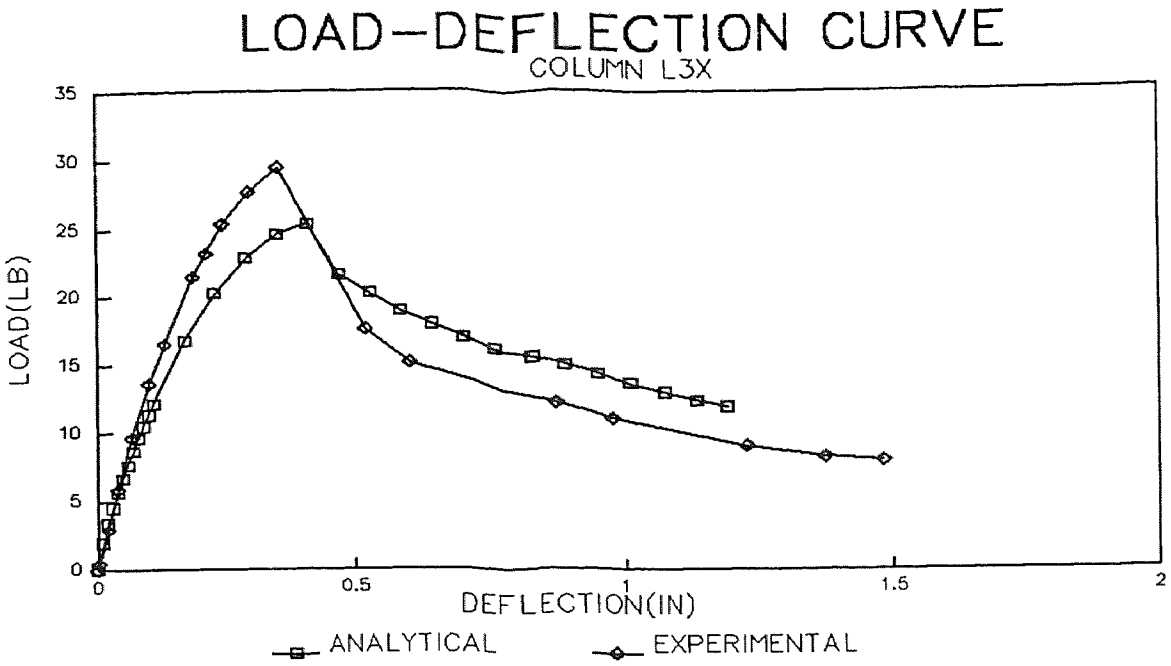

Figure N.3 Comparison of Load-Deflection Curve for High Strength Column L3 in X-Direction.

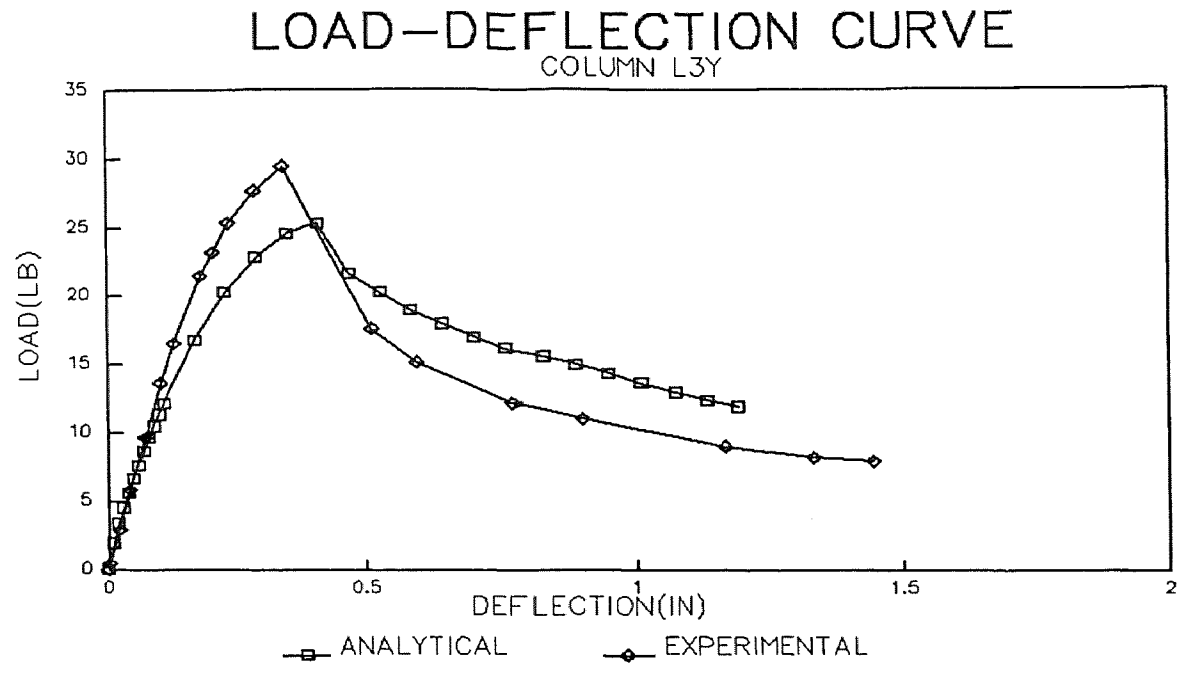

Figure N.4 Comparison of Load-Deflection Curve for High Strength Column L3 in Y-Direction.

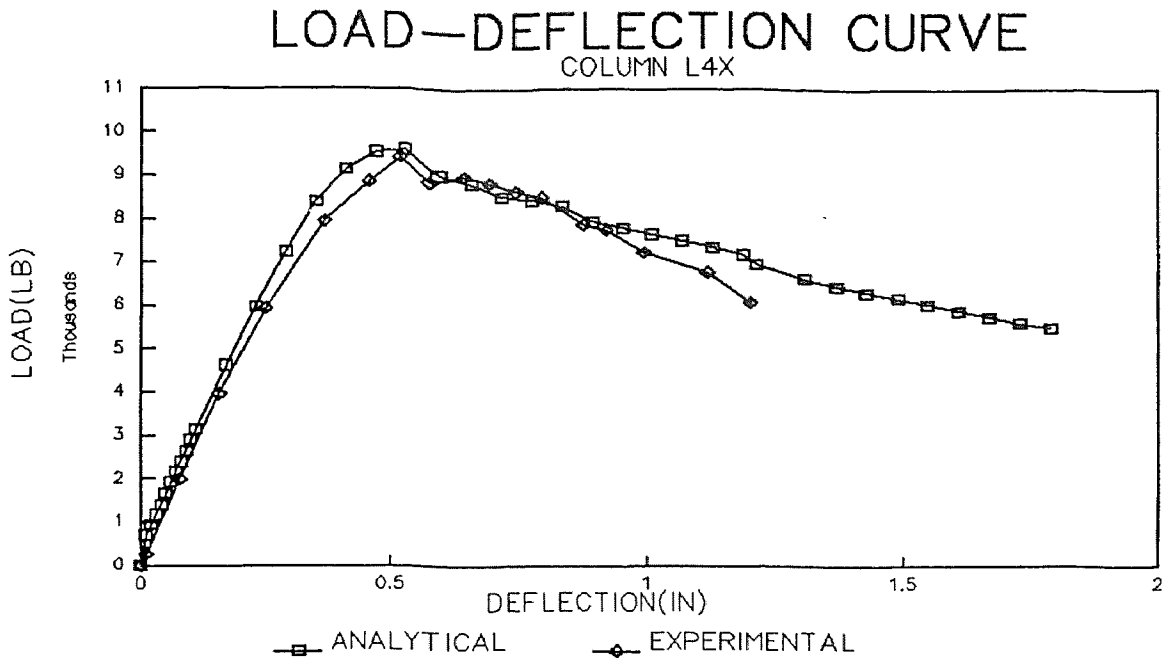

Figure N.5 Comparison of Load-Deflection Curve for High Strength Column L4 in X-Direction.

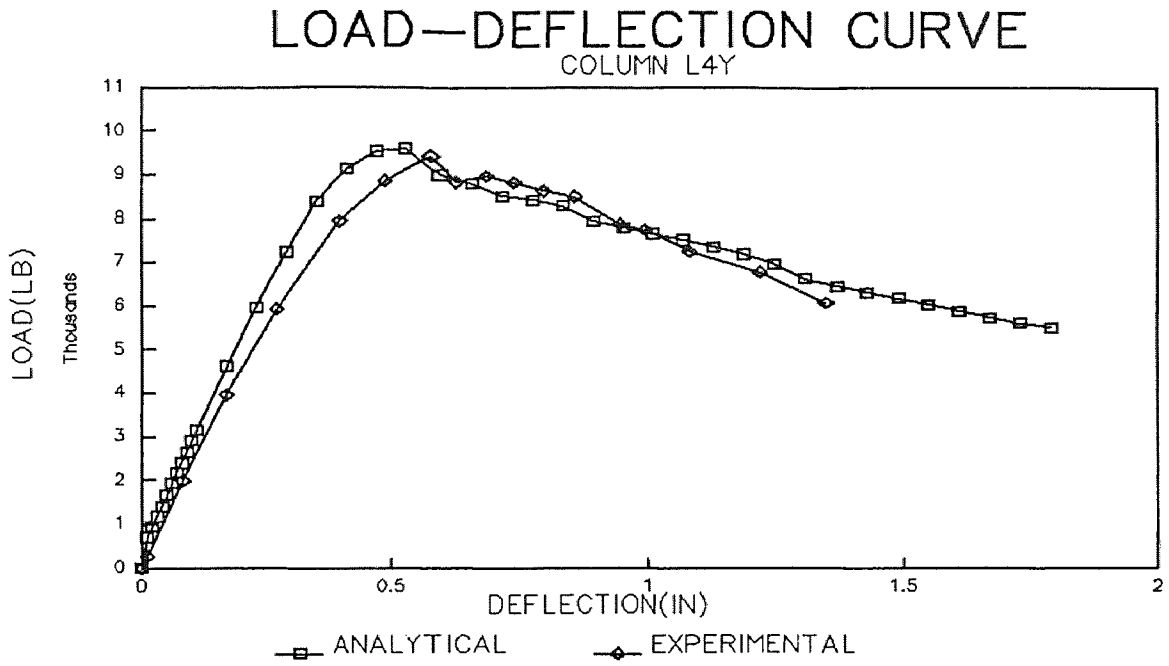

Figure N.6 Comparison of Load-Deflection Curve for High Strength Fibrous Column L4 in Y-Direction.

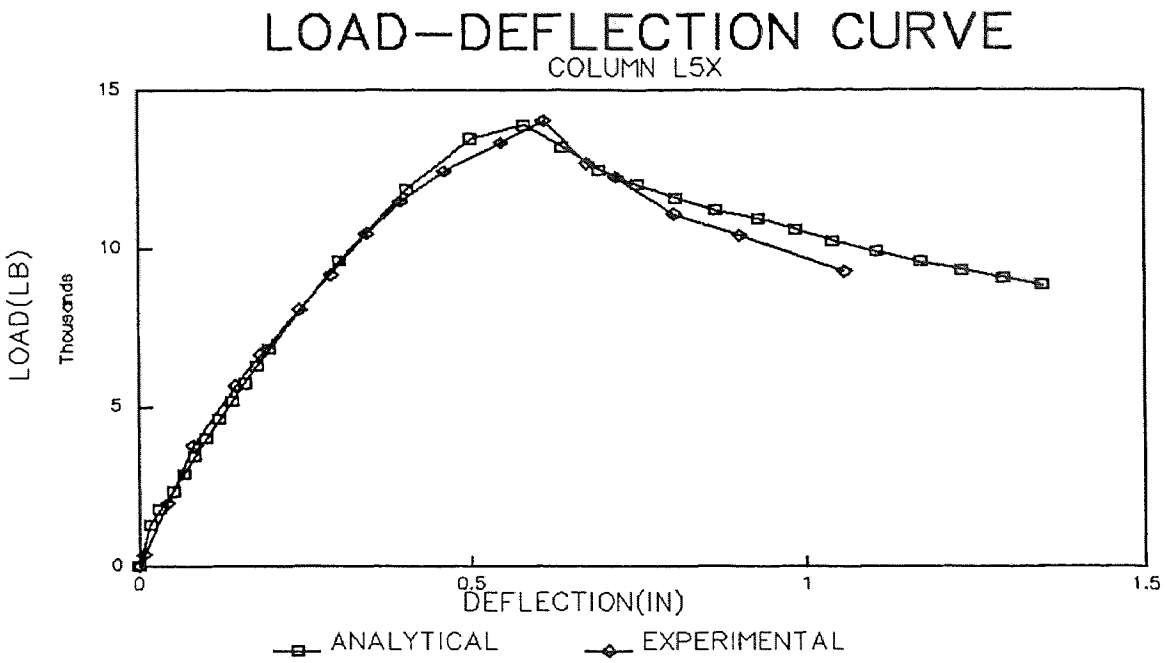

Figure N.7 Comparison of Load-Deflection Curve for High Strength Column L5 in X-Direction.

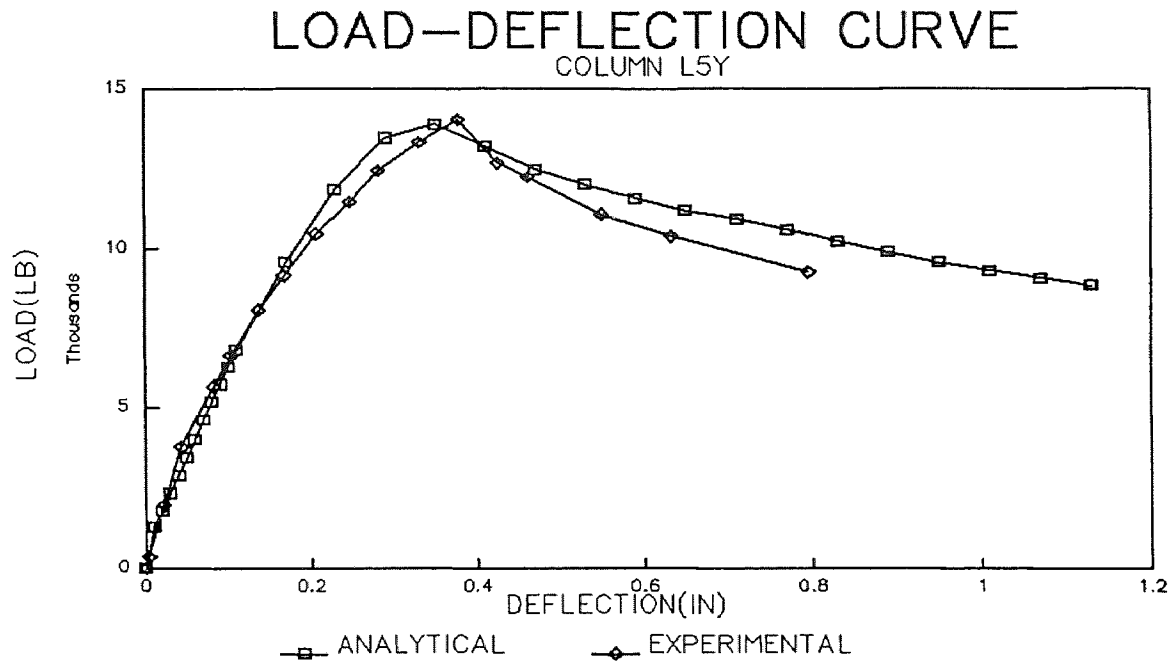

Figure N.8 Comparison of Load-Deflection Curve for High Strength Column L5 in Y-Direction.

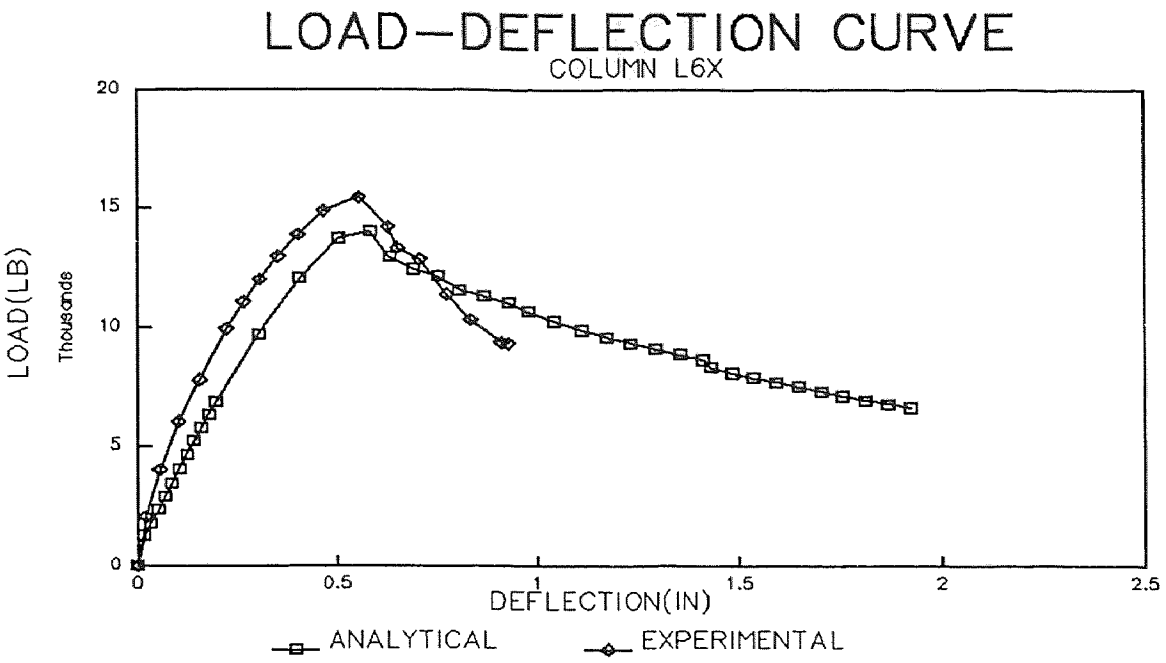

Figure N.9 Comparison of Load-Deflection Curve for High Strength Column L6 in X-Direction.

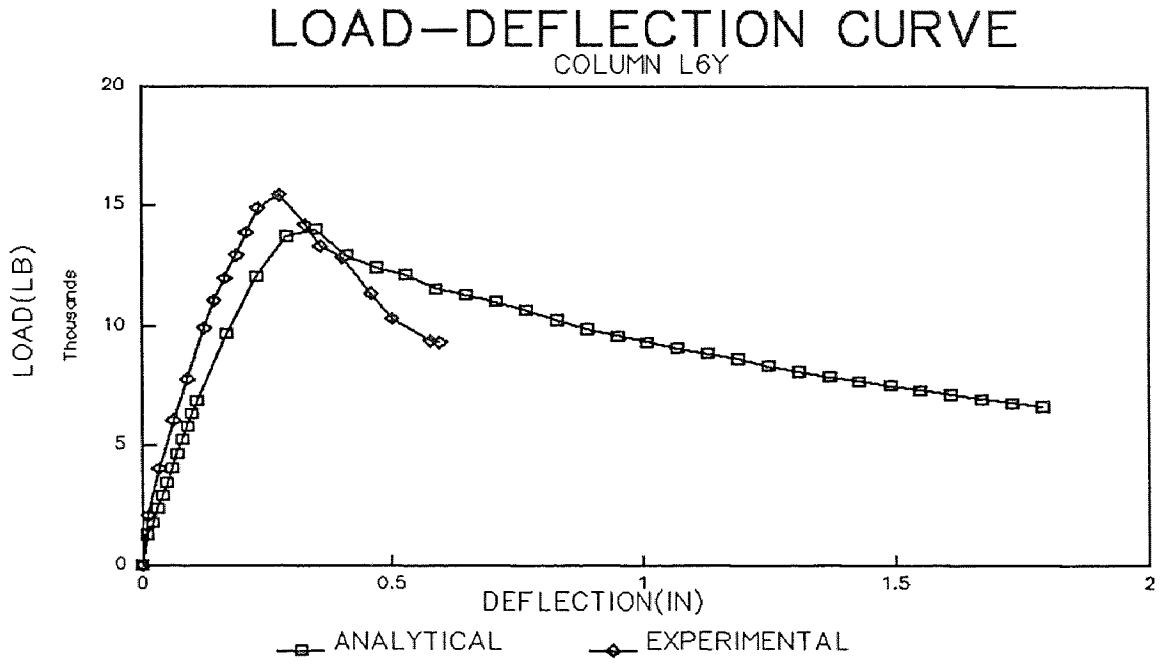

Figure N.10 Comparison of Load-Deflection Curve for High Strength Column L6 in Y-Direction.

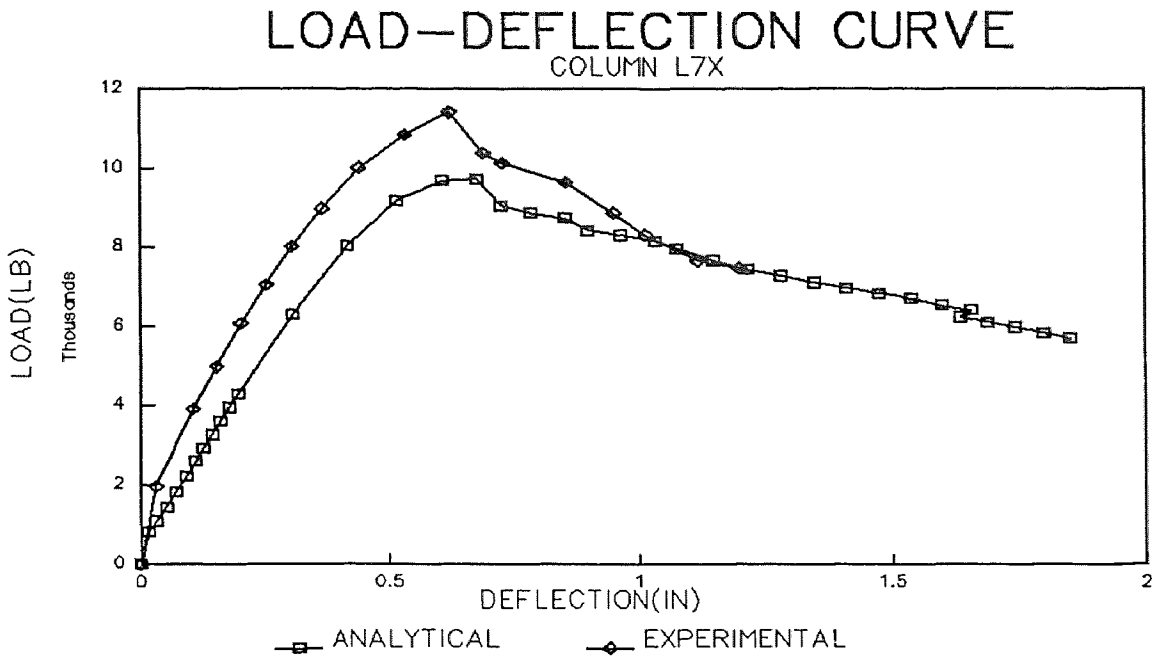

Figure N.11 Comparison of Load-Deflection Curve for High Strength Column L7 in X-Direction.

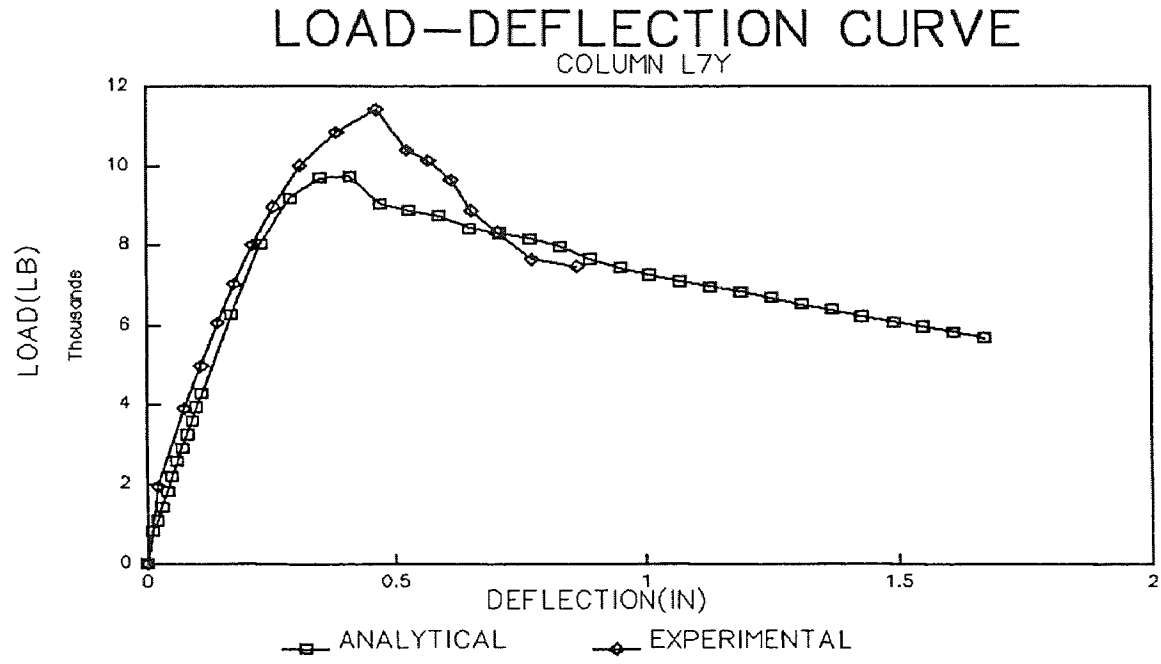

Figure N.12 Comparison of Load-Deflection Curve for High Strength Column L7 in Y-Direction.

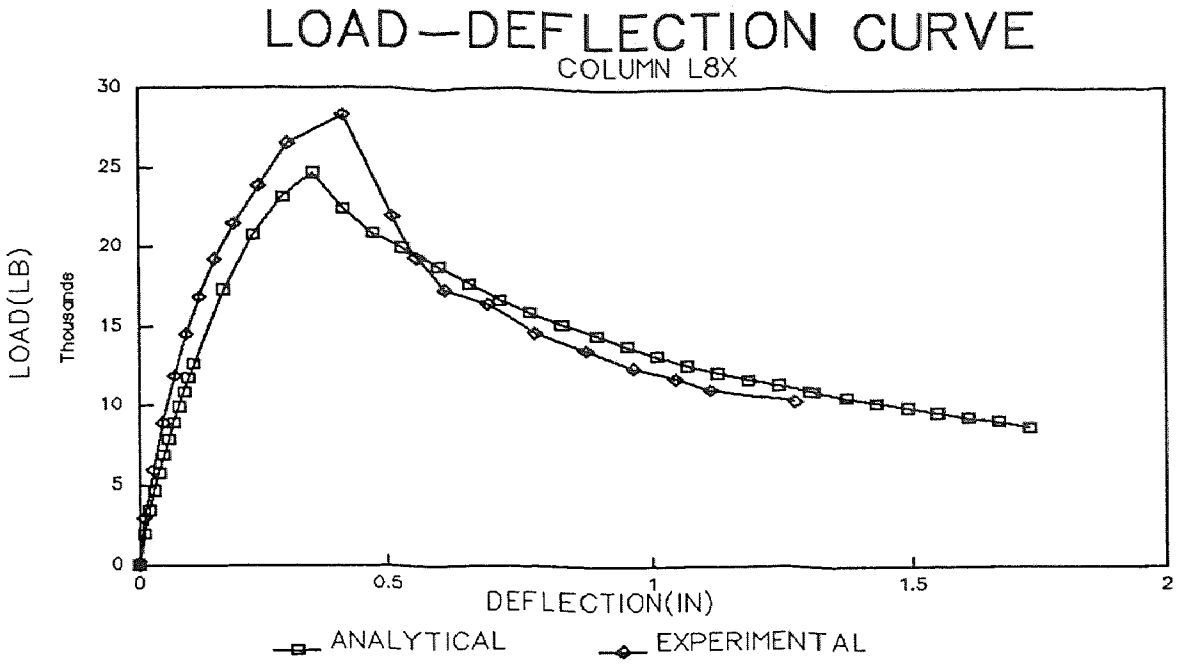

Figure N.13 Comparison of Load-Deflection Curve for High Strength Column L8 in X-Direction.

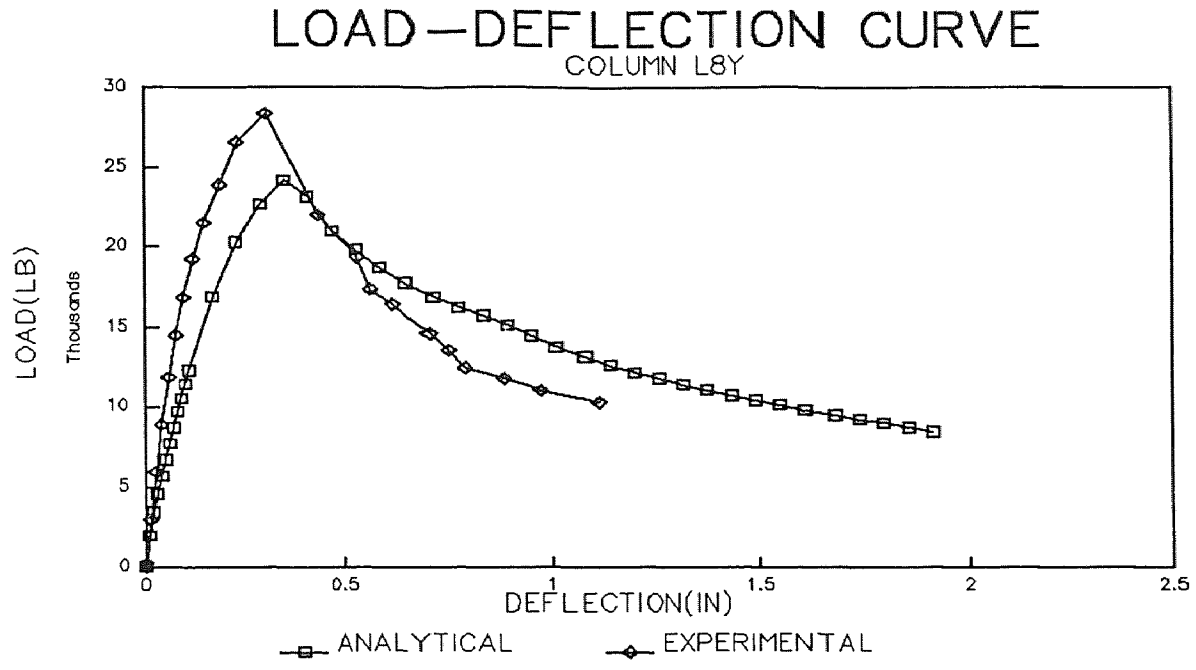

Figure N.14 Comparison of Load-Deflection Curve for High Strength Column L8 in Y-Direction.

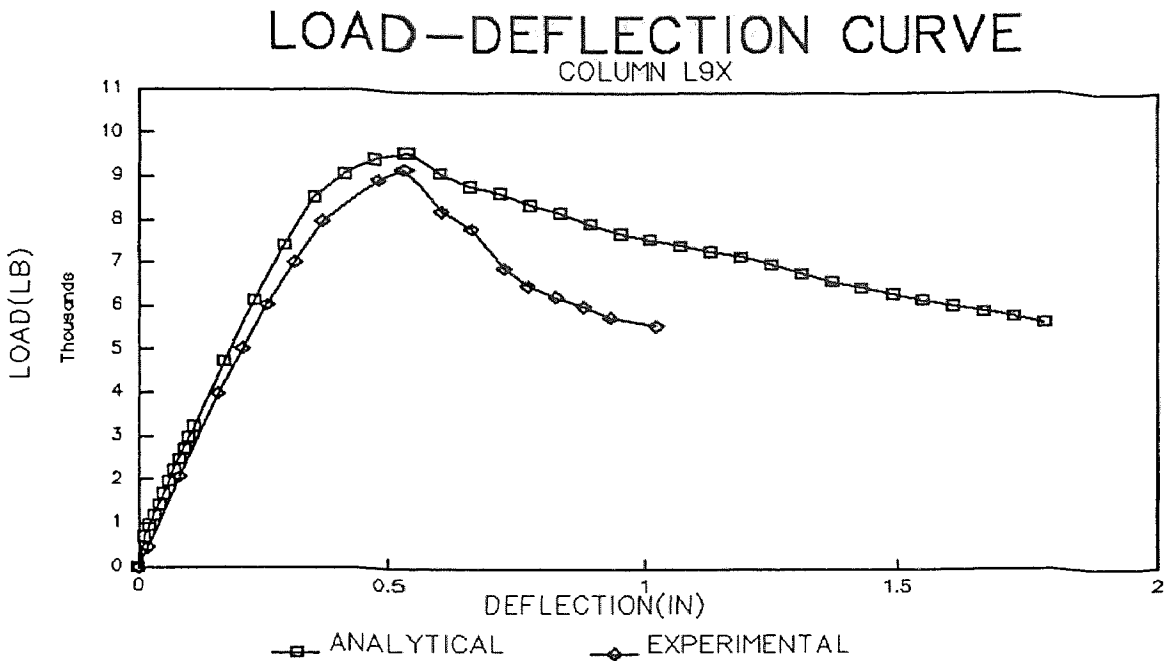

Figure N.15 Comparison of Load-Deflection Curve for High Strength Column L9 in X-Direction.

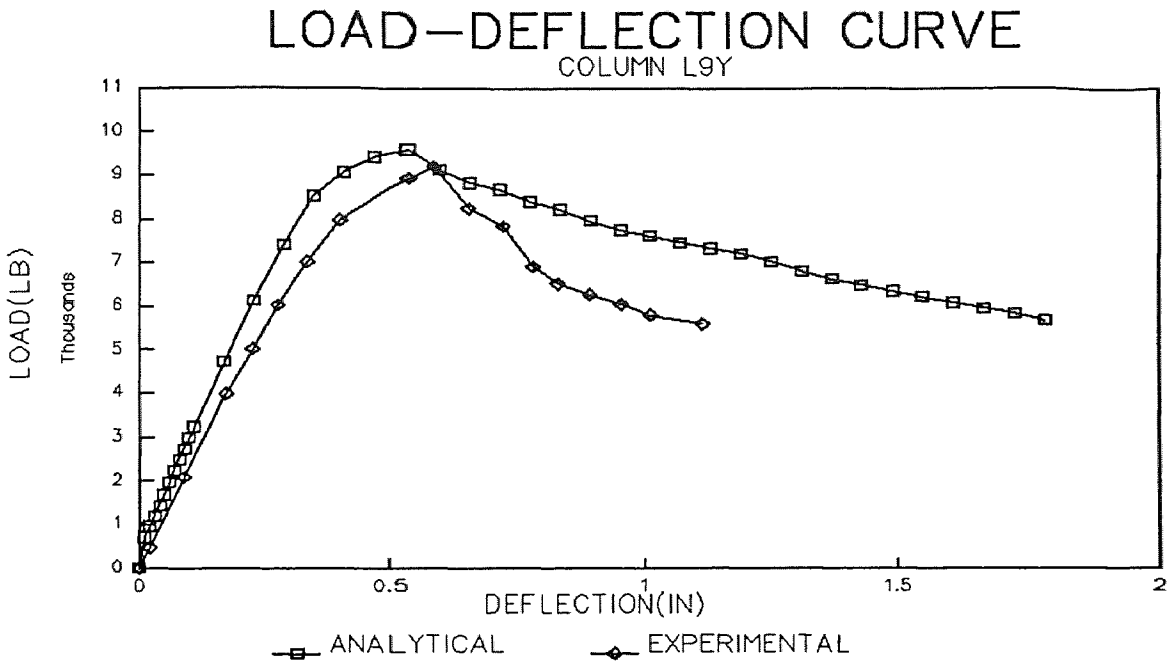

Figure N.16 Comparison of Load-Deflection Curve for High Strength Column L9 in Y-Direction.

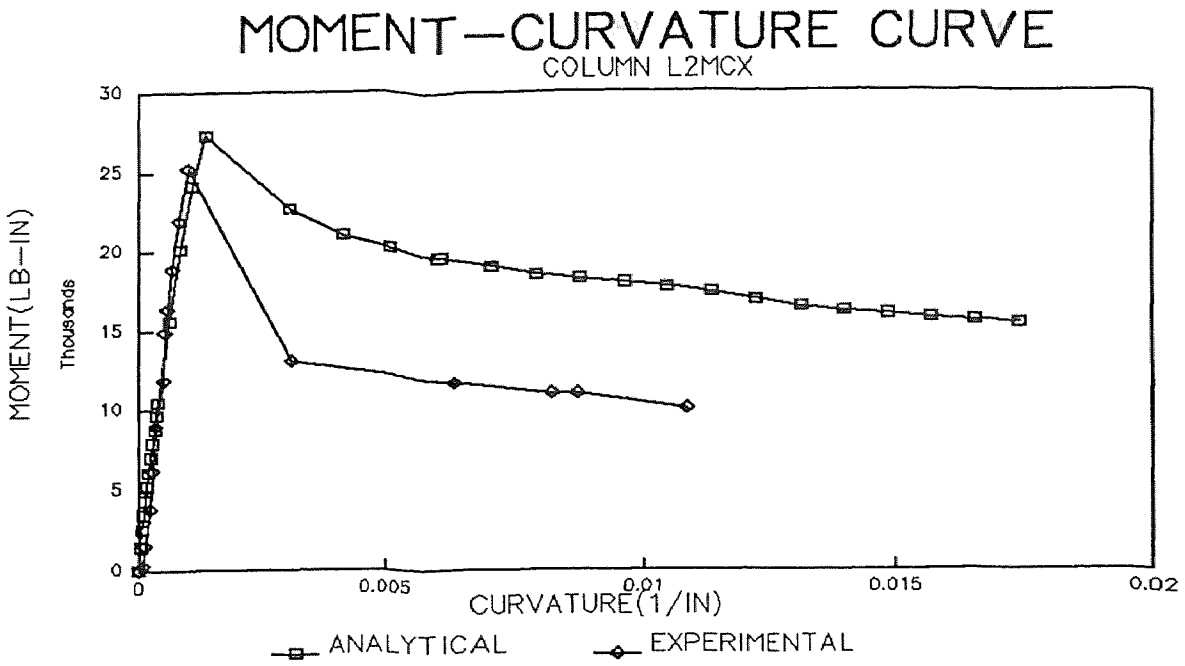

Figure N.17 Comparison of Moment-Curvature Curve for High Strength Column L2 in X-Direction.

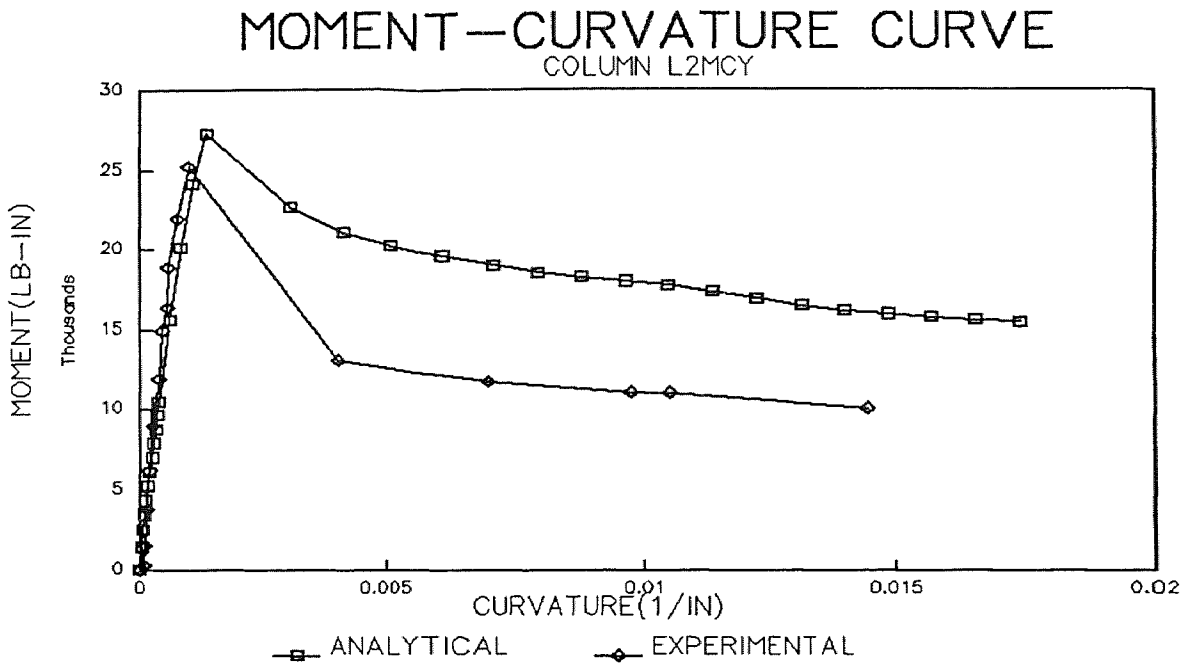

Figure N.18 Comparison of Moment-Curvature Curve for High Strength Column L2 in Y-Direction.

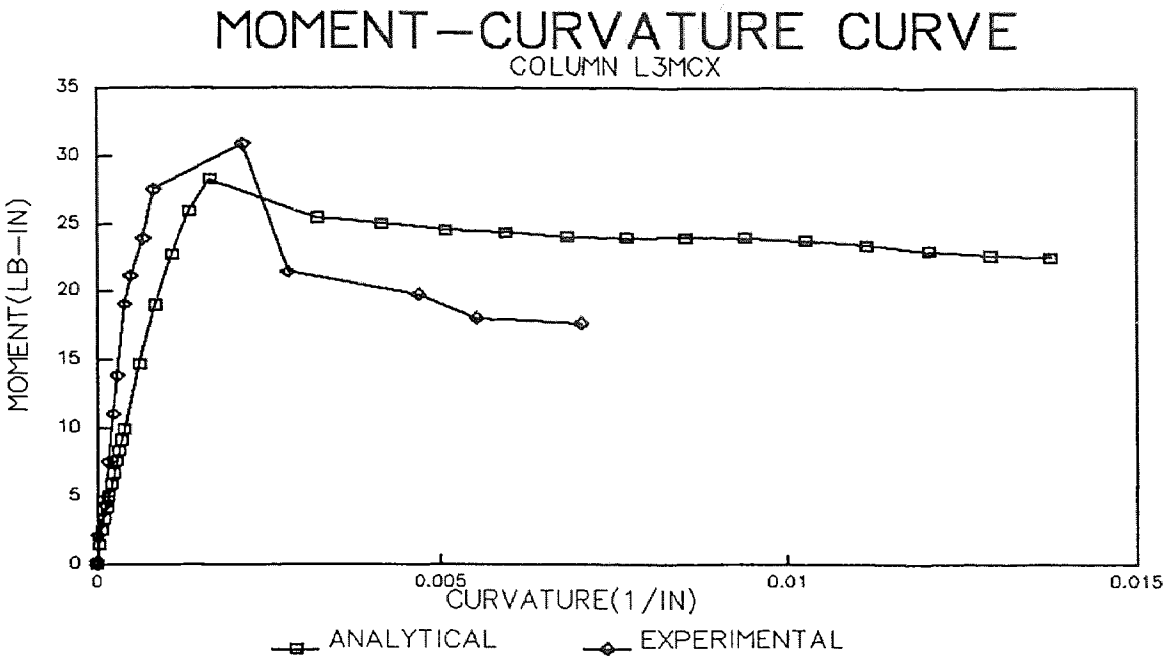

Figure N.19 Comparison of Moment-Curvature Curve for High Strength Column L3 in X-Direction.

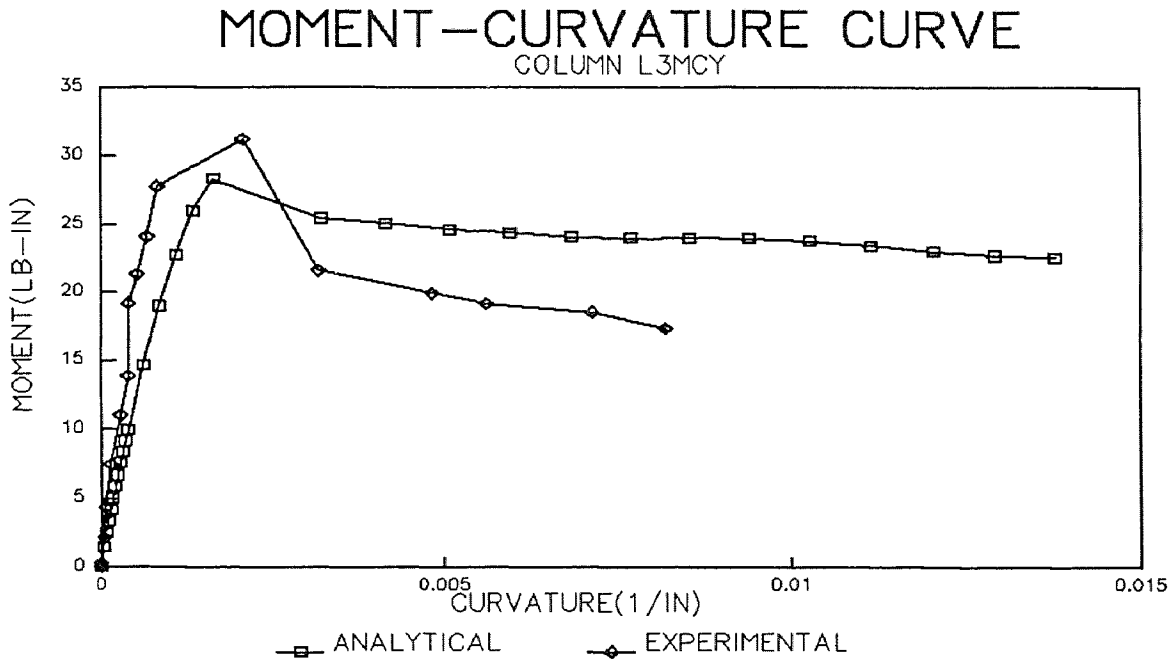

Figure N.20 Comparison of Moment-Curvature Curve for High Strength Column L3 in Y-Direction.

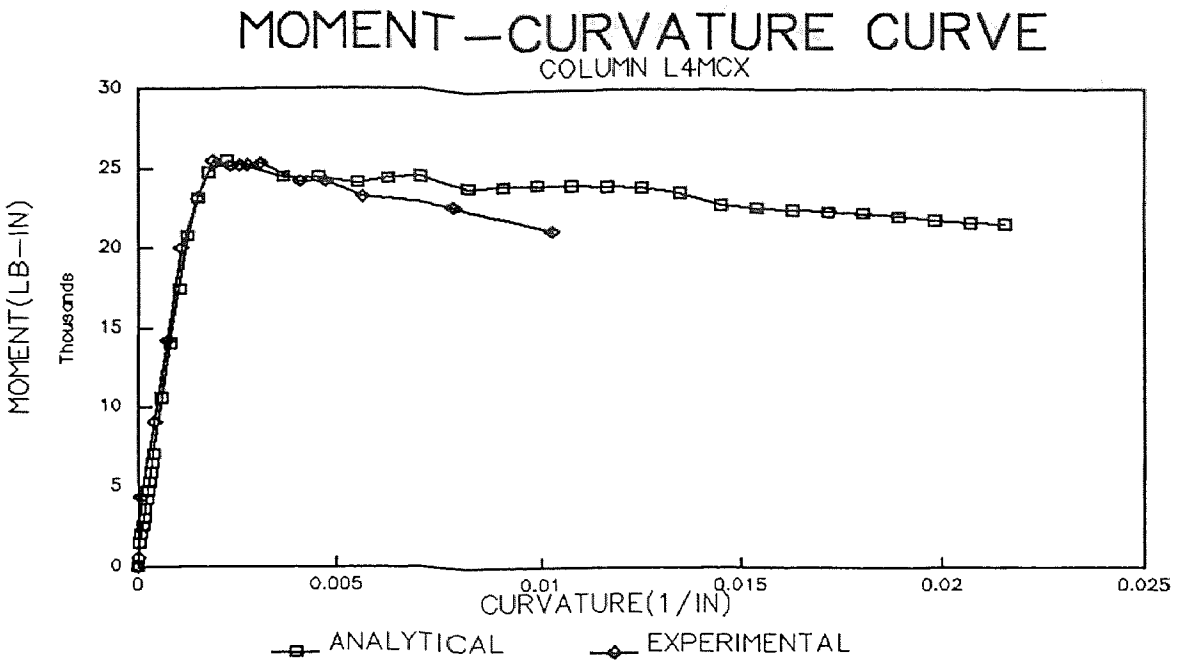

Figure N.21 Comparison of Moment-Curvature Curve for High Strength Column L4 in X-Direction.

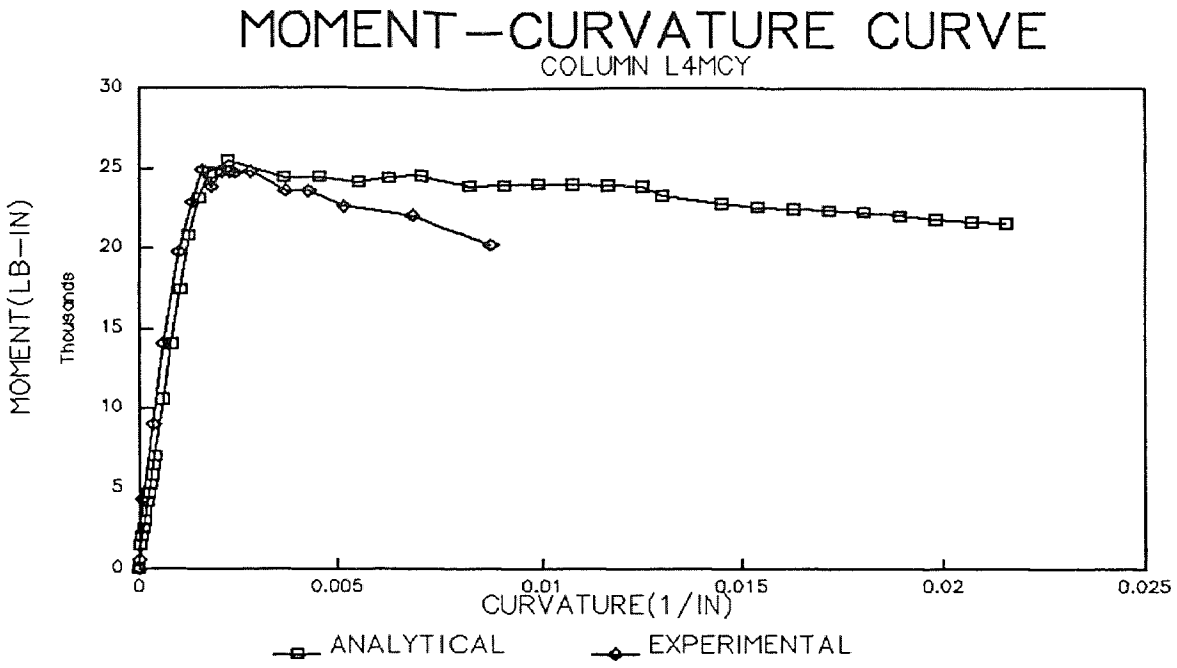

Figure N.22 Comparison of Moment-Curvature Curve for High Strength Column L4 in Y-Direction.

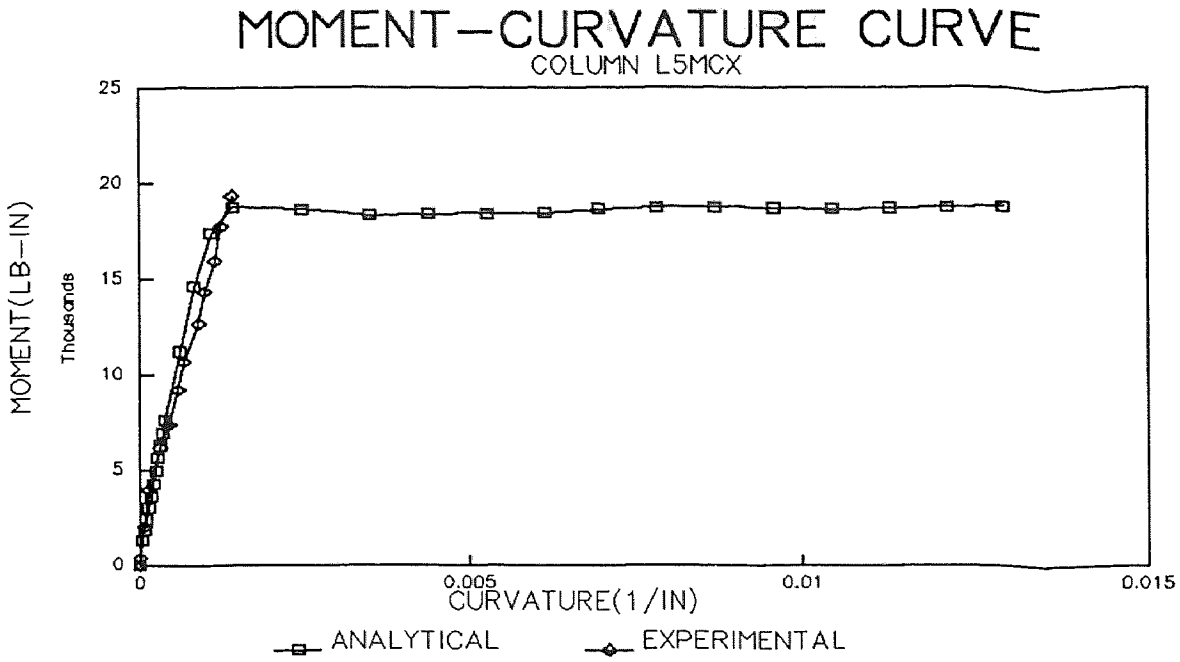

Figure N.23 Comparison of Moment-Curvature Curve for High Strength Column L5 in X-Direction.

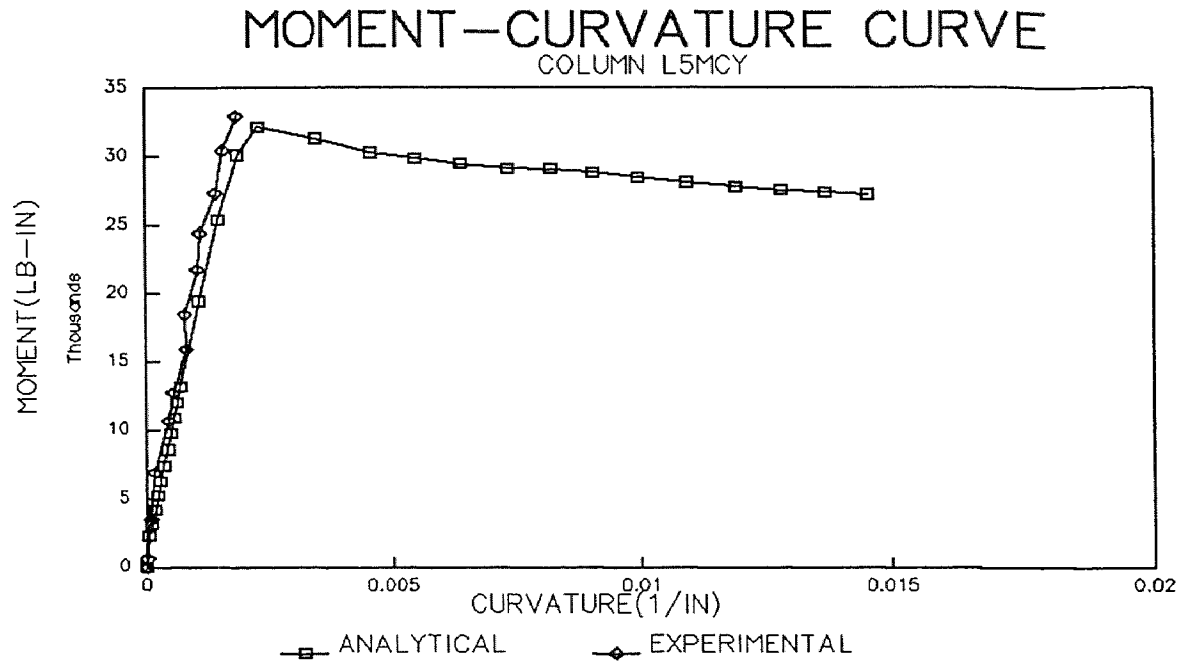

Figure N.24 Comparison of Moment-Curvature Curve for High Strength Column L5 in Y-Direction.

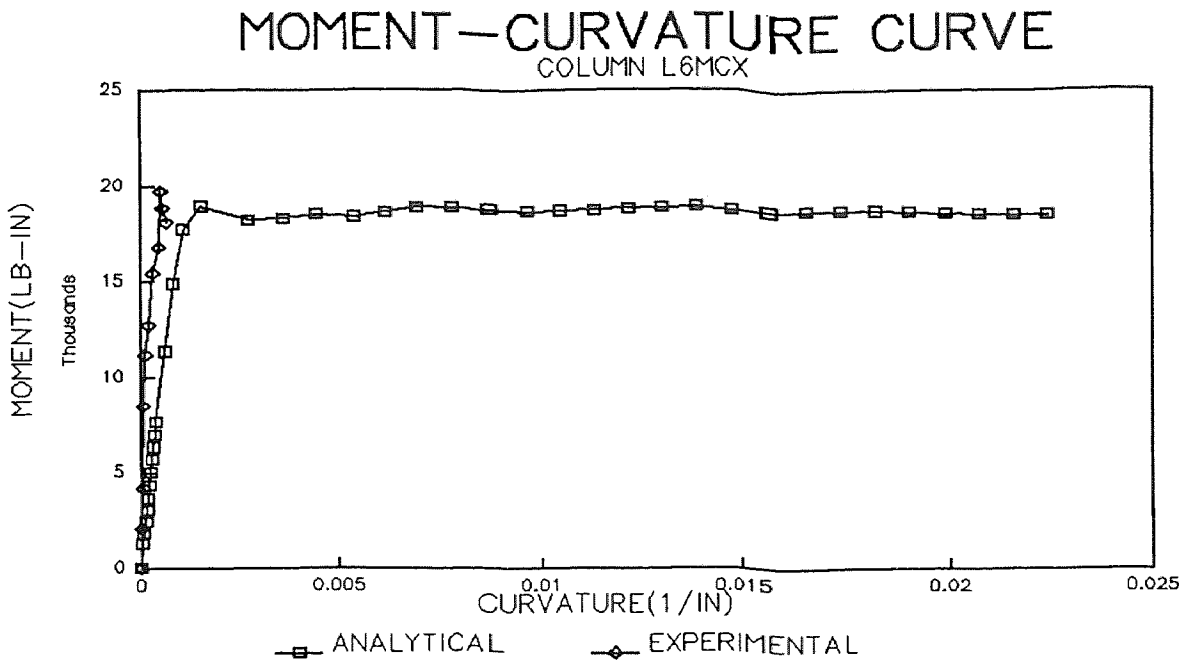

Figure N.25 Comparison of Moment-Curvature Curve for High Strength Column L6 in X-Direction.

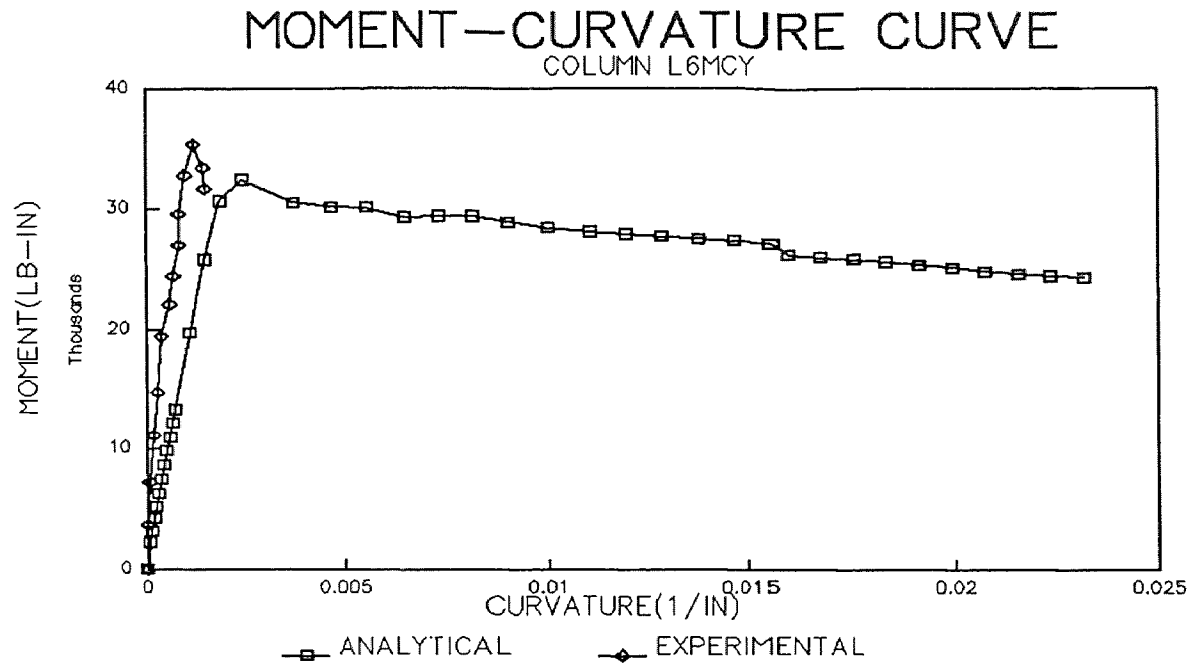

Figure N.26 Comparison of Moment-Curvature Curve for High Strength Column L6 in Y-Direction.

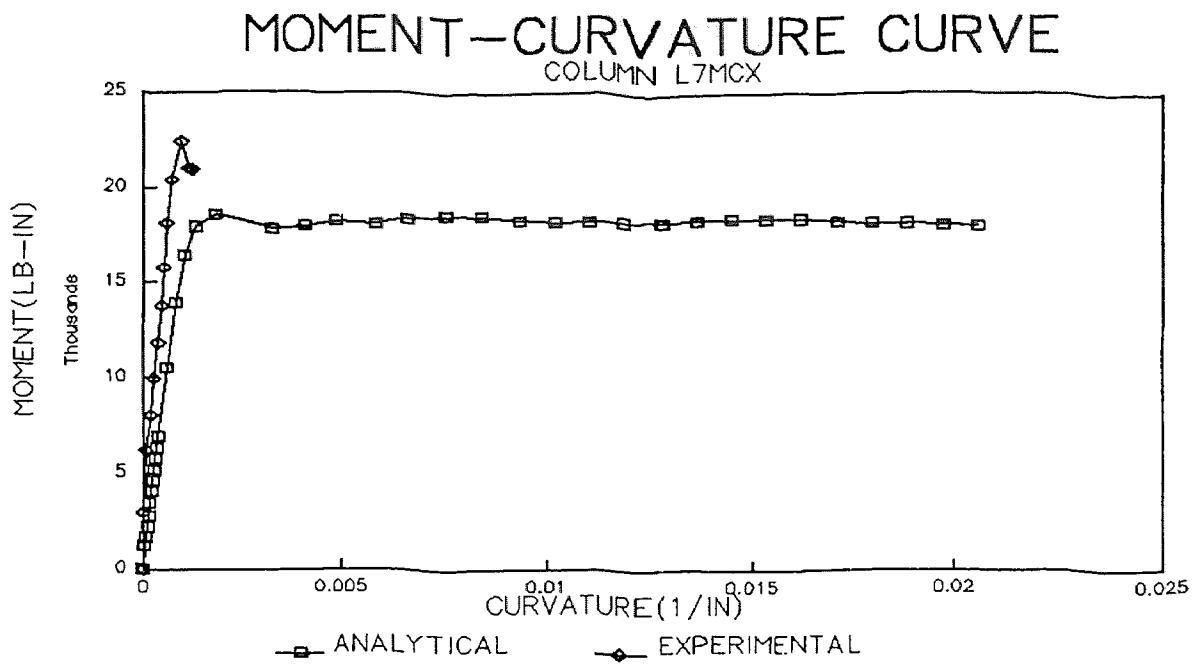

Figure N.27 Comparison of Moment-Curvature Curve for High Strength Column L7 in X-Direction.

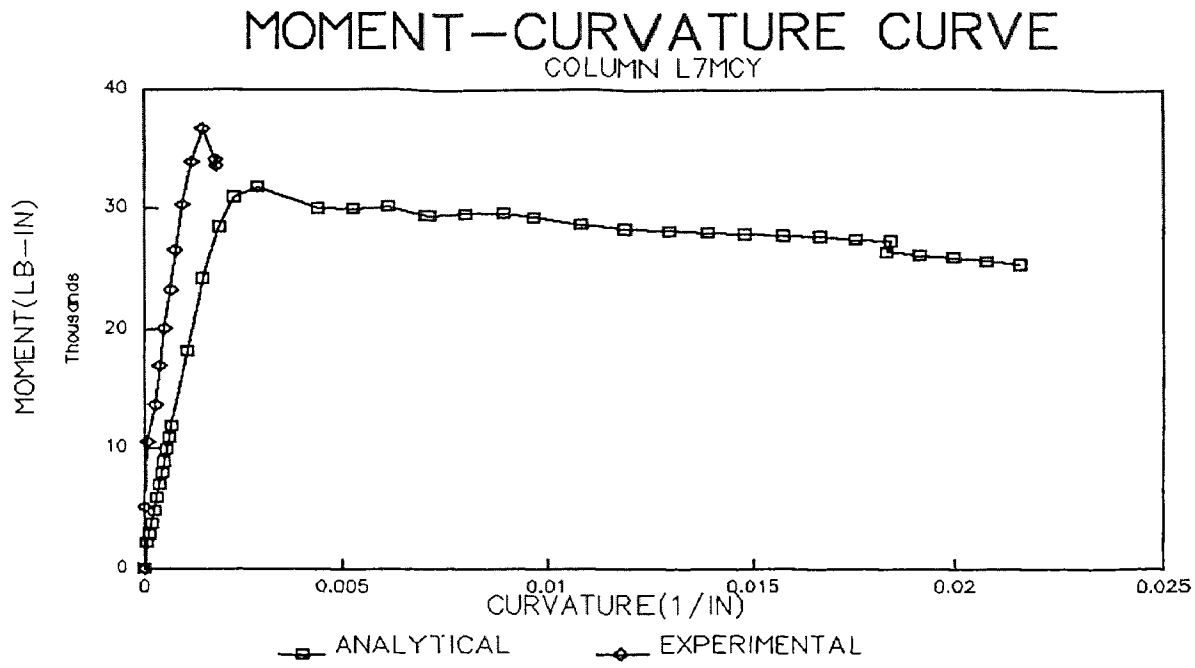

Figure N.28 Comparison of Moment-Curvature Curve for High Strength Column L7 in Y-Direction.

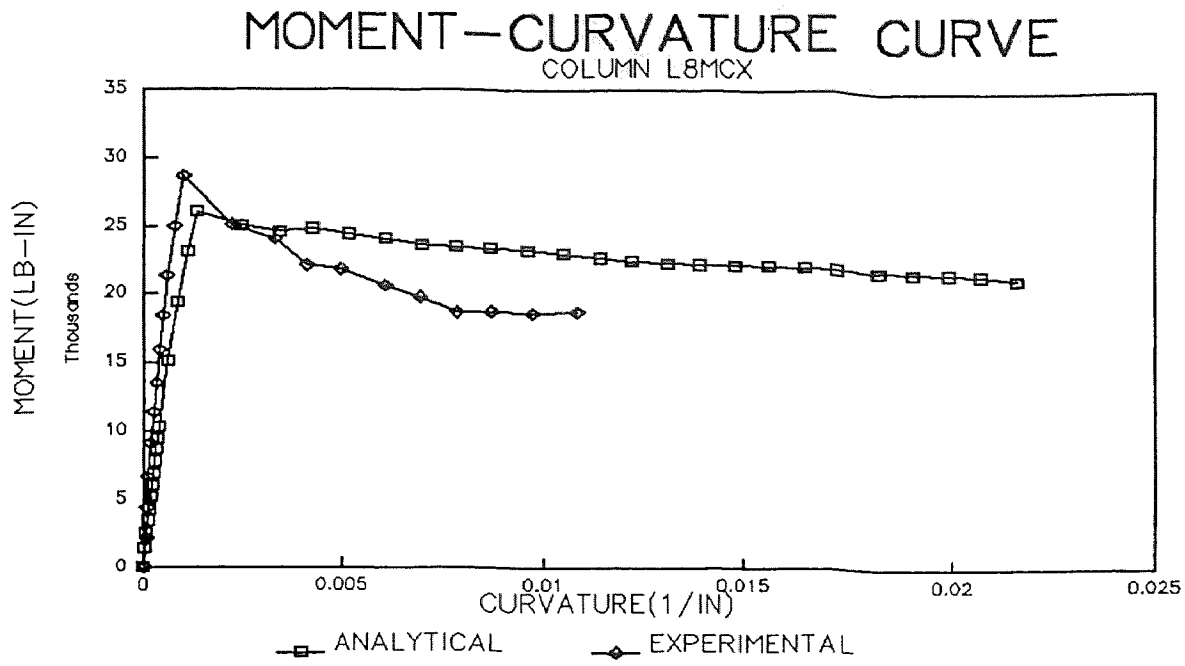

Figure N.29 Comparison of Moment-curvature Curve for High Strength Column L8 in X-Direction.

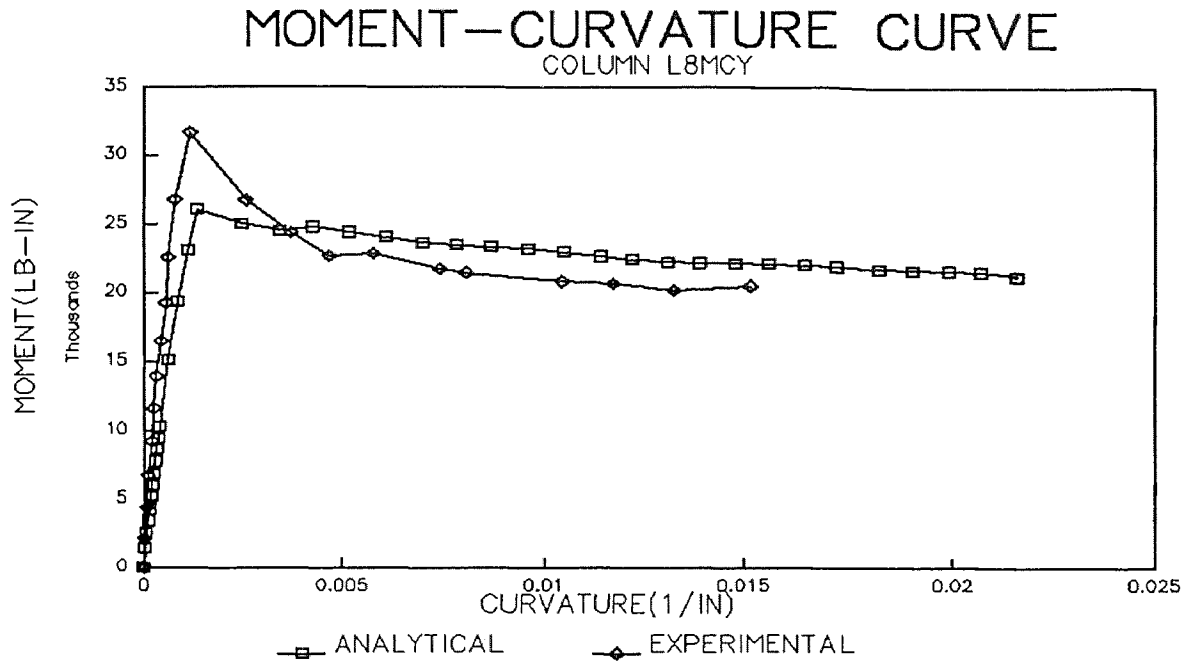

Figure N.30 Comparison of Moment-Curvature Curve for High Strength Column L8 in Y-Direction.

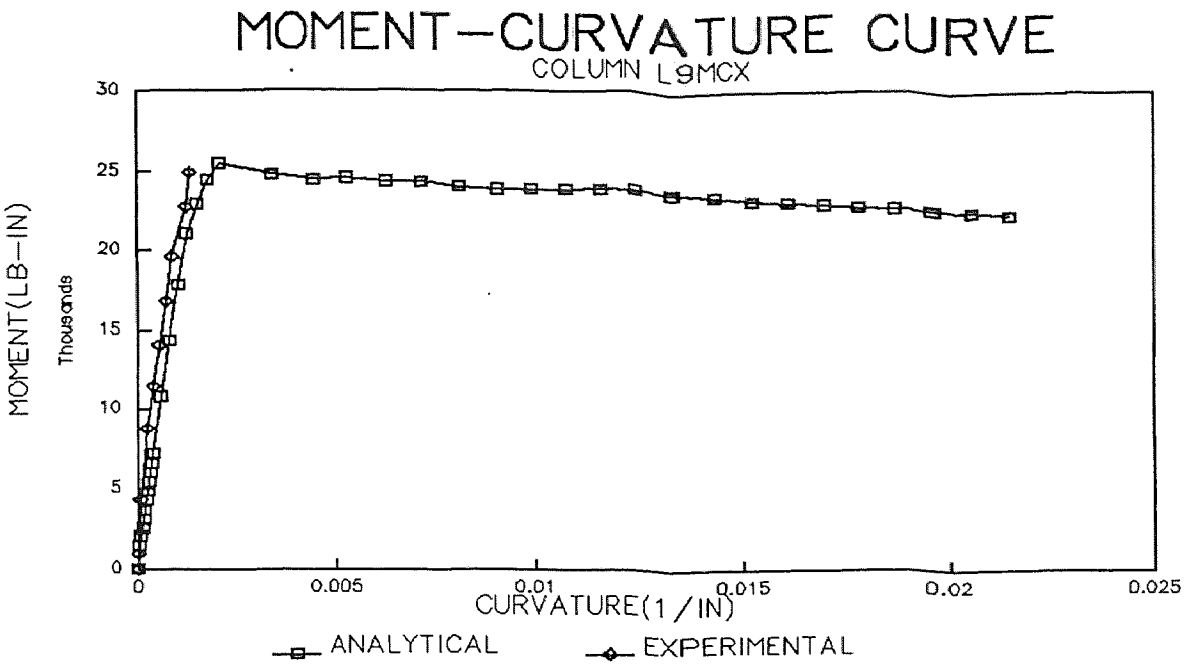

Figure N.31 Comparison of Moment-Curvature Curve for High Strength Column L9 in X-Direction.

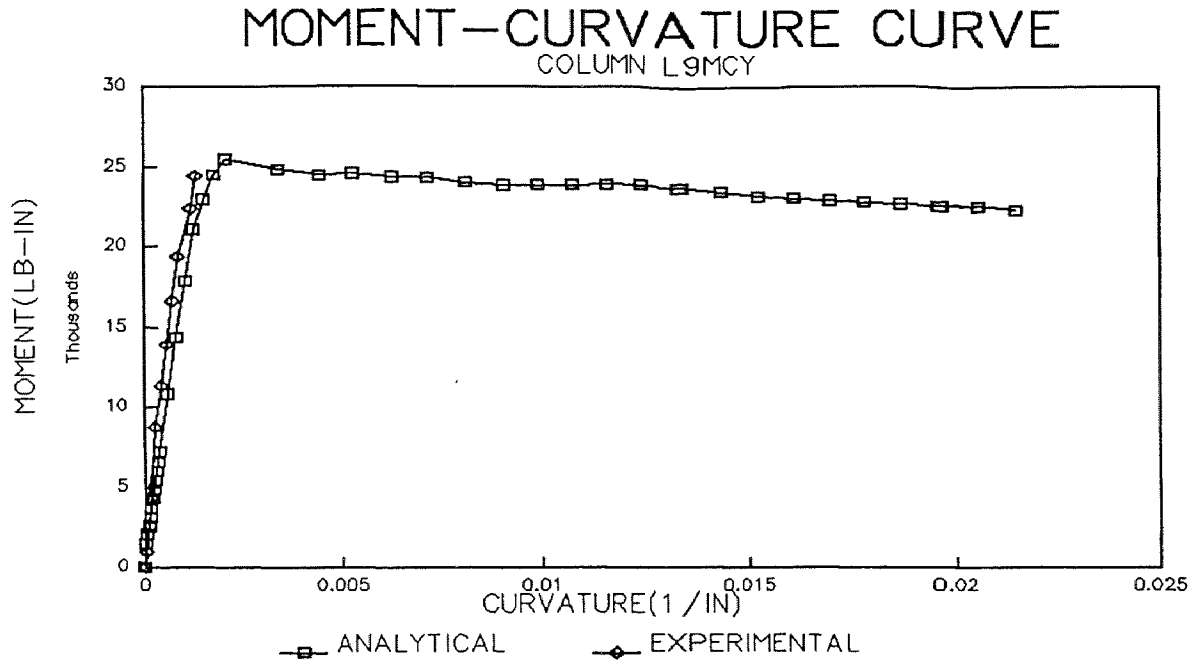

Figure N.32 Comparison of Moment-Curvature Curve for High Strength Column L9 in Y-Direction.

APPENDIX O
COMPARISON OF LOAD-DEFLECTION AND MOMENT-CURVATURE CURVES FOR HIGH STRENGTH FIBROUS COLUMNS

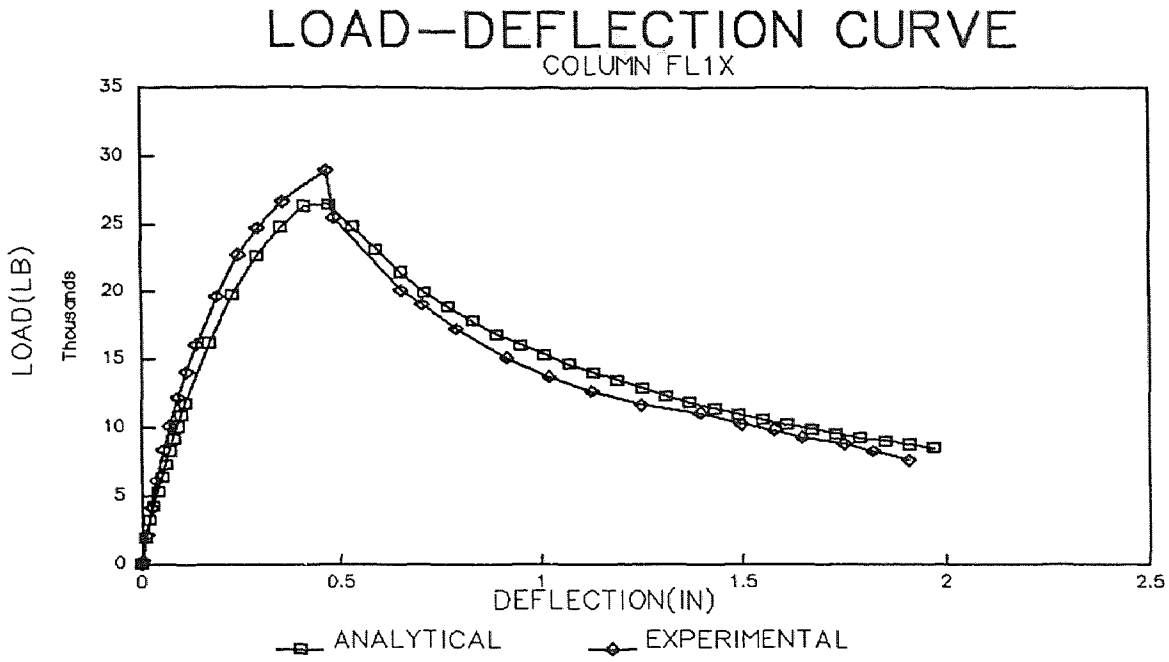

Figure O.1 Comparison of Load-Deflection Curve for High Strength Fibrous Column FL1 in X-Direction.

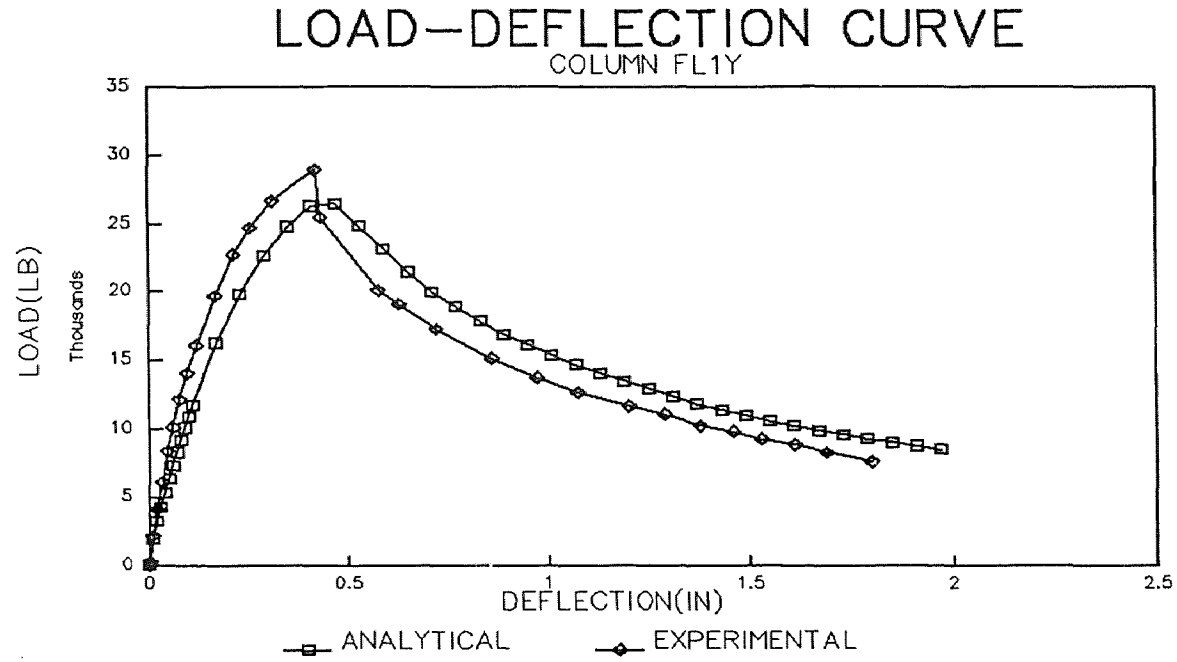

Figure O.2 Comparison of Load-Deflection Curve for High Strength Fibrous Column FL1 in Y-Direction.

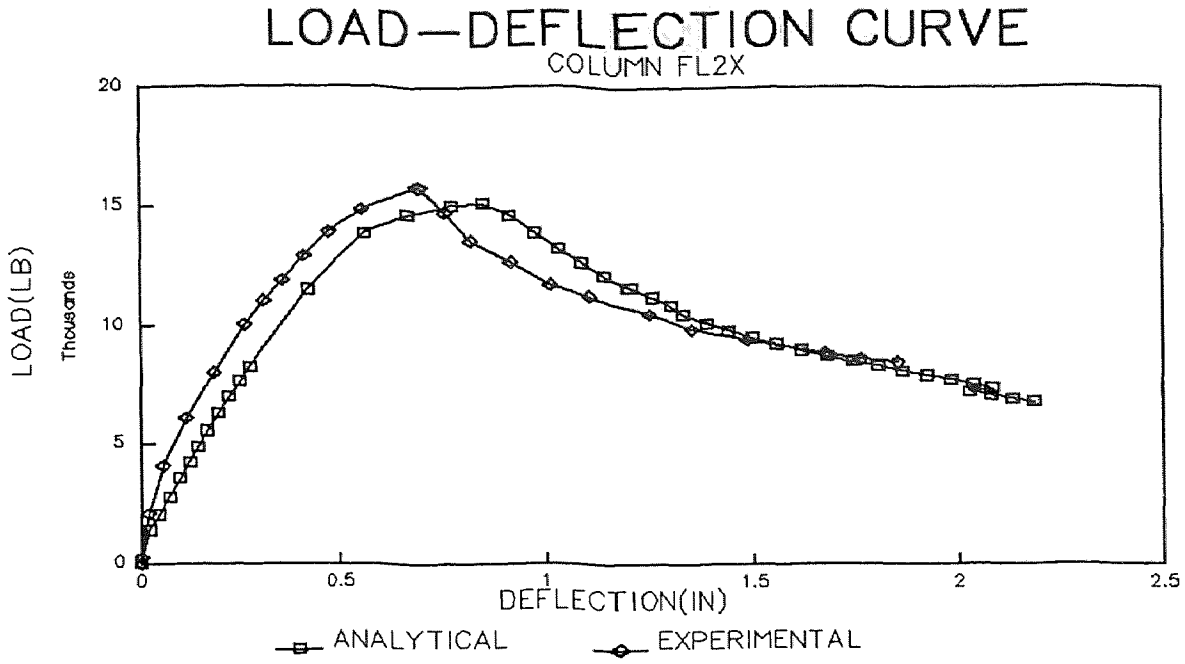

Figure O.3 Comparison of Load-Deflection Curve for High Strength Fibrous Column FL2 in X-Direction.

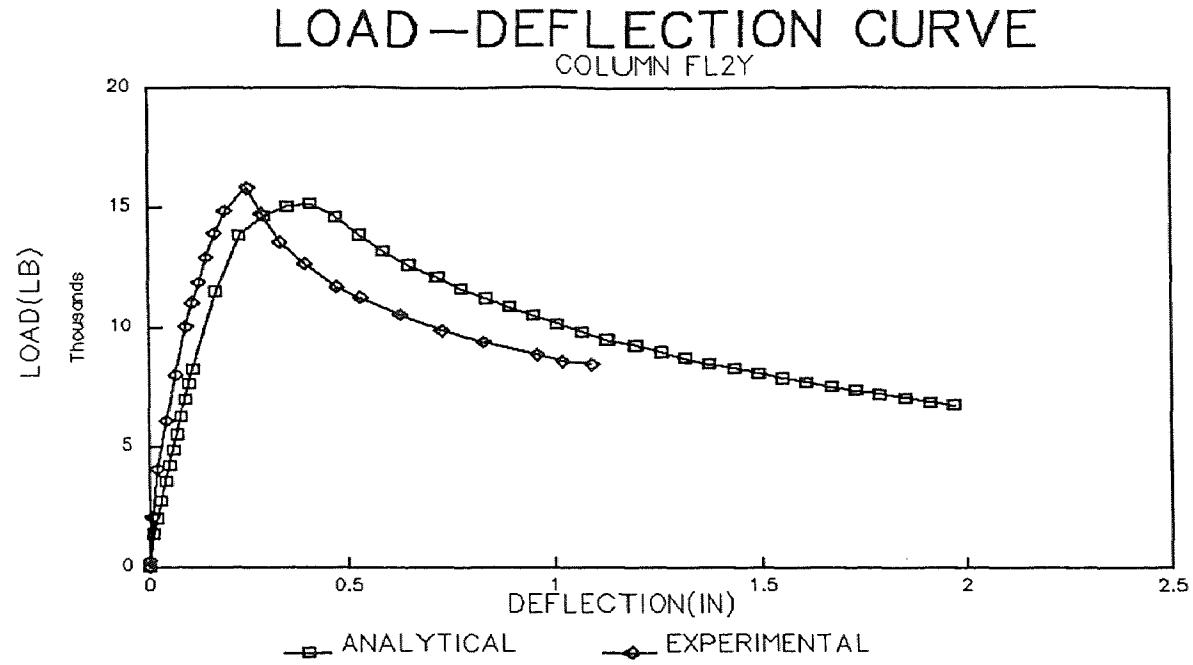

Figure O.4 Comparison of Load-Deflection Curve for High Strength Fibrous Column FL2 in Y-Direction.

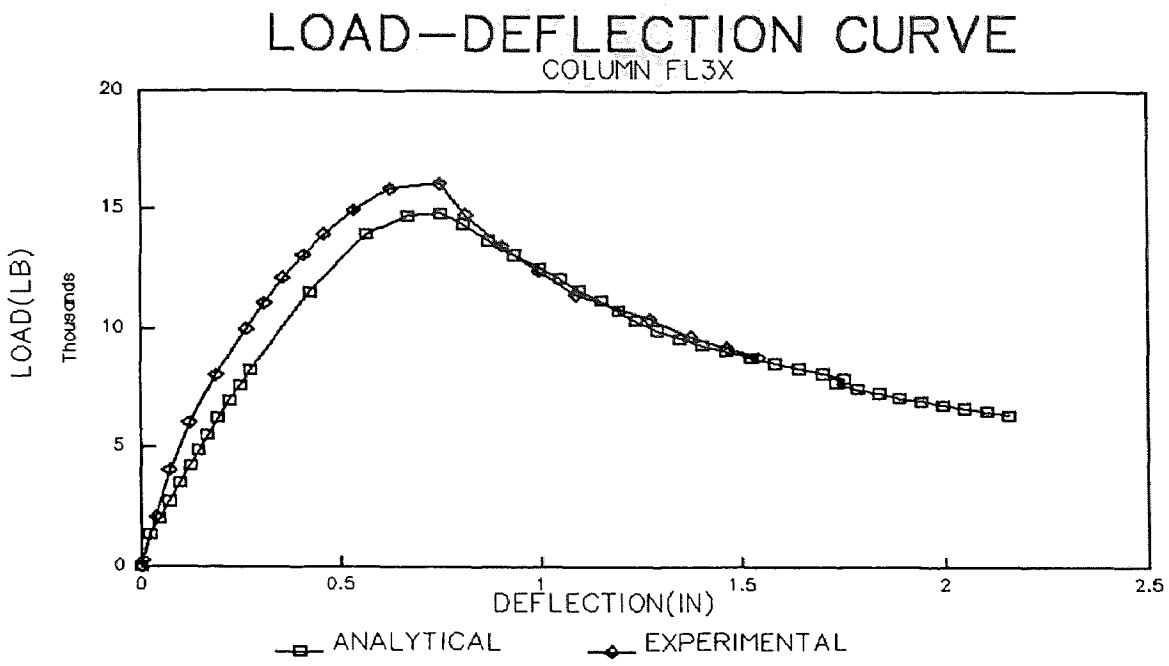

Figure O.5 Comparison Load-Deflection Curve for High Strength Fibrous Column FL3 in X-Direction.

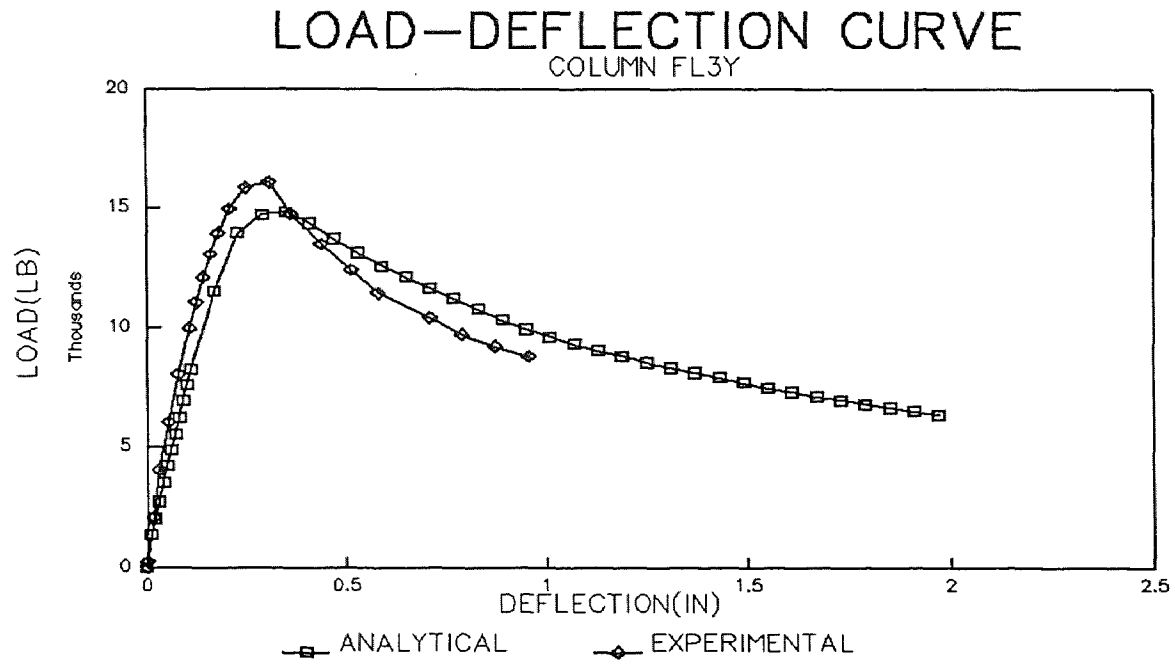

Figure O.6 Comparison of Load-Deflection for High Strength Fibrous Column FL3 in Y-direction.

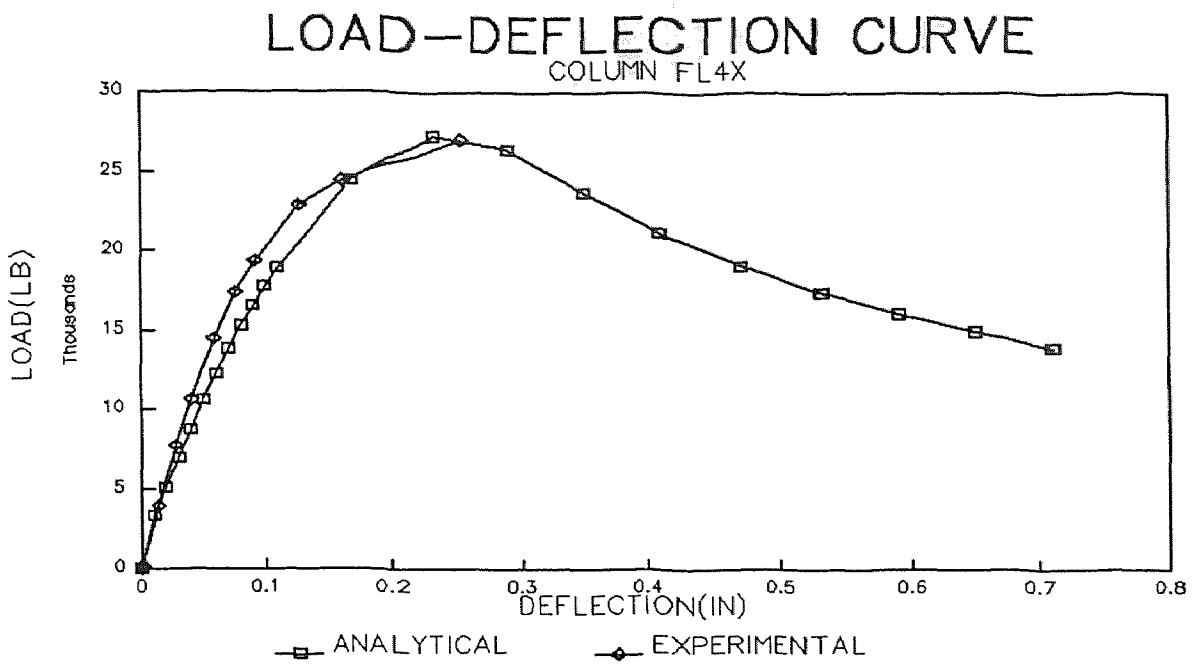

Figure O.7 Comparison of Load-Deflection Curve for High Strength Fibrous Column FL4 in X-Direction.

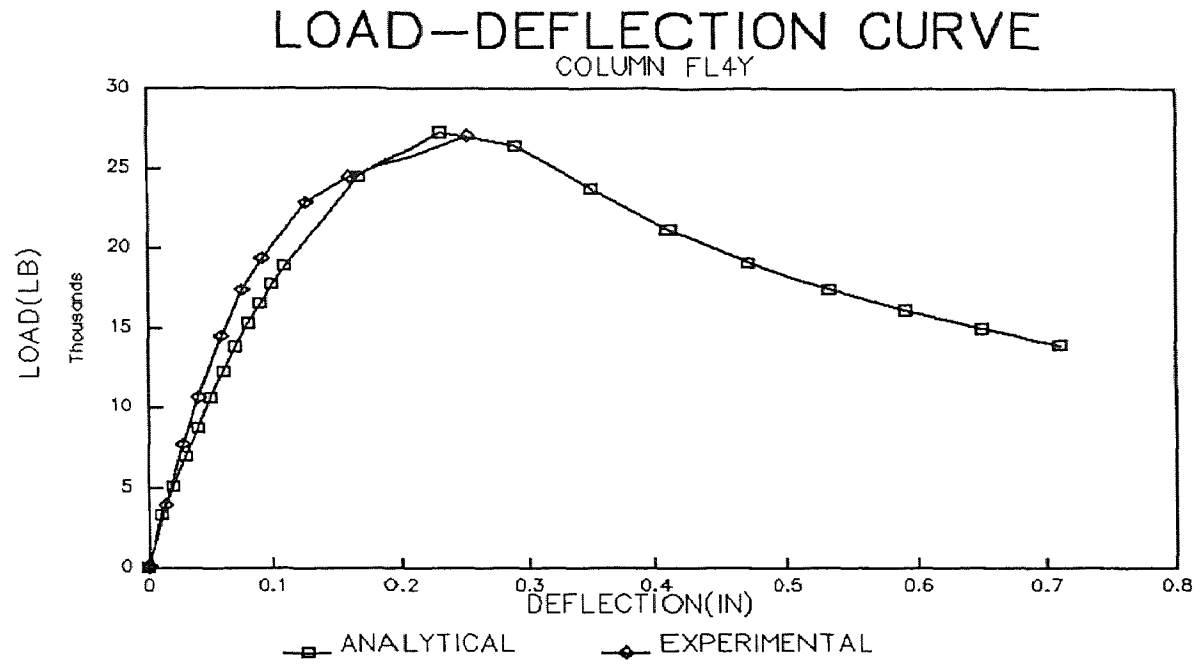

Figure O.8 Comparison of Load-Deflection Curve for High Strength Fibrous Column FL4 in Y-Direction.

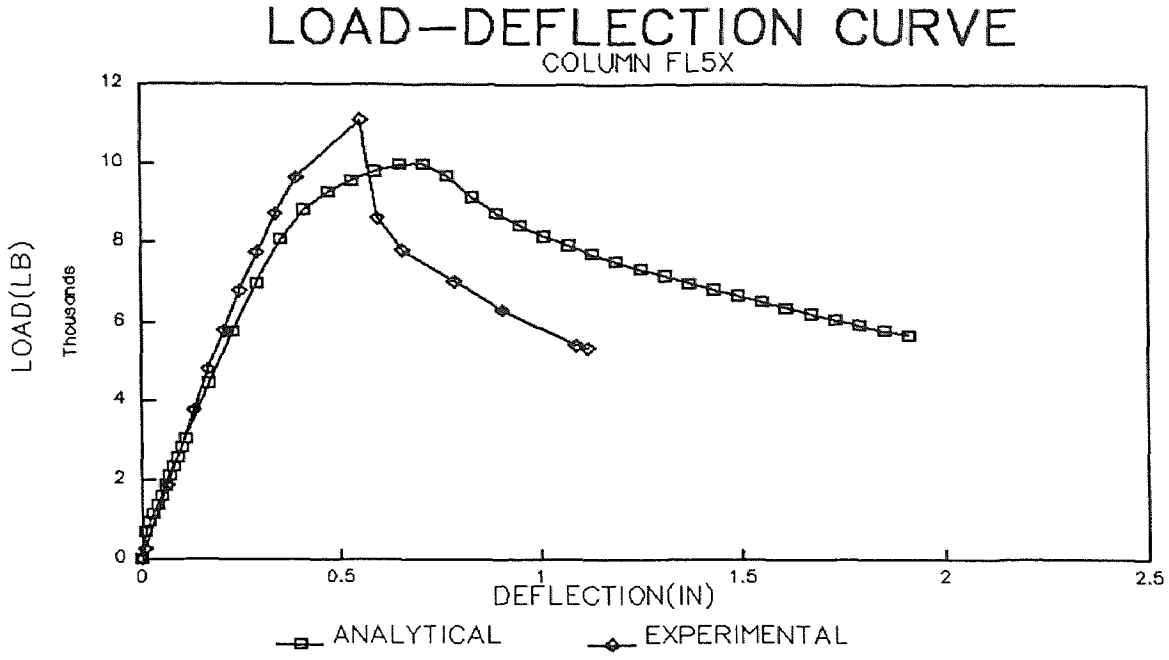

Figure O.9 Comparison of Load-Deflection Curve for High Strength Fibrous Column FL5 in X-Direction.

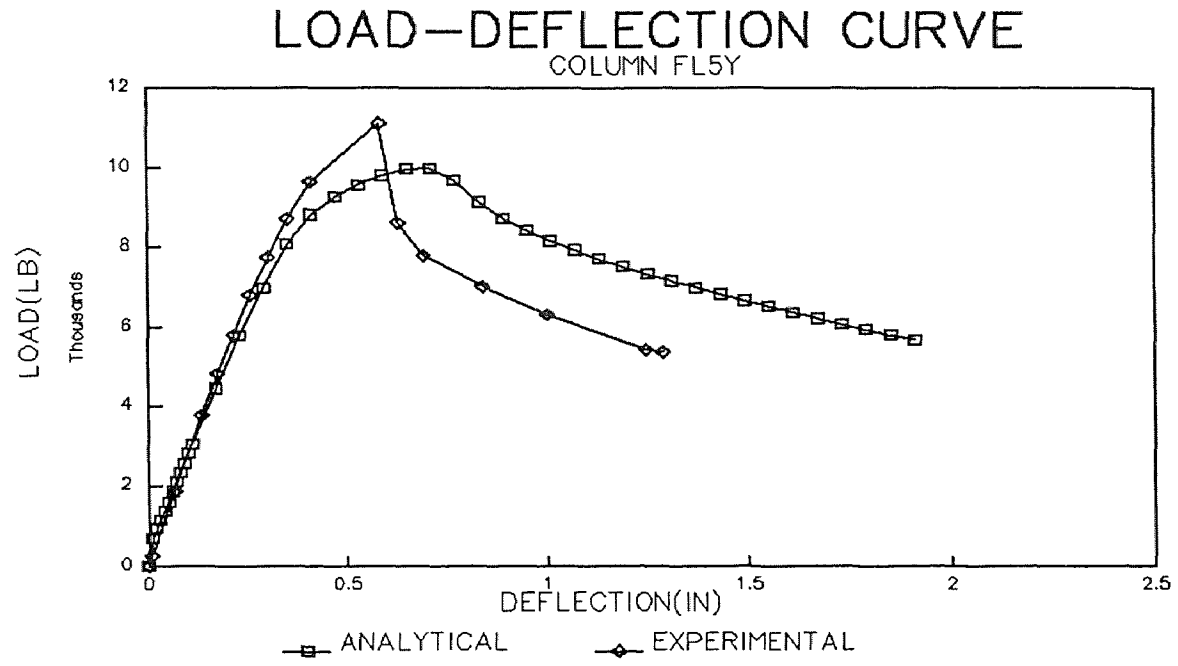

Figure O.10 Comparison of Load-Deflection Curve for High Strength Fibrous Column FL5 in Y-Direction.

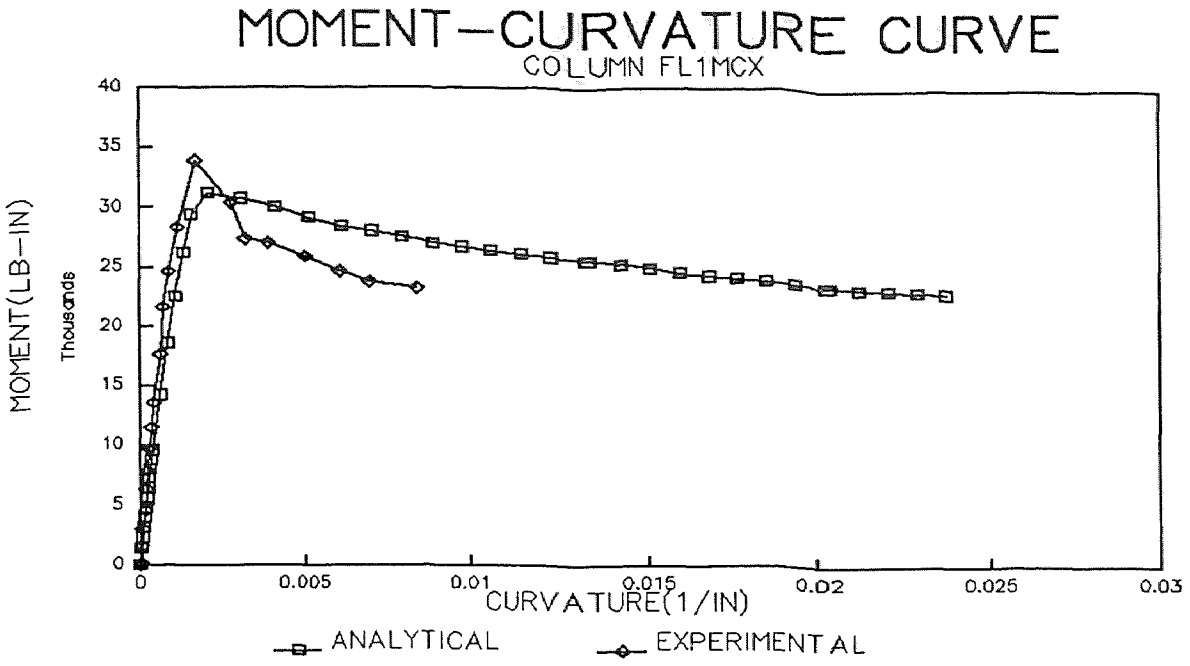

Figure O.11 Comparison of Moment-Curvature Curve for High Strength Fibrous Column FL1 in X-Direction.

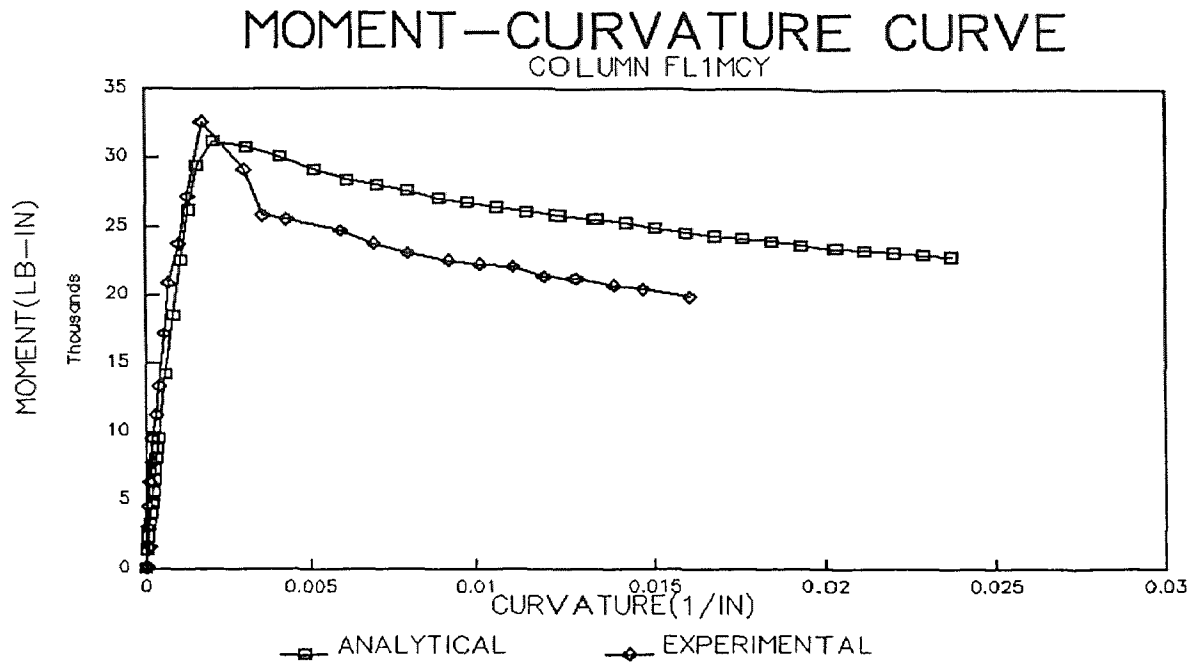

Figure O.12 Comparison of Moment-Curvature Curve for High Strength Fibrous Column FL1 in Y-Direction.

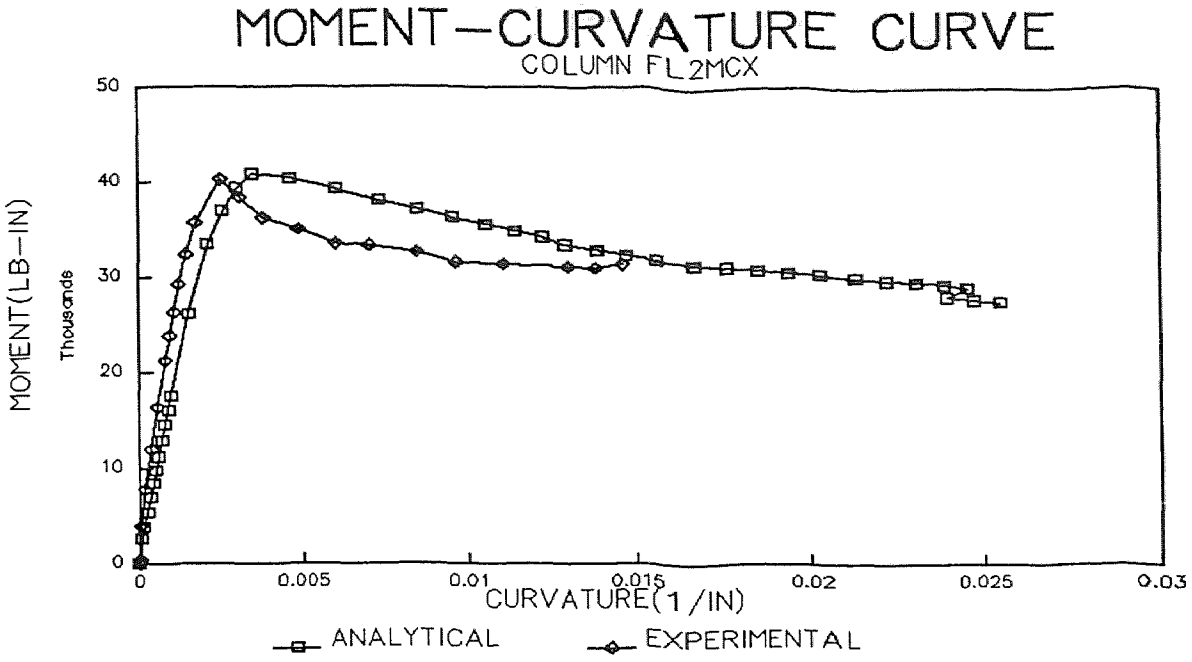

Figure O.13 Comparison of Moment Curvature Curve for High Strength Fibrous Column FL2 in X-Direction.

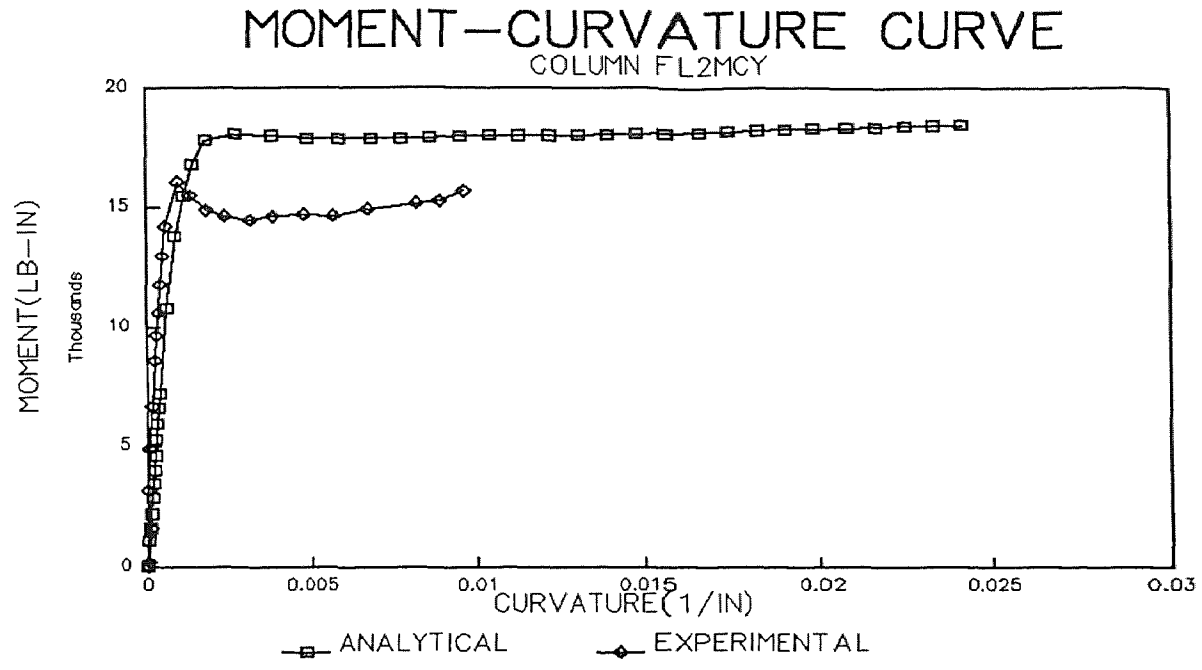

Figure O.14 Comparison of Moment-Curvature Curve for High Strength Fibrous Column FL2 in Y-Direction.

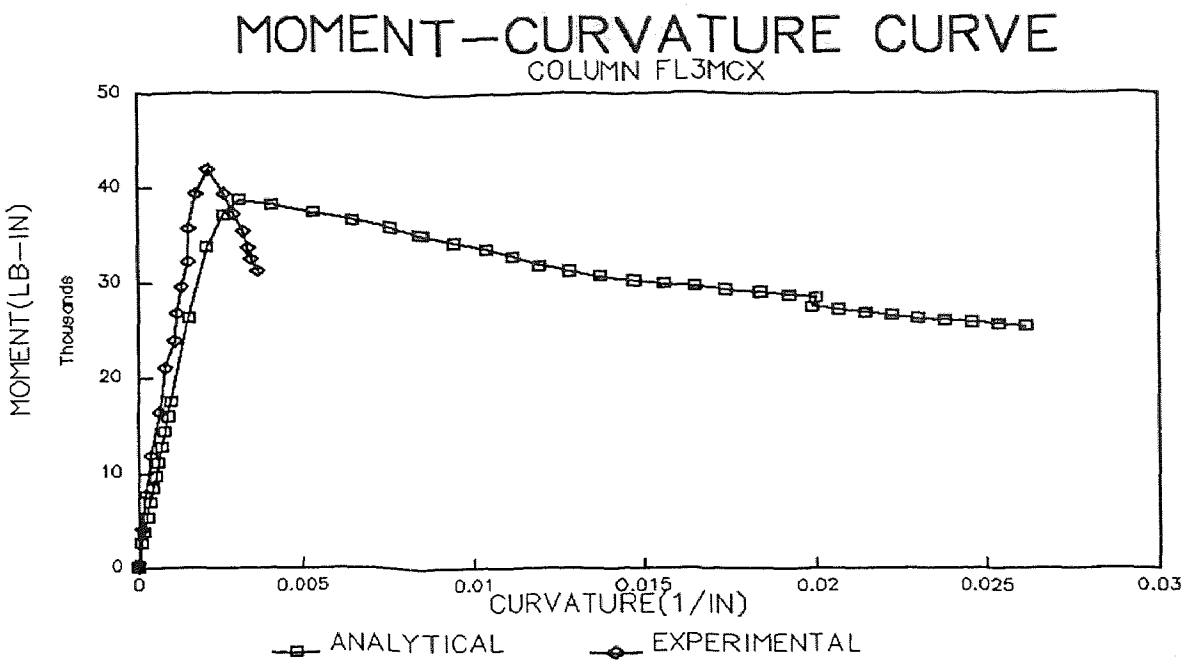

Figure O.15 Comparison of Moment-Curvature Curve for High Strength Fibrous Column FL3 in X-Direction.

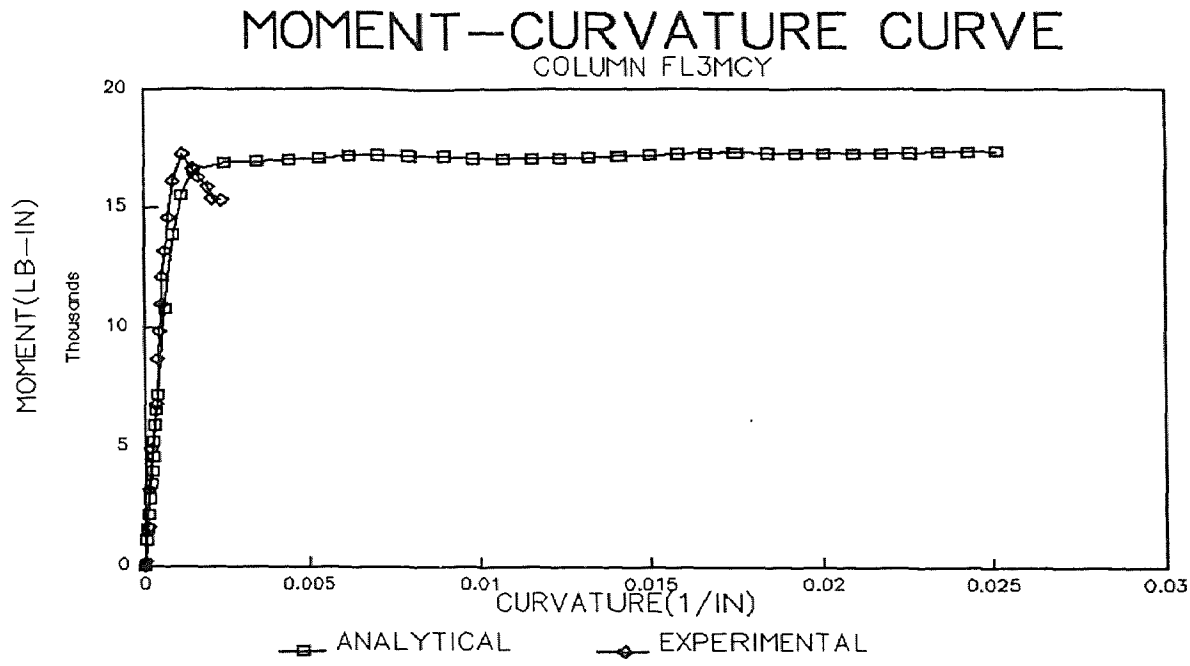

Figure O.16 Comparison of Moment-Curvature Curve for High Strength Fibrous Column FL3 in Y-Direction.

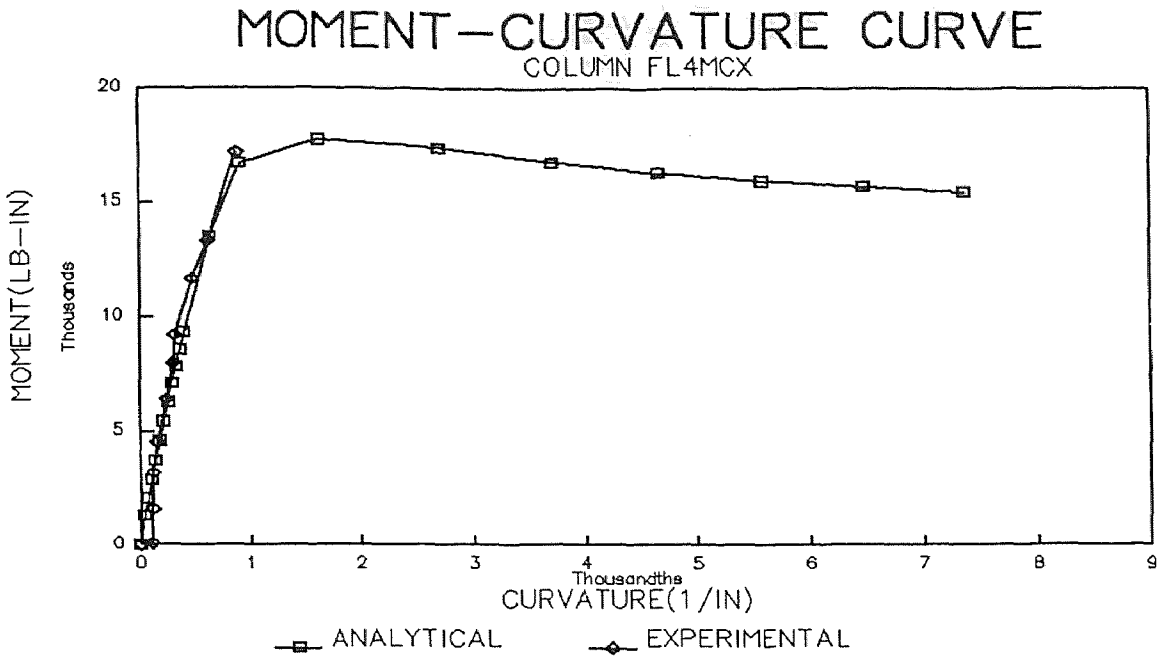

Figure O.17 Comparison of Moment-Curvature Curve for High Strength Fibrous Column FL4 in X-Direction.

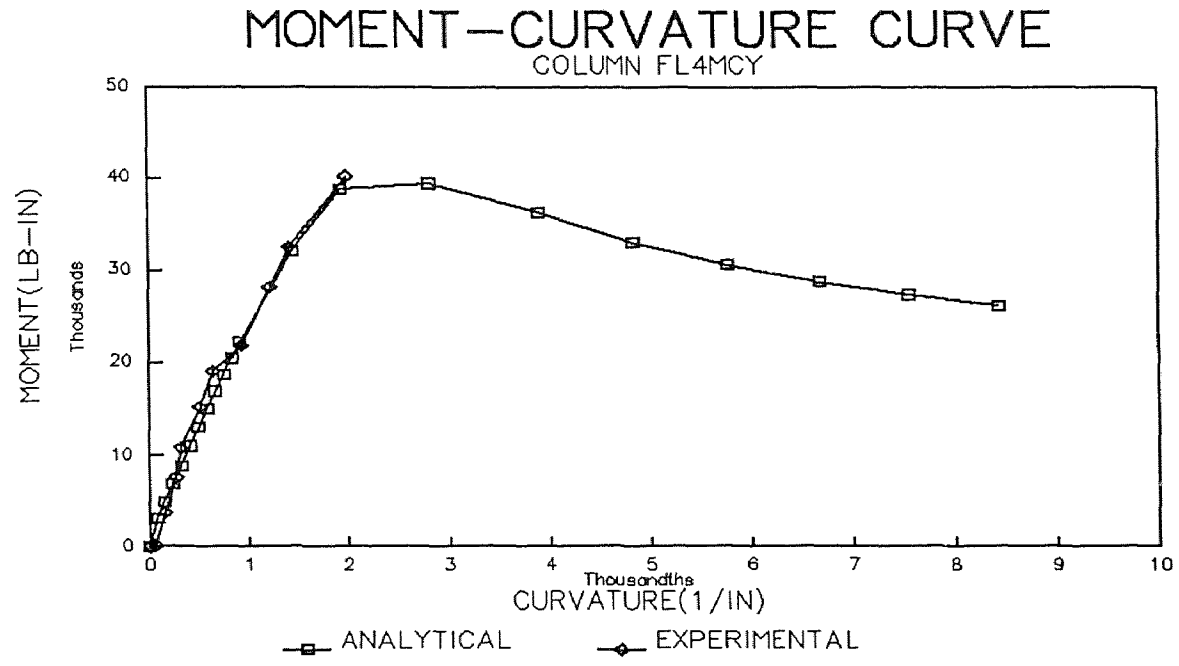

Figure O.18 Comparison of Moment-Curvature Curve for High Strength Fibrous Column FL4 in Y-Direction.

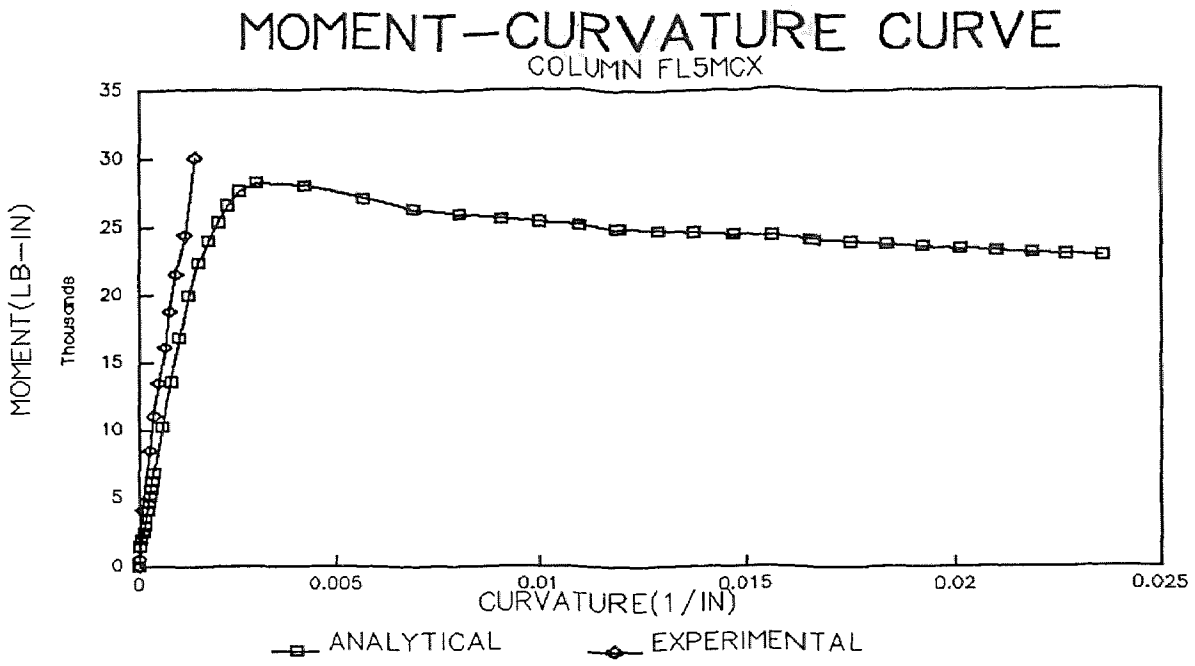

Figure O.19 Comparison of Moment-Curvature Curve for High Strength Fibrous Column FL5 in X-Direction.

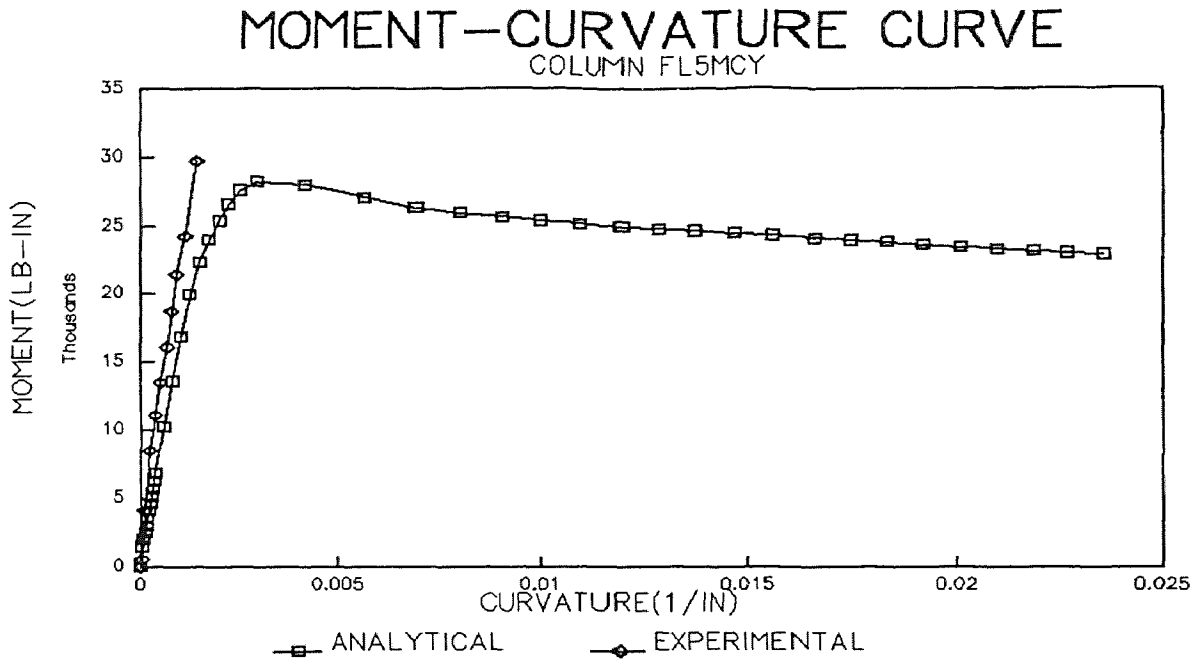

Figure O.20 Comparison of Moment-Curvature Curve for High Strength Fibrous Column FL5 in Y-Direction.

REFERENCE

ACI Committee 226. 1987. "Silica Fume in Concrete." *ACI Material Journal.* 2:158-166.

ACI Committee 363. 1987. "State-of-the-Art Report on High Strength Concrete." *ACI Journal.* SCM-15:364-411.

ACI Committee 544. 1974. "Fiber Reinforced Concrete." *ACI SP-44.*

ACI Committee 544. 1978. "Measurement of Properties of Fiber Reinforced Concrete." *ACI 544.2R-78.* American Concrete Institute. Detroit.

ACI Committee 544. 1982. "State-of-the-Art Report on Fiber Reinforced Concrete." *ACI 544.1R-82.* American Concrete Institute. Detroit.

ACI Committee 544. 1985. "State-of-the-Art Report on Fiber Reinforced Concrete." *ACI 544.1R-82.* Design with Fiber Reinforced Concrete. Illinois.

Ahmad, S. H., and S. P. Shah. 1979. "Complete Stress-Strain Curve of Concrete and Nonlinear Design." in *Proceedings. International Symposium on Nonlinear Design of Concrete Structures.* University of Waterloo. Waterloo. Ontario. Canada.

Ahmad, S. H., and S. P. Shah. 1982. "Stress-Strain Curves of Concrete Confined by Spiral Reinforcement." *ACI Journal.* Title no. 79-46. 6:484-490.

Aïtcin, P. C., and P. K. 1990. Mehta. "Effect of Coarse-Aggregate Characteristics on Mechanical Properties of High-Strength Concrete." *ACI Journal.* 2:103-107.

Albinger, J., and S. E. J. Moreno. 1981. "High Strength Concrete." *Chicago Style. Concrete Construction.* Vol. 26. 2:241-245.

Baalbaki, W., B. Benmokrane, O. Chaallal, and P. C. Aïtcin. 1991. "Influence of Coarse Aggregate on Elastic Properties of high-performance Concrete." *ACI Journal.* 5:499-503.

Bertero, V. V. 1979. "Proceedings of High Strength Concrete." *Workshop.* S. P. Shah. Editor. University of Illinois at Chicago. Circle. 2-4:96-167.

Carrasquillo, R. L., A. H. Nilson, and F. O. Slate. 1981. "Proporties of High Strength Concrete Subject to Short-Term Loads." *ACI Journal.* Proceedings Vol. 78. 3:171-178.

Carreira, D. J., and K. M. Chu. 1985. "Stress-Strain Relationship for Plain Concrete in Compression." *ACI Journal.* Proceedings. Vol. 82. 6:797-804.

Chan, W. W. L. 1955 "The Ultimate Strength and Deformation of plastic Hinges in Reinforced Concrete Frameworks." *Magazine of concrete Research.* Vol. 7. 21:121-132.

Chen, W. F., and J. L. Carson. 1971. "Stress-Strain Properties of Random Wire Reinforced Concrete." *ACI Journal.* 6:933-938.

Craig, R. J., S. Dunya, J. Riaz, and H. Shirazi. 1984. "Torsional Behavior of Reinforced Fibrous Concrete Columns." *Fiber Reinforced Concrete-International Symposium.* SP-81. American Concrete Institute. Detroit. SP-81:17-49.

Desayi, P., K. T. Sundara, R. Iyengar, and I. S. Reddy. 1978. "Equation for Stress-Strain Curve of Concrete Confined in Circular Steel Spiral." *Materiaux et Constructions.* Vol. 11. 65:339-345.

Desayi, P., and S. Krishnan. 1964. "Equation for Stress-Strain Curve of Concrete." *ACI Journal.* Proceedings. Vol. 61. 3:345-350.

Ezeldin, A. S. 1989. "Bond and Compression Behavior of Normal and High Strength Fiber Reinforced Concrete Subjected to Generalized Loading." Ph.D. Thesis. Rutgers University. New Brunswick.

Fanella, D. A., and A. E. Naaman. 1985. "Stress-Strain Properties of Fiber Reinforced Mortar in Compression." *ACI Journal.* Title No. 82-41. 4:475-482.

Freedman, S. 1970. "High-Strength Concrete. Part I: Materials." *Modern Concrete.*

Glavind, M., and T. AArre. 1991. "High-Strength Concrete with Increased Fracture-Toughness." *Materials Research Society. Mat. Res. Soc. Sympl Proc.* Vol. 211.

Gerstle, K. H. 1979. "Proceedings of High Strength Concrete." *Workshop.* S. P. Shah. Editor. University of Illinois at Chicago. Circle. 2-4:43-55.

Gregerson, J. 1991. "High-Strength Concrete Flexes Greater Muscle." *Building Design & Construction.* 1:64-67.

Hognestad, E. 1951. "A Study of Combined Bending and Axial Load in Reinforced Concrete Members." *Bulletin No. 399.* Engineering Experiment Station. University of Illinois. Urbana.

Hsu, C. T., and M. S. Mirza. 1969. "Generalized Moment-Curvature Relationships for Singly and Doubly Reinforced Beams." McGill University. *Structural Concrete Series* No. 24:1-48.

Hsu, C. T. 1974. "Behavior of Structural Concrete Subjected to Biaxial Flexure and Axial Compression." Ph. D. Thesis. McGill University. Aug.

Hughes, B. P., and N. I. Fattuhi. 1977 "Stress-Strain Curves for Fiber Reinforced Concrete in Compression." *Cement and Concrete Research.* 7:173-184.

Hundson, J. A., S. L. Crouch. and C. Fairhurst. 1972. "Soft. Stiff. and Servo-Controlled Testing Machines: A Review with Reference to Rock Failure." *Engineering Geology.* Vol. 6. No. 3:155-189.

Jahren, P. A. 1983. "Use of Silica Fume in Concrete." Fly Ash. Silica Fume. Slag and Other Mineral By-Products in Concrete. *ACI SP-79:* 825-842.

Kwak, K. H., J. Suh. and C. T. Thaomas Hsu. 1991. "Shear-Fatigue Behavior of Steel Fiber Reinforced Concrete Beams." *ACI Structural Journal.* Vol. 88. No. 2.:155-160.

Kent, D. C., and K. Park. 1971. "Flexural Members with Confined Concrete." *Journal of the Structural Division.* ASCE. ST. 7:1969-1974.

Lee, L. H. N. 1955. "Inelastic Behavior of Reinforced Concrete Members." *Transactions. ASCE.* Vol. 120:181-202.

Levi, F. 1961. "The Work of the European Concrete Committee." *ACI Journal. Proceedings* Vol. 57. No. 9:1041-1070.

Liebenberg, A. C. 1962. "A stress-Strain Function for Concrete Subjected to Short-Term Loading." *Magazine of Concrete Research.* Vol. 14. No. 41:85-99.

Macinnis, C., and D. V. Thomson. 1970. "Special Techniques for Producing High Strength Concrete." *ACI Journal.* 6:996-1002.

Martinez, S., A. H. Nilson. and F. O. Slate. 1984. "Spirally Reinforced High-Strength Concrete Columns." *ACI Journal.* 5:431-435.

Mather, K.1965. "High Strength. High Density Concrete." *ACI Journal.* Vol. 62. No. 8:951-962.

Mehta, P. K. 1983. "Pozzolanic and Cementitious By-Products as Miner Admixtures for Concrete-A Critical Review." Fly Ash. Silica Fume. Slag and Other Mineral By-Products in Concrete. *ACI SP-79*:1-46.

Rüsch, H. 1960. "Researches Toward a General Flexural Theory for Structural Concrete." *ACI Journal. Proceedings.* Vol. 57. No. 1:1-28.

Peterman, M. B., and R. L. Carrasquillo. 1986. "Production of High Strength Concrete." *Noyes Publication.* Park Ridge. New Jersey.

Popovics, S. 1970. "A Review of Stress-Strain Relationships for Concrete." *ACI Journal.* Title. No. 67-14:243-248.

Saenz.,L. P. Discussion of a paper by P. Desayi and S. Krishnan. 1964. " Equation for the Stress-Strain Curve of Concrete." *ACI Journal. Proceedings.* Vol. 61. No. 9:1229-1235.

Sandvik, M., and O. E. Gjorv. 1986. "Effect of Condensed Silica Fume on the Strength Development of Concrete." Fly Ash. Silica Fume. Slag and Natural Pozzlans in Concrete. *ACI SP-91*:893-902.

Sargin, M. 1971. "Stress-Strain Relationships for Concrete and the Analysis of Structural Concrete Sections." Study No. 4. Solid Mechanics Division. University of Waterloo. Waterloo. Ontario. Canada.

Sargin, M., and V. K. Handa. 1969. "A General Formulation for the Stress-Strain Properties of Concrete." Solid Mechanics Division. University of Waterloo Report No. 3. Waterloo. Ontario. Canada.

Sargin, M., S. K. Ghosh, and V. K. Handa. 1971. "Effects of Lateral Reinforcement upon the Strength and Deformation Properties of Concrete." *Magazine of Concrete Research.* Vol. 23. No. 75-76:99-110.

Saucier, K. L. 1979. "High Strength Concrete. Past. Present. Future." Paper Presented at *the 1979 Annual Convention. American Concrete Institute.* Milwaukee. 3:18-23.

Sellevold, E. J., and F. F. Radjy. 1983. "Condensed Silica Fume in Concrete: Water Demand and Strength Development." Fly Ash. Silica Fume. Slag and Other Mineral By-Products in Concrete. *ACI SP-79*:677-694.

Shah, S. P., and A. E. Naaman. 1976. "Mechanical Properties of Glass and Steel Fiber Reinforced Mortar." *ACI Journal.* 1:50-55.

Shah, S. P., U. Gokoz, and Farhad Ansari. 1981. "An Experimental Technique for Obtaining Complete Stress-Strain Curves for High Strength Concrete." *Cement. Concrete and Aggregates. CCAGDP.* Vol. 3. No. 1:21-27.

Shah, S. P., and G. Batson. Editors. 1987. "Fiber Reinforced Concrete Properties and Applications." *ACI SP-105.*

Shah, S. P., A. Fafitis, and R. Arnold. 1983. "Cyclic Loading of Spirally Reinforced Concrete." *Journal of the Structural Division.* ASCE. Vol. 109. No. 7:1695-1710.

Shah, S. P., P. Stroeven, D. Dalhuisen, and P. Van Stekelenburg. 1978. "Complete Stress-Strain Curves for Steel Fibre Reinforced Concrete in Uniaxial Tension and Compression." *Testing and Test Methods of Fibre Cement Composites (RILEM Symposium 1978)*. Construction Press. Lancaster. 128-138.

Smith, G. J., and F. N. Rad. 1989. "Economic Advantages of High-Strength Concrete in Columns." *Concrete International.* 4:37-43.

Smith, G. M., and L. E. Young. 1955. "Ultimate Theory in Flexure by Exponential Function." *ACI Journal. Proceedings.* Vol. 52. No. 3:349-360.

Soliman, M. T. M., and C. W. Yu. 1967. "The Flexural Stress-Strain Relationship of Concrete Confined by Rectangular Transverse Reinforcement." *Magazine of Concrete Research.* Vol. 19. No. 61:223-238.

Sturman, G. M., S. P. Shah, and G. Winter. 1965. "Effect of Flexural Strain Gradients on Microcracking and Stress-Strain Behavior of Concrete." *ACI Journal. Proceedings.* Vol. 62. No. 7:805-822.

Swamy, R. N. 1986. "Properties of High Strength Concrete." *Cement. Concrete. and Aggregates. CCAGPD.* Vol. 8. No. 1:33-41.

Szulczynski, T., and M. A. Sozen. 1961. "Load-Deformation Characteristics of Reinforced Concrete Prisms with Rectilinear Transverse Reinforcement." Structural Research Series No. 224. Civil Engineering Studies. University of Illinois. Urbana. September.

Taerwe, L. R. 1992. "Influence of Steel Fibers on Strain-Softening of High-Strength Concrete." *ACI Journal.* 1:54-60.

Tsao, W. H. 1991. "Behavior of Squarre and L-shaped Slender Reinforced Concrete Columns under Combined Biaxial Bending and Axial Compression." Ph.D Dissertation.

Wang, G., and C. T. Thomas Hsu. 1990. "Complete Load-Deformation Behavior of Biaxially Loaded RC Columns." Technical Report Structural Series. NO. 90-2. Dept. of Civil & Env. Eng. NJIT. 38 pp.

Wang, P. T., S. P. Shah, and A. E. Naaman. 1978. "Stress-Strain Curve for Normal and Lightweight Concrete in Compression." *J. of the American Concrete Institute.* Vol. 75. No. 11:603-611.

Wang, G., and C. T. Thomas Hsu. 1990. "Complete Load-Deformation Behavior of Biaxially Loaded Reinforced Concrete Columns." Technical Report Structural Series No. 90-2 Department of Civil and Environmental Engineering. New Jersey Institute of Technology.

Yong, Y. K., M. G. Nour, and E. G. Nawy. 1988. "Behavior of Laterally Confined High Strength Concrete under Axial Loads." *Journal of Structural Engineering.* Vol. 114. No. 2:332-351.

Young, L. E. 1960. "Simplifying Ultimate Flexural Theory by Minimizing the Moment of the Stress Block." *ACI Journal. Proceedings.* Vol. 57. No. 5:549-556.